6-24-2013 12:00 AM

Continuum Modeling on Size-dependent Properties of Piezoelectric Nanostructures

Zhi Yan
The University of Western Ontario

Supervisor
Dr. Liying Jiang
The University of Western Ontario

Graduate Program in Mechanical and Materials Engineering
A thesis submitted in partial fulfillment of the requirements for the degree in Doctor of Philosophy
© Zhi Yan 2013

Continuum Modeling on Size-dependent Properties of Piezoelectric Nanostructures

(Thesis format: Integrated Article)

by

Zhi Yan

Graduate Program in Engineering Science
Department of Mechanical and Materials Engineering

A thesis submitted in partial fulfillment
of the requirements for the degree of
Doctor of Philosophy

The School of Graduate and Postdoctoral Studies
The University of Western Ontario
London, Ontario, Canada

Abstract

Piezoelectric beam- and plate-based nanostructures hold a promise for device applications in the nanoelectromechanical systems (NEMS) due to their superior mechanical and electromechanical coupling properties. "Small is different", nanostructured piezoelectric materials exhibit size-dependent properties, which are different from their bulk counterparts. For predicting the unique physical and mechanical properties of these novel nanostructures, continuum mechanics modeling has been regarded as an efficient tool. However, the conventional continuum models fail to capture the size effects of nanostructures and thus are not directly applicable at the nanoscale. Therefore, it is necessary to develop modified continuum models for piezoelectric nanostructures by incorporating the size effects and investigate the size-dependent properties of piezoelectric nanostructures based on the developed models.

Nanoscale structures are characterized by a high surface to volume ratio. The atoms in the surface layers of a structure are exposed to a different environment compared to those in the bulk of the structure. Thus, surface has a considerable influence on the physical and mechanical behaviors of nanoscale structures and is believed to be responsible for their size-dependent properties. In addition, for nanostructured piezoelectric materials, the strain gradient induced flexoelectricity could be significant and contribute to their size-dependent properties. In this thesis, the influence of the surface effects and flexoelectric effect on the mechanical and electrical properties of piezoelectric nanostructures is investigated through modified continuum models. Firstly, based on a surface piezoelectricity model and the generalized Young-Laplace equations, modified continuum models with surface effects are developed to investigate the bending, vibration, buckling behaviors and electromechanical properties of piezoelectric nanobeams and nanoplates with different boundary conditions. Next, by accounting for the flexoelectric effect through the extended linear theory of piezoelectricity and conventional beam models, the static and dynamic responses of piezoelectric nanobeams are presented. It is demonstrated from this study that the size effects prominently influence the mechanical behaviors and the electroelastic responses of piezoelectric nanostructures.

This research carries out a theoretical methodology to predict the static bending, electroelastic field distribution, resonant frequencies of vibration and critical electric potential for the mechanical buckling of piezoelectric nanostructures with different structure geometries, loading conditions and boundary conditions, which is expected to provide a fundamental understanding on the electromechanical coupling behavior of piezoelectric structures at the nanoscale. It is helpful for understanding the size-dependent properties of nanostructured piezoelectric materials and performance improvement of the beam- and plate-based electronic devices in NEMS.

Keywords

Co-Authorship Statement

Title: Surface effects on the electromechanical coupling and bending behaviors of piezoelectric nanowires (Chapter 2)

Authors: Z. Yan and L. Y. Jiang

The preliminary idea of doing this work was from Dr. L. Y. Jiang. The derivation of formulations was done by Z. Yan. The analytical analysis and result interpretations were jointed conducted by Z. Yan and Dr. Jiang. The first draft of the manuscript was written by Z. Yan and the subsequent drafts were modified by Dr. Jiang. This paper was published by Journal of Physics D: Applied Physics, Vol. 44, 075404, (2011).

Title: The vibrational and buckling behaviors of piezoelectric nanobeams with surface effects (Chapter 3)

Authors: Z. Yan and L. Y. Jiang

The preliminary idea of doing this work was from Dr. Jiang. Z. Yan derived the formulations for calculations; Dr. Jiang gave valuable suggestions on defining boundary conditions. Simulation results were presented by Z. Yan under the constructive suggestions of Dr. Jiang. In discussion with Dr. Jiang, Z. Yan wrote the first draft of the manuscript and Dr. Jiang made the following modifications. This paper was published by Nanotechnology, Vol. 22, 245703, (2011).

Title: Electromechanical response of a curved piezoelectric nanobeam with the consideration of surface effects (Chapter 4)

Authors: Z. Yan and L. Y. Jiang

The derivation of the formulations was conducted by Z. Yan. Z. Yan presented the simulation results under the guidance of Dr. Jiang. Dr. Jiang gave valuable suggestions on interpreting the results. The first draft of the manuscript was written by Z. Yan in discussion with Dr. Jiang. Modifications were done by Dr. Jiang. This paper was published by Journal of Physics D: Applied Physics, Vol. 44, 365301, (2011).

Title: Surface effects on the electroelastic responses of a thin piezoelectric plate with nanoscale thickness (Chapter 5)

Authors: Z. Yan and L. Y. Jiang

Dr. Jiang gave the suggestion to do this work. The formulations were derived by Z. Yan. Simulations were conducted by Z. Yan under the guidance of Dr. Jiang. Z. Yan wrote the first draft of the manuscript in discussion with Dr. Jiang. Modifications were made by Dr. Jiang. This paper was published by Journal of Physics D: Applied Physics, Vol. 45, 255401, (2012).

Title: Vibration and buckling analysis of a piezoelectric nanoplate considering surface effects and in-plane constraints (Chapter 6)

Authors: Z. Yan and L. Y. Jiang

The preliminary idea of doing this work was from Dr. Jiang. All the formulations were derived by Z. Yan. Dr. Jiang gave valuable suggestions on how to define boundary conditions. All the simulations were done by Z. Yan under suggestions of Dr. Jiang. The result interpretations were jointly conducted by Z. Yan and Dr. Jiang. The first draft of the manuscript was written by Z. Yan and modifications were carried out by Dr. Jiang. This paper was published by Proceedings of the Royal Society A, Vol. 468, 3458-3475, (2012).

Title: Surface effects on the vibration and buckling of piezoelectric nanoplates (Chapter 7)

Authors: Z. Yan and L. Y. Jiang

The preliminary idea of doing this work was from Z. Yan and Dr. Jiang. All the formulations were derived by Z. Yan and the simulations were made by Z. Yan. Dr. Jiang gave valuable suggestions on how to present the results. The first draft of the manuscript was written by Z. Yan and modifications were carried out by Dr. Jiang. This paper was published by Europhysics Letters, Vol. 99, 27007, (2012).

Title: Flexoelectric effect on the electroelastic responses of bending piezoelectric nanobeams (Chapter 8)

Authors: Z. Yan and L. Y. Jiang

The preliminary idea of doing this work was from Dr. Jiang. All formulations were derived by Z. Yan. All the simulations were conducted by Z. Yan under valuable

suggestions of Dr. Jiang. The result interpretations were jointly conducted by Z. Yan and Dr. Jiang. The first draft of the manuscript was written by Z. Yan and Dr. Jiang made the following modifications. This paper was published by Journal of Applied Physics, Vol. 113, 194102, (2013).

Title: Size-dependent bending and vibration behavior of piezoelectric nanobeams aroused by flexoelectricity (Chapter 9)

Authors: Z. Yan and L. Y. Jiang

The preliminary idea of doing this work was from Dr. Jiang. Z. Yan derived all the formulations and conducted the simulations under valuable suggestions of Dr. Jiang. The result interpretations were jointed done by Z. Yan and Dr. Jiang. The first draft of the manuscript was prepared by Z. Yan and the subsequent modifications were carried out by Dr. Jiang. This manuscript has been submitted to Journal of Physics D: Applied Physics.

Acknowledgments

First and foremost, I would like to express my sincere gratitude to my supervisor Professor Liying Jiang for offering me the opportunity to pursue my graduate studies at Western. I would also like to thank Professor Jiang for her patient guidance, continuous support and invaluable suggestions throughout my graduate studies, which enabled me to complete this thesis.

I also sincerely appreciate Professor John R. Dryden, Professor Andy Sun and Professor Jun Yang's helps and supports during my studies at Western.

I would like to thank Professor Samuel Asokanthan, Professor José Herrera, Professor Peter Schiavone and Professor Anand Singh for devoting time to read my thesis.

Appreciation is also expressed to all the professors in the Department of Mechanical and Materials Engineering for their valuable knowledge imparted to me. In addition, I would like to thank all the staff members in my department for their assistance during the past years. I would also like to thank the current and former members of Professor Liying Jiang's group for their friendship and support.

Many thanks to the financial support from Natural Sciences and Engineering Research Council of Canada (NSERC) and Ontario ministry of training, colleges and universities.

Finally, I would like to thank my family and friends for their support and encouragement, especially my husband Wei Wu and my adorable fourteen-month-old daughter Yixi, whose love and sacrifice made this work possible.

Table of Contents

List of Figures

List of Appendices

Nomenclature

$\mathbf{a}$	reciprocal dielectric susceptibility tensor
$\mathbf{c}$	bulk elastic constant tensor
$\mathbf{c}^s$	surface elastic constant tensor
$\mathbf{D}$	bulk electric displacement vector
$\mathbf{D}^s$	surface electric displacement vector
$\mathbf{D}^0$	residual surface electric displacement vector
$\mathbf{e}$	bulk piezoelectric constant tensor
$\mathbf{e}^s$	surface piezoelectric constant tensor
$\mathbf{E}$	electric field vector
$\mathbf{f}$	flexocoupling constant tensor
h	thickness
H	electric enthalpy density
K	kinetic energy
L	length
$\mathbf{M}$	bending moment tensor
$\mathbf{N}$	in-plane force tensor
$\mathbf{P}$	electric polarization vector
P_{eff}	effective axial force
Q	shear force

$R(x)$	radius of curvature
u	displacement component
U	internal energy density
U_{oc}	internal energy under open circuit condition
U_{sc}	internal energy under short circuit condition
v	displacement component
V	electric voltage
V_{cr}	critical electric potential for the mechanical buckling
w	displacement component
X_i	coordinate functions
Y_i	coordinate functions
$(EI)_{eff}$	effective bending rigidity
ε	strain tensor
$\varPhi$	electric potential
κ	bulk dielectric constant tensor
κ^s	surface dielectric constant tensor
ξ_0	bulk electromechanical coupling coefficient
ξ_{eff}	electromechanical coupling coefficient
ψ	total slope of deflection of the curved beam

ρ	mass density
θ	rotation angle
$\boldsymbol{\sigma}$	bulk stress tensor
$\boldsymbol{\sigma}^s$	surface stress tensor
$\boldsymbol{\sigma}^0$	residual surface stress tensor
σ_{ijm}	components of higher order stress or moment stress tensor
ω	angular resonant frequency

Chapter 1

1   Introduction

1.1   Piezoelectricity

The earliest knowledge of electric effects goes back to ancient Greece, where it was found that rubbing fur on amber caused an attraction between the two. Owing to this reason, the modern word "electricity" derives from the Greek word "elektron" for amber. In later centuries, as people learn more about electricity, special prefixes have been added before the word "electricity" to distinguish various manifestations of electricity, *e.g.* "piezo-", which means "to press". Piezoelectricity was first discovered by Pierre and Jacques Curie brothers (1880), who found that by compressing certain crystals, electric charges were produced. The charges are proportional to the pressure and disappear when the pressure is withdrawn. This phenomenon is known as the direct piezoelectric effect. The converse piezoelectric effect is the deformation of piezoelectric crystal under an applied electric field, which was predicted by Lippmann (1881) based on thermodynamic principles. The converse piezoelectric effect was later verified by the Curies at the end of 1881. There are many materials which naturally have piezoelectricity, such as tourmaline, Rochelle salt, topaz, quartz, cane sugar, *etc*. However, the weakness of the electromechanical coupling effect in these natural materials strongly limits the application of piezoelectricity in the early days. The today's widespread application of the piezoelectric effect attributes to the introduction of artificial piezoelectric ceramics in the 1950's, including lead zirconate titanate (PZT), barium titanate ($BaTiO_3$), lead titanate ($PbTiO_3$), *etc*. Piezoelectric ceramics consists of a large number of small crystallites. Below Curie temperature, the electric dipoles near each other in the piezoelectric crystals tend to be aligned in regions called domains. The domains are usually randomly oriented, resulting in zero overall polarization or piezoelectric effect in the crystals. However, these crystals can acquire piezoelectricity under a strong electric field at a temperature slightly below the Curie point. Under the process, domains with different polarization directions are reoriented towards the direction of the applied electric field. A permanent polarization can be still aligned in the crystal after the process. This process, called poling, is an important manufacturing process and induces

piezoelectricity as well as material anisotropy. Due to the piezoelectric effects, piezoelectric materials have been widely used in the electronic devices such as sensors, actuators and transducers in research and industry.

1.2 Nanostructured piezoelectric materials and their size-dependent properties

Since the piezoelectric effect results from the relative displacements of atoms within crystals, devices based on piezoelectric materials can be made, in principle, to operate on atomic scales (Nguyen *et al*., 2013). With the development of nanotechnology and synthesis techniques, a collection of nanostructured piezoelectric materials has been successfully synthesized, including one-dimensional gallium nitride (GaN) nanowires and nanorods (Huang *et al*., 2002), $BaTiO_3$ nanowires (Spanier *et al*., 2006), zinc oxide (ZnO) nanowires, nanotubes, nanobelts, nanorods and nanorings (Wang, 2007), calcium sulfide (CaS) nanowires (Lin *et al*., 2008), aluminum nitride (AlN) nanowires (Yazdi *et al*., 2009), PZT nanofibers (Chen *et al*., 2010), *etc*. and two-dimensional $BaTiO_3$ nanofilms (Park *et al*., 2010), PZT nanoribbons (Qi *et al*., 2010), PZT nanofilms (Yamano *et al*., 2012), *etc*. The distinct mechanical and electromechanical coupling properties of these advanced materials make them attractive for a wide range of device applications in nanoelectromechanical systems (NEMS). One example that has received the most attention is nanogenerator based on piezoelectric nanowires with the first prototype being invented by Wang and Song (2006). In this device, piezoelectricity was employed to convert mechanical energy into electrical energy. Recently, nanogenerators have been fabricated by employing two-dimensional nanostructured piezoelectric materials including $BaTiO_3$ nanofilms, PZT nanoribbons and nanofilms to achieve high energy conversion efficiency (Park *et al*., 2010; Qi *et al*., 2010; Feng *et al*., 2011). Other applications of nanostructured piezoelectric materials include piezoelectric nanowire lasers (Johnson *et al*., 2002), resonators (Bai *et al*., 2003), field-effect transistors (Wang *et al*., 2006), diodes (He *et al*., 2007), sensors (Zhou *et al*., 2008) and strain-controlled logic gates (Wu *et al*., 2010). However, these fascinating devices are at the early research stage and still years away from commercially available due to the issues of reliability and optimal performance, which need to be further addressed. Therefore, it is of great

importance to conduct fundamental characterization of these advanced materials and qualitatively investigate their mechanical and electromechanical properties.

Different experimental techniques and computational tools have been developed to investigate the mechanical and electrical properties of nanostructured piezoelectric materials. Through these approaches, researchers have found that the materials at the nanoscale exhibit properties different from their bulk counterparts, *i.e.* size-dependent properties. For example, the Young's modulus of ZnO was experimentally observed to increase dramatically with decreasing diameters below 120 nm by the electric-field-induced resonance method (Chen *et al*., 2006). The elastic moduli of other nanostructured piezoelectric materials such as GaN nanowires, PZT nanofibers, CdS nanowires were also found to be size dependent in experiments (Nam *et al*., 2006; Xu *et al*., 2006; Gao *et al*., 2010). The fracture strain of ZnO wires was observed to vary from 5% to 15% with the decrease of diameters from 500 nm to 200 nm by performing experiments (Desai and Haque, 2006), while their ultimate tensile strength could be up to 40 times of the bulk one according to the controlled lateral force atomic force microscopy (AFM) measurement (Wen *et al*., 2008). Piezoelectric sensitive scanning force microscopy in the contact mode revealed a steep increase of the piezoelectric response of PZT films below lateral sizes of 200 nm (Bühlmann *et al*., 2002). From the piezoresponse force microscopy, the effective piezoelectric coefficient d_{33} of a ZnO nanobelt was measured and found to be frequency dependent and much larger than its bulk counterpart (Zhao *et al*., 2004). An experimental approach has been presented to measure the three independent piezoelectric coefficients of GaN nanowires (d_{13}, d_{33} and d_{15}) employing scanning probe microscopy (Minary-Jolandan *et al*., 2012). Experimental results demonstrated that the GaN nanowires exhibit strong piezoelectricity in three-dimensions, with up to six times of their bulk counterpart. In parallel to the above mentioned experimental work, atomistic simulations have also played a key role in predicting the size-dependent mechanical and electrical properties of nanostructured piezoelectric materials. For example, molecular dynamics simulations were performed to characterize the response of ZnO nanobelts with their ultimate tensile strength and Young's modulus being obtained as functions of size and growth orientation (Kulkarni *et al*., 2005). The elastic moduli of GaN nanowires for three major growth orientations were identified to be size dependent at small sizes by a computational-

experimental investigation (Bernal *et al*., 2011). By employing a shell-based molecular dynamics approach, the elastic modulus of $BaTiO_3$ nanowires was observed to differ dramatically from the bulk $BaTiO_3$ (Zhang *et al*., 2011). In addition, the piezoelectric coefficients of ZnO, GaN nanowires and ZnO nanobelt were also found to be size-dependent by using first-principle density functional theory (Xiang *et al*., 2006; Agrawal and Espinosa, 2011) and molecular dynamics approach (Momeni *et al*., 2012), respectively.

From the above mentioned studies, it has been clearly demonstrated that both experimental approaches and atomistic simulations provide unambiguous evidences of the size-dependent properties of nanostructured piezoelectric materials. However, experiments at the nanoscale are very difficult to control and they are not sufficient to provide a mechanistic explanation for a measured material property. Moreover, although atomistic simulation can be very accurate when employed to study a nanostructure by dealing with a cluster of atoms, this approach is largely limited by computation capabilities at both length and time scales considering the large number of atoms in a typical structure. Alternatively, many researchers have resorted to the continuum mechanics modeling to investigate the properties of nanostructures due to their superior computational efficiency and robustness. Nevertheless, the conventional continuum models ignore the variation of interatomic quantities and fail to capture the size effects of nanostructures. Therefore, modified continuum models incorporating the small scale features must be developed to overcome this limitation. Several modified continuum models have been developed to characterize the mechanical and physical properties of nanostructured materials, such as the non-local elasticity model, surface elasticity model and multiscale continuum model, which provide simulation results in good agreement with those from atomistic simulations, but more computational efficient and versatile. It is therefore has been claimed by Yakobson and Smalley (1997) that "the laws of continuum mechanics are amazing robust and allow one to treat even intrinsically discrete objects only a few atoms in diameter". A literature review on the investigation of size-dependent properties of nanostructured materials based on the continuum mechanics approaches will be provided later in Section 1.4.

1.3 Brief introduction of surface effects in solids and flexoelectricity phenomenon

Since the atoms at and near a free surface or an interface experience a different local environment in comparison to those in the bulk of a material due to reduced coordination, the equilibrium position and the energy associated with the atoms at and near a surface or an interface are generally different from those of the atoms in the bulk (Streitz *et al*., 1994). Therefore, the creation of a surface leads to excess free energy in a solid, *i.e.* the surface free energy, and the surface stress can be determined from the surface energy. The concepts and physics of surface energy and surface stress of solids were introduced by Gibbs (1906). In the Gibbs idealization, both the surface energy and surface stress are quantities in a continuum sense and they are ascribed to a "mathematical surface" with a zero thickness. As the influence of a surface on the physical properties of the atoms near it generally extends to a few atomic layers, there quite likely exists a transition interphase. This idealization is widely adopted, and the effect of the surface is therefore generally neglected in classical continuum mechanics theories (Wang *et al*., 2011). However, such an effect can no longer be neglected in nanostructures, in which the surface area to volume ratio is exceptional large at such a small scale. As a result, the surface effects could play a significant role in the size-dependent properties of nanostructures (including piezoelectric nanostructures).

Flexoelectricity refers to a spontaneous electric polarization in dielectrics induced by a non-uniform strain (or strain gradient) field. In contrast to piezoelectricity, which is restricted to certain crystals with noncentrosymmetry, flexoelectric effect can emerge even in centrosymmetric crystals. This phenomenon is explained by the non-uniform displacement of ions in the crystal under a strain gradient, which disrupts the inversion symmetry and leads to the formation of a net polarization in the crystal. Therefore, the piezoelectricity is induced by uniform strains while flexoelectricity results from non-homogeneous strain or strain gradient. The phenomenon of flexoelectricity was first predicted by Mashkevich and Tolpygo (1957) that electrostatic potential; could arise from non-homogeneous deformations of lattice in crystals such as silicon. The concept of flexoelectricity was introduced by Kogan in the 1960s (Kogan, 1964). However, the flexoelectricity has not received as much attention as piezoelectricity at the macroscopic

scale due to the mechanical restrictions on forming large stain gradients. Besides the magnitude of strain gradient, the strength of flexoelectricity also depends on the numerical value of the flexoelectric coefficient. Ma and Cross carried out a series of experimental work (2001a; b; 2002; 2003; 2006) and have observed strong flexoelectric effect in certain piezoelectric materials due to their large flexoelectric coefficient. These pioneer works have stimulated the recent scientific interests in investigating the phenomenon of flexoelectricity.

Flexoelectricity is a size-dependent effect, which becomes more significant at nanometer scale due to the increasing strain gradient. Numerous studies indicate that flexoelectric effect plays an important role in the physical characteristics of ferroelectric thin films and other nanostructures, such as the dielectric constant (Catalan *et al.*, 2004), the critical phase transition temperature (Eliseev *et al.*, 2009), the polarization hysteresis curves (Lee *et al.*, 2011) and the critical thickness of thin films below which the switchable spontaneous polarization vanishes (Zhou *et al.*, 2012). Since electric polarization can be induced by flexoelectricity even in non-piezoelectric materials, flexoelectricity can be exploited to produce "piezoelectric materials" by using non-piezoelectric constituent materials (Fousek *et al.*, 1999). It has also been shown that the physical properties of ferroelectric epitaxial thin films such as domain configurations and hysteresis curves can be tuned by means of the flexoelectric effect (Lee *et al.*, 2011). Furthermore, the flexoelectric effect can be used as a dynamic tool for polarization control and may enable data storage applications in which memory bits are written mechanically and read electrically (Lu *et al.*, 2012). Moreover, the electromechanical coupling of piezoelectric nanostructures may be enhanced by the flexoelectric effect (Majdoub *et al.*, 2008). Therefore, in addition to surface effects, the flexoelectric effect is also expected to be responsible for the size-dependent properties of nanostructured piezoelectric materials.

1.4   Literature review

Extensive theoretical studies have been devoted to investigate various problems with the consideration of surface effects, such as the elastic, bending and vibration properties of nanostructured elements, elastostatic solutions of nanoinhomogeneity problems, elastic

field around crack tip and effective properties of heterogeneous media (Wang *et al*., 2011). In addition, there is a surge of scientific interest in qualitatively studying the flexoelectric effect on the nanostructured dielectric materials. In this literature review, attention will be focused on the continuum modeling of one-dimensional nanowires/nanobeams and two-dimensional thin film, nanoplates with the surface effects and theoretical works on the flexoelectric effect, respectively.

1.4.1   Continuum modeling of nanostructures with surface effects

Gurtin and Murdoch (1975) proposed a theoretical framework based on continuum mechanics accounting the surface effects. In the surface elasticity model they proposed, the surface is regarded as a thin layer with negligible thickness adhered to the underlying bulk material without slipping. The surface properties and constitutive relations for the surface are different from those of the bulk and equilibrium of the surface is governed by the generalized Young-Laplace equations. It should be mentioned that the material properties of surface can be determined from experiments or atomistic simulations. This surface elasticity model has been served as a basis for many studies to investigate the mechanical properties of nanostructured materials. Miller and Shenoy (2000) investigated the size-dependent elastic properties of Al and Si nanowires and nanoplates taking into account the surface stress effect. The size dependence of torsional rigidity of nanosized bars has been found by the continuum analysis with the surface stress effect; the results were in good agreement with those from atomistic simulations (Shenoy, 2002). Dingreville *et al*. (2005) developed a framework to incorporate the surface energy into the continuum theory of mechanics and demonstrated that the overall elastic behavior of structural elements (such as particles, wires, films) were size-dependent. Guo and Zhao (2007a) studied the elastic bending properties of nanobeams based on a three-dimensional crystal model. Zhu (2008) investigated the influence of surface effects on the bending stiffness and hence the natural frequency of a coaxial core-shell nanowire. He and Lilley (2008a; b) studied the influence of surface effects on the static bending behavior and bending resonant frequencies of nanowires with different boundary conditions by incorporating the generalized Young-Laplace equation into the Euler-Bernoulli beam theory. Based on the surface elasticity model, Wang *et al*. (2008)

investigated the twisting deformation of nanowires due to anisotropic surface stresses and pointed out that the surface stresses might be responsible for the formation of some micro-/nanohelics. Wang and Feng (2009a; b) investigated the effects of both surface elasticity and residual surface tension on the buckling behaviors of nanowires based on Euler-Bernoulli and Timoshenko beam models, respectively. Zheng *et al*. (2010) investigated the size-dependent elastic property of nanowires induced by the surface effects using a core-shell model. Assadi and Farshi (2010) investigated the size-dependent vibration of curved nanobeams and rings including surface energies.

Two-dimensional nanostructures have also been widely studied with the consideration of the surface effects. He *et al*. (2004) studied the size-dependent mechanical response of a film with an arbitrary geometry and boundary conditions based on the surface elasticity model. Lim and He (2004), and Lu *et al*. (2006) conducted large-deflection analysis on the static and dynamic responses of nanoscale thin elastic films with the consideration of the surface effects. Guo and Zhao (2005; 2007b) presented a three dimensional continuum model to investigate the size-dependent elastic moduli of nanofilms with surface relaxation and surface energy effects. Huang (2008) proposed a modified continuum model of elastic films by incorporating surface effects into the conventional nonlinear von Karman plate theory. Wang and Zhao (2009) investigated the size-dependent self-buckling and bending behavior of nanoplates with surface effects. Zhu *et al*. (2009) studied the effects of surface and initial stresses on the bending stiffness of tri-layer plates and nanofilms. Lu *et al*. (2009) presented a study on nanoscale functionally graded films considering the surface effects, where the surface layers of the film were modeled by the continuum theory of surface elasticity. Assadi and Farshi (2011) conducted a size-dependent stability analysis of circular ultrathin films in elastic medium with the consideration of surface energies.

For piezoelectric nanomaterials, based on the surface elasticity model, Wang and Feng (2010) analyzed the influence of the residual stress and surface elasticity on the vibration and buckling behaviors of piezoelectric nanowires using the Euler-Bernoulli beam model. As an extension of the surface elasticity model, Huang and Yu (2006) proposed a surface piezoelectricity model by assuming that the surface energy density depended on the electric field at the surface in addition to the in-plane strains. They

studied a piezoelectric nanoring under an applied potential and showed that the surface piezoelectricity played an important role in the electromechanical behavior of piezoelectric nanostructures and the effect of surface piezoelectricity might be employed to improve some performances of nanostructures. However, the continuum modeling of surface effects including surface piezoelectricity on the mechanical and electromechanical coupling properties of nanostructured piezoelectric materials is far from complete. Therefore, it is necessary to conduct a systematic investigation to gain a fundamental understanding of how the surface effects influence the mechanical and physical properties of these structures.

1.4.2　Theoretical investigation on the flexoelectric effect

The theoretical studies on the influence of the flexoelectric effect on the mechanical and physical properties of nanostructured dielectrics are much fewer in comparison with those on the influence of surface effects on the properties of nanostructures. Tagantsev (1986, 1991) presented a phenomenological study on the flexoelectricity and found that the flexoelectric coefficient scaled with the dielectric susceptibility of the material. Maranganti *et al*. (2006) developed a complete mathematical framework for the flexoelectricity and solved the general embedded mismatched inclusion problems with explicit results for the inclusions spherical and cylindrical shapes. Based on this framework, Sharma *et al*. (2007) quantitatively demonstrated the possibility of designing "piezoelectric nanocomposites" without using piezoelectric materials. Majdoub *et al*. (2008) found a remarkable enhancement in piezoelectricity of piezoelectric nanostructures due to the flexoelectricity. Eliseev *et al*. (2009) investigated the renormalization in properties of ferroelectric nanostructures and elucidated the size-effects in such structures using Landau-Ginzburg-Devonshire phenomenological approach. Shen and Hu (2010) developed a more complete theoretical frame work for nanosized dielectrics with the consideration of the surface effects, flexoelectricity and electrostatic force. Sharma *et al.* (2010) presented closed-form analytical expressions for the flexoelectric response of various thin film and superlattice configurations under mechanical stress. They found that the interplay between thin film thickness, symmetry and flexoelectricity allowed the possibility of creating manufacturable piezoelectric thin

film superlattices without using piezoelectric materials. Yurkov (2011) pointed out that in the presence of the flexoelectric effect, the elastic boundary conditions were not coincident with the conventional ones. Liu *et al*. (2012) studied the effect of the flexoelectricity on the electrostatic potential in a bent piezoelectric nanowire and found that the flexoelectricity could explain the discrepancy between the results from classical piezoelectricity predictions and experimental measurements. However, the continuum modeling of the flexoelectric effect on the physical properties of piezoelectric nanostructures is still limited. Therefore, it is necessary to further explore the flexoelectricity on the mechanical and physical properties of these novel structures based on the modified continuum mechanics approaches.

1.5 Objectives

From the above introduction and literature review, it has demonstrated that understanding the size-dependent properties of piezoelectric nanostructures is essential for the design and applications of electronic devices in NEMS. The continuum mechanics approaches with the incorporation of the small scale features are successful in predicting the size-dependent properties of the nanostructured materials due to their simplicity and computation efficiency. However, these approaches were mostly developed to investigate the properties of elastic nanostructures, while investigation on the properties of piezoelectric nanostructures is very limited. Therefore, the main objective of this thesis is to provide a comprehensive theoretical study on the size-dependent properties of piezoelectric nanobeams and nanoplates based on the modified continuum mechanics modeling. Attention will be focused on:

(1) Proposing modified continuum models for piezoelectric nanostructures with the consideration of the size effects;

(2) Studying the size-dependent electroelastic responses of piezoelectric nanobeams and nanoplates with the size effects;

(3) Studying the surface effects on the bending, vibration and buckling behaviors of piezoelectric nanobeams with different boundary conditions;

(4) Studying the surface effects on the bending, vibration and buckling behaviors of piezoelectric nanoplates with different boundary conditions;

(5) Investigating the influence of the flexoelectric effect on the bending and vibration of piezoelectric nanobeams.

1.6 Thesis structure

A general introduction and literature review are presented in Chapter 1 while detailed introductions on each specific topic are presented in later chapters. Chapter 2 investigates the problem of a cantilevered piezoelectric nanobeam with surface effects, simulation results are provided to show the surface effects on the electromechanical coupling properties and static bending behavior of the piezoelectric nanobeams. Chapter 3 studies the vibration and buckling behavior of piezoelectric nanobeams with different boundary conditions. Results are presented to show how the surface effects, applied electrical load, applied axial strain and boundary conditions influence the vibration behavior of the piezoelectric nanobeams. The critical electric potential for the mechanical buckling of the piezoelectric nanobeam is analytically obtained and surface effects on this physical quantity are shown in the simulation results. Chapter 4 provides a study on the electromechanical responses of a curved piezoelectric nanobeam with surface effects. The explicit solutions for the electroelastic fields of a curved cantilever beam under both mechanical and electrical loads are obtained. Results are presented to show how the surface effects influence the displacement, stress and electric displacement fields of the curved beam. Chapter 5 presents a study on the size-dependent electroelastic responses of a simply-supported piezoelectric plate with nanoscale thickness. The size-dependent behaviors of the out-plane deflection, in-plane deformation, electric field, critical buckling load and critical electric potential for the mechanical buckling of the piezoelectric nanoplate under electromechanical loads are investigated. The vibration and buckling behaviors of simply supported and clamped-clamped piezoelectric nanoplates are presented in Chapter 6 and Chapter 7, respectively. In Chapter 6, analytical solutions for the piezoelectric nanoplate with surface effects under both traction free and clamped in-plane constraints are obtained. The transverse vibration of the plate is investigated under different applied electric potential, plate geometries, mode numbers and in-plane

conditions. Moreover, the critical electric potential for the plate is also examined under different length to thickness ratios. In Chapter 7, Ritz solutions are obtained and simulation results are presented to show the surface effects on the resonant frequency and critical electric potential of a piezoelectric nanoplate with clamped boundary conditions. Chapter 8 provides an investigation of the flexoelectric effect on the mechanical and electrical properties of piezoelectric nanobeams with different boundary conditions based on Euler-Bernoulli beam theory. The influence of the flexoelectricity on the static bending, axial relaxation strain, resultant axial forces and electric polarization will be presented. In Chapter 9, modified Timoshenko beam theory is developed with the consideration of the flexoelectricity. The static and dynamic behaviors of a simply supported piezoelectric nanobeam under distributed mechanical load are investigated based on the developed model. Finally, Chapter 10 concludes this thesis and some recommendations for the future work on the modeling of size-dependent properties of nanostructured piezoelectric materials are provided.

References

Agrawal, R. and Espinosa, H. D., 2011. Giant piezoelectric size effects in zinc oxide and gallium nitride nanowires. A first principles investigation. Nano Lett. **11**, 786-790.

Assadi, A. and Farshi, B., 2011. Size dependent stability analysis of circular ultrathin films in elastic medium with consideration of surface energies. Physica E **43**, 1111-1117.

Assadi, A., Farshi, B. and Alinia-Ziazi, A., 2010. Size dependent dynamic analysis of nanoplates. J. Appl. Phys. **107**, 124310.

Bai, X. D., Gao, P. X., Wang, Z. L. and Wang, E. G., 2003. Dual-mode mechanical resonance of individual ZnO nanobelts. Appl. Phys. Lett. **82**, 4806-4808.

Bernal, R. A., Agrawal, R., Peng, B., Bertness, K. A., Sanford, N. A., Davydov, A. V. and Espinosa, H. D., 2011. Effect of growth orientation and diameter on the elasticity of GaN nanowires. A combined in situ TEM and atomistic modeling investigation. Nano Lett. **11**, 548-555.

Bühlmann, S., Dwir, B., Baborowski, J. and Muralt, P., 2002. Size effect in mesoscopic epitaxial ferroelectric structures: increase of piezoelectric response with decreasing feature size. Appl. Phys. Lett. **80**, 3195.

Catalan, G., Sinnamon, L. J. and Gregg, J. M., 2004. The effect of flexoelectricity on the dielectric properties of inhomogeneously strained ferroelectric thin films. J. Phys.: Condens. Matter **16**, 2253.

Chen, C. Q., Shi, Y., Zhang, Y. S., Zhu, J. and Yan, Y. J., 2006. Size dependence of Young's modulus in ZnO nanowires. Phys. Rev. Lett. **96**, 075505.

Chen, X., Xu, S. Y., Yao, N. and Shi, Y., 2010. 1.6 V nanogenerator for mechanical energy harvesting using PZT nanofibers. Nano Lett. **10**, 2133-2137.

Curie, J. and Curie, P., 1880. Development par compression de l'eletricite polaire dans les cristaux hemiedres a faces inclines. Comptes Rendus Acad. Sci. **91**, 294-295.

Desai, A. V. and Haque, M. A., 2007. Mechanical properties of ZnO nanowires. Sensor. Actuat. A-Phys. **134**, 169-176.

Dingreville, R., Qu, J. M. and Cherkaoui, M., 2005. Surface free energy and its effect on the elastic behavior of nano-sized particles, wires and films. J. Mech. Phys. Solids **53**, 1827-1854.

Eliseev, E. A., Morozovska, A. N., Glinchuk, M. D. and Blinc, R., 2009. Spontaneous flexoelectric/flexomagnetic effect in nanoferroics. Phys. Rev. B **79**, 165433.

Feng, X., Yang, B. D., Liu, Y. M., Wang, Y., Dagdeviren, C., Liu, Z. J., Carlson, A., Li, J. Y., Huang, Y. G. and Rogers, J. A., 2011. Stretchable ferroelectric nanoribbons with wavy configurations on elastomeric substrates. ASC Nano **5**, 3326-3332.

Fousek, J., Cross, L. E. and Litvin, D. B., 1999. Possible piezoelectric composites based on the flexoelectric effect. Mater. Lett. **39**, 287-291.

Gao, P., Liu, K., Liu, L., Wang, Z., Liao, Z., Xu, Z., Wang, W., Bai, X., Wang, E. and Li, Y., 2010. Higher-order harmonic resonances and mechanical properties of individual cadmium sulphide nanowires measured by in situ transmission electron microscopy. J. Electron Microsc. **59**, 285-289.

Gibbs, J. W., 1906. The scientific papers of J. Willard Gibbs, Vol. 1. London: Longmans-Green.

Guo, J. G. and Zhao, Y. P., 2005. The size-dependent elastic properties of nanofilms with surface effects. J. Appl. Phys. **98**, 074306.

Guo, J. G. and Zhao, Y. P., 2007a. The size-dependent bending elastic properties of nanobeams with surface effects. Nanotechnology **18**, 295701.

Guo, J. G. and Zhao, Y. P., 2007b. The surface- and size-dependent elastic moduli of nanostructures. Surf. Rev. Lett. **14**, 667-670.

Gurtin, M. E. and Murdoch, A. I., 1975. A continuum theory of elastic material surfaces. Arch. Ration. Mech. Anal. **57**, 291-323.

He, J. and Lilley, C. M., 2008a. Surface effect on the elastic behavior of static bending Nanowires. Nano Lett. **8**, 1798-1802.

He, J. and Lilley, C. M., 2008b. Surface stress effect on bending resonance of nanowires with different boundary conditions. Appl. Phys. Lett. **93**, 263108.

He, J. H., Hsin, C. L., Liu, J., Chen, L. J. and Wang, Z. L., 2007. Piezoelectric gated diode of a single ZnO nanowire. Adv. Mater. **19**, 781-784.

He, L. H., Lim, C. W. and Wu, B. S., 2004. A continuum model for size-dependent deformation of elastic films of nano-scale thickness. Int. J. Solids Struct. **41**, 847-857.

Huang, D. W., 2008. Size-dependent response of ultra-thin films with surface effects. Int. J. Solids Struct. **45**, 568-579.

Huang, G. Y. and Yu, S. W., 2006. Effect of surface piezoelectricity on the electromechanical behaviour of a piezoelectric ring. Phys. Status Solidi B **243**, R22-R24.

Huang, Y., Duan, X. F., Cui, Y. and Lieber, C. M., 2002. Gallium nitride nanowire nanodevices. Nano Lett. **2**, 101-104.

Johnson, J. C., Choi, H.-J., Knutsen, K. P., Schaller, R. D., Yang, P. D. and Saykally, R. J., 2002. Single gallium nitride nanowire lasers. Nat. Mater. **1**, 106-110.

Kogan, S. M., 1964. Piezoelectric effect during inhomogeneous deformation and acoustic scattering of carriers in crystals. Sov. Phys. Solid. State **5**, 2069-2070.

Kulkarni, A. J., Zhou, M. and Ke, F. J., 2005. Orientation and size dependence of the elastic properties of zinc oxide nanobelts. Nanotechnology **16**, 2749.

Lee, D., Yoon, A., Jang, S. Y., Yoon, J. G., Chung, J.-S., Kim, M., Scott, J. F. and Noh, T. W., 2011. Giant flexoelectric effect in ferroelectric epitaxial thin films. Phys. Rev. Lett. **107**, 057602.

Lim, C. W. and He, L. H., 2004. Size-dependent nonlinear response of thin elastic films with nano-scale thickness. Int. J. Mech. Sci. **46**, 1715-1726.

Lin, Y. F., Song, J. H., Ding, Y., Lu, S.-Y. and Wang, Z. L., 2008. Alternating the output of a CdS nanowire nanogenerator by a white-light-stimulated optoelectronic effect. Adv. Mater. **20**, 3127-3130.

Lippmann, H. G., 1881. Sur le principle de la conversation de l'eletricite ou second principle de la theorie des phenomenes electriques. Comptes Rendus Acad. Sci **92**, 1049-1050.

Liu, C. C., Hu, S. L. and Shen, S. P., 2012. Effect of flexoelectricity on electrostatic potential in a bent piezoelectric nanowire. Smart Mater. Struct. **21**, 115024.

Lü, C. F., Chen, W. Q. and Lim, C.W., 2009. Elastic mechanical behavior of nano-scaled FGM films incorporating surface energies. Compos. Sci. Technol. **69**, 1124-1130.

Lu, H., Bark, C.-W., Esque de los Ojos, D., Alcala, J., Eom, C. B., Catalan, G. and Gruverman, A., 2012. Mechanical writing of ferroelectric polarization. Science **336**, 59-61.

Lu, P., He, L. H., Lee, H. P. and Lu, C., 2006. Thin plate theory including surface effects. Int. J. Solids Struct. **43**, 4631-4647.

Ma, W. H. and Cross, L. E., 2001a. Observation of the flexoelectric effect in relaxor $Pb(Mg_{1/3}Nb_{2/3})O_3$ ceramics. Appl. Phys. Lett. **78**, 2920.

Ma, W. H. and Cross, L. E., 2001b. Large flexoelectric polarization in ceramic lead magnesium niobate. Appl. Phys. Lett. **79**, 4420.

Ma, W. H. and Cross, L. E., 2002. Flexoelectric polarization of barium strontium titanate in the paraelectric state. Appl. Phys. Lett. **81**, 3440.

Ma, W. H. and Cross, L. E., 2003. Strain-gradient-induced electric polarization in lead zirconate titanate ceramics. Appl. Phys. Lett. **82**, 3293.

Ma, W. H. and Cross, L. E., 2006. Flexoelectricity of barium titanate. Appl. Phys. Lett. **88**, 232902.

Majdoub, M. S., Sharma, P. and Cagin, T., 2008. Enhanced size-dependent piezoelectricity and elasticity in nanostructures due to the flexoelectric effect. Phys. Rev. B **77**, 125424.

Maranganti, R., Sharma, N. D. and Sharma, P., 2006. Electromechanical coupling in nonpiezoelectric materials due to nanoscale nonlocal size effects: Green's function solutions and embedded inclusions. Phys. Rev. B **74**, 014110.

Mashkevich, V. S. and Tolpygo, K. B., 1957. Electrical, optical and elastic properties of diamond type crystals. Sov. Phys. JETP **5**, 435-439.

Miller, R. E. and Shenoy, V. B., 2000. Size-dependent elastic properties of nanosized structural elements. Nanotechnology **11**, 139-147.

Minary-Jolandan, M., Bernal, R. A., Kuljanishvili, I., Parpoil, V., Espinosa, H. D., 2012. Individual GaN nanowires exhibit strong piezoelectricity in 3D. Nano Lett. **12**, 970-976.

Momeni, K., Odegard, G. M. and Yassar, R. S., 2012. Finite size effect on the piezoelectric properties of ZnO nanobelts: A molecular dynamics approach. Acta Mater. **60**, 5117-5124.

Nam, C.-Y., Jaroenapibal, P., Tham, D., Luzzi, D. E., Evoy, S. and Fischer, J. E., 2006. Diameter-dependent electromechanical properties of GaN nanowires. Nano lett. **6**, 153-158.

Nguyen, T. D., Mao, S., Yeh, Y.-W., Purohit, P. K. and McAlpine, M. C., 2013. Nanoscale flexoelectricity. Adv. Mater. **25**, 946-974.

Park, K.-I., Xu, S., Liu, Y., Hwang, G.-T., Kang, S. J. L., Wang, Z. L. and Lee, K. J., 2010. Piezoelectric $BaTiO_3$ thin film nanogenerator on plastic substrates. Nano Lett. **10**, 4939-4943.

Qi, Y., Jafferis, N. T., Lyons, K., Lee, C. M., Ahmad, H. and McAlpine, M. C., 2010. Piezoelectric ribbons printed onto rubber for flexible energy conversion. Nano Lett. **10**, 524-528.

Sharma, N. D., Maranganti, R. and Sharma, P., 2007. On the possibility of piezoelectric nanocomposites without using piezoelectric materials. J. Mech. Phys. Solids **55**, 2328-2350.

Sharma, N. D., Landis, C. M. and Sharma, P., 2010. Piezoelectric thin-film superlattices without using piezoelectric materials. J. Appl. Phys. **108**, 024304.

Shen, S. P. and Hu, S. L., 2010. A theory of flexoelectricity with surface effect for elastic dielectrics. J. Mech. Phys. Solids **58**, 665-677.

Shenoy, V. B., 2002. Size-dependent rigidities of nanosized torsional elements. Int. J. Solids Struct. **39**, 4039-4052.

Spanier, J. E., Kolpak, A. M., Urban, J. J., Grinberg, I., Ouyang, L., Yun, W. S., Rappe, A. M. and Park, H., 2006. Ferroelectric phase transition in individual single-crystalline BaTiO3 nanowires. Nano Lett. **6**, 735-739.

Streitz, F. H., Cammarata, R. C. and Sieradzki, K., 1994. Surface-stress effects on elastic properties. I. Thin metal films. Phys. Rev. B **49**, 10699-10706.

Tagantsev, A. K., 1986. Piezoelectricity and flexoelectricity in crystalline dielectrics. Phys. Rev. B **34**, 5883-5889.

Tagantsev, A. K., 1991. Electric polarization in crystals and its response to thermal and elastic perturbations. Phase Transit. **35**, 119-203.

Wang, G. F. and Feng, X. Q., 2009a. Surface effects on buckling of nanowires under uniaxial compression. Appl. Phys. Lett. **94**, 141913.

Wang, G. F. and Feng, X. Q., 2009b. Timoshenko beam model for buckling and vibration of nanowires with surface effects. J. Phys. D: Appl. Phys. **42**, 155411.

Wang, G. F. and Feng, X. Q., 2010. Effect of surface stresses on the vibration and buckling of piezoelectric nanowires. EPL **91**, 56007.

Wang, J. S., Feng, X. Q., Wang, G. F. and Yu, S. W., 2008. Twisting of nanowires induced by anisotropic surface stresses. Appl. Phys. Lett. **92**, 191901.

Wang, J. X., Huang, Z. P., Duan, H. L., Yu, S. W., Feng, X. Q., Wang, G. F., Zhang, W. X. and Wang, T. J., 2011. Surface stress effect in mechanics of nanostructured materials. Acta Mech. Solida Sin. **24**, 52-82.

Wang, X. D., Zhou, J., Song, J. H., Liu, J., Xu, N. S. and Wang, Z. L., 2006. Piezoelectric field effect transistor and nanoforce sensor based on a single ZnO nanowire. Nano Lett. **6**, 2768-2772.

Wang, Z. L., 2007. Piezoelectric nanostructures: from growth phenomena to electric nanogenerators. MRS bull. **32**, 109-116.

Wang, Z. Q. and Zhao, Y. P., 2009. Self-instability and bending behaviors of nano plates. Acta Mech. Solida Sin. **22**, 630-643.

Wen, B., Sader, J. E. and Boland, J. J., 2008. Mechanical properties of ZnO nanowires. Phys. Rev. Lett. **101**, 175502.

Wu, W., Wei, Y. and Wang, Z. L., 2010. Strain-gated piezotronic logic nanodevices. Adv. Mater. **22**, 4711-4715.

Xiang, H. J., Yang, J. L., Hou, J. G. and Zhu, Q. S., 2006. Piezoelectricity in ZnO nanowires: A first-principles study. Appl. Phys. Lett. **89**, 223111.

Xu, S. Y., Shi, Y. and Kim, S. G., 2006. Fabrication and mechanical property of nano piezoelectric fibres. Nanotechnology **17**, 4497.

Yakobson, B. I. and Smalley, R., 1997. Fullerene Nanotubes: $C_{1,000,000}$ and Beyond. Am. Sci. **85**, 324-337.

Yamano, A., Takata, K. and Kozuka, H., 2012. Ferroelectric domain structures of 0.4-μm-thick Pb(Zr,Ti)O$_3$ films prepared by polyvinylpyrrolidone-assisted Sol-Gel method. J. Appl. Phys. **111**, 054109.

Yazdi, G. R., Persson, P. O., Gogova, D., Fornari, R., Hultman, L., Syväjärvi, M. and Yakimova, R., 2009. Aligned AlN nanowires by self-organized vapor–solid growth. Nanotechnology **20**, 495304.

Yurkov, A. S., 2011. Elastic boundary conditions in the presence of the flexoelectric effect. JETP Lett. **94**, 455-458.

Zhang, Y. H., Liu, B. and Fang, D. N., 2011. Stress-induced phase transition and deformation behavior of BaTiO$_3$ nanowires. J. Appl. Phys. **110**, 054109.

Zhao, M. H., Wang, Z. L. and Mao, S. X., 2004. Piezoelectric characterization on individual zinc oxide nanobelt under piezoresponse force microscope. Nano Lett. **4**, 587-590.

Zheng, X. P., Cao, Y. P., Li, B., Feng, X. Q. and Wang, G. F., 2010. Surface effects in various bending-based test methods for measuring the elastic property of nanowires. Nanotechnology **21**, 205702.

Zhou, H., Hong, J. W., Zhang, Y. H., Li, F. X., Pei, Y. M. and Fang, D. N., 2012. Flexoelectricity induced increase of critical thickness in epitaxial ferroelectric thin films. Physica B **407**, 3377-3381.

Zhou, J., Gu, Y., Fei, P., Mai, W., Gao, Y., Yang, R., Bao, G. and Wang, Z. L., 2008. Flexible piezotronic strain sensor. Nano Lett. **8**, 3035-3040.

Zhu, H. X., 2008. The effects of surface and initial stresses on the bending stiffness of nanowires. Nanotechnology **19**, 405703.

Chapter 2

2   Surface effects on the electromechanical coupling and bending behaviors of piezoelectric nanowires[1]

2.1   Introduction

Piezoelectric nanostructures hold tremendous potential for device applications, such as piezoelectric nanogenerators, mechanical-electrical triggers, sensors and nanoresonators (Song *et al*., 2006; Wang *et al*., 2006; Wang *et al*., 2007a; Lin *et al*., 2008; Zhou *et al*., 2008). Unlike their bulk counterparts, piezoelectric nanomaterials are observed to exhibit size-dependent properties when their dimensions approach to microns and nanometers. For example, the elastic and fracture properties of ZnO piezoelectric nanowires were found to vary with their cross-sectional dimensions according to the experimental measurements (Chen *et al*., 2006; Desai *et al*., 2007; Agrawal *et al*., 2008). In addition to the experimental work, size-dependent elastic properties of piezoelectric nanostructures were also reported using atomistic simulation (Kulkarni *et al*., 2005; Agrawal *et al*., 2009; Hu *et al*., 2009). The piezoelectric properties of ZnO nanobelts have also been explored by Zhao *et al*. (2004). They used piezoresponse force microscopy to measure the effective piezoelectric coefficient d_{33} of a ZnO nanobelt and found that d_{33} of the ZnO nanobelt was frequency dependent and much larger than their bulk counterpart. First principal energy theory was used to study the dielectric properties of nanoscale slabs in Ramprasad *et al*.'s work (2005), and their results indicated that the dielectric constant is dependent on the slab thickness. To achieve reliable and optimal performance of these nanostructures in the potential device applications, it is essential to find the underlying reason for the size-dependent properties of piezoelectric nanomaterials. Thus, the mechanical and electrical responses of the piezoelectric nanostructures can be properly characterized.

---

[1]A version of this chapter has been published.

Yan, Z. and Jiang, L. Y., J. Phys. D: Appl. Phys. 44, 075404, (2011).

For elastic nanostructures, it has been widely accepted that surface is largely responsible for the size-dependent mechanical properties of these materials due to the dramatic increasing ratio of surface area to volume at nanoscale. Recently, surface effects on the mechanical properties of elastic materials have been extensively studied by researchers. In addition to atomic studies (Makeev *et al*., 2006; Zhang *et al*., 2008; Rudd *et al*., 2008), researchers have accounted for the surface effects in continuum modeling by using the linear surface elastic theory developed by Gurtin and Murdoch (1975). Under a reasonable assumption, a surface can be regarded as a thin layer with negligible thickness *t* adhered to the bulk without slipping (Cammarata, 1994; Miller and Shenoy, 2000). The constitutive and equilibrium equations for the surface layer are different from those in the bulk of the solid. Following this surface-layer-based model, the surface effects on the bending, vibrational and buckling behaviors of nanowires were predicted by one-dimensional beam theory via the Young-Laplace equation (Wang and Feng, 2007; He and Lilley, 2008; Wang and Feng, 2009; Jiang and Yan, 2010). Through these studies and many others, it has been indicated that "the laws of continuum mechanics are amazing robust and allow one to treat even intrinsically discrete objects only a few atoms in diameter" (Yakobson, 1997). Therefore, it is natural to resort to continuum theory for modeling the electromechanical behavior of piezoelectric nanostructures due to the efficiency of such an approach.

It is worth to mention that Michalski *et al.* (2005) were the first to develop a continuum theory for the piezoelectric response of one-dimensional nanotubes and nanowires. However, their results failed to interpret the size-dependent properties of such materials. To investigate the underlying reason for the size-dependent properties of piezoelectric nanobeams, Sharma and his coworkers (Majdoub *et al*., 2008a; b) adopted the strain gradient induced flexoelectricity in the Euler-Bernoulli beam model to study the electromechanical coupling of piezoelectric nanobelts. Their results showed the enhanced size-dependent piezoelectricity in piezoelectric nanostructures. Inspired by the surface-layer-based model, it is natural to believe that surface effects may also play an important role in the electromechanical behavior of piezoelectric nanostructures. As argued earlier by Tagantsev (1986), surface piezoelectricity for piezoelectric materials may become important at small sizes. Therefore, it is essential to incorporate electric

field dependent surface effects when investigating the electromechanical coupling behavior of the nanoscale piezoelectric structures. Considering the surface piezoelectricity, Huang and Yu (2006) did pioneering work to study the electromechanical behavior of a piezoelectric ring. A considerable effect of surface piezoelectricity on the stress and electric fields was observed when the ring size scaled down to nanometers. As an extension of his previous work (Chen, 2007), Chen (2008) considered the macroscopic behavior of two-phase fibrous piezoelectric composites and found size-dependent electroelastic properties in the presence of surface effects.

Since most piezoelectric nanodevices are beam based, it is necessary to investigate the electromechanical properties as well as the bending behavior of piezoelectric nanobeams. Therefore, it is the objective of the current work to study the surface effects on the electromechanical coupling and static bending of piezoelectric nanowires using a conventional Euler-Bernoulli beam model. Following the similar surface-layer-based model in studying the surface effects on the mechanical properties of elastic materials, explicit expressions of electromechanical coupling (EMC) coefficient and effective bending rigidity accounting for surface effects are derived. It is indicated that the EMC coefficient is size-dependent and can be enhanced significantly with the scaling down of nanowire size. In addition, the surface effects on the stiffness and the electroelastic fields of the bending piezoelectric beam are also revealed.

2.2 Formulation of the problem

We adopt the foundation for the continuum modeling of elastic nanostructures considering the surface effects with using a surface-layer-based model, *i.e.* a nanostructure=bulk+surface. As proposed by Huang and Yu (2006), the constitutive equations for the surface are expressed as:

$$\sigma_{\alpha\beta}^{s} = \sigma_{\alpha\beta}^{0} + c_{\alpha\beta\gamma\delta}^{s}\varepsilon_{\gamma\delta} - e_{\alpha\beta k}^{s}E_{k}, \tag{2.1}$$

$$D_{i}^{s} = D_{i}^{0} + e_{\alpha\beta i}^{s}\varepsilon_{\alpha\beta} + \kappa_{ij}^{s}E_{j}, \tag{2.2}$$

with $c_{\alpha\beta\gamma\delta}^{s}$, $e_{\alpha\beta k}^{s}$ and κ_{ij}^{s} being the surface elastic, surface piezoelectric and surface

dielectric tensors. $\sigma_{\alpha\beta}^0$ and D_i^0 can be termed as residual surface stress and surface electric displacement without applied strain and electric field.

The constitutive relations in the bulk are the same as traditional piezoelectric materials, which are written in the form,

$$\sigma_{ij} = c_{ijkl}\varepsilon_{kl} - e_{ijk}E_k, \tag{2.3}$$

$$D_i = e_{kli}\varepsilon_{kl} + \kappa_{ij}E_j, \tag{2.4}$$

with c_{ijkl}, e_{ijk} and κ_{ij} being the bulk elastic, bulk piezoelectric and bulk dielectric tensors.
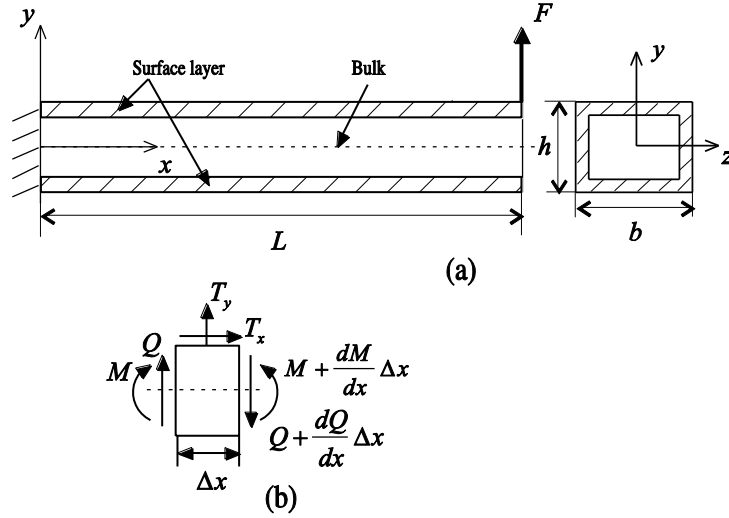
Figure 2.1: (a) Schematic of a piezoelectric cantilever beam with surface effects and (b) free-body diagram of an incremental beam element.

2.2.1   Static bending of a piezoelectric nanobeam

The problem envisaged is a cantilever piezoelectric beam subjected to a concentrated load F at the free end as shown in Fig. 2.1(a). A Cartesian coordinate system is used to describe the problem, where z-axis is the neutral axis of the beam, and y is the poling direction of the piezoelectric materials. L, h and b represent the length, thickness and width of the beam, respectively. Assuming beam thickness is much less than the radius of curvature induced by the mechanical load, then the axial strain ε_{xx} at any point in the beam can be defined as

$$\varepsilon_{xx} = -\frac{y}{R(x)}, \tag{2.5}$$

where $R(x)$ is the radius of curvature.

The electric field is assumed to exist only in y direction, therefore, the constitutive relation of the one-dimensional piezoelectric beam in the bulk can be written as

$$\sigma_{xx} = c_{11}\varepsilon_{xx} - e_{31}E_y, \tag{2.6}$$

$$D_y = e_{31}\varepsilon_{xx} + \kappa_{33}E_y. \tag{2.7}$$

Similarly, the constitutive equations for the surface layer of the beam are

$$\sigma_{xx}^s = \sigma_{xx}^0 + c_{11}^s\varepsilon_{xx} - e_{31}^sE_y, \tag{2.8}$$

$$D_x^s = D_x^0. \tag{2.9}$$

According to the generalized Young-Laplace equation derived by Chen *et al.* (2006b), the surface effects are represented by the traction jumps on the beam surfaces, *i.e.*

$$T_x = \frac{\partial \sigma_{xx}^s}{\partial x}; \ T_y = \frac{\sigma_{xx}^s}{R_c}, \tag{2.10}$$

where R_c is the radius of curvature defined positively when the unit normal of surface is pointed towards the center of curvature. Therefore, $R_c = R(x)$ for the upper surface layer and $R_c = -R(x)$ for the lower surface layer. Under the open circuit condition where the electric displacement $D_y = 0$ on the beam surfaces, we have

$$T_y^u = \frac{\left[\sigma_{xx}^0 + \left(c_{11}^s + \frac{e_{31}^s e_{31}}{\kappa_{33}}\right)\left(-\frac{h}{2R(x)}\right)\right]}{R(x)}, \tag{2.11}$$

$$T_y^l = -\frac{\left[\sigma_{xx}^0 + \left(c_{11}^s + \frac{e_{31}^s e_{31}}{\kappa_{33}}\right)\left(\frac{h}{2R(x)}\right)\right]}{R(x)}, \tag{2.12}$$

as the traction jumps along y direction for the upper and lower surfaces of the rectangle

beam, while T_y=0 for the side surfaces. It should also be mentioned that the electric displacement jump across surfaces is zero.

To derive the governing equation for the piezoelectric beam considering surface effects, we follow the same procedure in Liu and Rajapakse's work (2010) for an elastic nanobeam. We take an incremental beam element of length Δx and draw the free body diagram as shown in Fig. 2.1(b), in which T_x and T_y are tractions induced by the existence of the surfaces, M and Q are bending moment and shear force, respectively. It should be mentioned that we only draw T_x and T_y on the upper surface of the element; however, they exist on the circumferential surfaces of the beam. The equilibrium equations of the element can be expressed as,

$$\frac{\mathrm{d}M}{\mathrm{d}x} - \int_s T_x y \mathrm{d}s - Q = 0 \;, \tag{2.13}$$

$$\int_s T_y \mathrm{d}s - \frac{\mathrm{d}Q}{\mathrm{d}x} = 0 \;, \tag{2.14}$$

where s is the perimeter of the beam cross section. Differentiating Eq. (2.13) with respect to x and using Eq. (2.14) result in

$$\frac{\mathrm{d}^2 M}{\mathrm{d}x^2} - \frac{\mathrm{d}}{\mathrm{d}x} \int_s T_x y \mathrm{d}s - \int_s T_y \mathrm{d}s = 0 \;, \tag{2.15}$$

where $M = -\int_A \sigma_{xx} y \mathrm{d}A$, with A and σ_{xx} being the beam cross-sectional area and the axial stress.

Assuming the deflection of the beam in the y direction is $v(x)$, for a beam with small deformation, the curvature is approximated by the second derivative of the beam deflection, *i.e.* $1/R(x) \approx \mathrm{d}^2 v(x)/\mathrm{d}x^2$. Substituting Eq. (2.10) into Eq. (2.15) and using Eqs. (2.5), (2.8), (2.11) and (2.12), the governing equation for a piezoelectric beam including the surface effects is derived as

$$(EI)_{\mathrm{eff}} \frac{\mathrm{d}^4 v}{\mathrm{d}x^4} = 2b\sigma_{xx}^0 \frac{\mathrm{d}^2 v}{\mathrm{d}x^2} \;, \tag{2.16}$$

where $(EI)_{\text{eff}}$ is the effective bending rigidity of the piezoelectric beam, which can be expressed as

$$(EI)_{\text{eff}} = \frac{1}{12}\left(c_{11} + \frac{e_{31}^2}{\kappa_{33}}\right)bh^3 + \left(c_{11}^s + \frac{e_{31}^s e_{31}}{\kappa_{33}}\right)\left(\frac{1}{6}h^3 + \frac{1}{2}bh^2\right). \tag{2.17}$$

It is noted that $q(x) = 2b\sigma_{xx}^0\left(\mathrm{d}^2v/\mathrm{d}x^2\right)$ at the right hand side of Eq. (2.16) is induced by the residual surface stress and can be regarded as a distributed load acting normal to the beam axis. When the surface piezoelectricity and the electromechanical coupling are not considered, Eq. (2.17) recovers to the effective bending rigidity of an elastic nanobeam with surface effects (He and Lilley, 2008).

For the cantilever beam considered here, the corresponding boundary conditions are

$$v(0) = 0; \quad \left.\frac{\mathrm{d}v(x)}{\mathrm{d}x}\right|_{x=0} = 0, \tag{2.18}$$

$$M(L) = 0; \quad Q(L) = -F. \tag{2.19}$$

Based on boundary conditions (2.18) and (2.19), Eq. (2.16) can be solved. Then the deflection of the piezoelectric beam can be obtained as

$$v(x) = \frac{FL}{4\sigma_{xx}^0 b\sqrt{\eta}}(-e^{\frac{\sqrt{\eta}}{L}x - \sqrt{\eta}} + e^{-\frac{\sqrt{\eta}}{L}x + \sqrt{\eta}} + e^{-\sqrt{\eta}} - e^{\sqrt{\eta}}) + \frac{Fx}{4\sigma_{xx}^0 b}(e^{-\sqrt{\eta}} + e^{\sqrt{\eta}}), \tag{2.20}$$

with $\eta = 2\sigma_{xx}^0 bL^2/(EI)_{\text{eff}}$. Corresponding, the other electroelastic fields in the beam can also be determined.

2.2.2 Derivation of EMC coefficient

The EMC coefficient is a measurement of the effectiveness of the electromechanical coupling and has been used as an important parameter for piezoelectric energy harvesting (Beeby et al., 2006; Anton and Sodano, 2007; Majdoub et al., 2008). It can be defined as the square root of the ratio of electrical energy stored in the volume of a piezoelectric body to the total mechanical energy supplied to the body (or vice versa) and can be obtained by measuring variations of the energy stored in the electromechanical structure

with changing electric boundary conditions (Trindade and Benjeddou, 2009). The total internal energy can be expressed as

$$U = \frac{1}{2}\int_V \sigma_{xx}\varepsilon_{xx}\,\mathrm{d}V + \frac{1}{2}\int_\Gamma \sigma_{xx}^s\varepsilon_{xx}\,\mathrm{d}\Gamma,$$ (2.21)

V and Γ represent the volume and the surface area of the beam, respectively.

(i) *Open circuit condition*. In this case, electric displacement is $D_y=0$. From the constitutive Eqs. (2.6) and (2.8) for both bulk and surface, the total internal energy stored U_{oc} in the piezoelectric body can be expressed as

$$U_{oc} = \frac{1}{2}(c_{11} + \frac{e_{31}^2}{\kappa_{33}})\int_A y^2\,\mathrm{d}A\int_0^L\left(\frac{\mathrm{d}^2 v(x)}{\mathrm{d}x^2}\right)^2\mathrm{d}x + \frac{1}{2}(c_{11}^s + \frac{e_{31}^s e_{31}}{\kappa_{33}})\int_s y^2\,\mathrm{d}s\int_0^L\left(\frac{\mathrm{d}^2 v(x)}{\mathrm{d}x^2}\right)^2\mathrm{d}x,$$ (2.22)

which can then be reduced to

$$U_{oc} = \frac{1}{2}\left[\frac{1}{12}\left(c_{11} + \frac{e_{31}^2}{\kappa_{33}}\right)bh^3 + \left(c_{11}^s + \frac{e_{31}^s e_{31}}{\kappa_{33}}\right)\left(\frac{1}{2}bh^2 + \frac{1}{6}h^3\right)\right]\int_0^L\left(\frac{\mathrm{d}^2 v(x)}{\mathrm{d}x^2}\right)^2\mathrm{d}x.$$ (2.23)

(ii) *Short circuit condition*. In this case, electric field $E_y=0$. Following the same procedure for open circuit condition, the total internal energy of the piezoelectric body can be calculated as

$$U_{sc} = \frac{1}{2}\left[\frac{1}{12}c_{11}bh^3 + c_{11}^s\left(\frac{1}{2}bh^2 + \frac{1}{6}h^3\right)\right]\int_0^L\left(\frac{\mathrm{d}^2 v(x)}{\mathrm{d}x^2}\right)^2\mathrm{d}x.$$ (2.24)

Under the same nonuniform strain ε_{xx} condition (Trindade and Benjeddou, 2009), the square of EMC coefficient can then be determined as

$$\xi_{\mathrm{eff}}^2 = \frac{U_{oc} - U_{sc}}{U_{oc}} = \frac{e_{31}^2 bh + e_{31}^s e_{31}(2h + 6b)}{(c_{11}\kappa_{33} + e_{31}^2)bh + (c_{11}^s\kappa_{33} + e_{31}^s e_{31})(2h + 6b)}.$$ (2.25)

It is evident that the EMC coefficient is size-dependent when considering the surface effects. If the surface effects are ignored, the above equation is reduced to the EMC coefficient of bulk piezoelectric materials as $\xi_0^2 = e_{31}^2/\left(e_{31}^2 + c_{11}\kappa_{33}\right)$.

2.3   Results and discussion

For case study, PZT-5H is chosen as the piezoelectric material and the bulk material properties are $c_{11} = 126\,\text{GPa}$, $e_{31} = -6.5\,\text{C m}^{-2}$, $\kappa_{33} = 1.3 \times 10^{-8}\,\text{C V}^{-1}\,\text{m}^{-1}$. The surface properties can be obtained by atomistic calculations. For example, Miller and Shenoy (2000) calculated the free surface properties of aluminum based on the embedded-atom method for some crystallographic direction. Usually, the surface elasticity could be on the order of $1-10\,\text{N m}^{-1}$ (Miller and Shenoy, 2000; Lachut and Sader, 2007; He and Lilley, 2008; Ru, 2009). However, due to the lack of such work on piezoelectric materials, it is difficult to choose the appropriate surface piezoelectric and dielectric constants. Following Huang and Yu's work (2006), we choose $c_{11}^{s} = 7.56\,\text{N m}^{-1}$ and $e_{31}^{s} = -3 \times 10^{-8}\,\text{C m}^{-1}$ as a reasonable approximation for these surface material properties based on some previous work.

To investigate how the surface effects influence the electromechanical coupling of piezoelectric materials, the variation of EMC coefficient ξ_{eff} normalized by the classical EMC coefficient ξ_0 for the bulk material with the beam thickness h is plotted in Fig. 2.2. The width of the beam is assumed as $b=0.5h$. It is observed in this figure that the EMC coefficient is size-dependent and surface effects become more prominent with a decrease in beam thickness. A high apparent piezoelectric response is seen at smaller sizes, for example, at $h=12$ nm, the EMC coefficient is almost doubled compared with the EMC coefficient of the bulk materials. Since this EMC coefficient is an important measurement of the effectiveness of the electromechanical coupling, which governs the electricity generation of piezoelectric generators in energy harvesting, the giant increase in EMC coefficient at the nanoscale due to the surface effects is expected to be helpful for the performance improvement of piezoelectric nanogenerators.

With the consideration of surface effects, the bending rigidity of the piezoelectric beam is changed accordingly as shown in Eq. (2.17). Therefore, it will be interesting to investigate the surface effects on the compliance or the stiffness of the piezoelectric bending beam. As an example, the material constants are the same as those in Fig. 2.2 and the geometric parameters of the beam are taken as $h=20$ nm, $b=0.5h$ and $L=500$ nm.
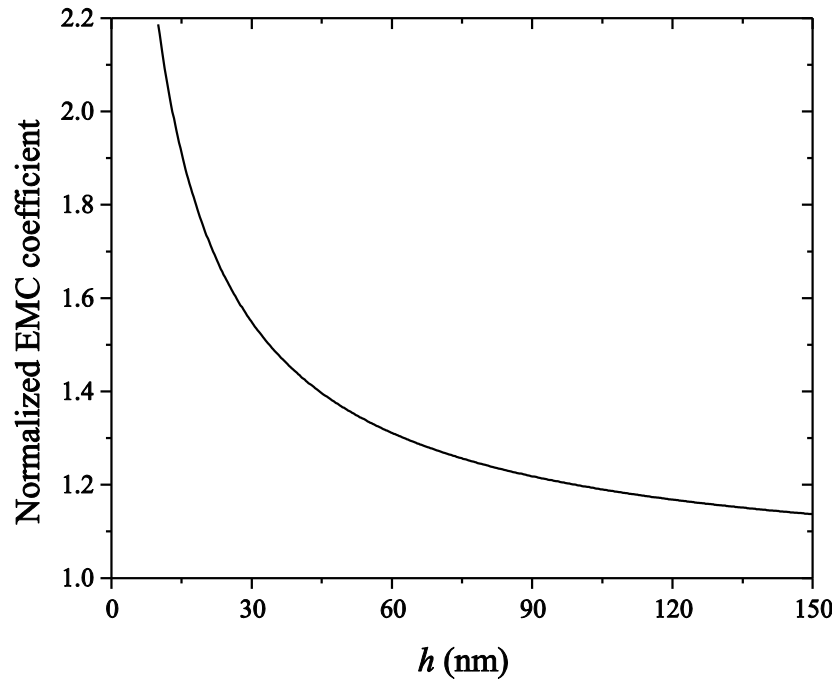
Figure 2.2: The variation of the normalized EMC coefficient with the beam thickness h.
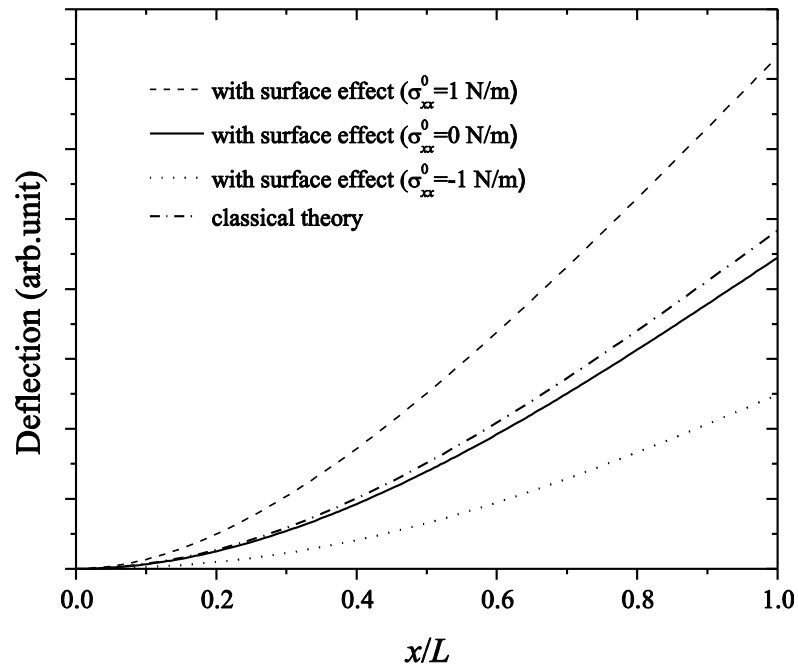
Figure 2.3: Deflection of the piezoelectric cantilever beam along the longitudinal axis.

The deflections along the beam longitudinal axis are plotted in Fig. 2.3 and compared to see the surface effects. From this figure, we found a similar phenomenon which was observed for an elastic nanobeam (He and Lilley, 2008), *i.e.* a positive residual surface
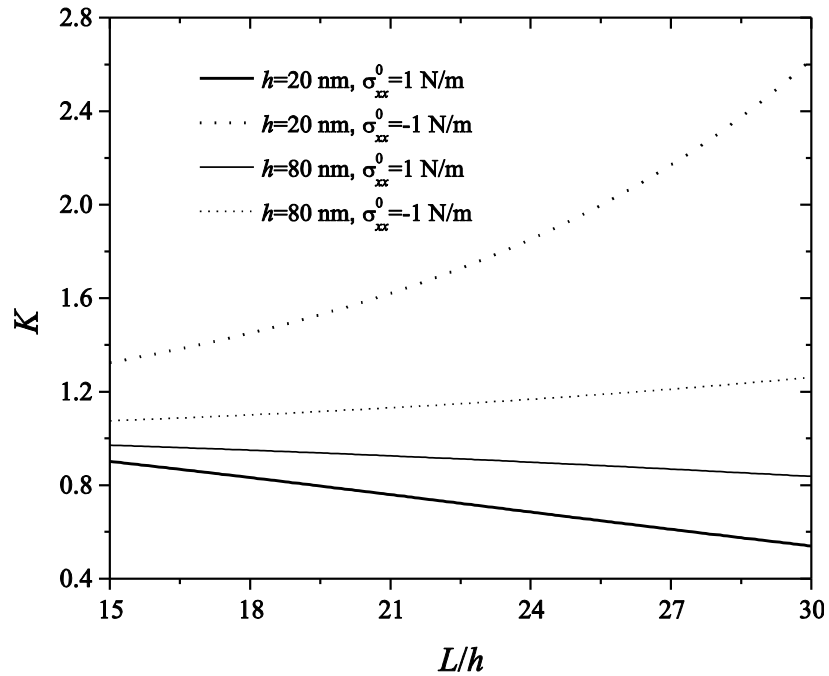
Figure 2.4: The variation of the normalized stiffness K with L/h.
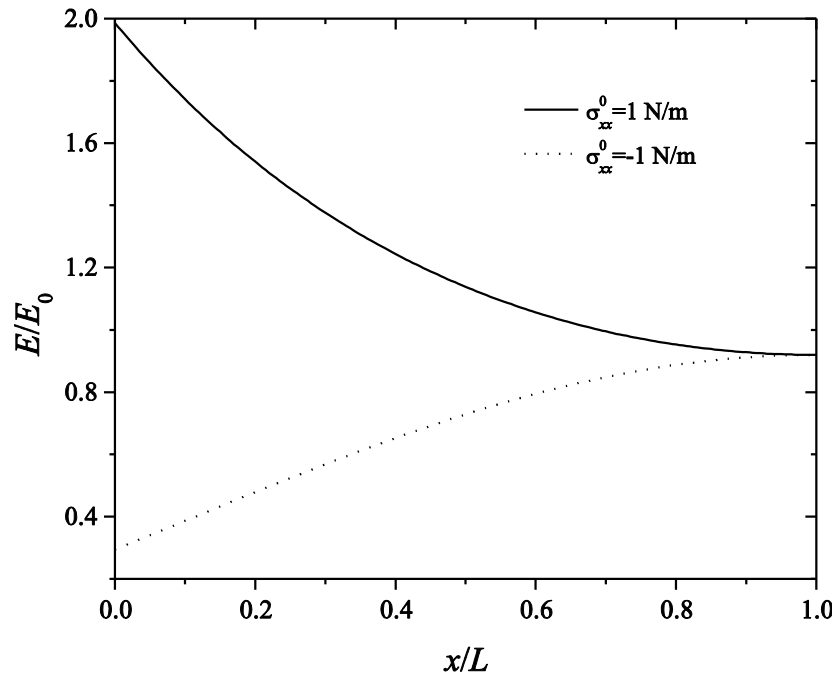
Figure 2.5: The normalized electric field distribution along the longitudinal axis.

stress $\sigma_{xx}^0 > 0$ softens the cantilever beam while a negative residual stress $\sigma_{xx}^0 < 0$ stiffens the cantilever beam compared with the bulk beam without surface effects. It is also

observed in this figure that without considering the surface residual stress $\sigma_{xx}^0 = 0$, the combined effect of surface elasticity and surface piezoelectricity is to stiffen the beam as evidenced by the bending curve for the beam with surface effects ($\sigma_{xx}^0 = 0$) being below that for the classical beam. Here we also study the nanobeam contact stiffness k defined by Jing *et al.* (2006), *i.e.* the ratio of the applied force F to the induced deflection v at the same point sustaining the applied force. For nanobeams with thickness h=20 nm and h=80 nm and varying length-to-thickness ration L/h, Fig. 2.4 plots the variation of normalized stiffness $K=k/k_0$ with $k_0=F/v_0$ representing the stiffness of a conventional beam without surface effects. It is found that stiffness has a significant dependence on the beam thickness: smaller beams appear softer or stiffer due to the surface effects. It is also observed from this figure that surface effects are more significant for the slender beams with larger length-to-thickness ratio (L/h). It is concluded from these two figures that surface effects have a significant influence on the static bending behavior of piezoelectric nanobeam.
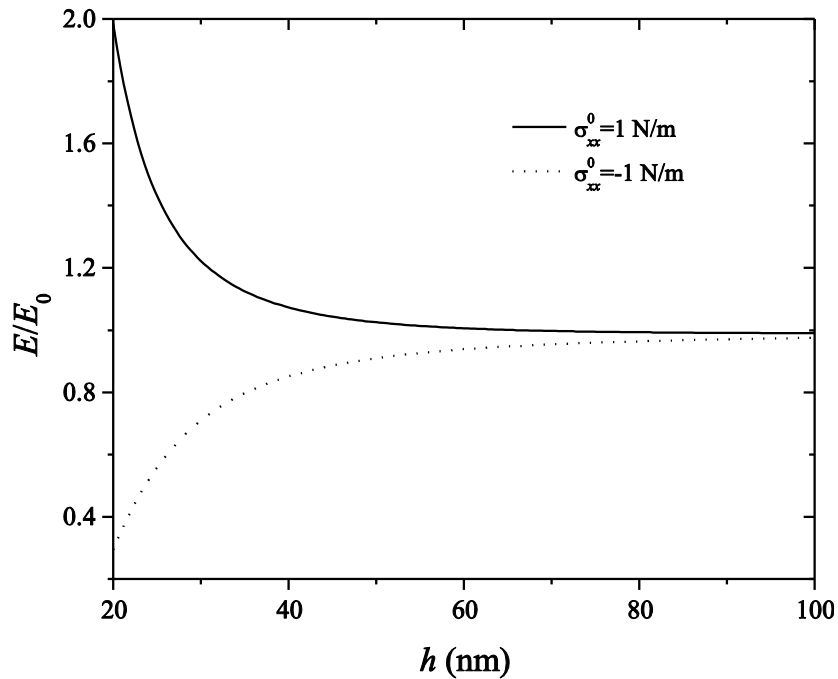
Figure 2.6: The variation of the normalized electric field distribution with h.

To show the influence of surface effects upon the electric field, Fig. 2.5 displays the variation of electric field along the beam longitudinal axis, where the electric field E is

normalized by E_0 for the classical beam without surface effects. It is found in this figure that surface effects on the electric field are prominent at the fixed end, and the residual surface stress has no effect at the free end. This phenomenon is attributed to the zero curvature at the free end of the beam; therefore, the residual surface stress has no effect on the electroelastic fields of the beam as shown in Eq. (2.16). The variation of this normalized electric field with the beam thickness is plotted in Fig. 2.6. It is found in this figure that when the beam thickness h is small, the electric field deviates more from their conventional bulk counterpart, and approaches it with the increase in beam thickness.

2.4   Conclusions

Based on the Euler-Bernoulli beam theory and the generalized Young-Laplace equation, we have investigated the combined surface effects of residual surface stress, surface elasticity and surface piezoelectricity on electromechanical coupling and bending behaviors of a cantilever piezoelectric nanobeam. Explicit solutions for elastic bending are obtained to assess surface effects on the stiffness of nanobeams. It is found that surface effects play a significant role in the electroelastic fields of piezoelectric nanobeams. It is observed that the influence of surface effects upon the beam stiffness is more prominent for slender beams. The significant enhancement of electromechanical coupling coefficient due to surface effects has also been observed with the decrease in the nanobeam thickness, which implies that surface effects may be employed for performance improvement of nanostructured piezoelectric materials in the potential applications as nanogenerators. The obtained results are envisaged to benefit understanding of the size-dependent electromechanical properties of nanostructured piezoelectric materials and are very helpful for the design of piezoelectric beam-based nanogenerators.

References

Agrawal, R., Peng, B. and Espinosa, H. D., 2009. Experimental-computational investigation of ZnO nanowires strength and fracture. Nano Lett. **9**, 4177-4183.

Agrawal, R., Peng, B., Gdoutos, E. E. and Espinosa, H. D., 2008. Elasticity size effects in ZnO nanowires-a combined experimental-computational approach. Nano Lett. **8**, 3668-3674.

Anton, S. R. and Sodano, H. A., 2007. A review of power harvesting using piezoelectric materials (2003–2006). Smart Mater. Struct. **16**, R1.

Beeby, S. P., Tudor, M. J. and White, N. M., 2006. Energy harvesting vibration sources for microsystems applications. Meas. Sci. Technol. **17**, R175.

Cammarata, R. C., 1994. Surface and interface stress effects in thin films. Prog. Surf. Sci. **46**, 1-38.

Chen, C. Q., Shi, Y., Zhang, Y. S., Zhu, J. and Yan, Y. J., 2006a. Size dependence of Young's modulus in ZnO nanowires. Phys. Rev. Lett. **96**, 075505.

Chen, T., 2008. Exact size-dependent connections between effective moduli of fibrous piezoelectric nanocomposites with interface effects. Acta Mech. **196**, 205-217.

Chen, T., Dvorak, G. J. and Yu, C. C., 2007. Size-dependent elastic properties of unidirectional nano-composites with interface stresses. Acta Mech. **188**, 39-54.

Chen, T. Y., Chiu, M. S. and Weng, C. N., 2006b. Derivation of the generalized Young-Laplace equation of curved interfaces in nanoscaled solids. J. Appl. Phys. **100**, 074308.

Desai, A. V. and Haque, M. A., 2007. Mechanical properties of ZnO nanowires. Sensor. Actuat. A-Phys. **134**, 169-176.

Gurtin, M. E. and Murdoch, A. I, 1975. A continuum theory of elastic material surfaces. Arch. Ration. Mech. Anal. **57**, 291-323.

He, J. and Lilley, C. M., 2008. Surface effect on the elastic behavior of static bending nanowires. Nano Lett. **8**, 1798-1802.

Huang, G. Y. and Yu, S. W., 2006. Effect of surface piezoelectricity on the electromechanical behaviour of a piezoelectric ring. Phys. Status Solidi-Rapid Res. Lett. **243**, R22-R24.

Hu, J. and Pan, B. C., 2009. Surface effect on the size- and orientation-dependent elastic properties of single-crystal ZnO nanostructures. J. Appl. Phys. **105**, 034302.

Jiang, L. Y. and Yan, Z., 2010. Timoshenko beam model for static bending of nanowires with surface effects. Physica E **42**, 2274-2279.

Jing, G. Y., Duan, H. L., Sun, X. M., Zhang, Z. S., Xu, J., Li, Y. D., Wang, J. X. and Yu, D. P., 2006. Surface effects on elastic properties of silver nanowires: Contact atomic-force microscopy. Phys. Rev. B **73**, 235409.

Kulkarni, A. J., Zhou, M. and Ke, F. J., 2005. Orientation and size dependence of the elastic properties of zinc oxide nanobelts. Nanotechnology **16**, 2749.

Lachut, M. J. and Sader, J. E., 2007. Effect of surface stress on the stiffness of cantilever plates. Phys. Rev. Lett. **99**, 206102.

Lin, Y. F., Song, J. H., Ding, Y., Lu, S. Y. and Wang, Z. L., 2008. Piezoelectric nanogenerator using CdS nanowires. Appl. Phys. Lett. **92**, 022105.

Liu, C. and Rajapakse, R. K. N. D., 2010. Continuum models incorporating surface energy for static and dynamic response of nanoscale beams. IEEE Trans. Nanotechnol. **9**, 422-431.

Majdoub, M. S., Sharma, P. and Cagin, T., 2008a. Dramatic enhancement in energy harvesting for a narrow range of dimensions in piezoelectric nanostructures. Phys. Rev. B **78**, 121407(R).

Majdoub, M. S., Sharma, P. and Cagin, T., 2008b. Enhanced size-dependent piezoelectricity and elasticity in nanostructures due to the flexoelectric effect. Phys. Rev. B **77**, 125424.

Makeev, M. A., Srivastava, D. and Menon, M., 2006. Silicon carbide nanowires under external loads: An atomistic simulation study. Phys. Rev. B **74**, 165303.

Michalski, P. J., Sai, N. and Mele, E. J., 2005. Continuum theory for nanotube piezoelectricity. Phys. Rev. Lett. **95**, 116803.

Miller, R. E. and Shenoy, V. B., 2000. Size-dependent elastic properties of nanosized structural elements. Nanotechnology **11**, 139.

Ramprasad, R. and Shi, N., 2005. Dielectric properties of nanoscale HfO_2 slabs. Phys. Rev. B **72**, 052107.

Ru, C. Q., 2009. Thermoelastic dissipation of nanowire resonators with surface stress. Physica E **41**, 1243-1248.

Rudd, R. E. and Lee, B., 2008. Mechanics of silicon nanowires: size-dependent elasticity from first principles. Mol. Simul. **34**, 1-8.

Song, J. H., Zhou, J. and Wang, Z. L., 2006. Piezoelectric and semiconducting coupled power generating process of a single ZnO belt/wire. A technology for harvesting electricity from the environment. Nano Lett. **6**, 1656-1662.

Tagantsev, A. K., 1986. Piezoelectricity and flexoelectricity in crystalline dielectrics. Phys. Rev. B **34**, 5883-5889.

Trindade, M. A. and Benjeddou, A., 2009. Effective electromechanical coupling coefficients of piezoelectric adaptive structures: critical evaluation and optimization. Mech. Adv. Mater. Struct. **16**, 210-223.

Wang, G. F. and Feng, X. Q., 2007. Effects of surface elasticity and residual surface tension on the natural frequency of microbeams. Appl. Phys. Lett. **90**, 231904.

Wang, G. F. and Feng, X. Q., 2009. Surface effects on buckling of nanowires under uniaxial compression. Appl. Phys. Lett. **94**, 141913.

Wang, X. D., Song, J. H., Liu, J. and Wang, Z. L., 2007. Direct-current nanogenerator driven by ultrasonic waves. Science **316**, 102-105.

Wang, Z. L. and Song, J. H., 2006. Piezoelectric nanogenerators based on zinc oxide nanowire arrays. Science **312**, 242-246.

Yakobson, B. I. and Smalley, R., 1997. Fullerene Nanotubes: $C_{1,000,000}$ and Beyond. Am. Sci. **85**, 324-337.

Zhang, T. Y., Luo, M. and Chan, W. K., 2008. Size-dependent surface stress, surface stiffness and Young's modulus of hexagonal prism [111] β-SiC nanowires. J. Appl. Phys. **103**, 104308.

Zhao, M. H., Wang, Z. L. and Mao, S. X., 2004. Piezoelectric characterization of individual zinc oxide nanobelt probed by piezoresponse force microscope. Nano Lett. **4**, 587-590.

Zhou, J., Fei, P., Gao, Y. F., Gu, Y. D., Liu, J., Bao, G. and Wang, Z. L., 2008. Mechanical-electrical triggers and sensors using piezoelectric micowires/nanowires. Nano Lett. **8**, 2725-2730.

Chapter 3

3 The vibrational and buckling behaviors of piezoelectric nanobeams with surface effects[2]

3.1 Introduction

Recently, one-dimensional piezoelectric nanostructures, such as nanowires (NWs) or nanobelts, have been attracting a great deal of interest from research communities due to their potential applications as nanoresonators (Bai *et al*., 2003; Tanner *et al*., 2007), field effect transistors (Wang *et al*., 2006; Fei *et al*., 2009), diodes (He *et al*., 2007), chemical sensors (Wang *et al*., 2004) and nanogenerators (Wang and Song, 2006; Su *et al*., 2007). Determination of the mechanical and physical properties of piezoelectric nanostructures is a critical issue in the design process of these nanodevices. For example, in their applications as nanoresonators (Bai *et al*., 2003; Chen *et al*., 2006; Huang *et al*., 2006), the vibrational behavior of piezoelectric nanostructures needs to be accurately predicted.

Although many efforts have been devoted to the study of the properties of macroscopic piezoelectric materials, there are much fewer studies investigating the properties of nanoscale piezoelectric materials with electromechanical coupling. Gao and Wang (2007) applied the perturbation theory to quantitatively predict the piezoelectric potential distribution in a nanowire by applying a lateral force at its tip. By means of the first piezoelectric effect approximation, the piezoelectric potential generated in a bent ZnO nanorod was derived using the continuum modeling approach (Shao *et al.*, 2010). Sun *et al*. (2010) numerically estimated the potential, the output power and the energy conversion efficiency of three different piezoelectric nanostructures by applying both static and dynamic loads. In these studies, all the material property coefficients of nanoscale piezoelectric materials were considered constants and the same as their bulk counterparts. However, existing work indicated that the material properties of

---

[2]A version of this chapter has been published. It should be noted that the influence of the axial boundary constraint of the piezoelectric nanobeams is ignored in this study. To consider the axial boundary constraint, a supplementary work is provided in Appendix A.

Yan, Z. and Jiang, L.Y., Nanotechnology 22, 245703, (2011).

piezoelectric nanostructures were size-dependent. The Young's modulus of piezoelectric NWs was observed to increase with the decrease of the nanowire diameter at the nanoscale (Chen *et al*., 2006; Stan *et al*., 2007; Agrawal *et al*., 2008). In Zhao *et al*.'s work (2004), the effective piezoelectric coefficient of the ZnO nanowire was found to be frequency-dependent and was much larger than that of the bulk material. By conducting a molecular dynamics study, size effects were also found to influence the piezoelectric coefficient of the $BaTiO_3$ nanowire (Zhang *et al*., 2010). From the first-principles calculations, it was also demonstrated that piezoelectric nanomaterials have larger piezoelectric constants than their bulk counterparts (Xiang *et al*., 2006; Li *et al*., 2007). These studies provide direct evidence of the size dependence of material properties for nanoscale piezoelectric materials. Such size-dependent properties of piezoelectric nanomaterials are believed to be attributed to both the strain-gradient-induced flexoelectricity (Majdoub *et al*., 2008a; b) and surface effects (Tagantsev, 1986). In addition to the surface elasticity and residual surface stress as in elastic materials, the surface effects of piezoelectric materials also include surface piezoelectricity.

The surface effects on the size-dependent elastic properties of nanomaterials have been well investigated. Among these existing studies, continuum mechanics approaches based on the linear surface elasticity theory proposed by Gurtin and Murdoch (1975) have been widely adopted to model the influence of surface effects on the properties of nanostructures. Under a reasonable assumption, a surface can be regarded as a thin layer with negligible thickness *t* adhered to the bulk without slipping (Cammarata, 1994; Miller and Shenoy, 2000). The constitutive and equilibrium equations for the surface layer are different from those in the bulk of the solid. Following this surface elasticity model, He and Lilley (He and Lilley, 2008a; b) investigated the influence of surface effects on the elastic behavior of static bending and the resonant frequencies of NWs with different boundary conditions. The vibrational and buckling behaviors of elastic NWs were also predicted by considering surface effects in Wang and Feng's work (2007; 2009a; b). However, the work on continuum modeling of piezoelectric nanostructures considering surface effects is very limited. Wang and Feng (2010) investigated the effect of surface stress on the vibration and buckling of piezoelectric nanowires using the surface elasticity model by ignoring the surface piezoelectricity effect. It should be mentioned that the

physical origin of the surface effects is that atoms at the free surface are exposed to a different environment compared to the atoms in the bulk of a material (Cammarata, 1994). Consequently, the surface atom will be in a higher energy state than the atom in the bulk due to the missing of its neighboring atoms, *i.e.* the source of surface energy. Since nanostructures have high specific surface area, the surface energy becomes a significant part of the total elastic energy. In the surface elasticity model, the surface energy density depends on the in-plane strain at the surface. For piezoelectric nanostructures, it is natural to believe that the surface energy density may also depend on the electric field at the surface, which inspired the extension of the surface elasticity model to the surface piezoelectricity model proposed by Huang and Yu (2006). Similar to the surface elasticity model, constitutive relations for the surface and the bulk of the piezoelectric nanomaterial are different. In their work, the mechanical and electrical responses of a piezoelectric ring were studied using this developed surface piezoelectricity model. The results indicated that the electroelastic fields of a piezoelectric nanostructure were significantly influenced by the surface effects, which were more prominent at a few nanometers. The surface effects on the electromechanical coupling and static bending of piezoelectric NWs were studied in our recent work (Yan and Jiang, 2010). It was found that the electromechanical coupling coefficient could be dramatically increased due to the surface effects.

Since most nanodevices with piezoelectric nanowires or nanobelts as fundamental elements are beam-based, it is necessary to investigate the vibrational and buckling behaviors of piezoelectric nanobeams. However, it appears that the influence of the surface effects on such behaviors of piezoelectric nanobeams has not been investigated thus far. Hence, the objective of the current work is to study the combined surface effects and electromechanical coupling on the vibration and buckling of piezoelectric nanobeams using the conventional Euler-Bernoulli beam model. By using the surface piezoelectricity model (Huang and Yu, 2006), the surface effects on the resonant frequencies and the critical electrical buckling load will be revealed. This work is expected to predict the mechanical and electrical responses of piezoelectric nanostructures more accurately and provide a guideline for the design and applications of the piezoelectric-nanobeam-based devices.

3.2 Problem formulation and solution

The case study in the current work will be conducted on a piezoelectric nanobeam with a rectangular cross section. Fig. 3.1(a) shows an example of a piezoelectric cantilever nanobeam with L, b and h denoting its length, width and thickness, respectively. The bending displacement along the z-direction is w. Based on the Euler-Bernoulli beam theory; the axial strain ε_x at any point in the beam can be defined as

$$\varepsilon_x = \varepsilon_0 - z\frac{\partial^2 w(x,t)}{\partial x^2},$$ (3.1)

with ε_0 being the applied axial strain. The electric field is assumed to exist only in the z direction, and can be determined by the electric potential Φ as

$$E_z = -\frac{\partial \Phi}{\partial z}.$$ (3.2)
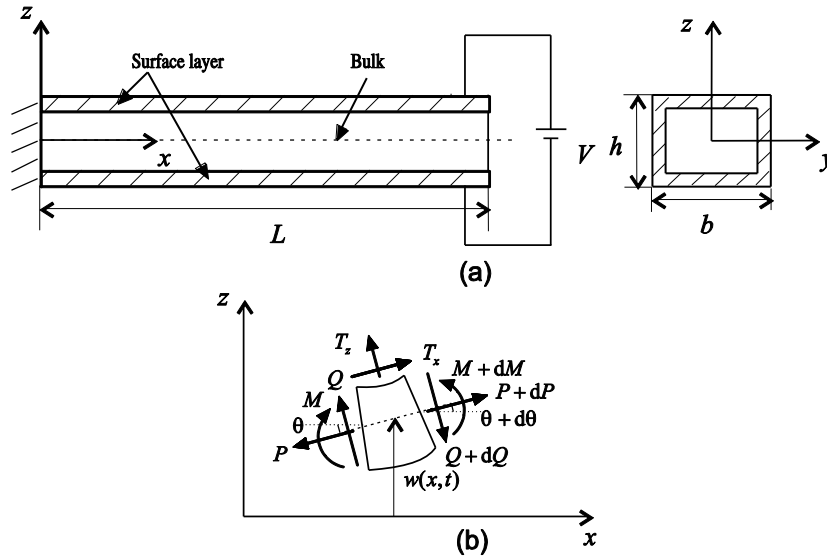
Figure 3.1: (a) Schematic of a piezoelectric nanobeam with surface effects and (b) free-body diagram of an incremental beam element.

For the surface piezoelectricity model, the constitutive equations of the surface are different from those of the bulk. If the poling direction for the piezoelectric medium is assumed to be along the z-direction, the constitutive equations for the surface of the one-dimensional beam can be obtained based on Huang and Yu's work (2006)

$$\sigma_x^s = \sigma_x^0 + c_{11}^s \varepsilon_x - e_{31}^s E_z, \tag{3.3}$$

$$D_x^s = D_x^0, \tag{3.4}$$

where σ_x^s and D_x^s are axial surface stress and surface electric displacement; σ_x^0 and D_x^0 are residual surface stress and residual surface electric displacement without applied strain and electric field; and c_{11}^s and e_{31}^s are surface elastic and surface piezoelectric constants. The constitutive relations in the bulk are the same as conventional piezoelectric materials, *i.e.*

$$\sigma_x = c_{11}\varepsilon_x - e_{31}E_z, \tag{3.5}$$

$$D_z = e_{31}\varepsilon_x + \kappa_{33}E_z, \tag{3.6}$$

where σ_x is axial stress, D_z is electric displacement, and c_{11}, e_{31} and κ_{33} are elastic, piezoelectric and dielectric constants for the bulk medium, respectively.

According to the surface elasticity model, distributed traction results from the surface stress and acts on the nanobeam in bending. The traction jumps can be described by the generalized Young-Laplace equations derived by Chen *et al.* (2006), *i.e.*

$$T_x = \frac{\partial \sigma_x^s}{\partial x}; \qquad T_z = \frac{\sigma_x^s}{R_c}, \tag{3.7}$$

where R_c is the radius of curvature, defined as positive when the unit normal of the surface is pointed towards the center of curvature. It is noted that T_z only exists on the top and bottom surfaces of the beam, but not on the left and right surfaces. In addition, it should be mentioned that the electric displacement jump across surfaces is zero.

To derive the governing equation for the piezoelectric nanobeam with surface effects, we follow the same procedure for an elastic nanobeam (Liu and Rajapakse, 2010). The forces acting on a beam element of length dx are shown in Fig. 3.1(b), where $\theta = \partial w(x,t)/\partial x$ is the rotation angle of the beam cross section; P is the axial normal force including the induced forces by the applied axial strain ε_0 and the applied electrical load; Q is the shear force and M is the bending moment. T_x and T_z are induced by the

surface effects and exist on the circumferential surfaces of the bulk beam. The governing equations for the beam element according to bending can be written as

$$-\frac{\partial Q}{\partial x}+\int_S T_z \mathrm{d}S = \rho A \frac{\partial^2 w(x,t)}{\partial t^2}, \tag{3.8}$$

$$P\frac{\partial w(x,t)}{\partial x}+Q+\int_S T_x z \mathrm{d}S - \frac{\partial M}{\partial x}=0, \tag{3.9}$$

where S and A are the perimeter and the area of the beam cross section, ρ is the mass density, $P=\int_A \sigma_x \mathrm{d}A$ and $M=-\int_A \sigma_x z \mathrm{d}A$. Differentiating Eq. (3.9) with respect to x and using Eq. (3.8) results in

$$\frac{\partial^2 M}{\partial x^2}-P\frac{\partial^2 w(x,t)}{\partial x^2}-\frac{\partial}{\partial x}\int_S T_x z \mathrm{d}S - \int_S T_z \mathrm{d}S = -\rho A \frac{\partial^2 w(x,t)}{\partial t^2}. \tag{3.10}$$

In the absence of free electric charges, Gauss's law requires that

$$\frac{\partial D_z}{\partial z}=0. \tag{3.11}$$

Substituting Eq. (3.6) into Eq. (3.11) and using Eqs. (3.1) and (3.2), the electric potential distribution can be determined based on the electrical boundary conditions $\Phi(-h/2)=0$ and $\Phi(h/2)=V$, i.e.

$$\Phi = -\frac{e_{31}}{2\kappa_{33}}\frac{\partial^2 w(x,t)}{\partial x^2}\left(z^2-\frac{h^2}{4}\right)+\frac{V}{h}z+\frac{V}{2}. \tag{3.12}$$

Then the axial stresses for the surface and the bulk in Eqs. (3.3) and (3.5) can be determined as

$$\sigma_x^s = \sigma_x^0 + c_{11}^s \varepsilon_0 + e_{31}^s \frac{V}{h}-\left(c_{11}^s+\frac{e_{31}^s e_{31}}{\kappa_{33}}\right)z\frac{\partial^2 w(x,t)}{\partial x^2}, \tag{3.13}$$

$$\sigma_x = c_{11}\varepsilon_0 + e_{31}\frac{V}{h}-\left(c_{11}+\frac{e_{31}^2}{\kappa_{33}}\right)z\frac{\partial^2 w(x,t)}{\partial x^2}. \tag{3.14}$$

Applying equations (3.13) and (3.14), the governing equation (3.10) for the piezoelectric nanobeam with surface effects is rewritten as

$$\left(EI\right)_{\text{eff}}\frac{\partial^4 w(x,t)}{\partial x^4}-P_{\text{eff}}\frac{\partial^2 w(x,t)}{\partial x^2}=-\rho A\frac{\partial^2 w}{\partial t^2}, \tag{3.15}$$

where $\left(EI\right)_{\text{eff}}$ and P_{eff} are the effective bending rigidity and the effective axial load of the piezoelectric nanobeam, respectively. They are expressed as

$$\left(EI\right)_{\text{eff}}=\frac{1}{12}\left(c_{11}+\frac{e_{31}^2}{\kappa_{33}}\right)bh^3+\left(c_{11}^{s}+\frac{e_{31}^{s}e_{31}}{\kappa_{33}}\right)\left(\frac{1}{2}bh^2+\frac{1}{6}h^3\right), \tag{3.16}$$

$$P_{\text{eff}}=c_{11}\varepsilon_0 bh+e_{31}Vb+2b\left(\sigma_x^0+c_{11}^{s}\varepsilon_0+e_{31}^{s}\frac{V}{h}\right). \tag{3.17}$$

It should be mentioned that the current formulation is conducted for a piezoelectric nanobeam with rectangular cross section. However, such a formulation procedure is also applicable to the piezoelectric nanobeam with circular cross section, such as a nanowire. The corresponding effective bending rigidity and effective axial load for the nanobeam with circular cross section are

$$\left(EI\right)_{\text{eff}}=\frac{\pi D^4}{64}\left(c_{11}+\frac{e_{31}^2}{\kappa_{33}}\right)+\frac{\pi D^3}{8}\left(c_{11}^{s}+\frac{e_{31}^{s}e_{31}}{\kappa_{33}}\right), \tag{3.18}$$

$$P_{\text{eff}}=\frac{\pi D^2}{4}\left(c_{11}\varepsilon_0+e_{31}\frac{V}{D}\right)+2\left(\sigma_x^0+c_{11}^{s}\varepsilon_0+e_{31}^{s}\frac{V}{D}\right)D, \tag{3.19}$$

where D is the diameter of the nanowire. It is indicated in Eqs. (3.16)-(3.19) that the surface effects, including the residual surface stress, the surface elasticity and the surface piezoelectricity, may significantly influence the vibration and buckling behaviors of the piezoelectric nanobeam.

The resonant frequencies for beams with different boundary conditions, for example, simply supported (S-S), cantilever (C-F) and clamped-clamped (C-C) piezoelectric nanobeams, can be determined from the following characteristic equations

$$\sin\left(s_2 L\right)=0 \qquad \left(\text{S-S}\right), \tag{3.20}$$

$$s_1^4+s_2^4+s_1 s_2\left(s_2^2-s_1^2\right)\sinh\left(s_1 L\right)\sin\left(s_2 L\right)+2s_1^2 s_2^2\cosh\left(s_1 L\right)\cos\left(s_2 L\right)=0 \quad \left(\text{C-F}\right), \tag{3.21}$$

$$2s_1s_2 - 2s_1s_2\cos(s_2L)\cosh(s_1L) + (s_1^2 - s_2^2)\sin(s_2L)\sinh(s_1L) = 0 \quad \text{(C-C)}, \tag{3.22}$$

where

$$s_1 = \left(\frac{P_{\text{eff}} + \sqrt{P_{\text{eff}}^2 + 4\rho A\omega^2 (EI)_{\text{eff}}}}{2(EI)_{\text{eff}}}\right)^{\frac{1}{2}}, \tag{3.23}$$

and

$$s_2 = \left(\frac{\sqrt{P_{\text{eff}}^2 + 4\rho A\omega^2 (EI)_{\text{eff}}} - P_{\text{eff}}}{2(EI)_{\text{eff}}}\right)^{\frac{1}{2}}, \tag{3.24}$$

with ω being the angular resonant frequencies.

Since the applied electric potential may induce a compressive axial force due to the electromechanical coupling, the determination of the critical electric potential for buckling is essential. According to the buckling theory (Timoshenko and Gere, 1961), a piezoelectric nanobeam buckles under the following condition

$$P_{\text{eff}} = -\frac{\pi^2 (EI)_{\text{eff}}}{(KL)^2}, \tag{3.25}$$

where K is the effective-length factor which depends on the end conditions of the beam. For example, $K = 1$ for the S-S beam, $K = 0.5$ for the C-C beam and $K = 2$ for the C-F beam, respectively. Accounting for the surface effects, the critical electric potential corresponding to the buckling of the piezoelectric nanobeam is then determined as

$$V_{\text{cr}} = -\frac{\left(c_{11}bh\varepsilon_0 + 2bc_{11}^s\varepsilon_0 + 2b\sigma_x^0 + \dfrac{\pi^2 (EI)_{\text{eff}}}{(KL)^2}\right)}{\left(e_{31}b + e_{31}^s \dfrac{2b}{h}\right)}. \tag{3.26}$$

These equations derived above depict the dependence of the resonant frequencies and the critical electric potential for buckling on the surface effect parameters as well as the boundary conditions. It may be noted that, if surface effects are excluded in the analysis, these equations reduce to those for the conventional piezoelectric beams.

3.3 Results and discussion

To qualitatively understand the mechanical and electrical responses of a piezoelectric nanobeam, we choose one kind of lead zirconate titanate material, PZT-5H, for the case study and their bulk material property constants are $c_{11} = 126\,\text{GPa}$, $e_{31} = -6.5\,\text{C m}^{-2}$, $\kappa_{33} = 1.3 \times 10^{-8}\,\text{C V}^{-1}\,\text{m}^{-1}$ and $\rho = 7.5 \times 10^{3}\,\text{kg m}^{-3}$. The formulations in section 3.2 suggest that the behaviors of piezoelectric nanobeams significantly depend on their surface properties, which could be determined by experiments or atomistic simulations (Miller and Shenoy, 2000; He and Lilley, 2008a). Following Huang and Yu's work (2006), the surface elastic and surface piezoelectric constants are chosen as $c_{11}^{\text{s}} = 7.56\,\text{N m}^{-1}$ and $e_{31}^{\text{s}} = -3 \times 10^{-8}\,\text{C m}^{-1}$ as a reasonable approximation. In addition, the typical residual surface stress is of the order of $0.1 - 1\,\text{N m}^{-1}$ (Miller and Shenoy, 2000; Lachut and Sader, 2007; He and Lilley, 2008a). In this work, $\sigma_x^0 = 1.0\,\text{N m}^{-1}$ is taken for the simulation when the residual surface stress is considered and the beam width b is assumed to be equal to the beam thickness h.

Firstly, the influence of surface effects on the resonant frequencies of the piezoelectric nanobeam is studied. The normalized first-mode resonant frequency ω_1 / ω_1^0 against the beam thickness for a simply supported (S-S) nanobeam under different electrical loads V is plotted in Fig. 3.2, where ω_1^0 is calculated from the classical beam theory without considering the surface effects and the applied voltage. The length to thickness ratio of the nanobeam is fixed at L/h=20 and no initial axial strain exists $(\varepsilon_0 = 0)$. It is observed from this figure that the surface effects obviously influence the resonant frequency of the piezoelectric nanobeam. Within some range of applied voltage, the surface effects become more dominant with the decrease of the beam thickness. However, with the increase of the applied positive voltage, V=0.2 V for example, it is observed that the resonant frequency drops down with the decrease of the beam thickness, which indicates a possible mechanical buckling of the piezoelectric
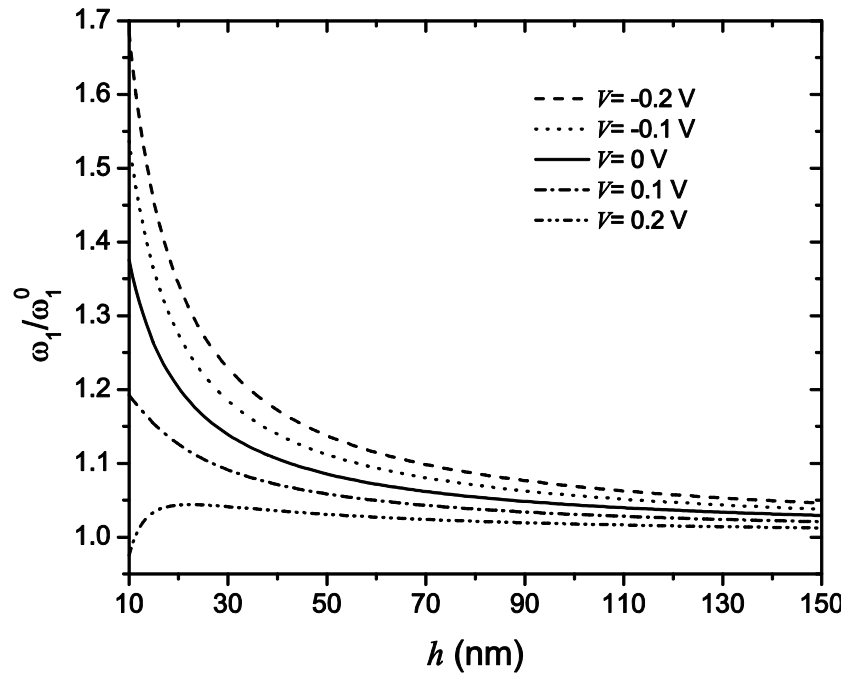
Figure 3.2: Variation of the normalized frequency with the beam thickness for a nanobeam with simply supported (S-S) boundary condition.
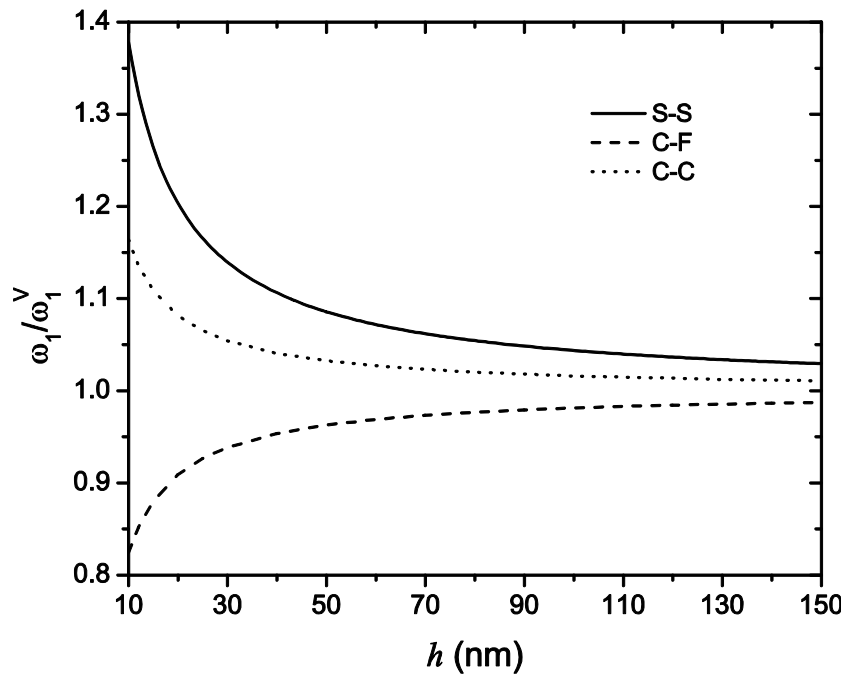
Figure 3.3: Normalized frequency versus beam thickness for a nanobeam with different boundary conditions.

nanobeam with a sufficiently large positive voltage or a sufficiently small beam thickness. This phenomenon is due to the fact that a compressive axial load is induced by an applied

voltage in the positive direction as indicted in Eq. (3.17) and will be discussed later. Moreover, it is also observed from this figure that the electromechanical coupling of piezoelectric materials can be explored for frequency tuning of nanobeams, as shown by the variation of the natural frequencies with the applied voltages.

Fig. 3.3 displays the effect of boundary conditions on the first mode resonant frequency ω_1 for a piezoelectric nanobeam with the same geometric dimensions as the beam studied in Fig. 3.2. In this figure, the resonant frequency is normalized by ω_1^V, which is calculated for the beam without considering the surface effects but with the applied voltage $V = -0.1\,\text{V}$. It is observed that the influence of surface effects on the resonant frequencies depends on the beam size and the boundary conditions. The resonant frequencies calculated for both simply supported (S-S) and clamped-clamped (C-C) nanobeams are higher than those calculated without the surface effects, while an opposite trend occurs for the cantilever (C-F) nanobeam. It is concluded from this figure that the influence of the surface effects on the resonant frequencies of the piezoelectric nanobeam is more pronounced for a simply supported beam. A similar phenomenon has also been observed for elastic nanowires (He and Lilley, 2008b). It will also be interesting to study the effect of surface elasticity, residual surface stress and surface piezoelectricity on the resonant frequencies separately. For a simply supported (S-S) nanobeam as studied in Fig. 3.3, Fig. 3.4 plots the variation of the normalized first mode resonant frequency with the beam thickness considering the surface elasticity $\left(\sigma_x^0 = 0, e_{31}^s = 0, c_{11}^s \neq 0\right)$, the residual surface stress $\left(\sigma_x^0 \neq 0, e_{31}^s = 0, c_{11}^s = 0\right)$ and the surface piezoelectricity $\left(\sigma_x^0 = 0, e_{31}^s \neq 0, c_{11}^s = 0\right)$, respectively. It is found that the effect of the residual surface stress and the surface piezoelectricity on the resonant frequencies is more prominent than the surface elasticity effect within the considered values of surface property constants in the current case study. However, such an effect of surface piezoelectricity was ignored in Wang and Feng's work (2010). To see the axial load effect, Fig. 3.5 depicts the variation of the resonant frequency with the beam thickness h ($L/h = 20$) for an S-S nanobeam subjected to different initial axial strain ε_0. The applied electrical load is $V = -0.1\,\text{V}$. As expected, the resonant frequency decreases with the

compressive axial strain since this applied load softens the beam, while it increases with the tensile axial strain due to the stiffening effect.
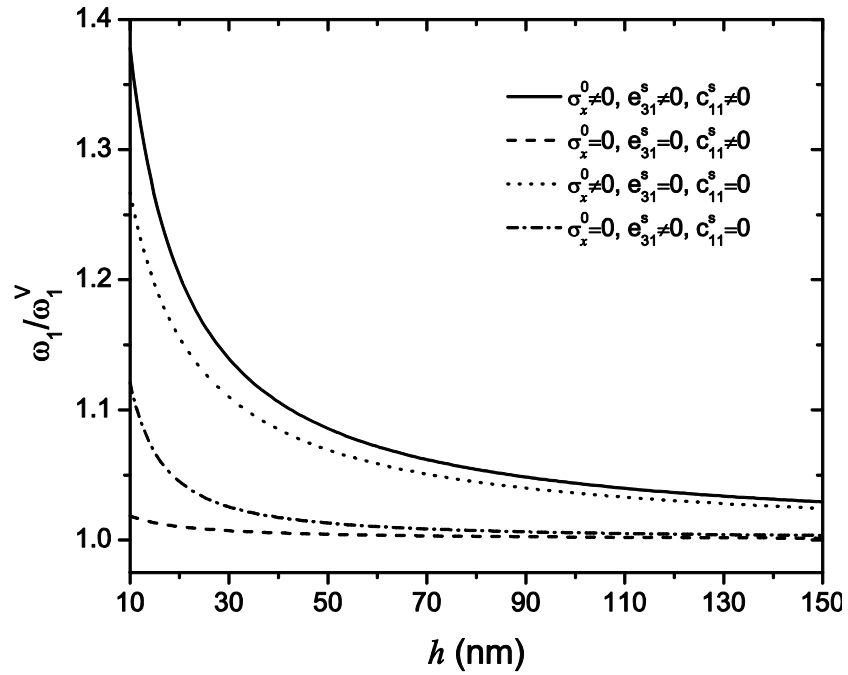
Figure 3.4: Normalized frequency versus beam thickness for a simply supported (S-S) nanobeam considering surface elasticity, residual surface stress and surface piezoelectricity separately.
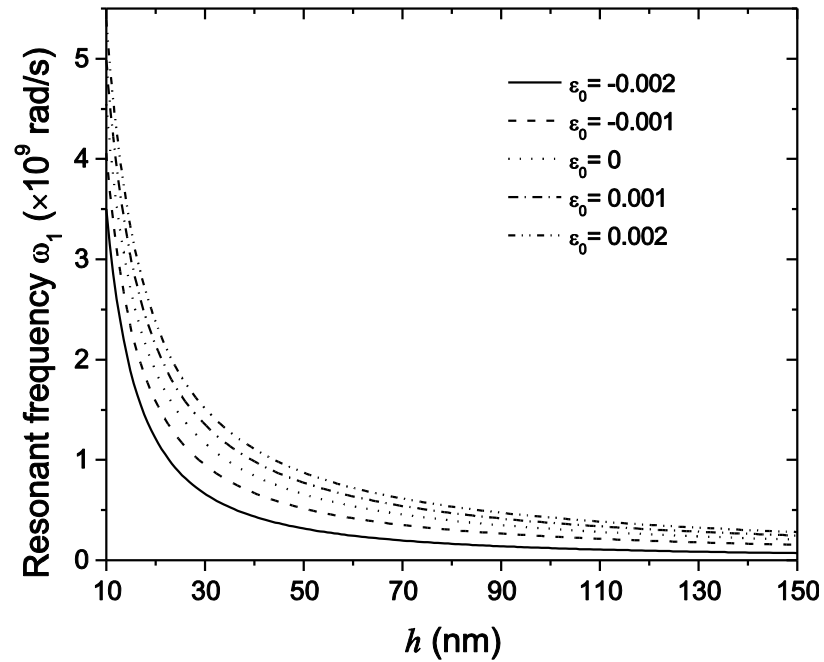
Figure 3.5: Variation of the resonant frequency with the beam thickness for a simply supported (S-S) nanobeam considering axial load effect.
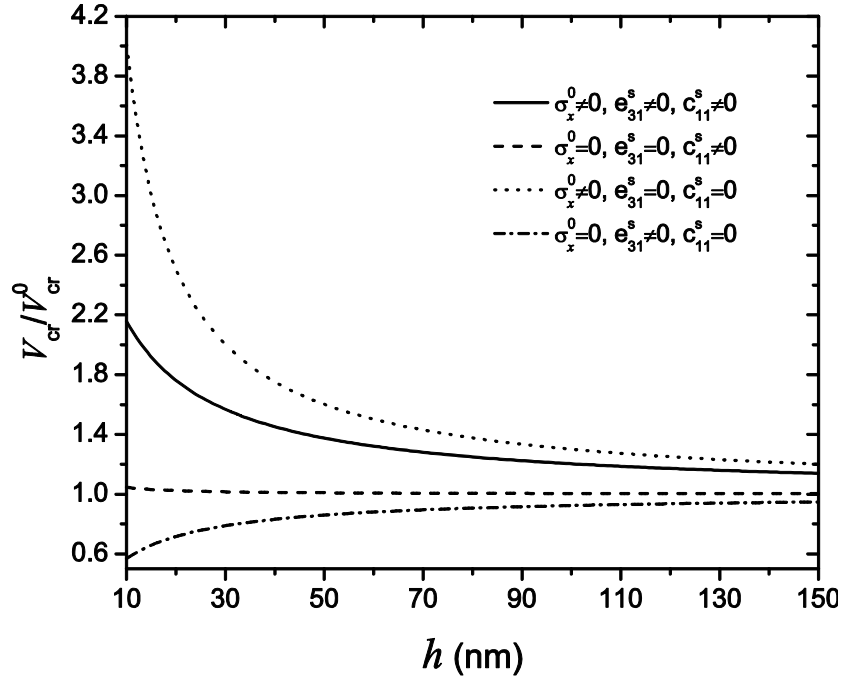
Figure 3.6: Variation of the normalized critical electric potential with the beam thickness for a cantilever (C-F) nanobeam.

The buckling of piezoelectric nanobeams is also an interesting issue for engineering applications. Without an applied axial load ($\varepsilon_0 = 0$), the applied electrical load V which generates axial stress due to the piezoelectricity may cause the buckling of the nanobeams. Since the surface effects also contribute to the effective axial load acting on the nanobeam, as discussed in section 3.2, they may have a significant influence on this buckling behavior. For a piezoelectric cantilever nanobeam, the normalized critical electric potential for buckling V_{cr}/V_{cr}^0, versus beam thickness h is plotted in Fig. 3.6, where V_{cr}^0 is the critical electric potential for the buckling of the beam without surface effects. It is observed in this figure that the influence of the surface effects on the critical electric potential becomes more pronounced with the decrease of nanobeam size h. Similar to Fig. 3.4, the surface elasticity effect on the critical electric potential for buckling is relatively small compared to the effects of the residual surface stress and the surface piezoelectricity. However, the effects of the residual surface stress and the surface piezoelectricity on the buckling electric potential are opposite, *i.e.* the residual surface stress increases the critical electric potential, while the surface piezoelectricity decreases it. The results obtained from the current work indicate the significance of considering

surface piezoelectricity in predicting the vibration and buckling behaviors of piezoelectric nanostructures in addition to the elastic surface effects of nanomaterials.

3.4 Conclusions

Based on the surface piezoelectricity model and the generalized Young-Laplace equations, the influence of surface effects including residual surface stress, surface elasticity and surface piezoelectricity on the vibration and buckling behaviors of piezoelectric nanobeams has been studied using an Euler-Bernoulli beam model. The resonant frequencies and the critical electric potential for buckling of piezoelectric nanobeams with different boundary conditions have been derived. The results indicate that the surface effects, the boundary conditions, the applied electrical load and axial strain influence the mechanical behaviors of the piezoelectric nanobeams significantly. It is found that the influence of the residual surface stress and the surface piezoelectricity on the resonant frequencies and the critical electric potential for buckling is more prominent than the surface elasticity. It is also observed that the resonant frequencies can be tuned by adjusting the applied electrical load. The present study is expected to provide guidelines for the design and applications of piezoelectric-nanobeam-based devices.

References

Agrawal, R., Peng, B., Gdoutos, E. E. and Espinosa, H. D., 2008. Elasticity size effects in ZnO nanowires-a combined experimental-computational approach. Nano Lett. **8**, 3668-3674.

Bai, X. D., Gao, P. X., Wang, Z. L. and Wang, E. G., 2003. Dual-mode mechanical resonance of individual ZnO nanobelts. Appl. Phys. Lett. **82**, 4806-4808.

Cammarata, R. C., 1994. Surface and interface stress effects in thin films. Prog. Surf. Sci. **46**, 1-38.

Chen, C. Q., Shi, Y., Zhang, Y. S., Zhu, J. and Yan, Y. J., 2006. Size dependence of Young's modulus in ZnO nanowires. Phys. Rev. Lett. **96**, 075505.

Chen, T. Y., Chiu, M. S. and Weng, C. N., 2006. Derivation of the generalized Young-Laplace equation of curved interfaces in nanoscaled solids. J. Appl. Phys. **100**, 074308.

Fei, P., Yeh, P. H., Zhou, J., Xu, S., Gao, Y. F., Song, J. H., Gu, Y. D., Huang, Y. Y. and Wang, Z. L., 2009. Piezoelectric potential gated field-effect transistor based on a free-standing ZnO wire. Nano Lett. **9**, 3435-3439.

Gao, Y. and Wang, Z. L., 2007. Electrostatic potential in a bent piezoelectric nanowire. The fundamental theory of nanogenerator and nanopiezotronics. Nano Lett. **7**, 2499-2505.

Gurtin, M. E. and Murdoch, A. I., 1975. A continuum theory of elastic material surfaces. Arch. Ration. Mech. Anal. **57**, 291-323.

He, J. and Lilley, C. M., 2008a. Surface effect on the elastic behavior of static bending nanowires. Nano Lett. **8**, 1798-1802.

He, J. and Lilley, C. M., 2008b. Surface stress effect on bending resonance of nanowires with different boundary conditions. Appl. Phys. Lett. **93**, 263108.

He, J. H., Hsin, C. L., Liu, J., Chen, L. J. and Wang, Z. L., 2007. Piezoelectric gated diode of a single ZnO nanowire. Adv. Mater. **19**, 781-784.

Huang, G. Y. and Yu, S. W., 2006. Effect of surface piezoelectricity on the electromechanical behaviour of a piezoelectric ring. Phys. Status Solidi B-Basic Solid State Phys. **243**, R22-R24.

Huang, Y. H., Bai, X. D. and Zhang, Y., 2006. In situ mechanical properties of individual ZnO nanowires and the mass measurement of nanoparticles. J. Phys.: Condens. Matter **18**, L179-L184.

Lachut, M. J. and Sader, J. E., 2007. Effect of surface stress on the stiffness of cantilever plates. Phys. Rev. Lett. **99**, 206102.

Li, C., Guo, W. L., Kong, Y. and Gao, H. J., 2007. Size-dependent piezoelectricity in zinc oxide nanofilms from first-principle calculations. Appl. Phys. Lett. **90**, 033108.

Liu, C. and Rajapakse, R. K. N. D., 2010. Continuum models incorporating surface energy for static and dynamic response of nanoscale beams. IEEE Trans. Nanotechnol. **9**, 422-431.

Majdoub, M. S., Sharma, P. and Cagin, T., 2008a. Dramatic enhancement in energy harvesting for a narrow range of dimensions in piezoelectric nanostructures. Phys. Rev. B **78**, 121407(R).

Majdoub, M. S., Sharma, P. and Cagin, T., 2008b. Enhanced size-dependent piezoelectricity and elasticity in nanostructures due to the flexoelectric effect. Phys. Rev. B **77**, 125424.

Miller, R. E. and Shenoy, V. B., 2000. Size-dependent elastic properties of nanosized structural elements. Nanotechnology **11**, 139-147.

Shao, Z. Z., Wen, L. Y., Wu, D. M., Wang, X. F., Zhang, X. A. and Chang, S. L., 2010. A continuum model of piezoelectric potential generated in a bent ZnO nanorod. J. Phys. D: Appl. Phys. **43**, 245403.

Stan, G., Ciobanu, C. V., Parthangal, P. M. and Cook, R. F., 2007. Diameter-dependent radial and tangential elastic moduli of ZnO nanowires. Nano Lett. **7**, 3691-3697.

Su, W. S., Chen, Y. F., Hsiao, C. L. and Tu, L. W., 2007. Generation of electricity in GaN nanorods induced by piezoelectric effect. Appl. Phys. Lett. **90**, 063110.

Sun, C. L., Shi, J. and Wang, X. D., 2010. Fundamental study of mechanical energy harvesting using piezoelectric nanostructures. J. Appl. Phys. **108**, 034309.

Tagantsev, A. K., 1986. Piezoelectricity and flexoelectricity in crystalline dielectrics. Phys. Rev. B **34**, 5883-5889.

Tanner, S. M., Gray, J. M., Rogers, C. T., Bertness, K. A. and Sanford, N. A., 2007. High-Q GaN nanowire resonators and oscillators. Appl. Phys. Lett. **91**, 203117.

Timoshenko, S. P. and Gere, J. M., 1961. Theory of elastic stability, McGraw-Hill, New York.

Wang, G. F. and Feng, X. Q., 2007. Effects of surface elasticity and residual surface tension on the natural frequency of microbeams. Appl. Phys. Lett. **90**, 231904.

Wang, G. F. and Feng, X. Q., 2009a. Surface effects on buckling of nanowires under uniaxial compression. Appl. Phys. Lett. **94**, 141913.

Wang, G. F. and Feng, X. Q., 2009b. Timoshenko beam model for buckling and vibration of nanowires with surface effects. J. Phys. D: Appl. Phys. **42**, 155411.

Wang, G. F. and Feng, X. Q., 2010. Effect of surface stresses on the vibration and buckling of piezoelectric nanowires. EPL **91**, 56007.

Wang, Q., Li, Q. H., Chen, Y. J., Wang, T. H., He, X. L., Li, J. P. and Lin, C. L., 2004. Fabrication and ethanol sensing characteristics of ZnO nanowire gas sensors. Appl. Phys. Lett. **84**, 3654-3656.

Wang, X. D., Zhou, J., Song, J. H., Liu, J., Xu, N. S. and Wang, Z. L., 2006. Piezoelectric field effect transistor and nanoforce sensor based on a single ZnO nanowire. Nano Lett. **6**, 2768-2772.

Wang, Z. L. and Song, J. H., 2006. Piezoelectric nanogenerators based on zinc oxide nanowire arrays. Science **312**, 242-246.

Xiang, H. J., Yang, J. L., Hou, J. G. and Zhu, Q. S., 2006. Piezoelectricity in ZnO nanowires: A first-principles study. Appl. Phys. Lett. **89**, 223111.

Yan, Z. and Jiang, L. Y., 2011. Surface effects on the electromechanical coupling and bending behaviours of piezoelectric nanowires. J. Phys. D: Appl. Phys. **44**, 075404.

Zhang, Y. H., Hong, J. W., Liu, B. and Fang, D. N., 2010. Strain effect on ferroelectric behaviors of $BaTiO_3$ nanowires: a molecule dynamics study. Nanotechnology **21**, 015701.

Zhao, M. H., Wang, Z. L. and Mao, S. X., 2004. Piezoelectric characterization of individual zinc oxide nanobelt probed by piezoresponse force microscope. Nano Lett. **4**, 587-590.

Chapter 4

4 Electromechanical response of a curved piezoelectric nanobeam with the consideration of surface effects[3]

4.1 Introduction

Due to their coupled piezoelectric and semiconductive properties, piezoelectric nanostructured materials are considered as ideal candidates for constructing nanodevices, such as chemical and biological nanosensors (Wang *et al*., 2004), nanoresonators (Bai *et al*., 2003; Tanner *et al*., 2007) and nanogenerators (Wang and Song, 2006; Su *et al*., 2007). In recent years, various one-dimensional piezoelectric nanostructures have been successfully synthesized, including nanowires, nanobelts, nanosprings and nanorings (Wang, 2009). This wide range of novel structures of piezoelectric nanomaterials enables the design of more complicated and fascinating devices in nanoelectromechanical systems (NEMS). To fulfill the potential applications of those advanced nanodevices, it is necessary to qualitatively understand the electromechanical coupling of the piezoelectric nanostructured materials and predict their responses to external loadings.

Unlike their bulk counterparts, existing experiments and atomistic simulations have found that the elastic and piezoelectric coefficients of piezoelectric nanomaterials vary with their structure dimensions (Zhao *et al*., 2004; Chen *et al*., 2006; Stan *et al*., 2007; Agrawal *et al*., 2008; Zhang *et al*., 2010). Understanding this size-dependent property is essential for the performance prediction and the design of piezoelectric nanodevices. Due to the extreme difficulties in conducting experiments on nanoscale materials and computing expensiveness of atomic studies, it is natural to pursue the analysis of piezoelectric nanomaterials by continuum models. When the characteristic sizes of these piezoelectric structures shrink to nanometers, new physics may emerge and the theories typically applied to macroscale materials do not immediately translate to the nanoscale structures. For example, conventional continuum models ignore the variation of

---

[3]A version of this chapter has been published.

Yan, Z. and Jiang, L.Y., J. Phys. D: Appl. Phys. 44, 365301, (2011).

interatomic quantities and thus fail to capture the size effects of materials at the nanoscale. Therefore, modified continuum models are required to incorporate the size effects into the conventional continuum mechanics framework. One proposed modified continuum theory studying the nanoscale materials is the Eringen's nonlocal theory of elasticity (Eringen, 2002), in which the stress at a specific point is related to the strains of the entire domain mathematically formulated by integral equation. Using this theory, the size effects are captured by the nonlocal parameters of the kernel function in the integration. This nonlocal theory has been applied to study the nanostructured materials, such as nanobeam (Lu *et al*., 2006), nanorod (Aydogdu, 2009), nanoring (Wang and Duan, 2008) and nanoplate (Duan and Wang, 2007) in the literature. Due to the inherently large surface area-to-volume ratio that is exhibited by typical nanoscale structures, surface effects may play a crucial role in the behavior of piezoelectric nanomaterials. These surface effects have been incorporated into the continuum modeling of nanostructures using the linear surface elastic theory developed by Gurtin and Murdoch (1975) and the generalized Young-Laplace equations (Cammarata, 1994; Miller and Shenoy, 2000; Chen *et al*., 2006). Such a surface-layer-based model has been widely adopted to investigate the bending (Miller and Shenoy, 2000; He and Lilley, 2008a), vibration (Wang and Feng, 2007; He and Lilley, 2008b) and buckling (Wang *et al*., 2007) behaviors of nanostructures. In these studies, the surface effects are found to be responsible for the size-dependent behaviors of nanostructures and the simulation results have been validated by atomistic studies and experiments (Miller and Shenoy, 2000; He and Lilley, 2008a; b).

The size-dependent elastic properties of nanomaterials have been well studied by modified continuum theories as mentioned above. However, the investigation on the properties of piezoelectric nanostructures using continuum modeling approaches is still limited. It is worth mentioning that Michalski *et al*. (2005) were the first to develop a continuum theory to predict the piezoelectric responses of nanotubes and nanowires. While their results failed to interpret the size-dependent properties of these nanoscale materials. As discussed earlier by Tagantsev (1986), the strain gradient induced flexoelectricity as well as surface effects may play a substantial role in the size-dependent electromechanical coupling of piezoelectric nanomaterials. The flexoelectric effects have been studied by Sharma's group (Majdoub *et al*., 2008a; b) and their results suggested a

significant enhancement of electromechanical coupling of piezoelectric nanostructures due to the nonuniform strain gradient developed in a nanoscale bending beam. Huang and Yu (2006) were the first to incorporate the surface effects in the continuum modeling to study the electromechanical behavior of a piezoelectric ring. In their work, the surface effects include the surface elasticity, residual surface stress and surface piezoelectricity. A considerable influence of surface piezoelectricity on the stress and electric fields was observed when the ring size scaled down to nanometers. Wang and Feng (2010) investigated the vibration and buckling behaviors of piezoelectric nanowires using the elastic surface-layer-based model by ignoring the surface piezoelectricity effect. Recently, we studied the influence of surface effects on the electromechanical coupling and static bending of piezoelectric nanobeam (Yan and Jiang, 2011) by considering the combined effects of surface elasticity, residual surface stress and surface piezoelectricity. It was found that the effect of surface piezoelectricity on the size-dependent properties was significant compared with the effects of residual surface stress and surface elasticity.

Since curved structures, such as arch or ring like piezoelectric structures, are common shapes in practical applications, it will be very interesting to study the electromechanical responses of curved piezoelectric nanobeams. The free vibrations of elastic nanorings or curved nanobeams have been studied using nonlocal theory (Wang and Duan, 2008) and surface elasticity theory (Assadi *et al*., 2011), in which the size effects were clearly identified. However, it appears that the influence of surface effects on the electromechanical behavior of curved piezoelectric nanobeams has not been investigated thus far. Hence, the objective of this work is to study the surface effects on the electroelastic responses of a curved piezoelectric nanobeam under external stimulus. The surface effects are accounted by applying a surface-layer-based model. Based on the conventional Euler-Bernoulli curved beam theory, explicit expressions of the electroelastic fields of the curved piezoelectric nanobeam will be derived to show the influence of the surface effects. This work is expected to provide useful guidelines for the design of NEMS devices based on curved piezoelectric nanobeams or nanoring structures.

4.2   Formulation of the problem

Various behaviors of elastic nanostructures have been successfully predicted using a surface-layer-based model (Miller and Shenoy, 2000; He and Lilley, 2008a; b; Wang and Feng, 2007; Wang *et al.*, 2007; Assadi and Farshi, 2011), *i.e.* a nanostructure=bulk+surface. In this study, this model will be further explored to investigate the electromechanical behavior of a curved piezoelectric nanobeam. An element of this curved beam is shown in Fig. 4.1 with x representing a local coordinate axis, which is pointed from the centroidal axis of the curved beam to the center o. It is assumed that the curved beam has a radius R, which is much larger than the beam thickness h, and the poling direction of the piezoelectric body is along the radial direction. u_r and u_θ are the radial and circumferential displacements, respectively. When the piezoelectric body is subjected to a voltage V, the flexural and extensional deformations of the beam will be induced. According to the curved beam theory and Euler-Bernoulli beam assumptions, the tangential strain ε_θ in the beam element can be expressed as (Rao, 2007)

$$\varepsilon_\theta = \frac{1}{R}\left[-u_r + \frac{\partial u_\theta}{\partial \theta} - \frac{x}{R}\frac{\partial}{\partial \theta}\left(u_\theta + \frac{\partial u_r}{\partial \theta}\right)\right], \tag{4.1}$$
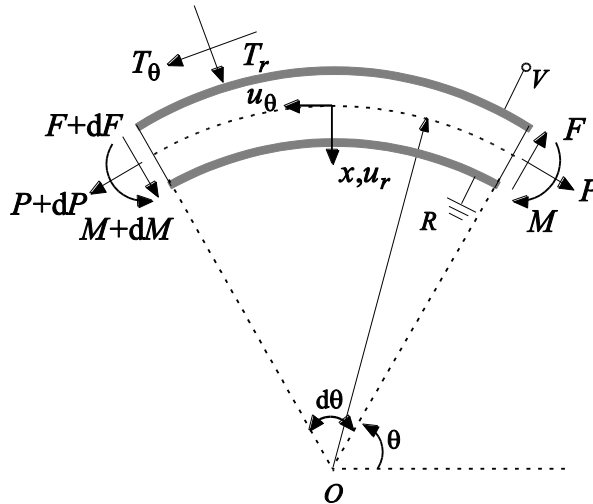
Figure 4.1: Free-body diagram of an incremental element of a curved piezoelectric nanobeam with surface effects.

and the total slope of the deflection curve is

$$\psi = \frac{1}{R}\frac{\partial u_r}{\partial \theta} + \frac{u_\theta}{R}. \tag{4.2}$$

It is assumed that the nonzero electric field exists only along the radial direction. Since the piezoelectric structure is very thin, this electric field E_r can be considered as a constant (Crawley and Deluis, 1987), *i.e.*

$$E_r = \frac{V}{h}. \tag{4.3}$$

In the surface-layer-based model, since the atoms within the surfaces experience a different local environment from that experienced by atoms in the bulk, the constitutive equations of the surfaces are different from the bulk. From Huang and Yu's work (2006), the constitutive relations for the surface of this one-dimensional curved piezoelectric beam can be expressed as

$$\sigma_\theta^s = \sigma_\theta^0 + c_{11}^s \varepsilon_\theta - e_{31}^s E_r, \tag{4.4}$$

$$D_\theta^s = D_\theta^0, \tag{4.5}$$

where σ_θ^s and D_θ^s are the surface stress and surface electric displacement; σ_θ^0 and D_θ^0 are the residual surface stress and surface electric displacement without applied strain and electric field; c_{11}^s and c_{31}^s are the surface elastic and surface piezoelectric constants. It should be mentioned that the surface effects for a piezoelectric medium include the surface piezoelectricity in addition to the surface elasticity and residual surface stress, which is evidenced by the e_{31}^s and D_θ^0 in the constitutive equations.

The constitutive relations in the bulk are the same as conventional piezoelectric materials, *i.e.*

$$\sigma_\theta = c_{11}\varepsilon_\theta - e_{31}E_r, \tag{4.6}$$

$$D_r = e_{31}\varepsilon_\theta + \kappa_{33}E_r, \tag{4.7}$$

with σ_θ and D_r being the bulk stress and the bulk electric displacement, c_{11}, e_{31} and κ_{33} being the conventional elastic, piezoelectric and dielectric constants.

According to the generalized Young-Laplace equations derived by Chen *et al.* (2006), the surface effects are represented by the traction jumps T_θ and T_r on the beam surfaces as shown in Fig. 4.1. Under the assumption of $h \ll R$ and small deformation, these traction jumps can be expressed as

$$T_\theta = \frac{1}{R}\frac{\partial \sigma_\theta^s}{\partial \theta}, \tag{4.8}$$

$$T_r\left(r = R - \frac{h}{2}\right) = \sigma_\theta^s\left(r = R - \frac{h}{2}\right)/R; \ T_r\left(r = R + \frac{h}{2}\right) = -\sigma_\theta^s\left(r = R + \frac{h}{2}\right)/R. \tag{4.9}$$

It is noted that T_r only exists on the top and bottom surfaces of the beam, while the left and right surfaces do not contribute such a traction on the beam. In addition, the electric displacement jump across surfaces is zero.

To derive the governing equations for this curved beam, we follow the same procedure for an elastic nanobeam with the consideration of surface effects (Liu and Rajapakse, 2010). In Fig. 4.1, T_r and T_θ are circumferential traction induced by the surface effects, P, F and M are the axial force, shear force and bending moment of the beam. The governing equations of the curved piezoelectric nanobeam considering surface effects are then derived from the equilibrium condition of the curved element, *i.e.*

$$P + \frac{dF}{d\theta} + \int_s T_r \, ds R = 0, \tag{4.10}$$

$$\frac{dP}{d\theta} - F + \int_s T_\theta \, ds R = 0, \tag{4.11}$$

$$\frac{dM}{d\theta} + FR - \int_s T_\theta x \, ds R = 0, \tag{4.12}$$

where s is the perimeter of the beam cross-section and the integration in these equations accounts for the surface effects. The axial force F and the bending moment M are defined in the same way as those of the conventional elastic beam, which are expressed as

$P = \int_{-h/2}^{h/2} \sigma_\theta b \mathrm{d}x$ and $M = -\int_{-h/2}^{h/2} \sigma_\theta x b \mathrm{d}x$. Then after lengthy manipulation of equations

(4.10) – (4.12) with the consideration of Eqs. (4.1), (4.3), (4.4), (4.6), (4.8) and (4.9), the governing equations in terms of u_r and u_θ can be rewritten as

$$A\frac{\mathrm{d}^5 u_r}{\mathrm{d}\theta^5} + (A+C)\frac{\mathrm{d}^3 u_r}{\mathrm{d}\theta^3} + C\frac{\mathrm{d}u_r}{\mathrm{d}\theta} = 0, \tag{4.13}$$

$$\frac{\mathrm{d}u_\theta}{\mathrm{d}\theta} = \frac{AB}{(A+B)C}\left(\frac{\mathrm{d}^2 u_r}{\mathrm{d}\theta^2} + \frac{\mathrm{d}^4 u_r}{\mathrm{d}\theta^4}\right) + \frac{D}{C} + u_r, \tag{4.14}$$

in which *A, B, C* and *D* are constants defined as

$$\left. \begin{array}{l} A = \dfrac{c_{11}}{R}bh + \dfrac{c_{11}^s}{R}(2b+2h); \ B = \dfrac{c_{11}bh^3}{12R^3} + \dfrac{c_{11}^s}{R^3}\left(\dfrac{1}{2}bh^2 + \dfrac{1}{6}h^3\right); \\[3mm] C = \dfrac{c_{11}}{R}bh + \dfrac{2c_{11}^s}{R}b; \ D = \left(bhe_{31} + 2e_{31}^s b\right)\dfrac{V}{h} - 2\sigma_\theta^0 b. \end{array} \right\} \tag{4.15}$$

4.3 Solutions of the problem

From the governing equations (4.13) and (4.14), the solutions of u_r and u_θ can be expressed as

$$u_r = C_1 + C_2 \sin\theta + C_3 \cos\theta + C_4 \sin\left(\sqrt{\frac{C}{A}}\theta\right) + C_5 \cos\left(\sqrt{\frac{C}{A}}\theta\right), \tag{4.16}$$

and

$$\begin{aligned} u_\theta = {}& C_1\theta - C_2 \cos\theta + C_3 \sin\theta + \frac{D}{C}\theta + C_6 \\[2mm] & + \frac{A^2 + BC}{A(A+B)}\sqrt{\frac{A}{C}}\left[-C_4 \cos\left(\sqrt{\frac{C}{A}}\theta\right) + C_5 \sin\left(\sqrt{\frac{C}{A}}\theta\right)\right], \end{aligned} \tag{4.17}$$

in which $C_1 - C_6$ are constants and will be determined from boundary conditions.

For the case without considering surface effects, *i.e.* all the constants related to surface effects are zero, it results in $A=C$ in Eq. (4.15). Correspondingly, the solutions of u_r and u_θ are expressed as

$$u_r = C_1 + C_2 \sin\theta + C_3 \cos\theta + C_4\theta\sin\theta + C_5\theta\cos\theta, \tag{4.18}$$

and

$$
\begin{aligned}
u_\theta &= C_1\theta - C_2\cos\theta + C_3\sin\theta + C_4\left[\frac{AC+BC-2AB}{(A+B)C}\sin\theta - \theta\cos\theta\right] \\
&+ C_5\left[\frac{AC+BC-2AB}{(A+B)C}\cos\theta + \theta\sin\theta\right] + C_6 + \frac{D}{C}\theta.
\end{aligned}
\tag{4.19}
$$

In order to apply appropriate boundary conditions to the curved piezoelectric nanobeam with the consideration of surface effects, it is necessary to determine the effective loads on the boundary surfaces. We rewrite Eqs. (4.10)-(4.12) as

$$P^* + \frac{\mathrm{d}F^*}{\mathrm{d}\theta} = 0; \quad \frac{\mathrm{d}P^*}{\mathrm{d}\theta} - F^* = 0; \quad \frac{\mathrm{d}M^*}{\mathrm{d}\theta} + F^*R = 0. \tag{4.20}$$

Thus, the above equations are in the same format as the governing equations for conventional curved beams, *i.e.* Eqs. (4.10)-(4.12) with integrations being zero. P^*, F^* and M^* are defined as the effective axial force, effective shear force and effective bending moment, which are derived as

$$P^* = A\left(-u_r + \frac{\mathrm{d}u_\theta}{\mathrm{d}\theta}\right) + \frac{2c_{11}^{\mathrm{s}}h}{R}\frac{B}{A+B}u_r - D, \tag{4.21}$$

$$F^* = -B\left(\frac{\mathrm{d}^2u_\theta}{\mathrm{d}\theta^2} + \frac{\mathrm{d}^3u_r}{\mathrm{d}\theta^3}\right) + \frac{2c_{11}^{\mathrm{s}}h}{R}\frac{B}{A+B}\frac{\mathrm{d}u_r}{\mathrm{d}\theta}, \tag{4.22}$$

$$M^* = BR\left(\frac{\mathrm{d}u_\theta}{\mathrm{d}\theta} + \frac{\mathrm{d}^2u_r}{\mathrm{d}\theta^2}\right) - 2c_{11}^{\mathrm{s}}h\frac{B}{A+B}u_r. \tag{4.23}$$

It can be seen from Eqs. (4.21)-(4.23) that when the surface effects are excluded, P^*, F^* and M^* reduce to the axial force P, shear force F and bending moment M for a conventional curved piezoelectric beam, *i.e.*

$$P = \frac{bhc_{11}}{R}\left(-u_r + \frac{\mathrm{d}u_\theta}{\mathrm{d}\theta}\right) - be_{31}V, \tag{4.24}$$

$$F = -\frac{c_{11}bh^3}{12R^3}\left(\frac{d^2u_\theta}{d\theta^2} + \frac{d^3u_r}{d\theta^3}\right), \tag{4.25}$$

$$M = \frac{c_{11}bh^3}{12R^2}\left(\frac{du_\theta}{d\theta} + \frac{d^2u_r}{d\theta^2}\right). \tag{4.26}$$

For a cantilever beam, the mechanical boundary conditions are defined as

(1) Free end ($\theta = \alpha$):

$$F^* = f; \qquad P^* = p; \qquad M^* = m, \tag{4.27}$$

(2) Fixed end ($\theta = \beta$):

$$u_r = 0; \qquad u_\theta = 0; \qquad \psi = 0, \tag{4.28}$$

where f, p and m are applied point loads, α and β are measured for the free and fixed ends of the beam from the designated horizontal line, as shown in Fig. 4.1.

Based on these boundary conditions, the constants $C_1 - C_6$ in solutions (4.16) and (4.17) can be determined. Correspondingly, the electroelastic fields of the curved piezoelectric nanobeam are thus obtained, which will be used later to predict the surface effects on the electromechanical response of the curved piezoelectric nanobeam.

4.4 Results and discussion

In case study, the original configuration of the curved piezoelectric nanobeam is assumed to have a constant radius-to-thickness ratio $R/h = 15$ and the angles at the free end and the fixed end are $\alpha = \frac{\pi}{2}$ and $\beta = 0$, respectively. PZT- 5H is chosen as the piezoelectric material with bulk material properties $c_{11} = 126$ GPa , $e_{31} = -6.5$ C m^{-2} and $\kappa_{33} = 1.3\times10^{-8}$ C V^{-1} m^{-1}. The surface properties can be determined by experiments and atomistic simulations; however, such quantities are not available for PZT-5H in the open literature. In Huang and Yu's work (2006), $c_{11}^s = 7.56$ N m^{-1} and $e_{31}^s = -3\times10^{-8}$ C m^{-1} were chosen for such material as reasonable approximations according to experiments. The residual surface stress is taken as $\sigma_\theta^0 = 1.0$ N m^{-1} (Miller and Shenoy, 2000; Lachut

and Sader, 2007; He and Lilley, 2008a), which is on the same order as surface elasticity constants displayed by atomistic simulations. In this study, these data will be adopted to qualitatively understand the electromechanical response of a curved piezoelectric nanobeam. As discussed in He and Lilley's work (2008a), the surface-layer-based model ignores the effects of the edge and corner atoms, which are expected to play an important role in the properties of truly small nanostructures but can be only captured by the atomistic simulations. Therefore, we only conduct the simulation for the beam with the thickness h higher than 10 nm.

Firstly, we consider the mechanical response of a curved cantilever beam (with width to thickness ratio $b/h = 3$) when it is subjected to an applied electrical load $V = 0.1$ V. For the considered range of the piezoelectric beam size, the applied voltage will induce an electric field below the poling electric field 1×10^7 V m^{-1} of PZT nanomaterials (Xu et al., 2010). Fig. 4.2 shows the radial displacement u_r at the beam free end versus the beam thickness h. The result from the conventional beam model without considering surface effects is also provided for comparison. It is clearly indicated in this figure that the surface effects have a significant influence on this displacement field, and such surface effects are more pronounced for the nanobeam with smaller cross-sectional dimension h. The separate influence of the surface elasticity $\left(\sigma_\theta^0 = 0, \ e_{31}^s = 0, \ c_{11}^s \neq 0 \right)$, the surface piezoelectricity $\left(\sigma_\theta^0 = 0, \ e_{31}^s \neq 0, \ c_{11}^s = 0 \right)$, the residual surface stress $\left(\sigma_\theta^0 \neq 0, \ e_{31}^s = 0, \ c_{11}^s = 0 \right)$ and the combined influence of the surface elasticity and the surface piezoelectricity $\left(\sigma_\theta^0 = 0, \ e_{31}^s \neq 0, \ c_{11}^s \neq 0 \right)$ are also compared in this figure. It is seen that the separate effect of c_{11}^s and σ_θ^0 on the displacement field of the curved piezoelectric nanobeam is much larger than the effect of e_{31}^s for the considered range of the surface parameters. However, the combined effect of the surface piezoelectricity with the surface elasticity and the residual surface stress is significant, indicating that the surface effects are not the simple summation but the coupling of each individual effect. Therefore, it is of great importance to consider the surface piezoelectricity despite its
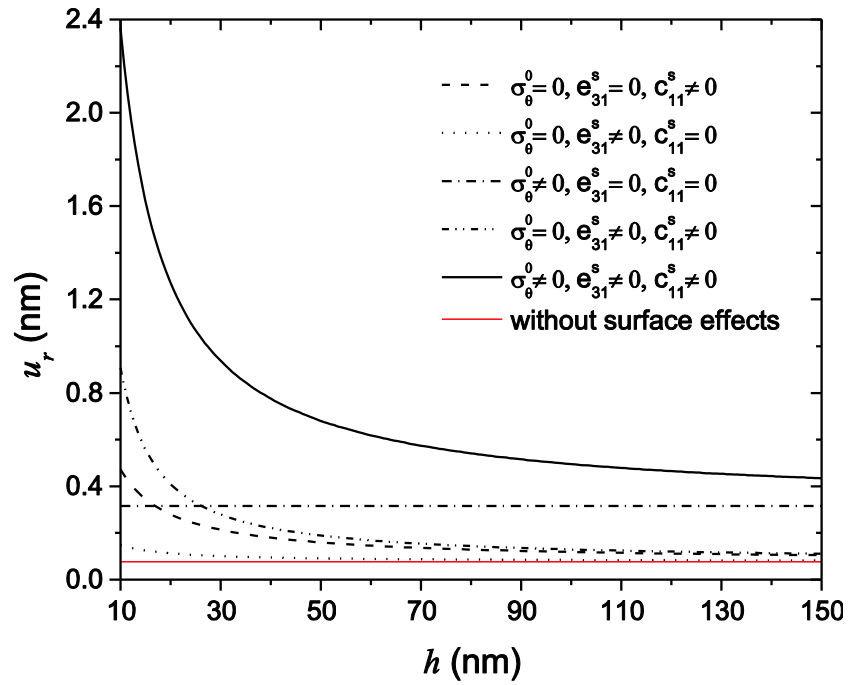
Figure 4.2: Variation of radial displacement u_r at the free end of a cantilever beam with beam thickness h.
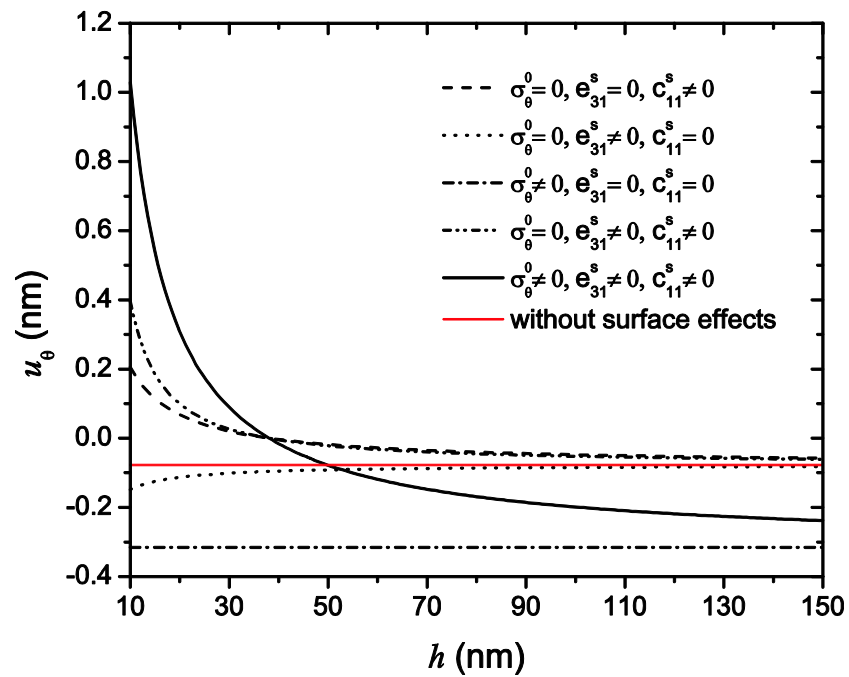
Figure 4.3: Variation of circumferential displacement u_θ at the free end of a cantilever beam with beam thickness h.

small separate effect under some circumstances. For this cantilever nanobeam, the free end surface ($\theta = \alpha$) of the beam is free to move in the radial and circumferential directions, thus the existence of the residual surface stress will cause the relaxation displacement in both the radial and the circumferential directions. Such a phenomenon has been discussed by Park and Klein for a flat cantilever nanowire (2007), in which the free end of the beam is constrained to move only in the longitudinal direction. When only the residual surface stress is considered, a constant radial relaxation displacement at the beam free end is observed for the beam with different thickness but fixed radius to thickness ratio, which is the difference between curves for ($\sigma_\theta^0 \neq 0$, $e_{31}^s = 0$, $c_{11}^s = 0$) and for the conventional beam model in this figure. Correspondingly, the radial displacement for the current model with the consideration of the combined surface effects tends to approach this constant displacement with the increasing of the beam thickness h. If this residual surface stress is excluded, it is also found in this figure that the displacement for the beam with the consideration of the combined surface elasticity and surface piezoelectricity approaches the conventional beam result as expected. A similar phenomenon is observed for the circumferential displacement at the beam free end as shown in Fig. 4.3. Since the radius-to-thickness ratio of the curved beam is fixed, this surface stress driven relaxation for the radial and circumferential displacements is constant as shown in these two figures. It is interesting to mention that the circumferential displacement u_θ could be either positive or negative,

depends on the coupled effect of the surface effects with the electromechanical coupling. When the surface effects are excluded, the electromechanical coupling (1-3 type coupling of piezoelectric materials, *i.e.* an electrical load in r direction results in a mechanical deformation in θ direction) causes the contraction of the curved beam along the circumferential direction as shown by the red solid curve in Fig. 4.3. However, once the surface effects are considered, the coupled effect with the electromechanical coupling could significantly change the profile of the circumferential displacement distribution. As demonstrated in this figure that at the beam free end, both surface piezoelectricity and residual surface stress induce a negative displacement with respect to the electromechanical coupling displacement without surface effects, while the surface elasticity induces a positive one. The separate influence of these surface effects varies

with the beam thickness. Once the surface elasticity is significantly over dominant the coupling of surface piezoelectricity and residual surface stress when thickness h scales
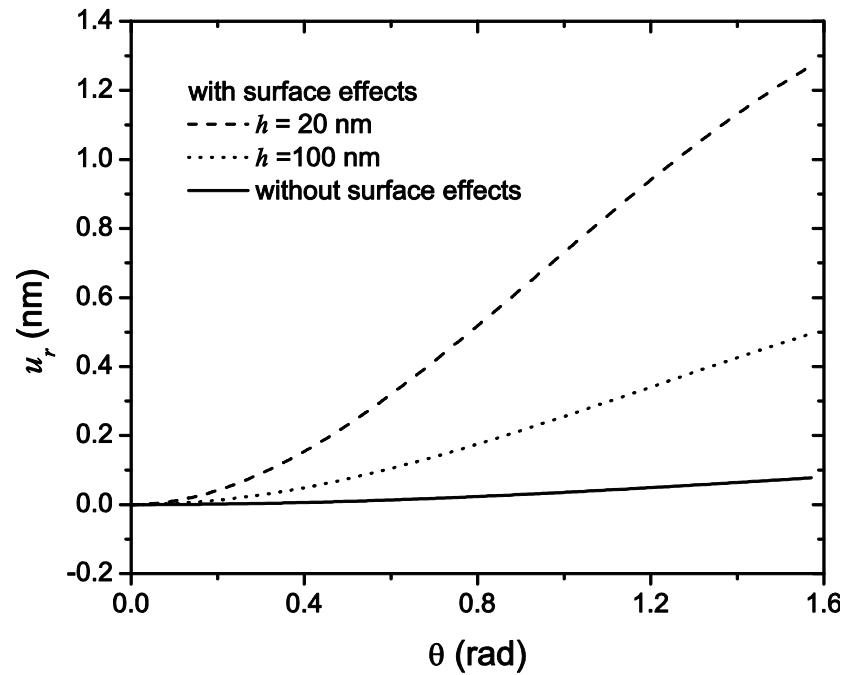
Figure 4.4: Distribution of radial displacement u_r along the curved beam with different thickness h.
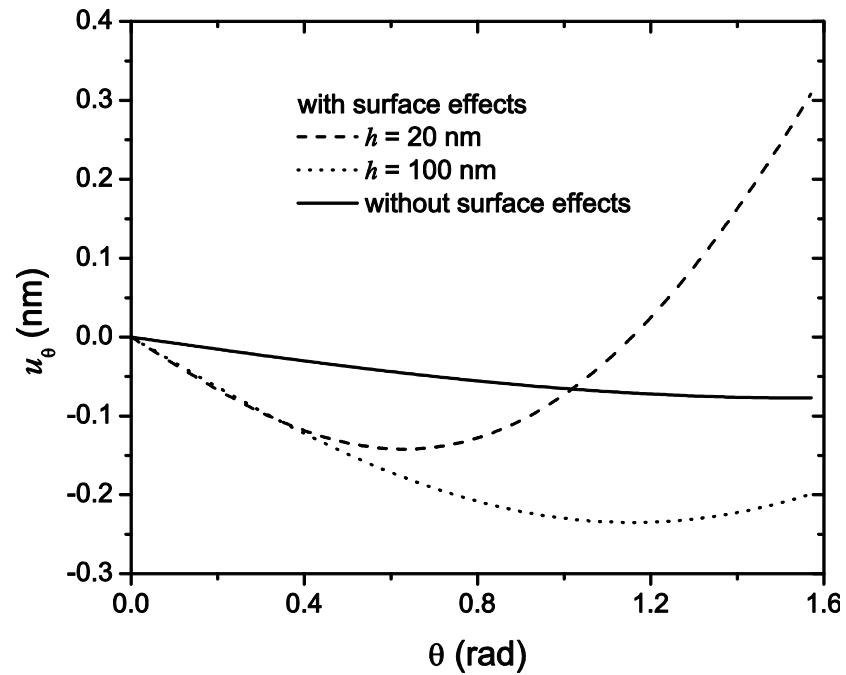
Figure 4.5: Distribution of circumferential displacement u_θ along the curved beam with different thickness h.

down to a particular value, a positive displacement occurs. Otherwise, the free end circumferential displacement is negative. Therefore, the sign of the circumferential displacement u_θ may change with the beam thickness h.

The displacement field distributions along the circumferential direction are displayed in Figs. 4.4 and 4.5 for a curved nanobeam with different thicknesses. The influence of surface effects on the displacement field distribution is evidenced by the difference between the results from the current model and the conventional one for a nanobeam with different sizes. Again such discrepancy is larger for the beam with smaller thickness, $h = 20$ nm for example when the width b is fixed. It is also interesting to see how the influence of surface effects on the electroelastic fields of the curved beam varies with the beam width. The radial displacement distribution along the curved beam with different beam width when the beam thickness is fixed at h=20 nm is plotted in Fig. 4.6 for this purpose. As expected, the influence of surface effects also depends on the beam width (another cross-sectional dimension of the beam). With the decrease in the beam width, the influence of the surface effects increases. It should be mentioned that the displacement at any particular point of the curved beam is the combined result of the geometry of the beam, the location of the point, the electromechanical coupling, the surface effects and the applied loads. Therefore, both positive and negative circumferential displacement could occur along the beam depending on the above mentioned combined effects as shown in Fig. 4.5. As a result, a minimum of the circumferential displacement may occur at a particular position of the beam. The implication of these results is that the surface effects could significantly change the deformation profile of a curved piezoelectric nanobeam when subjected to an electrical load, which will definitely influence the operation of such cantilever beams. All these results indicate that it is necessary to consider surface effects for the design and applications of curved piezoelectric nanobeams, such as curved nanoswitches, the displacement control for curved structures using piezoelectric nanoactuators and potential surface tension sensors using piezoelectric read-out. The exclusion of surface effects using conventional beam models for structures with nanoscale length may lead to significant errors in modeling and performance prediction.
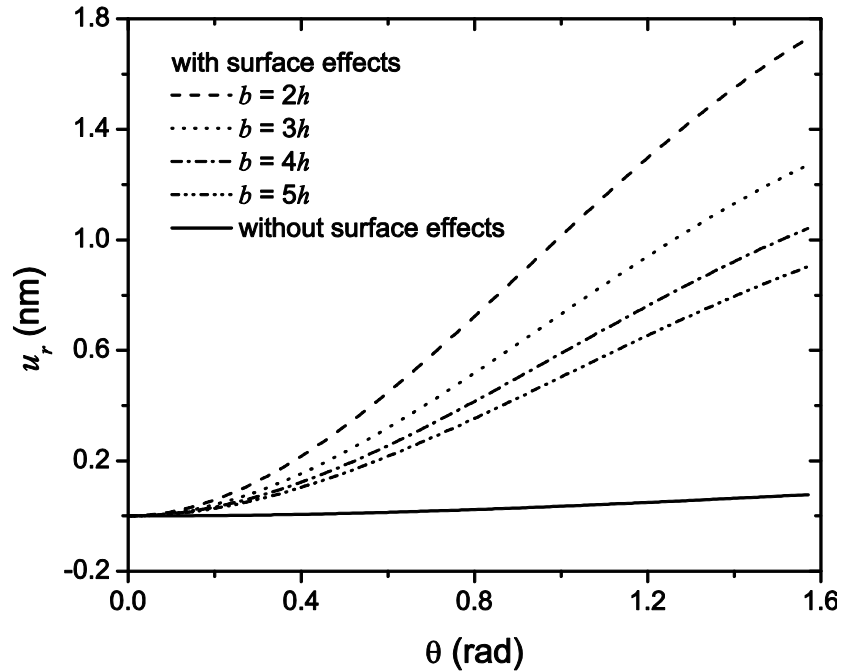
Figure 4.6: Distribution of radial displacement u_r along the curved beam with different beam width b.
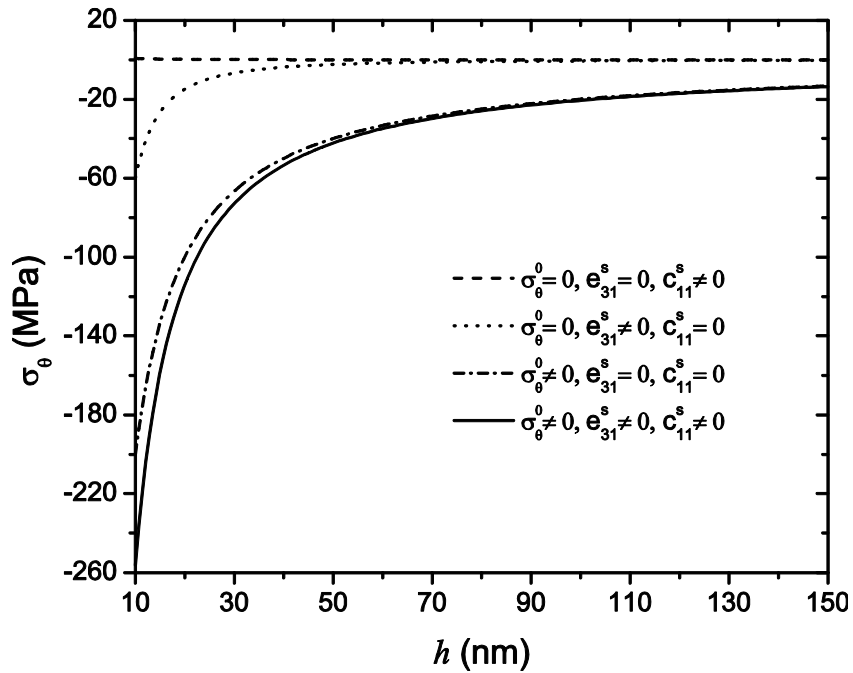
Figure 4.7: Variation of hoop stress σ_θ at the fixed end of a cantilever beam with thickness h.

For a curved cantilever piezoelectric beam subjected to an electrical load V, there will be no stress developed in the beam based on the conventional beam theory. However, the existence of surface effects may significantly intervene in the stress field. Fig. 4.7
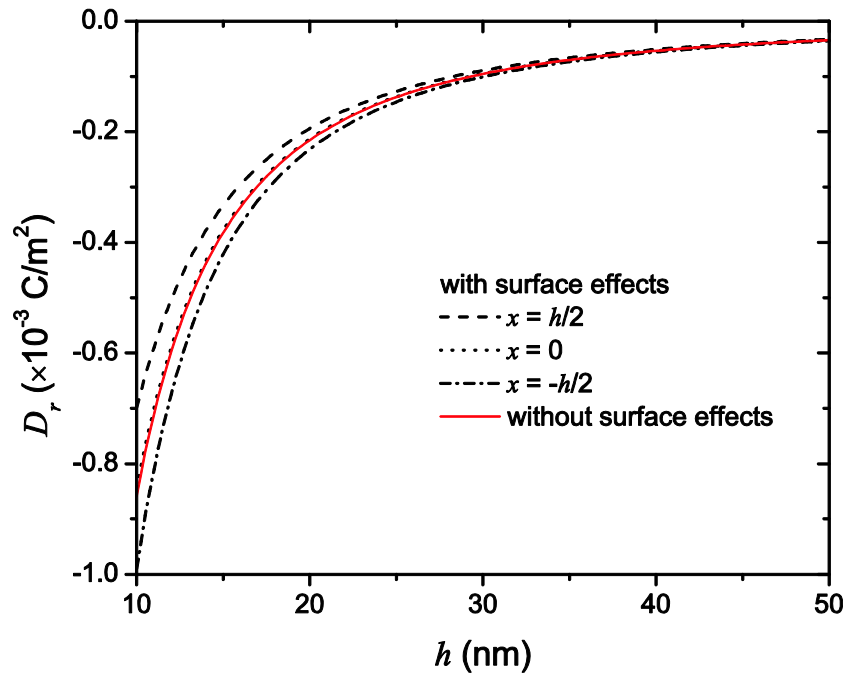
Figure 4.8: Variation of electric displacement D_r at the free end of a cantilever beam with beam thickness h under an axial load.
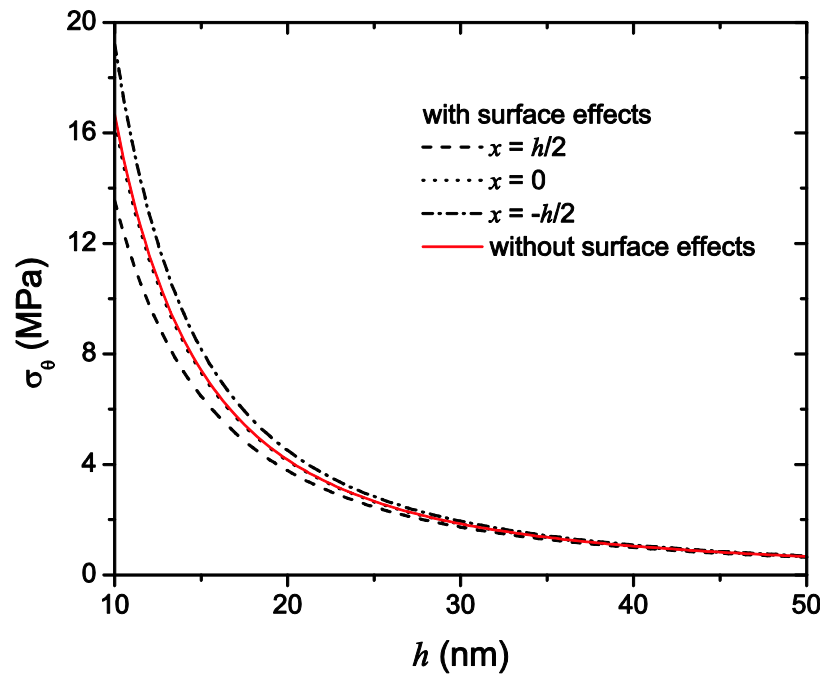
Figure 4.9: Variation of hoop stress σ_θ at the free end of a cantilever beam with beam thickness h under an axial load.

plots the variation of the hoop stress σ_θ at the central line ($x = 0$) of the fixed end ($\theta = \beta$) with the beam thickness. It is seen that the surface elasticity has a negligible influence on σ_θ, while the surface piezoelectricity, especially the residual surface stress influences this hoop stress significantly. These surface effects can be ignored with the increasing of the beam thickness.

To show the surface effects on the electroelastic fields of the curved piezoelectric beam under a mechanical load, Figs. 4.8 and 4.9 plot the variation of the electric displacement D_r and the hoop stress σ_θ at the beam free end ($\theta = \alpha$) with the beam thickness h. Since the effect of residual surface stress is equivalent to an applied voltage, as indicated in Eq. (4.15), we assume $\sigma_\theta^0 = 0$ in the case study to see the electroelastic response of the piezoelectric beam to an applied axial load $p = 5$ nN at the beam free end. It is observed in these figures that the influence of the surface piezoelectricity and the surface elasticity on the electric displacement and the hoop stress is very significant for smaller h. For example, the surface effects disturb the uniform distribution of the electric displacement and the hoop stress through the thickness direction as evidenced by the discrepancy between the curves for $x=h/2$, $x=0$ and $x=-h/2$. With the increasing of h, surface effects are negligible and the distribution of both the electric displacement and the hoop stress becomes uniform as predicted by the conventional beam model.

4.5 Conclusions

In this work, the influence of surface effects including residual surface stress, surface elasticity and surface piezoelectricity on the electromechanical response of a curved piezoelectric nanobeam under electrical and mechanical loads has been studied. Based on the Euler-Bernoulli curved beam theory, surface effects are incorporated into the governing equations through the surface-layer-based model and the generalized Young-Laplace equations. Explicit expressions for the electroelastic fields have been derived. The results show that combined influence of the residual surface stress, surface elasticity and surface piezoelectricity on the displacement, stress and electric displacement fields of the curved beam is significant. Although some individual influence of the residual surface stress, surface elasticity and surface piezoelectricity is small under some

circumstances, exclusion of such individual influence may lead to significant errors in evaluating the electroelastic fields since these effects are coupled. Surface effects are more prominent for the beams with smaller cross-sectional dimensions. This work is envisaged to be helpful for the design and applications of curved beam based piezoelectric nanodevices in NEMS.

References

Agrawal, R., Peng, B., Gdoutos, E. E. and Espinosa, H. D., 2008. Elasticity size effects in ZnO nanowires-a combined experimental-computational approach. Nano Lett. **8**, 3668-3674.

Assadi, A. and Farshi, B., 2011. Size dependent vibration of curved nanobeams and rings including surface energies. Physica E **43**, 975-978.

Aydogdu, M., 2009. Axial vibration of the nanorods with the nonlocal continuum rod model. Physica E **41**, 861-864.

Bai, X. D., Gao, P. X., Wang, Z. L. and Wang, E. G., 2003. Dual-mode mechanical resonance of individual ZnO nanobelts. Appl. Phys. Lett. **82**, 4806-4808.

Cammarata, R. C., 1994. Surface and interface stress effects in thin films. Prog. Surf. Sci. **46**, 1-38.

Chen, C. Q., Shi, Y., Zhang, Y. S., Zhu, J. and Yan, Y. J., 2006. Size dependence of Young's modulus in ZnO nanowires. Phys. Rev. Lett. **96**, 075505.

Chen, T. Y., Chiu, M. S. and Weng, C. N., 2006. Derivation of the generalized Young-Laplace equation of curved interfaces in nanoscaled solids. J. Appl. Phys. **100**, 074308.

Crawley, E. F. and de Luis, J., 1987. Use of piezoelectric actuators as elements of intelligent structures. AIAA J. **25**, 1373-1385.

Duan, W. H. and Wang, C. M., 2007. Exact solutions for axisymmetric bending of micro/nanoscale circular plates based on nonlocal plate theory. Nanotechnology **18**, 385704.

Eringen, A. C., 2002. Nonlocal continuum field theories, Springer, New York.

Gurtin, M. E. and Murdoch, A. I., 1975. A continuum theory of elastic material surfaces. Arch. Ration. Mech. Anal. **57**, 291-323.

He, J. and Lilley, C. M., 2008a. Surface effect on the elastic behavior of static bending nanowires. Nano Lett. **8**, 1798-1802.

He, J. and Lilley, C. M., 2008b. Surface stress effect on bending resonance of nanowires with different boundary conditions. Appl. Phys. Lett. **93**, 263108.

Huang, G. Y. and Yu, S. W., 2006. Effect of surface piezoelectricity on the electromechanical behaviour of a piezoelectric ring. Phys. Status Solidi-Rapid Res. Lett. **243**, R22-R24.

Lachut, M. J. and Sader, J. E., 2007. Effect of surface stress on the stiffness of cantilever plates. Phys. Rev. Lett. **99**, 206102.

Liu, C. and Rajapakse, R. K. N. D., 2010. Continuum models incorporating surface energy for static and dynamic response of nanoscale beams. IEEE Trans. Nanotechnol. **9**, 422-431.

Lu, P., Lee, H. P., Lu, C. and Zhang, P. Q., 2006. Dynamic properties of flexural beams using a nonlocal elasticity model. J. Appl. Phys. **99**, 073510.

Majdoub, M. S., Sharma, P. and Cagin, T., 2008a. Dramatic enhancement in energy harvesting for a narrow range of dimensions in piezoelectric nanostructures. Phys. Rev. B **78**, 121407(R).

Majdoub, M. S., Sharma, P. and Cagin, T., 2008b. Enhanced size-dependent piezoelectricity and elasticity in nanostructures due to the flexoelectric effect. Phys. Rev. B **77**, 125424.

Michalski, P. J., Sai, N. and Mele, E. J., 2005. Continuum theory for nanotube piezoelectricity. Phys. Rev. Lett. **95**, 116803.

Miller, R. E. and Shenoy, V. B., 2000. Size-dependent elastic properties of nanosized structural elements. Nanotechnology **11**, 139-147.

Park, H. S. and Klein, P. A., 2007. Surface Cauchy-Born analysis of surface stress effects on metallic nanowires. Phys. Rev. B **75**, 085408.

Rao, S. S., 2007. Vibration of Continuous Systems, Wiley, New York.

Song, J. H., Zhou, J. and Wang, Z. L., 2006. Piezoelectric and semiconducting coupled power generating process of a single ZnO belt/wire. A technology for harvesting electricity from the environment. Nano Lett. **6**, 1656-1662.

Stan, G., Ciobanu, C. V., Parthangal, P. M. and Cook, R. F., 2007. Diameter-dependent radial and tangential elastic moduli of ZnO nanowires. Nano Lett. **7**, 3691-3697.

Su, W. S., Chen, Y. F., Hsiao, C. L. and Tu, L. W., 2007. Generation of electricity in GaN nanorods induced by piezoelectric effect. Appl. Phys. Lett. **90**, 063110.

Tagantsev, A. K., 1986. Piezoelectricity and flexoelectricity in crystalline dielectrics. Phys. Rev. B **34**, 5883-5889.

Tanner, S. M., Gray, J. M., Rogers, C. T., Bertness, K. A. and Sanford, N. A., 2007. High-Q GaN nanowire resonators and oscillators. Appl. Phys. Lett. **91**, 203117.

Wang, C. M. and Duan, W. H., 2008. Free vibration of nanorings/arches based on nonlocal elasticity. J. Appl. Phys. **104**, 014303.

Wang, G. F. and Feng, X. Q., 2007. Effects of surface elasticity and residual surface tension on the natural frequency of microbeams. Appl. Phys. Lett. **90**, 231904.

Wang, G. F. and Feng, X. Q., 2010. Effect of surface stresses on the vibration and buckling of piezoelectric nanowires. EPL **91**, 56007.

Wang, G. F., Feng, X. Q. and Yu, S. W., 2007. Surface buckling of a bending microbeam due to surface elasticity. EPL **77**, 44002.

Wan, Q., Li, Q. H., Chen, Y. J., Wang, T. H., He, X. L., Li, J. P. and Lin, C. L., 2004. Fabrication and ethanol sensing characteristics of ZnO nanowire gas sensors. Appl. Phys. Lett. **84**, 3654.

Wang, Z. L., 2009. ZnO nanowire and nanobelt platform for nanotechnology. Mater. Sci. Eng: R. **64**, 33-71.

Wang, Z. L. and Song, J. H., 2006. Piezoelectric nanogenerators based on zinc oxide nanowire arrays. Science **312**, 242-246.

Xu, S., Hansen, B. J. and Wang, Z. L., 2010. Piezoelectric-nanowire-enabled power source for driving wireless microelectronics. Nature Commun. **1**, 93.

Yan, Z. and Jiang, L. Y., 2011. Surface effects on the electromechanical coupling and bending behaviours of piezoelectric nanowires. J. Phys. D: Appl. Phys. **44**, 075404.

Zhang, Y. H., Hong, J. W., Liu, B. and Fang, D. N., 2010. Strain effect on ferroelectric behaviors of $BaTiO_3$ nanowires: a molecular dynamics study. Nanotechnology **21**, 015701.

Zhao, M. H., Wang, Z. L. and Mao, S. X., 2004. Piezoelectric characterization of individual zinc oxide nanobelt probed by piezoresponse force microscope. Nano Lett. **4**, 587-590.

Chapter 5

5 Surface effects on the electroelastic responses of a thin piezoelectric plate with nanoscale thickness[4]

5.1 Introduction

Piezoelectric nanostructured materials have attracted tremendous attention from the research community due to their potential applications as field effect transistors (Wang *et al*., 2006), diodes (He *et al*., 2007), chemical sensors (Lao *et al*., 2007), phototronic devices (He *et al.*, 2010) and generators (Wang and Song, 2006; Su *et al*., 2007; Wang *et al*., 2007; Lin *et al*., 2008; Wang *et al*., 2010; Xu *et al*., 2010) in nanoelectromechanical systems (NEMS). Recently, researchers have attempted to transfer piezoelectric nanoribbons and nanofilms (PZT and $BaTiO_3$ materials for example) onto flexible substrates for the purpose of utilizing the high electromechanical coupling of piezoelectric materials in conformable energy harvesting (Park *et al*., 2010; Qi *et al*., 2010; Feng *et al*., 2011). These attempts allow for the integration of high performance energy conversion devices to operate in a stretchable mode and may open up new avenues for energy harvesting. To further explore the design and application possibilities of piezoelectric nanostructured materials, it is essential to qualitatively understand their electromechanical coupling behavior and predict their electroelastic responses to external loads.

Since controlled experiments on materials are extremely difficult at the nanoscale and atomistic simulations are restricted by computation capacities, continuum modeling has been naturally pursued as an alternative tool. It should be mentioned that conventional continuum theories ignoring the variations of interatomic quantities cannot capture the atomic features of materials, hence, they fail to predict the size-dependent properties of materials when the characteristic size of structures scales down to the nanoscale. On the other hand, existing experimental observations (Zhao *et al*., 2004;

---

[4]A version of this chapter has been published.

Yan, Z. and Jiang, L.Y., J. Phys. D: Appl. Phys. 45, 255401, (2012).

Chen *et al*., 2006; Stan *et al*., 2007) and atomistic simulations (Agrawal *et al*., 2008; Zhang *et al*., 2010) have demonstrated that the electromechanical properties of piezoelectric materials at the nanoscale are intrinsically size dependent. Therefore, capturing the nature of such size dependence is a new challenge in the theoretical modeling of piezoelectric nanostructures.

Modified continuum models with the incorporation of size effects in the conventional continuum framework have thus been attempted to interpret the size-dependent properties of various nanostructures. One such model is based on Eringen's nonlocal elasticity theory (Eringen, 2002), in which the stress at a material point is expressed in terms of strains of all material points in the entire domain by integral equation accounting for long ranged atomistic interactions. Using this theory, the size effects are introduced into the classical continuum model through the nonlocal influence parameter. The size-dependent phenomena at small scale can also be understood by resorting to the concept of surface effects. Due to the inherent large surface area-to-volume ratio exhibited by typical nanostructures, surface effects are believed to contribute to their size-dependent properties. These surface effects for elastic nanostructured solids have been incorporated into the linear surface elasticity model developed by Gurtin and Murdoch (1975), in which the surface is modeled as a thin layer with different material properties and constitutive equations from the underlying bulk material. The presence of surface effects results in nonclassical boundary conditions on the bulk part through the generalized Young-Laplace equations (Cammarata, 1994; Miller and Shenoy, 2000). These models have been successfully adopted to study the size-dependent mechanical properties of elastic nanobeams, nanorings and nanoplates from different perspectives (Lim and He, 2004; Lu *et al*., 2006a; b; Duan and Wang, 2007; Wang and Feng, 2007; Wang *et al*., 2007; He and Lilley, 2008a; b; Wang and Duan, 2008; Aydogdu, 2009; Assadi *et al*., 2010; Assadi and Farshi, 2011). As an extension of the surface elasticity model, Huang and Yu (2006) developed a surface piezoelectricity model, which incorporates surface piezoelectricity in addition to the surface elasticity and residual surface stress, to study the mechanical and electrical responses of a piezoelectric ring. It was found that the electroelastic responses of the nanoring were size dependent and significantly influenced by the surface effects. The

static and dynamic analysis of piezoelectric nanobeams were also investigated with the surface piezoelectricity model in our previous work (Yan and Jiang, 2011a; b; c). It was found that the surface elasticity, residual surface stress and surface piezoelectricity influence the electromechanical coupling, bending, vibration and buckling behaviors of piezoelectric nanobeams significantly. In parallel to the surface piezoelectricity model, Sharma and his co-works (Majdoub *et al*., 2008a; b) adopted the higher order continuum theory (*i.e.* strain gradient theory) in their work and found that the strain gradient induced flexoelectricity also played an important role in the size-dependent electromechanical properties of piezoelectric nanobeams.

For two-dimensional nanostructures such as nanoribbons and nanofilms, modified conventional plate theories have been developed by researchers to study their size-dependent mechanical properties. For example, the nonlocal elastic plate theory has been implemented by Murmu and Pradhan (2009) to study the vibration response of single-layered graphene sheets. Based on the surface elasticity model, Kirchhoff and Mindlin plate theories including surface effects have been developed to investigate size-dependent static and dynamic behaviors of thin plates with nanoscale thickness (Lim and He, 2004; Lu *et al*., 2006b). This model was also employed to study the buckling delamination of an ultra-thin film-substrate system recently (Lu *et al*., 2011). However, the modeling and analysis of piezoelectric plates at the nanoscale have not been reported thus far. Therefore, it is the first attempt in this work to investigate the electroelastic responses of a piezoelectric nanoplate with the consideration of surface effects. The formulation is based on the Kirchhoff plate theory and the surface effects are incorporated into the governing differential equations of the thin piezoelectric plates via the surface piezoelectricity model and the generalized Young-Laplace equations. Simulation results will be demonstrated to show the effects of the surface elasticity, residual surface stress and surface piezoelectricity upon the electroelastic responses of the plate. This work is expected to provide more accurate predictions on the electromechanical coupling behavior of nanoribbon or nanoplate based piezoelectric devices in NEMS.

5.2 Formulation of the problem

The problem envisaged in this work is a rectangular piezoelectric nanoplate with thickness h, and in-plane length a and width b. In order to derive the governing equations for the plate, a differential element as shown in Fig. 5.1 is considered, in which a Cartesian coordinate system $oxyz$ is used to describe the element. The oxy plane
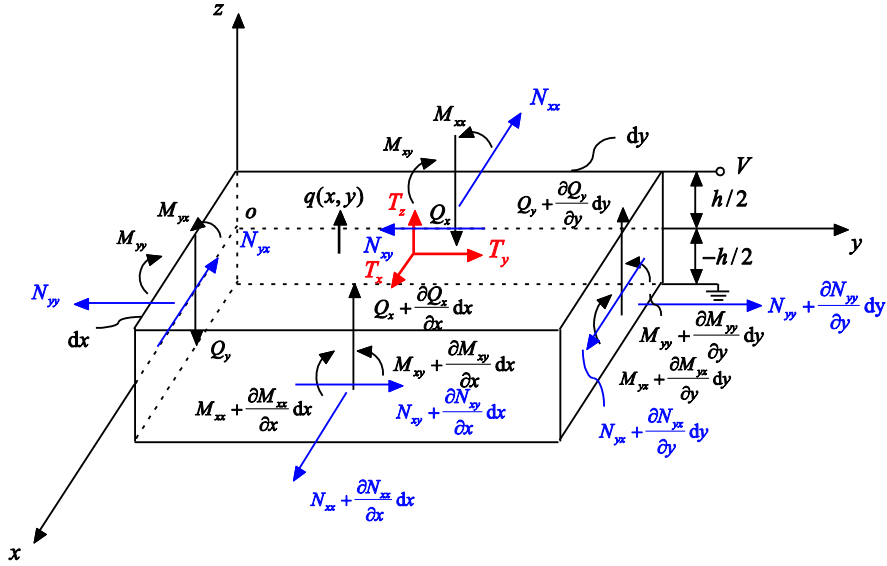
Figure 5.1: Schematic of a differential element of the piezoelectric nanoplate with surface effects.

coincides with the undeformed midplane of the plate and the upper and lower surfaces of the plate are defined by $z = h/2$ and $z = -h/2$, respectively. The piezoelectric body is poled along the z direction and is subjected to a transversely distributed mechanical load $q(x, y)$ and an electric potential V. According to Kirchhoff's hypotheses, the displacements of the plate can be represented as

$$\left. \begin{aligned} u(x, y, z) &= u^0(x, y) - z\frac{\partial w(x, y)}{\partial x}; \\ v(x, y, z) &= v^0(x, y) - z\frac{\partial w(x, y)}{\partial y}; \\ w(x, y, z) &= w(x, y), \end{aligned} \right\} \tag{5.1}$$

where $u^0(x, y)$ and $v^0(x, y)$ are in-plane displacements of the midplane, and $w(x, y)$ is out-plane displacement of the midplane. It should be mentioned that such in-plane displacements of the midplane may be induced by the applied mechanical load, the

applied electrical load due to the electromechanical coupling and the residual surface stress induced relaxation. As discussed in the literature (Park and Klein, 2007; Zhang *et al*., 2010), without any applied external load, the nanostructured material undergoes an in-plane relaxation to fulfill its own equilibrium, resulting in an initial strain. However, such relaxation depends on the in-plane constraints of the plate; for example, the ends of the plate could be free to move resulting in the relaxation displacement but could be fixed without allowing in-plane motion. The effect of the in-plane constraints on the electroelastic fields of the plate will be discussed later in this work. Correspondingly, the strains can be expressed as

$$
\left.
\begin{aligned}
\varepsilon_x &= \frac{\partial u^0(x,y)}{\partial x} - z\frac{\partial^2 w(x,y)}{\partial x^2}; \\
\varepsilon_y &= \frac{\partial v^0(x,y)}{\partial y} - z\frac{\partial^2 w(x,y)}{\partial y^2}; \\
\gamma_{xy} &= \frac{\partial u^0(x,y)}{\partial y} + \frac{\partial v^0(x,y)}{\partial x} - 2z\frac{\partial^2 w(x,y)}{\partial x \partial y}.
\end{aligned}
\right\}
\tag{5.2}
$$

The electric field is assumed to exist only along the *z* direction and can be determined from the electric potential Φ by

$$
E_z = -\frac{\partial \Phi}{\partial z}.
\tag{5.3}
$$

For the surface piezoelectricity model adopted in this work, the constitutive equations of the surface layer are different from the bulk. The surface stresses σ_x^s, σ_y^s and σ_{xy}^s, and the surface electric displacements D_x^s and D_y^s can be expressed according to (Huang and Yu, 2006; Yan and Jiang, 2011a; b) as

$$
\left.
\begin{aligned}
\sigma_x^s &= \sigma_x^0 + c_{11}^s \varepsilon_x + c_{12}^s \varepsilon_y - e_{31}^s E_z; \\
\sigma_y^s &= \sigma_y^0 + c_{12}^s \varepsilon_x + c_{11}^s \varepsilon_y - e_{31}^s E_z; \\
\sigma_{xy}^s &= \sigma_{xy}^0 + c_{66}^s \gamma_{xy}; \\
D_x^s &= D_x^0; \\
D_y^s &= D_y^0.
\end{aligned}
\right\}
\tag{5.4}
$$

with c_{11}^s, c_{12}^s and c_{66}^s being the surface elastic constants, and e_{31}^s being the surface piezoelectric constant. σ_x^0, σ_y^0 and σ_{xy}^0 are the residual surface stresses and D_x^0 and D_y^0 are the residual surface electric displacements. The interior bulk material obeys the same constitutive relations as those for the conventional piezoelectric materials. Following the assumption (Zhao *et al.*, 2007) that the stress component in the *z*-direction is $\sigma_z = 0$, the constitutive relation for the bulk of the piezoelectric plate can be written in the matrix notation format, as

$$\left.\begin{aligned}
\sigma_x &= \tilde{c}_{11}\varepsilon_x + \tilde{c}_{12}\varepsilon_y - \tilde{e}_{31}E_z; \\
\sigma_y &= \tilde{c}_{12}\varepsilon_x + \tilde{c}_{11}\varepsilon_y - \tilde{e}_{31}E_z; \\
\sigma_{xy} &= c_{66}\gamma_{xy}; \\
D_z &= \tilde{e}_{31}\varepsilon_x + \tilde{e}_{31}\varepsilon_y + \tilde{\kappa}_{33}E_z,
\end{aligned}\right\} \tag{5.5}$$

where σ_x, σ_y and σ_{xy} are the bulk stresses and D_z is the bulk electric displacement; the reduced elastic constants $\tilde{c}_{11}$, $\tilde{c}_{12}$, piezoelectric constant $\tilde{e}_{31}$ and dielectric constant $\tilde{\kappa}_{33}$ are $\tilde{c}_{11} = c_{11} - c_{13}^2/c_{33}$, $\tilde{c}_{12} = c_{12} - c_{13}^2/c_{33}$, $\tilde{e}_{31} = e_{31} - c_{13}e_{33}/c_{33}$ and $\tilde{\kappa}_{33} = \kappa_{33} + e_{33}^2/c_{33}$. The numerical values of the macroscopic elastic constants c_{11}, c_{12}, c_{13}, c_{33}, c_{66}, piezoelectric constants e_{31}, e_{33} and dielectric constant κ_{33} for PZT-5H are given in the discussion section.

According to the generalized Young-Laplace equations (Chen *et al.*, 2006), the existence of surfaces can be represented by the traction jumps T_x, T_y and T_z exerting on the bulk of the plate, which can be expressed in terms of the surface stresses as

$$\left.\begin{aligned}
T_x^u &= T_x^l = \frac{\partial \sigma_x^s}{\partial x} + \frac{\partial \sigma_{yx}^s}{\partial y}; \\
T_y^u &= T_y^l = \frac{\partial \sigma_{xy}^s}{\partial x} + \frac{\partial \sigma_y^s}{\partial y}; \\
T_z^u &= \sigma_x^s \frac{\partial^2 w(x,y)}{\partial x^2} + 2\sigma_{xy}^s \frac{\partial^2 w(x,y)}{\partial x \partial y} + \sigma_y^s \frac{\partial^2 w(x,y)}{\partial y^2}; \\
T_z^l &= -\sigma_x^s \frac{\partial^2 w(x,y)}{\partial x^2} - 2\sigma_{xy}^s \frac{\partial^2 w(x,y)}{\partial x \partial y} - \sigma_y^s \frac{\partial^2 w(x,y)}{\partial y^2},
\end{aligned}\right\} \tag{5.6}$$

where the superscripts 'u' and 'l' denote the upper and lower surfaces of the plate, respectively. Note that we only consider T_x and T_y on both the upper and the lower surfaces of the plate due to the small thickness of the plate, which are not sketched in detail in Fig. 5.1. It should also be mentioned that in addition to the traction jumps induced by the surface stresses, for piezoelectric materials, there will also exist an electric displacement jump across the surfaces due to the existence of surface electric displacement. However, for the problem investigated in this work, the electric displacement jump across the surfaces is zero, which can be derived from the generalized Young-Laplace equations (Chen *et al.*, 2006) with the consideration of the fourth and fifth equations of Eqs. (5.4).

For the differential element of the plate composed of the surface and the bulk parts as shown in Fig. 5.1, the force and moment equilibrium yields the following equations

$$\left.\begin{aligned}
\frac{\partial N_{xx}}{\partial x} + \frac{\partial N_{yx}}{\partial y} + T_x^{\mathrm{u}} + T_x^{\mathrm{l}} &= 0; \\
\frac{\partial N_{xy}}{\partial x} + \frac{\partial N_{yy}}{\partial y} + T_y^{\mathrm{u}} + T_y^{\mathrm{l}} &= 0; \\
\frac{\partial Q_x}{\partial x} + \frac{\partial Q_y}{\partial y} + T_z^{\mathrm{u}} - T_z^{\mathrm{l}} &= -q(x,y); \\
\frac{\partial M_{xx}}{\partial x} + \frac{\partial M_{yx}}{\partial y} + Q_x - \left(T_x^{\mathrm{u}} - T_x^{\mathrm{l}}\right)\frac{h}{2} &= 0; \\
\frac{\partial M_{xy}}{\partial x} + \frac{\partial M_{yy}}{\partial y} + Q_y - \left(T_y^{\mathrm{u}} - T_y^{\mathrm{l}}\right)\frac{h}{2} &= 0,
\end{aligned}\right\} \tag{5.7}$$

where N_{ij} and $Q_i\,(i,j=x,y)$ are the axial and shear forces with dimension of force per unit length and M_{ij} is the bending moment with dimension of moment per unit length. The axial forces and bending moments are related to stresses by $N_{ij} = \int_{-h/2}^{h/2} \sigma_{ij}\mathrm{d}z$ and $M_{ij} = -\int_{-h/2}^{h/2} \sigma_{ij} z\mathrm{d}z$, respectively.

In the absence of free electric charges, the electric displacement should satisfy the Gauss's law

$$\frac{\partial D_x}{\partial x} + \frac{\partial D_y}{\partial y} + \frac{\partial D_z}{\partial z} = 0. \tag{5.8}$$

In order to determine the electric field distribution, appropriate electrical boundary conditions must be prescribed. According to Dorfmann and Ogden's work (2005), the electrical boundary conditions can be set either for the electric displacement or for the electric field. In this study, it is assumed that the upper and lower surfaces of the piezoelectric body are fully electroded and an electric voltage V is applied between these two electrodes as shown in Fig. 5.1. For this closed-circuit condition, the electrical boundary conditions can be prescribed in terms of the electric potential, *i.e.* $\Phi(h/2)=V$ and $\Phi(-h/2)=0$ (Pan *et al.*, 2011). Substituting Eqs. (5.3) and the fourth equation of Eqs. (5.5) into Eq. (5.8) and applying the electrical boundary conditions, the electric potential and the electric field distribution can be determined as

$$\Phi = -\frac{\tilde{e}_{31}}{2\tilde{\kappa}_{33}} \left(\frac{\partial^2 w}{\partial x^2} + \frac{\partial^2 w}{\partial y^2} \right) \left(z^2 - \frac{h^2}{4} \right) + \frac{V}{h} z + \frac{V}{2}, \tag{5.9}$$

and

$$E_z = \frac{\tilde{e}_{31}}{\tilde{\kappa}_{33}} \left(\frac{\partial^2 w}{\partial x^2} + \frac{\partial^2 w}{\partial y^2} \right) z - \frac{V}{h}. \tag{5.10}$$

It should be mentioned that the first term in Eq. (5.10) for the electric field is caused by the electromechanical coupling, and the surface effects also contribute to it.

From Eqs. (5.2), (5.4)-(5.7) and (5.10), the governing equations of the piezoelectric nanoplate with the surface effects can be derived as

$$\left(\tilde{c}_{11}h + 2c_{11}^s \right) \frac{\partial^2 u^0}{\partial x^2} + \left(c_{66}h + 2c_{66}^s \right) \frac{\partial^2 u^0}{\partial y^2} + \left(\tilde{c}_{12}h + c_{66}h + 2c_{12}^s + 2c_{66}^s \right) \frac{\partial^2 v^0}{\partial x \partial y} = 0, \tag{5.11}$$

$$\left(c_{66}h + 2c_{66}^s \right) \frac{\partial^2 v^0}{\partial x^2} + \left(\tilde{c}_{11}h + 2c_{11}^s \right) \frac{\partial^2 v^0}{\partial y^2} + \left(\tilde{c}_{12}h + c_{66}h + 2c_{12}^s + 2c_{66}^s \right) \frac{\partial^2 u^0}{\partial x \partial y} = 0, \tag{5.12}$$

and

$$\left[\left(\tilde{c}_{11}+\frac{\tilde{e}_{31}^2}{\tilde{\kappa}_{33}}\right)\frac{h^3}{12}+\left(c_{11}^{\text{s}}+\frac{e_{31}^{\text{s}}\tilde{e}_{31}}{\tilde{\kappa}_{33}}\right)\frac{h^2}{2}\right]\left(\frac{\partial^4 w}{\partial x^4}+\frac{\partial^4 w}{\partial y^4}\right)$$

$$+\left[\left(\tilde{c}_{12}+\frac{\tilde{e}_{31}^2}{\tilde{\kappa}_{33}}\right)\frac{h^3}{6}+\frac{c_{66}h^3}{3}+\left(2c_{66}^{\text{s}}++c_{12}^{\text{s}}+\frac{e_{31}^{\text{s}}\tilde{e}_{31}}{\tilde{\kappa}_{33}}\right)h^2\right]\frac{\partial^4 w}{\partial x^2\partial y^2}=q(x,y)$$

$$+\left[\left(\tilde{c}_{11}\frac{\partial u^0}{\partial x}+\tilde{c}_{12}\frac{\partial v^0}{\partial y}+\tilde{e}_{31}\frac{V}{h}\right)h+2\left(\sigma_x^0+c_{11}^{\text{s}}\frac{\partial u^0}{\partial x}+c_{12}^{\text{s}}\frac{\partial v^0}{\partial y}+e_{31}^{\text{s}}\frac{V}{h}\right)\right]\frac{\partial^2 w}{\partial x^2} \qquad (5.13)$$

$$+\left[\left(\tilde{c}_{12}\frac{\partial u^0}{\partial x}+\tilde{c}_{11}\frac{\partial v^0}{\partial y}+\tilde{e}_{31}\frac{V}{h}\right)h+2\left(\sigma_y^0+c_{12}^{\text{s}}\frac{\partial u^0}{\partial x}+c_{11}^{\text{s}}\frac{\partial v^0}{\partial y}+e_{31}^{\text{s}}\frac{V}{h}\right)\right]\frac{\partial^2 w}{\partial y^2}$$

$$+2\left[c_{66}\left(\frac{\partial u^0}{\partial y}+\frac{\partial v^0}{\partial x}\right)h+2\sigma_{xy}^0+2c_{66}^{\text{s}}\left(\frac{\partial u^0}{\partial y}+\frac{\partial v^0}{\partial x}\right)\right]\frac{\partial^2 w}{\partial x\partial y}.$$

In order to apply the appropriate mechanical boundary conditions to the nanoplate with surface effects, the generalized resultant forces and moments are defined as (Lu *et al.*, 2006b)

$$N_{ij}^*=N_{ij}+\left(\sigma_{ij}^{\text{s}}\right)^{\text{u}}+\left(\sigma_{ij}^{\text{s}}\right)^1;\ M_{ij}^*=M_{ij}-\frac{h}{2}\left[\left(\sigma_{ij}^{\text{s}}\right)^{\text{u}}-\left(\sigma_{ij}^{\text{s}}\right)^1\right]. \qquad (5.14)$$

Then equilibrium equations (5.7) can be simplified as

$$\left.\begin{array}{l}\dfrac{\partial N_{xx}^*}{\partial x}+\dfrac{\partial N_{yx}^*}{\partial y}=0;\\[3mm]\dfrac{\partial N_{xy}^*}{\partial x}+\dfrac{\partial N_{yy}^*}{\partial y}=0;\\[3mm]\dfrac{\partial^2 M_{xx}^*}{\partial x^2}+2\dfrac{\partial^2 M_{xy}^*}{\partial x\partial y}+\dfrac{\partial^2 M_{yy}^*}{\partial y^2}=q(x,y)+N_{xx}^*\dfrac{\partial^2 w}{\partial x^2}+2N_{xy}^*\dfrac{\partial^2 w}{\partial x\partial y}+N_{yy}^*\dfrac{\partial^2 w}{\partial y^2},\end{array}\right\} \qquad (5.15)$$

which are in the same format as the governing equations for a conventional piezoelectric plate (Zhao *et al.*, 2007).

For case study, we will investigate the static bending of a simply supported piezoelectric nanoplate with the following mechanical boundary conditions for the out-plane displacement and the generalized resultant moments,

$$w=0,\ M_{xx}^*=0\ \text{at} \qquad\qquad w=0,\ M_{yy}^*=0\ \text{at}\ y=0,\ y=b. \qquad (5.16)$$

The in-plane mechanical boundary conditions can be defined according to different in-plane constraints, which are listed as the following two cases:

Case 1: $N_{xx}^* = N_{xy}^* = 0$ at $x = 0, x = a$; $N_{yy}^* = N_{xy}^* = 0$ at $y = 0, y = b$

Traction free conditions are satisfied on the side surfaces of the plate for this case. Assuming the residual surface stresses $\sigma_x^0 = \sigma_y^0 = \sigma^0$, $\sigma_{xy}^0 = 0$ and the plate is subjected to a uniformly distributed transverse load $q(x, y) = q_0$, the displacements satisfying all the boundary conditions can be derived as

$$
\left.\begin{aligned}
u^0(x, y) &= \varepsilon x;\ v^0(x, y) = \varepsilon y; \\
w(x, y) &= \sum_{m=1}^{\infty}\sum_{n=1}^{\infty} A_{mn} \sin\left(\frac{m\pi x}{a}\right)\sin\left(\frac{n\pi y}{b}\right),
\end{aligned}\right\}
\tag{5.17}
$$

where

$$
\varepsilon = -\frac{\tilde{e}_{31}V + 2\left(\sigma^0 + e_{31}^s \dfrac{V}{h}\right)}{\left(\tilde{c}_{11} + \tilde{c}_{12}\right)h + 2\left(c_{11}^s + c_{12}^s\right)},
\tag{5.18}
$$

and

$$
A_{mn} = \frac{16 q_0}{mn\pi^2 X} \qquad (m, n = 1, 3, 5...),
\tag{5.19}
$$

with

$$
\begin{aligned}
X &= \left[\left(\tilde{c}_{11} + \frac{\tilde{e}_{31}^2}{\tilde{\kappa}_{33}}\right)\frac{h^3}{12} + \left(c_{11}^s + \frac{e_{31}^s \tilde{e}_{31}}{\tilde{\kappa}_{33}}\right)\frac{h^2}{2}\right]\left[\left(\frac{m\pi}{a}\right)^4 + \left(\frac{n\pi}{b}\right)^4\right] \\
&+ \left[\left(\tilde{c}_{12} + \frac{\tilde{e}_{31}^2}{\tilde{\kappa}_{33}}\right)\frac{h^3}{6} + \frac{c_{66}h^3}{3} + \left(2c_{66}^s + c_{12}^s + \frac{e_{31}^s \tilde{e}_{31}}{\tilde{\kappa}_{33}}\right)h^2\right]\frac{m^2 n^2 \pi^4}{a^2 b^2}.
\end{aligned}
\tag{5.20}
$$

It is obvious from Eqs. (5.17) and (5.18) that the in-plane displacements are induced by the applied electric potential and the residual surface stress. Without the applied electrical load $V=0$, an in-plane relaxation strain develops due to the residual surface stress σ^0, *i.e.*

$$\varepsilon = -\frac{2\sigma^0}{\left(\tilde{c}_{11} + \tilde{c}_{12}\right)h + 2\left(c_{11}^s + c_{12}^s\right)}. \tag{5.21}$$

Such a relaxation phenomenon has also been found by Park and Kein (2007) for an elastic nanowire using the surface Cauchy-Born model.

Case 2: $u^0\left(x, y\right) = 0, v^0\left(x, y\right) = 0$.

In this case, the in-plane displacements are constrained to zero, which are the same as assumed by Zhao *et al.* (2007) for a conventional piezoelectric plate. Under this condition, the in-plane displacements are trivial as assumed for a conventional Kirchhoff plate theory. Thus the governing equation (5.13) can be simplified as

$$\left[\left(\tilde{c}_{11} + \frac{\tilde{e}_{31}^2}{\tilde{\kappa}_{33}}\right)\frac{h^3}{12} + \left(c_{11}^s + \frac{e_{31}^s \tilde{e}_{31}}{\tilde{\kappa}_{33}}\right)\frac{h^2}{2}\right]\left(\frac{\partial^4 w}{\partial x^4} + \frac{\partial^4 w}{\partial y^4}\right)$$

$$+\left[\left(\tilde{c}_{12} + \frac{\tilde{e}_{31}^2}{\tilde{\kappa}_{33}}\right)\frac{h^3}{6} + \frac{c_{66}}{3}h^3 + \left(2c_{66}^s + c_{12}^s + \frac{e_{31}^s \tilde{e}_{31}}{\tilde{\kappa}_{33}}\right)h^2\right]\frac{\partial^4 w}{\partial x^2 \partial y^2} = q\left(x, y\right) \tag{5.22}$$

$$+\left[\tilde{e}_{31}V + 2\left(\sigma_x^0 + e_{31}^s \frac{V}{h}\right)\right]\frac{\partial^2 w}{\partial x^2} + 4\sigma_{xy}^0 \frac{\partial^2 w}{\partial x \partial y} + \left[\tilde{e}_{31}V + 2\left(\sigma_y^0 + e_{31}^s \frac{V}{h}\right)\right]\frac{\partial^2 w}{\partial y^2}.$$

Adopting the same assumptions for the residual surface stresses as case 1, the analytical solution for the above differential governing equation according to a uniformly distributed transverse load $q\left(x, y\right) = q_0$ can be obtained as

$$w\left(x, y\right) = \sum_{m=1}^{\infty}\sum_{n=1}^{\infty} A_{mn}\sin\left(\frac{m\pi x}{a}\right)\sin\left(\frac{n\pi y}{b}\right), \tag{5.23}$$

with

$$A_{mn} = \frac{16q_0}{mn\pi^2 Y} \qquad \left(m, n = 1, \ 3, \ 5...\right), \tag{5.24}$$

and

$$Y = \left[\left(\tilde{c}_{11} + \frac{\tilde{e}_{31}^2}{\tilde{\kappa}_{33}} \right) \frac{h^3}{12} + \left(c_{11}^{s} + \frac{e_{31}^{s} \tilde{e}_{31}}{\tilde{\kappa}_{33}} \right) \frac{h^2}{2} \right] \left[\left(\frac{m\pi}{a} \right)^4 + \left(\frac{n\pi}{b} \right)^4 \right]$$

$$+ \left[\left(\tilde{c}_{12} + \frac{\tilde{e}_{31}^2}{\tilde{\kappa}_{33}} \right) \frac{h^3}{6} + \frac{c_{66}}{3} h^3 + \left(2c_{66}^{s} + c_{12}^{s} + \frac{e_{31}^{s} \tilde{e}_{31}}{\tilde{\kappa}_{33}} \right) h^2 \right] \frac{m^2 n^2 \pi^4}{a^2 b^2} \qquad (5.25)$$

$$+ \left[\tilde{e}_{31} V + 2 \left(\sigma^0 + e_{31}^{s} \frac{V}{h} \right) \right] \left(\frac{m^2 \pi^2}{a^2} + \frac{n^2 \pi^2}{b^2} \right).$$

It should be mentioned that this in-plane displacement constraint has been widely adopted in studying the surface effects of nanobeams (Wang and Feng, 2007; Wang *et al*., 2007; He and Lilley, 2008a; b). Correspondingly, the residual surface stress induced displacement relaxation has not been observed in these studies. In this work, the electroelastic responses of the piezoelectric nanoplate to the applied electromechanical loads will be discussed according to these two types of the in-plane constraints.

Due to the inherent electromechanical coupling of piezoelectric materials, the applied electrical load may generate in-plane forces under certain boundary conditions. For case 2 discussed above, the in-plane loads due to the applied electric potential V can be obtained as

$$N_{xx}^{*} = \tilde{e}_{31} V + 2 \left(\sigma_x^0 + e_{31}^{s} \frac{V}{h} \right); \quad N_{yy}^{*} = \tilde{e}_{31} V + 2 \left(\sigma_y^0 + e_{31}^{s} \frac{V}{h} \right). \qquad (5.26)$$

These forces may be compressive depending on the magnitude and the direction of the applied electric field, in addition, the existence of the surface effects also contributes to these in-plane loads. These compressive forces may induce the mechanical buckling of the piezoelectric nanoplate. Therefore, it is necessary to consider the buckling behavior of the piezoelectric nanoplate with surface effects.

For simplicity, we only consider the cylindrical buckling of an infinitely wide (in y direction) piezoelectric plate with finite length l in the x direction under a compressive force N at $x = 0$ and $x = l$. In this case, all the electroelastic fields depend on the x coordinate only. Without considering the transverse load, *i.e.* $q(x,y) = 0$, the equilibrium equations (5.15) can be rewritten as

$$\frac{dN^*_{xx}}{dx} = 0; \quad \left[\left(\tilde{c}_{11} + \frac{\tilde{e}^2_{31}}{\tilde{\kappa}_{33}} \right) \frac{h^3}{12} + \left(c^s_{11} + \frac{e^s_{31}\tilde{e}_{31}}{\tilde{\kappa}_{33}} \right) \frac{h^2}{2} \right] \frac{d^4 w}{dx^4} = N^*_{xx} \frac{d^2 w}{dx^2}. \tag{5.27}$$

For the simply supported boundary conditions, *i.e.* at $x = 0$ and $x = l$,

$$N^*_{xx} = -N; \quad w = 0; \quad M^*_{xx} = 0, \tag{5.28}$$

with N being a compressive force applied to the bulk, a nontrivial solution of Eq. (5.27) can be expressed as

$$w(x) = \sum_{n=1}^{\infty} w_n \sin \left(\frac{n\pi x}{l} \right), \tag{5.29}$$

in which n is a positive integer. Substituting Eq. (5.29) into Eq. (5.27), the critical buckling load can be obtained as,

$$N_{cr} = \left[\left(\tilde{c}_{11} + \frac{\tilde{e}^2_{31}}{\tilde{\kappa}_{33}} \right) \frac{h^3}{12} + \left(c^s_{11} + \frac{e^s_{31}\tilde{e}_{31}}{\tilde{\kappa}_{33}} \right) \frac{h^2}{2} \right] \frac{\pi^2}{l^2}. \tag{5.30}$$

It is obvious that this critical buckling load depends on the electromechanical coupling and the surface effects of the piezoelectric plate.

When the displacement of the piezoelectric plate is constrained along the x direction, *i.e.* $u^0 = 0$, the electromechanical coupling induced compressive force may also cause the mechanical buckling of the plate as discussed before. In this case, the critical electric potential for the buckling can be derived as

$$V_{cr} = \frac{-N_{cr} - 2\sigma^0}{\tilde{e}_{31} + \frac{2e^s_{31}}{h}}. \tag{5.31}$$

From all these equations derived above, it is indicated that the electroealstic responses of the piezoelectric nanoplate depend on the surface effects which will be illustrated in the following section. It should be noted that if surface effects are excluded in the analysis, these equations will reduce to those for the conventional piezoelectric plates.

5.3   Results and discussion

In case study, PZT-5H is chosen as the example material, with the macroscopic material properties being $c_{11} = 126$ GPa , $c_{12} = 55$ GPa , $c_{13} = 53$ GPa , $c_{33} = 117$ GPa , $e_{31} = -6.5$ C m^{-2} , $e_{33} = 23.3$ C m^{-2} and $\kappa_{33} = 1.3 \times 10^{-8}$ C V^{-1} m^{-1} . It should be mentioned exact values of the surface parameters can be obtained from detailed atomistic calculations or experiments. However, such quantities for PZT-5H are not completely available in the literature. In this work, we adopt the surface elasticity as $c_{11}^{s} = 7.56$ N m^{-1} and the surface piezoelectricity as $e_{31}^{s} = -3.0 \times 10^{-8}$ C m^{-1}, which are the same as given in Huang and Yu's work (2006). The residual surface stress is taken as $\sigma^{0} = 1.0$ N m^{-1}, c_{12}^{s} is assumed as $c_{12}^{s} = c_{12} c_{11}^{s} / c_{11}$ and c_{66}^{s} is obtained from $c_{66}^{s} = \left(c_{11}^{s} - c_{12}^{s} \right) / 2$.

Firstly, we will focus on investigating the static bending of a piezoelectric nanoplate with surface effects. The maximum deflection of the plate under external loads occurs in the middle of the plate ($x = a/2$, $y = b/2$) as indicated in Eqs. (5.17). For a simply supported piezoelectric plate with $a = b = 30h$ and its in-plane constraints being set as described in case 1 of the previous section, when it is subjected to a mechanical load q_0 only, the dimensionless maximum deflection $w_{max} \tilde{c}_{11} / (q_0 h)$ with the variation of the plate thickness h is plotted in Fig 5.2. It is obvious that this dimensionless deflection is independent of the absolute size of the plate when the surface effects are excluded. However, the existence of the surface effects leads to the size-dependent bending response of the plate. It is observed in this figure that the maximum deflection decreases with the decrease of the nanoplate thickness. With the increase in the plate thickness h, the influence of the surface effects diminishes and the predicted deflection from the current model tends to approach a constant as predicted by the conventional Kirchhoff plate model without the consideration of the surface effects. The separate influence of the surface elasticity and the surface piezoelectricity is also compared in Fig. 5.2. Within the considered range of the surface parameters in this work, the surface elasticity has a relatively smaller effect on the static bending in comparison to the surface piezoelectricity. Similar observation for the out-plane displacement of the piezoelectric nanoplate with the in-plane constraints described by case 2 in the previous section has
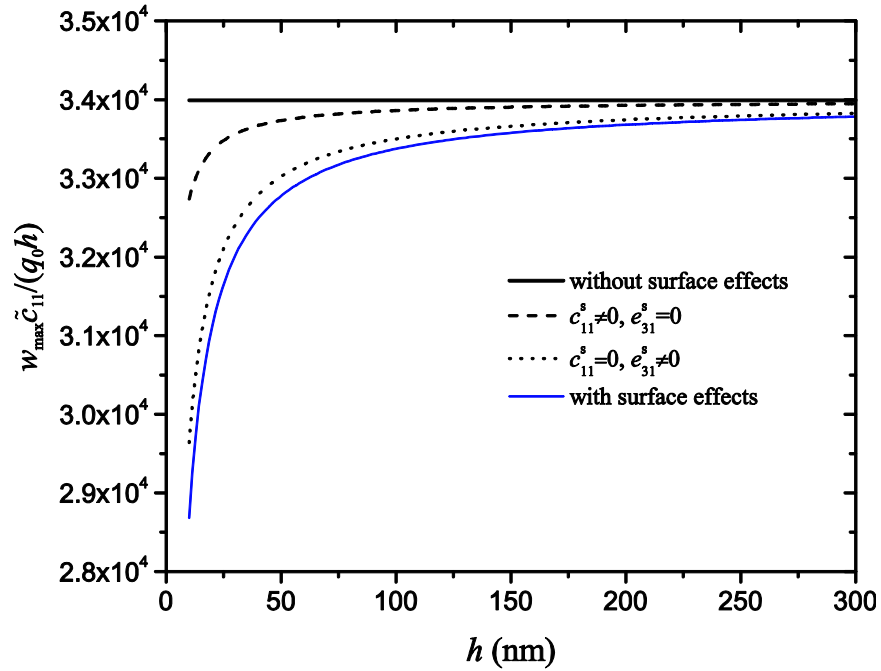
Figure 5.2: Variation of the dimensionless maximum deflection with plate thickness h ($a = b = 30h$).
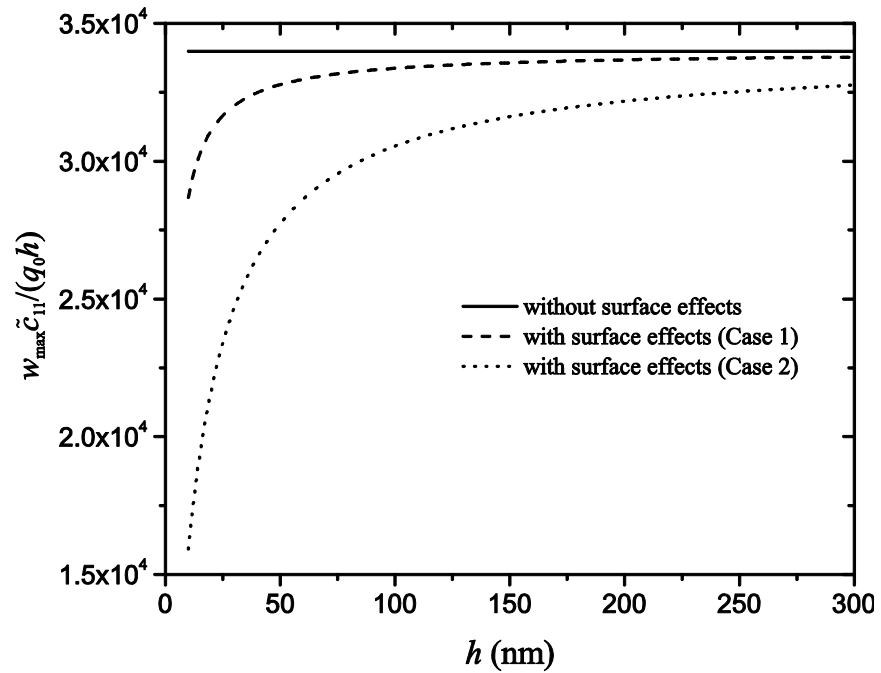
Figure 5.3: Influence of in-plane constraints on the out-plane deflection of the nanoplate.

also been obtained. It should be mentioned that when the in-plane constraint is set for the traction (case 1), the residual surface stress σ^0 induces the in-plane displacement relaxation, but has no effect on the out-plane deflection of the plate. However, when the

in-plane displacement is controlled without allowing for the displacement relaxation (case 2), the residual surface stress has a significant effect on the out-plane deflection as shown by the big discrepancy between the results predicted for two types of in-plane constraints in Fig. 5.3. These results indicate the significance of considering in-plane constraints for accurately modeling the physical properties of nanostructured materials.

For a plate with the in-plane constraints defined in case 2, when it is subjected to both a mechanical load q_0 and an electrical load V, the variation of the normalized deflection w_{max} / w_{max}^0 in the middle of the plate ($x = a/2$, $y = b/2$) with the plate thickness h is shown in Fig. 5.4 for the plate with different in-plane dimensions. w_{max}^0 is the deflection at the same point of the plate induced by the same electrical and mechanical loads without considering the surface effects. In order to avoid the mechanical buckling due to the applied voltage, negative voltage is applied to show this effect. Under this situation, the generalized effective axial forces N_{xx}^* and N_{yy}^* due to the applied V are tensile as indicated in Eqs. (5.26), therefore, no mechanical buckling of the plate will occur. From this figure, it is observed that the influence of the surface effects on the bending of the plate depends on the applied electrical load, $i.e.$ in general, the influence of the surface effects decreases with the increase in the applied electrical voltage amplitude. However, such dependence of the surface effects upon the electrical load varies with the in-plane dimensions of the plate. For example, when the length and the width are set as $a = b = 50h$ for a square plate, the influence of the applied voltage is very obvious when the plate thickness h is small. When the plate in-plane dimensions decrease, $a = b = 30h$ for example, such influence of the applied voltage becomes less. It is also indicated in this figure that with the increase of the plate in-plane dimensions, $i.e.$ a and b increase, the influence of the surface effects on the electroelastic responses is enhanced. Therefore, the surface effects are more prominent for the plate with larger aspect ratio. With the increase in the plate thickness, surface effects will eventually disappear as indicated by all the curves tending to approach unity.

When the in-plane constraints are set for the traction as discussed in case 1 in the previous section, the applied voltage in the z direction will induce the in-plane strain ε in both the x and y directions due to the 1-3 electromechanical coupling of the piezoelectric
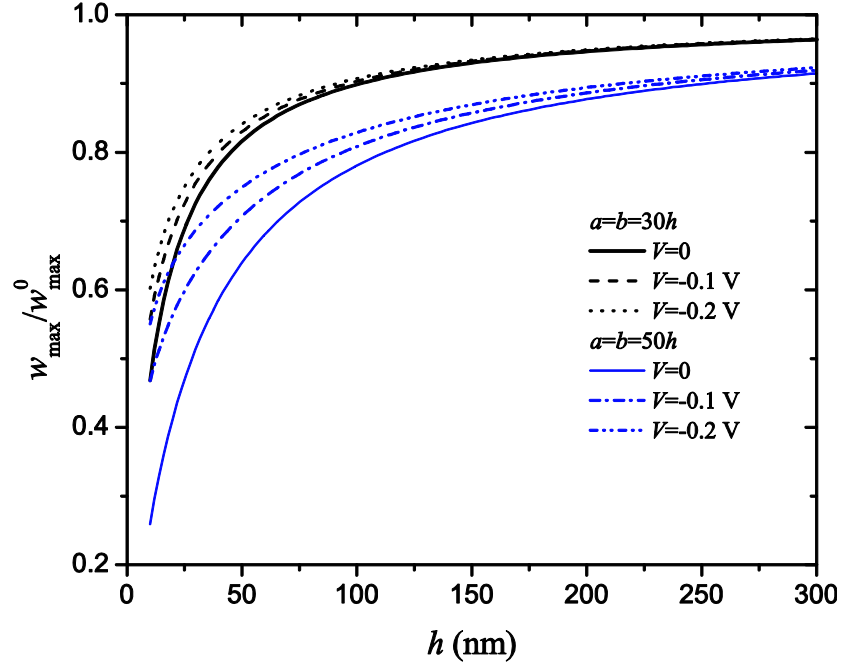
Figure 5.4: Variation of the normalized maximum deflection w_{max} / w_{max}^0 with plate thickness h.
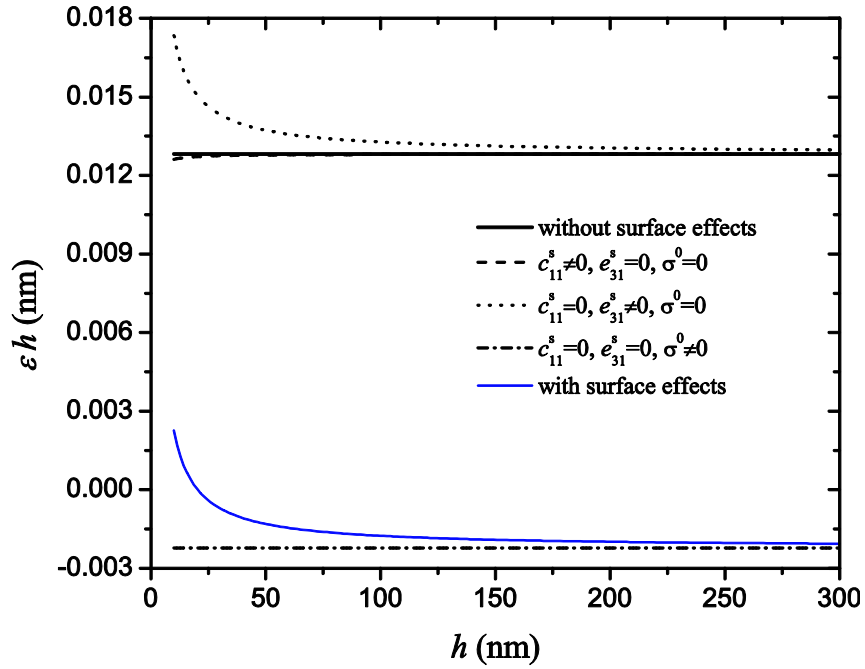
Figure 5.5: Variation of the in-plane strain with plate thickness h ($V = 0.1$ V).

materials. It is obvious from Eq. (5.18) that εh is a constant without the consideration of the surface effects. Therefore, the surface effects are represented by the size-dependence of this parameter εh as depicted in Fig. 5.5, in which the influence of the surface elasticity,

the residual surface stress and the surface piezoelectricity are studied separately for the plate. It is found that the surface elasticity has a negligible influence on the in-plane strain, while the influence of the surface piezoelectricity is prominent. Due to the in-plane displacement relaxation, the residual surface stress induces a constant εh as shown in Eq. (5.18) without considering the other surface effects. Thus, this relaxation significantly influences the electromechanical coupling of the piezoelectric nanoplate as shown by the big discrepancy between the two straight lines in this figure. It should be noted that this relaxation is independent of the plate in-plane dimensions a and b, which could be clearly observed from Eq. (5.18). Such a relaxation phenomenon has been observed and discussed by Park and Klein (2007) for an elastic nanowire using atomistic simulation. As indicated by Eq. (5.10), the surface effects may significantly influence the electric field distribution due to the electromechanical coupling, *i.e.* the first term in Eq. (5.10),

$$E_c = \frac{\tilde{e}_{31}}{\tilde{\kappa}_{33}}\left[\frac{\partial^2 w(x,y)}{\partial x^2} + \frac{\partial^2 w(x,y)}{\partial y^2}\right]z.$$ When the plate is subjected to a mechanical load q_0,

Fig. 5.6 plots the E_c / q_0 along the plate thickness z direction in the middle line of the plate ($x = a/2$ and $y = b/2$). It is observed in this figure that this electromechanical coupling induced electric field distributes linearly along the thickness direction, and is significantly influenced by the surface effects when the plate thickness is relatively small. For example $E_c / q_0 = \pm 2.97$ VmN^{-1} at $z/h = \pm 0.5$, decreasing 8.3% compared with $E_c / q_0 = \pm 3.24$ VmN^{-1} from the conventional plate model when $h = 20$ nm. When the plate thickness increases to $h = 100$ nm, surface effects are reduced as expected, $E_c / q_0 = \pm 3.19$ VmN^{-1} at $z/h = \pm 0.5$, decreasing 1.5% compared with the results from the conventional plate model.

The mechanical buckling of the piezoelectric plate is also an important issue for consideration. The cylindrical buckling of the piezoelectric nanoplate ($l = 30h$) with the surface effects is investigated when it is subjected to an in-plane compressive force along the x direction. Similar to the results obtained in Fig. 5.2, the dimensionless critical buckling load $N_{\text{cr}} / (h\tilde{c}_{11})$ from Eq. (5.30) is independent of the thickness of the nanoplate without the consideration of surface effects, as shown in Fig. 5.7. The separate
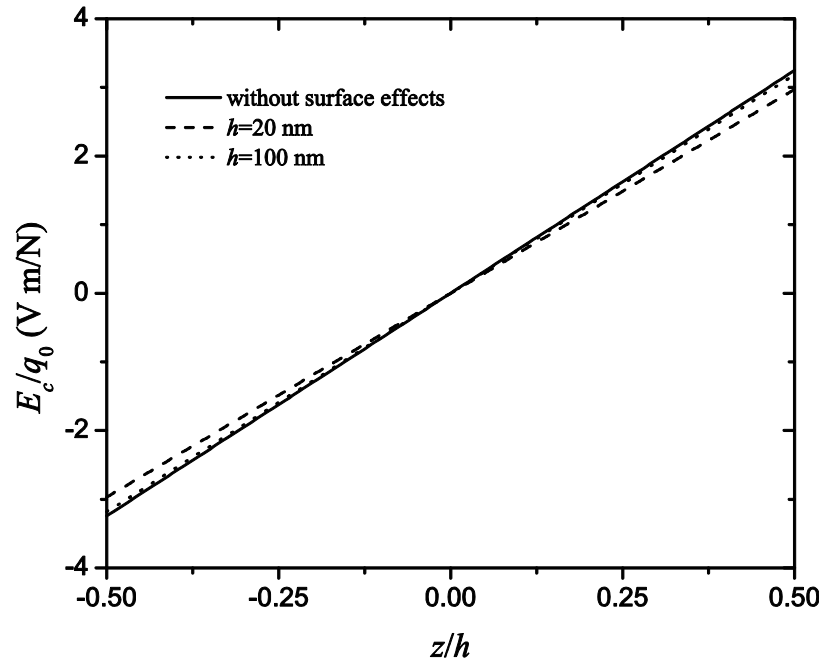
Figure 5.6: Variation of the electric field induced by the electromechanical coupling along the plate thickness z direction ($a = b = 30h$).
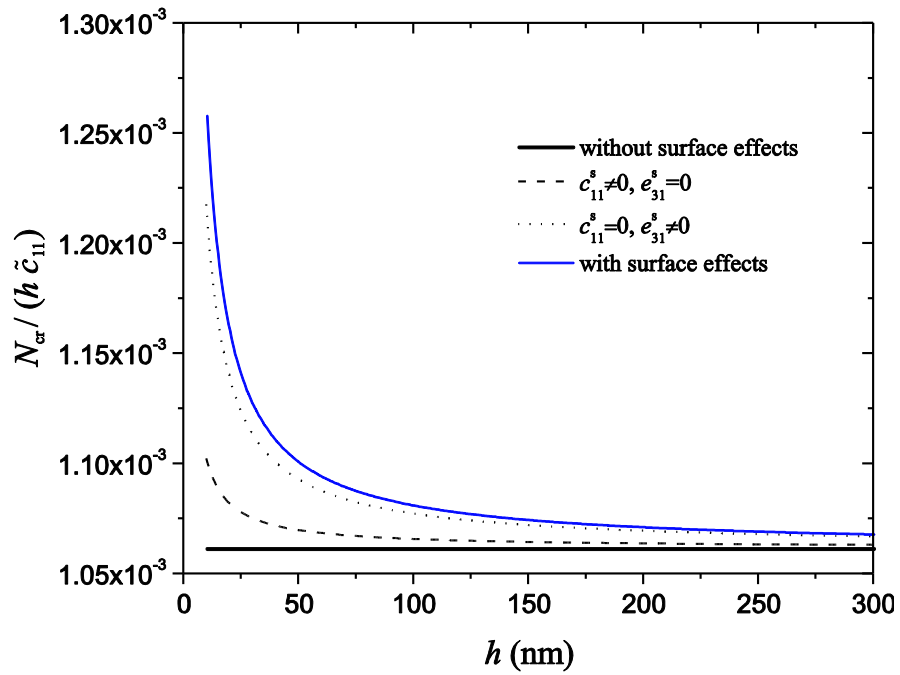
Figure 5.7: Variation of the dimensionless critical cylindrical buckling load with plate thickness h ($l = 30h$).
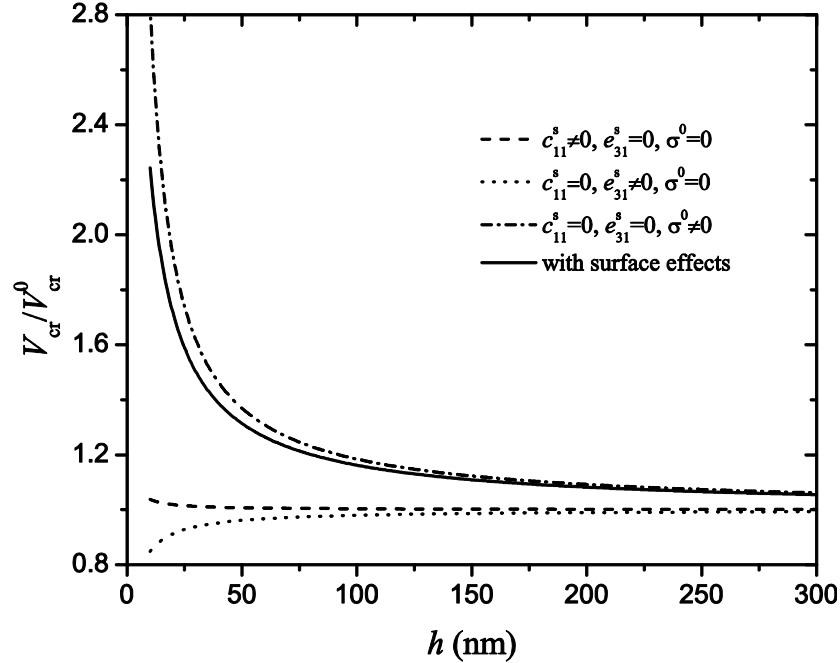
Figure 5.8: Variation of the normalized critical electric potential for cylindrical buckling with plate thickness h ($l = 30h$).

influence of the surface elasticity and the surface piezoelectricity upon this critical compressive load is studied. It is found in this figure that the surface piezoelectricity has more prominent effect in comparison with the surface elasticity, which means the necessity of using this surface piezoelectricity model in predicting the electroelastic responses of the piezoelectric plate, which has been ignored in the existing literature (Wang and Feng, 2010). It is also observed that the surface effects increase the critical buckling load significantly when h is small and this influence decreases with the increase in the nanoplate thickness. As discussed in the previous section, the applied electrical load may generate compressive force and induce the mechanical buckling when the in-plane displacements are constrained to zero. Fig. 5.8 depicts the normalized critical electric potential V_{cr} / V_{cr}^0 for buckling with the variation of the plate thickness h (V_{cr}^0 is the critical electric potential for buckling without the consideration of the surface effects). It is obvious that the influence of the surface effects on the critical electric potential for buckling is prominent when the plate thickness is small. For example, when the plate thickness $h = 10$ nm, the critical electric potential for buckling is more than 2.2 times the critical electric potential without considering the surface effects. The separate influence

of the surface elasticity, residual surface stress and surface piezoelectricity is also compared in Fig. 5.8. It is found that the surface elasticity and the residual surface stress increase this critical electric potential for buckling while the surface piezoelectricity decreases it. These results indicate the importance of considering surface effects in predicting the buckling behavior of piezoelectric plates at the nanoscale.

5.4   Conclusions

The size-dependent electroelastic responses of a piezoelectric plate with the nanoscale thickness have been theoretically and qualitatively investigated in this work. Based on the Kirchhoff plate theory, the surface effects including the surface elasticity, residual surface stress and surface piezoelectricity are incorporated into the differential governing equations and the boundary conditions via the surface piezoelectricity model and the generalized Young-Laplace equations. Simulation results are provided to show the surface effects upon the static bending and buckling behaviors of a simply supported piezoelectric nanoplate with different in-plane constraints. It is found that the out-plane deflection, the in-plane deformation, the electric field, the critical buckling load and the critical electric potential for mechanical buckling of the piezoelectric nanoplate under electromechanical loads are size dependent and such size dependence attributes to the surface effects. The influence of the surface effects on the electromechanical coupling of the piezoelectric plate is very significant when the plate thickness scales down to nanometers. With the increase of the plate thickness, such influence on the electroelastic responses of the plate diminishes and the predicted electromechanical behavior of the piezoelectric nanoplate approaches that for the conventional piezoelectric plate as expected. This work with more accurate modeling methodology for piezoelectric nanostructures is expected to provide helpful guidelines for the design and application of nanoplate based piezoelectric devices in NEMS.

References

Agrawal, R., Peng, B., Gdoutos, E. E. and Espinosa, H. D., 2008. Elasticity size effects in ZnO nanowires-a combined experimental-computational approach. Nano Lett. **8** 3668-3674.

Assadi, A. and Farshi, B., 2011. Size dependent vibration of curved nanobeams and rings including surface energies. Physica E **43**, 975-978.

Assadi, A., Farshi, B. and Alinia-Ziazi, A., 2010. Size dependent dynamic analysis of nanoplates. J. Appl. Phys. **107**, 124310.

Aydogdu, M., 2009. Axial vibration of the nanorods with the nonlocal continuum rod model. Physica E **41**, 861-864.

Cammarata, R. C., 1994. Surface and interface stress effects in thin films. Prog. Surf. Sci. **46**, 1-38.

Chen, C. Q., Shi, Y., Zhang, Y. S., Zhu, J. and Yan, Y. J., 2006a. Size dependence of Young's modulus in ZnO nanowires. Phys. Rev. Lett. **96**, 075505.

Chen, T. Y., Chiu, M. S. and Weng, C. N., 2006b. Derivation of the generalized Young-Laplace equation of curved interfaces in nanoscaled solids. J. Appl. Phys. **100**, 074308.

Dorfmann, A. and Ogden, R. W., 2005. Nonlinear electroelasticity. Acta Mech. **174**, 167-183.

Duan, W. H. and Wang, C. M., 2007. Exact solutions for axisymmetric bending of micro/nanoscale circular plates based on nonlocal plate theory. Nanotechnology **18**, 385704.

Eringen, A. C., 2002. Nonlocal continuum field theories, Springer, New York.

Feng, X., Yang, B. D., Liu, Y. M., Wang, Y., Dagdeviren, C., Liu, Z. J., Carlson, A., Li, J. Y., Huang, Y. G. and Rogers, J. A., 2011. Stretchable ferroelectric nanoribbons with wavy configurations on elastomeric substrates. ACS Nano **5**, 3326-3332.

Gurtin, M. E. and Murdoch, A. I., 1975. A continuum theory of elastic material surfaces. Arch. Ration. Mech. Anal. **57**, 291-323.

He, J. and Lilley, C. M., 2008a. Surface effect on the elastic behavior of static bending nanowires. Nano Lett. **8**, 1798-1802.

He, J. and Lilley, C. M., 2008b. Surface stress effect on bending resonance of nanowires with different boundary conditions. Appl. Phys. Lett. **93**, 263108.

He, J. H., Hsin, C. L., Liu, J., Chen, L. J. and Wang, Z. L., 2007. Piezoelectric gated diode of a single ZnO nanowire. Adv. Mater. **19**, 781-784.

Hu, Y. F., Chang, Y. L., Fei, P., Snyder, R. L. and Wang, Z. L., 2010. Designing the electric transport characteristics of ZnO micro/nanowire devices by coupling piezoelectric and photoexcitation effects. ACS Nano **4**, 1234-1240.

Huang, G. Y. and Yu, S. W., 2006. Effect of surface piezoelectricity on the electromechanical behaviour of a piezoelectric ring. Phys. Status Solidi-Rapid Res. Lett. **243**, R22-R24.

Lao, C. S., Kuang, Q., Wang, Z. L., Park, M. C. and Deng, Y. L., 2007. Polymer functionalized piezoelectric-FET as humidity/chemical nanosensors. Appl. Phys. Lett. **90**, 262107.

Lim, C. W. and He, L. H., 2004. Size-dependent nonlinear response of thin elastic films with nano-scale thickness. Int. J. Mech. Sci. **46**, 1715-1726.

Lin, Y. F., Song, J. H., Ding, Y., Lu, S. Y. and Wang, Z. L., 2008. Alternating the output of a CdS nanowire nanogenerator by a white-light-stimulated optoelectronic effect. Adv. Mater. **20**, 3127-3130.

Lu, P., Lee, H. P., Lu, C. and Zhang, P. Q., 2006a. Dynamic properties of flexural beams using a nonlocal elasticity model. J. Appl. Phys. **99**, 073510.

Lu, P., He, L. H., Lee, H. P. and Lu, C., 2006b. Thin plate theory including surface effects. Int. J. Solids Struct. **43**, 4631-4647.

Lu, T. Q., Zhang, W. X. and Wang, T. J., 2011. The surface effect on the strain energy release rate of buckling delamination in thin film–substrate systems. Int. J. Eng. Sci. **49**, 967-975.

Majdoub, M. S., Sharma, P. and Cagin, T., 2008a. Dramatic enhancement in energy harvesting for a narrow range of dimensions in piezoelectric nanostructures. Phys. Rev. B **78**, 121407(R).

Majdoub, M. S., Sharma, P. and Cagin, T., 2008b. Enhanced size-dependent piezoelectricity and elasticity in nanostructures due to the flexoelectric effect. Phys. Rev. B **77**, 125424.

Miller, R. E. and Shenoy, V. B., 2000. Size-dependent elastic properties of nanosized structural elements. Nanotechnology **11**, 139-147.

Murmu, T. and Pradhan, S. C., 2009. Vibration analysis of nano-single-layered graphene sheets embedded in elastic medium based on nonlocal elasticity theory. J. Appl. Phys. **105**, 064319.

Pan, X. H., Yu, S. W. and Feng, X. Q., 2011. A continuum theory of surface piezoelectricity for nanodielectrics. Sci. China-Phys. Mech. Astron. **54**, 564-573.

Park, H. S. and Klein, P. A., 2007. Surface Cauchy-Born analysis of surface stress effects on metallic nanowires. Phys. Rev. B **75**, 085408.

Park, K.-I., Xu, S., Liu, Y., Hwang, G.-T., Kang, S. J. L., Wang, Z. L. and Lee, K. J., 2010. Piezoelectric $BaTiO_3$ thin film nanogenerator on plastic substrates. Nano Lett. **10**, 4939-4943.

Qi, Y., Jafferis, N. T., Lyons, K., Lee, C. M., Ahmad, H. and McAlpine, M. C., 2010. Piezoelectric ribbons printed onto rubber for flexible energy conversion. Nano Lett. **10**, 524-528.

Stan, G., Ciobanu, C. V., Parthangal, P. M. and Cook, R. F., 2007. Diameter-dependent radial and tangential elastic moduli of ZnO nanowires. Nano Lett. **7**, 3691-3697.

Su, W. S., Chen, Y. F., Hsiao, C. L. and Tu, L. W., 2007. Generation of electricity in GaN nanorods induced by piezoelectric effect. Appl. Phys. Lett. **90**, 063110.

Xu, S., Hansen, B. J. and Wang, Z. L., 2010. Piezoelectric-nanowire-enabled power source for driving wireless microelectronics. Nature Commun. **1**, 93.

Wang, C. M. and Duan, W. H., 2008. Free vibration of nanorings/arches based on nonlocal elasticity. J. Appl. Phys. **104**, 014303.

Wang, G. F. and Feng, X. Q., 2007. Effects of surface elasticity and residual surface tension on the natural frequency of microbeams. Appl. Phys. Lett. **90**, 231904.

Wang, G. F. and Feng, X. Q., 2010. Effect of surface stresses on the vibration and buckling of piezoelectric nanowires. EPL **91**, 56007.

Wang, G. F., Feng, X. Q. and Yu, S. W., 2007. Surface buckling of a bending microbeam due to surface elasticity. EPL **77**, 44002.

Wang, X. B., Song, J. H., Zhang, F., He, C. Y., Hu, Z. and Wang, Z. L., 2010. Electricity generation based on one-dimensional group-III nitride nanomaterials. Adv. Mater. **22**, 2155-2158.

Wang, X. D., Zhou, J., Song, J. H., Liu, J., Xu, N. S. and Wang, Z. L., 2006. Piezoelectric field effect transistor and nanoforce sensor based on a single ZnO nanowire. Nano Lett. **6**, 2768-2772.

Wang, Z. L. and Song, J. H., 2006. Piezoelectric nanogenerators based on zinc oxide nanowire arrays. Science **312**, 242-246.

Wang, Z. Y., Hu, J., Suryavanshi, A. P., Yum, K. and Yu, M. F., 2007. Voltage generation from individual $BaTiO_3$ nanowires under periodic tensile mechanical load. Nano Lett. **7**, 2966-2969.

Yan, Z. and Jiang, L. Y., 2011a. Surface effects on the electromechanical coupling and bending behaviours of piezoelectric nanowires. J. Phys. D: Appl. Phys. **44**, 075404.

Yan, Z. and Jiang, L. Y., 2011b. The vibrational and buckling behaviors of piezoelectric nanobeams with surface effects. Nanotechnology **22**, 245703.

Yan, Z. and Jiang, L. Y., 2011c. Electromechanical response of a curved piezoelectric nanobeam with the consideration of surface effects. J. Phys. D: Appl. Phys. **44**, 365301.

Zhang, T. Y., Wang, Z. J. and Chan, W. K., 2010. Eigenstress model for surface stress of solids. Phys. Rev. B **81**, 195427.

Zhang, Y. H., Hong, J. W., Liu, B. and Fang, D. N., 2010. Strain effect on ferroelectric behaviors of $BaTiO_3$ nanowires: a molecular dynamics study. Nanotechnology **21**,015701.

Zhao, M. H., Wang, Z. L. and Mao, S. X., 2004. Piezoelectric characterization of individual zinc oxide nanobelt probed by piezoresponse force microscope. Nano Lett. **4**, 587-590.

Zhao, M., Qian, C., Lee, S. W. R., Tong, P., Suemasu, H. and Zhang, T. Y., 2007. Electro-elastic analysis of piezoelectric laminated plates. Adv. Compos. Mater. **16**, 63-81.

Chapter 6

6 Vibration and buckling analysis of a piezoelectric nanoplate considering surface effects and in-plane constraints[5]

6.1 Introduction

Since the first prototyping of a nanogenerator by means of piezoelectric nanowire arrays (Wang and Song, 2006), piezoelectric nanostructured materials have attracted tremendous interests in the research community for potential applications of various devices in the nanotechnology, such as nanosensors, nanoresonators, nanogenerators and nanotransistors (Lao *et al*., 2007; Su *et al*., 2007; Tanner *et al*., 2007; Fei *et al*., 2009). Most recently, piezoelectric thin films or nanoribbons (lead zirconate titanate (PZT) and BaTiO$_3$) have been successfully transferred onto flexible substrates for stretchable energy harvesting, which suggest new possible applications of piezoelectric nanomaterials (Park *et al*., 2010; Feng *et al*., 2011; Qi *et al*., 2011). Among these novel nanodevices, nanoscale piezoelectric beam or plate structures are the key components. Therefore, understanding the mechanical and physical behaviors of piezoelectric nanostructures with these configurations is essential for their design and applications.

"Small is different", the mechanical properties of piezoelectric nanostructures can differ markedly from their macroscopic counterparts. Owing to the increasing aspect ratio of surface area to volume at the nanoscale, it is believed that size dependence of the mechanical properties and piezoelectricity due to the surface effects will arise. Existing experiments and atomistic simulations have confirmed that the elastic and piezoelectric coefficients of piezoelectric nanostructures vary with their dimensions (Zhao *et al*., 2004; Chen *et al*., 2006a; Zhang and Huang, 2006; Stan *et al*., 2007; Agrawal *et al*., 2008; Zhang *et al*., 2010a). Owing to the extreme difficulty in conducting experiments and computational expensiveness of atomistic studies, modified continuum theories

---

[5]A version of this chapter has been published.

Yan, Z. and Jiang, L.Y., Proc. R. Soc. A 468, 3458-3475, (2012).

incorporating the surface effects have been naturally pursued as alternative and effective tools in mechanical and physical property characterization of nanostructured materials.

For elastic nanostructures, the size-dependent properties have been well studied using modified continuum theories based on the well-known surface elasticity model developed by Gurtin and Murdoch (1975). In addition to the studies on the static and dynamic behaviors of nanobeams (Wang and Feng, 2007; 2009; He and Lilley, 2008a; b; Liu and Rajapakse, 2010), this surface elasticity model has also been adopted for modeling the elastic nanoplates. For example, Lim and He (2004) investigated surface effects on the large deflection of an ultra-thin film using the von Karman plate theory. Lu *et al*. (2006) used modified Kirchhoff and Mindlin plate models to characterize the bending, vibration and buckling behaviors of nanoscale plates with surface effects. The transverse vibration of a rectangular nanoplate was investigated by Assadi *et al*. (2010) considering the influence of surface properties and temperature. The free vibration of a circular nanoplate, including the surface effects, was also investigated using a modified laminated plate theory (Assadi and Farshi, 2010). However, the investigation on the size-dependent properties of piezoelectric nanostructures using continuum modeling approaches is still very limited, especially for piezoelectric nanoplates (PNPs). The surface elasticity model was used by Wang and Feng (2010) to study the vibration and buckling of a piezoelectric nanobeam, while the surface piezoelectricity was ignored. As an extension of the surface elasticity model, Huang and Yu (2006) carried out pioneering work in proposing a surface piezoelectricity model to study the effect of piezoelectric surface layers on the static deformation of a piezoelectric nanoring. This surface piezoelectricity model has been further applied in our previous work (Yan and Jiang, 2011a; b; c) to study the surface effects on the static electroelastic responses and vibration behavior of flat and curved piezoelectric nanobeams. Li *et al*. (2011) studied surface effects on the wrinkling of a piezoelectric nanofilm on a compliant substrate by modeling the film structure as a von Karman beam. Recently, a comprehensive model has been developed for dielectric nanomaterials by Shen and Hu (2010) with the consideration of surface effects, flexoelectricity and electrostatic forces. It should be mentioned that another type of modified continuum model has also been explored by researchers to investigate the size effects. For example, the vibration of piezoelectric

nanobeams was investigated recently either based on a linear or a von Karman strain-displacement relation (Ke and Wang, 2012; Ke *et al*., 2012). They discussed the influence of the non-local parameter, temperature change and external electric voltage on the thermo-electro-mechanical vibration characteristics of the piezoelectric nanobeams. These studies have demonstrated the significance of considering size effects in studying the mechanical and physical properties of piezoelectric nanostructures.

To the authors' best knowledge, the influence of the surface effects on the vibrational behavior of PNPs has not been studied thus far. This work, therefore, will carry out an investigation for this purpose. Owing to the intrinsic electromechanical coupling of piezoelectric materials and the existence of surface stresses in surface layers, either in-plane forces or in-plane displacements may develop in the PNP depending on the in-plane constraints prescribed. It should be mentioned that such in-plane relaxation strains of elastic nanowires owing to the surface stresses have been discussed in literature by using atomistic or atomistic-based theories (Park and Klein, 2007; Zhang *et al*., 2010b; Park, 2012). In addition, by considering a relaxation process before bending deformation, Song *et al.* (2011) studied the mechanical behavior of nanowires by using a continuum model. The results in these studies suggest that accounting for axial strain relaxation may be necessary to improve the accuracy and predictive capability of analytical surface elastic theories. However, this surface-stress-induced relaxation phenomenon has not been accounted in the previous investigations of the nanoplates with surface effects (Lim and He, 2004; Lu *et al*., 2006; Assadi and Farshi, 2010; Assadi *et al*., 2010), owing to their particular prescribed in-plane boundary conditions. Therefore, different in-plane constraints will be defined in this work in order to catch all the possible phenomena induced by the surface effects. As a result, distinct vibration behavior and in-plane motions of the PNPs will be observed under different in-plane boundary conditions.

6.2 Formulation

The vibration analysis of a rectangular PNP with length a, width b and thickness h as illustrated in Fig. 6.1a is conducted in the current work. A Cartesian coordinate system (x, y, z) is used to describe the plate with z along the plate thickness direction and the x-y plane sitting on the midplane of the undeformed plate. The piezoelectric body is poled

along the *z*-direction and subjected to an electric potential *V* between the upper and lower surfaces of the plate. For a piezoelectric nanobeam subjected to an electric potential across its thickness (Wang and Feng, 2010), the authors argued that the electric field component in the length direction is negligible compared with that in the thickness direction according to the available numerical simulation results (Gao and Wang, 2007). Therefore, for a thin piezoelectric plate with large in-plane dimension to thickness ratio, it is reasonable to neglect the in-plane electric field components when the plate is subjected to an electric potential across its thickness, which has been adopted by Zhao *et al.* (2007). Therefore, in this work, the electric field is assumed to exist only along the *z*-direction and can be expressed in terms of the electric potential Φ

$$E_z = -\frac{\partial \Phi}{\partial z},$$
(6.1)

The electric boundary conditions are prescribed as Φ(*h*/2)=*V* and Φ(−*h*/2)=0 according to Fig. 6.1a.
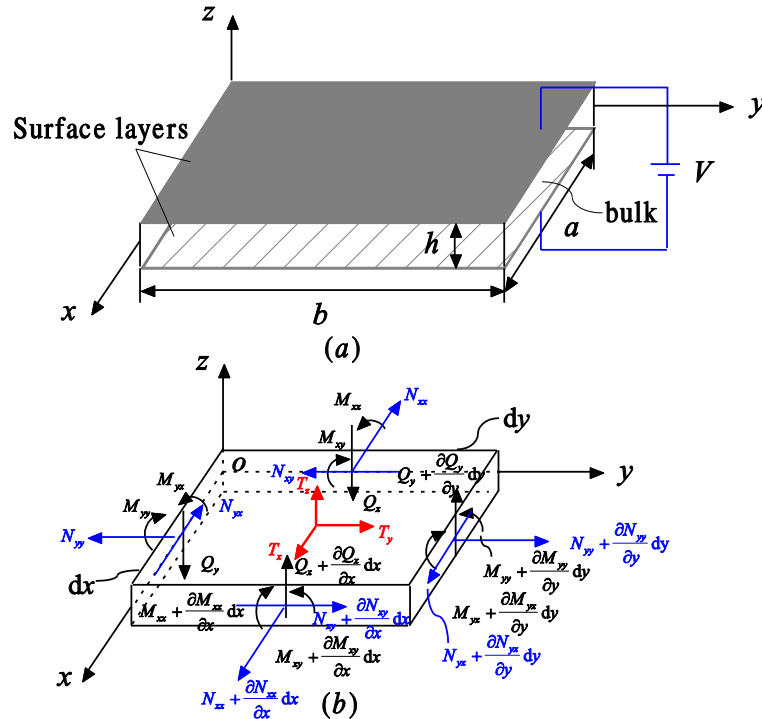
Figure 6.1: (*a*) A piezoelectric nanoplate with both bulk and surface parts. (*b*) Schematic of a differential element of the piezoelectric nanoplate.

To account for the surface effects, a surface piezoelectricity model (Huang and Yu, 2006; Yan and Jiang 2011a; b) is adopted here. According to this model, the PNP is considered as being composed of a bulk part and the upper and lower surface layers with negligible thickness. For the bulk part, the material obeys the same constitutive relations as the conventional piezoelectric materials. With the plane stress assumption that the stress component in the z-direction is negligible (Zhao *et al.*, 2007), the linear constitutive equations for the bulk part are written as

$$\left.\begin{aligned}
\sigma_{xx} &= c_{11}\varepsilon_{xx} + c_{12}\varepsilon_{yy} - e_{31}E_z; \\
\sigma_{yy} &= c_{12}\varepsilon_{xx} + c_{11}\varepsilon_{yy} - e_{31}E_z; \\
\sigma_{xy} &= c_{66}\gamma_{xy}; \\
D_z &= e_{31}\varepsilon_{xx} + e_{31}\varepsilon_{yy} + \kappa_{33}E_z,
\end{aligned}\right\} \tag{6.2}$$

where c_{11}, c_{12} and c_{66} are bulk elastic constants; e_{31} and κ_{33} are bulk piezoelectric and dielectric constants, respectively.

For the surface layers, the constitutive equations are different from those of the bulk, which can be expressed according to the surface piezoelectricity model (Huang and Yu, 2006)

$$\left.\begin{aligned}
\sigma_{xx}^{s} &= \sigma_{xx}^{0} + c_{11}^{s}\varepsilon_{xx} + c_{12}^{s}\varepsilon_{yy} - e_{31}^{s}E_z; \\
\sigma_{yy}^{s} &= \sigma_{yy}^{0} + c_{12}^{s}\varepsilon_{xx} + c_{11}^{s}\varepsilon_{yy} - e_{31}^{s}E_z; \\
\sigma_{xy}^{s} &= \sigma_{xy}^{0} + c_{66}^{s}\gamma_{xy}; \\
D_x^{s} &= D_x^{0}; \\
D_y^{s} &= D_y^{0},
\end{aligned}\right\} \tag{6.3}$$

where $\sigma_{\alpha\beta}^{s}(\alpha,\beta=x,y)$ and $D_{\alpha}^{s}(\alpha=x,y)$ are surface stresses and surface electric displacements; c_{11}^{s}, c_{12}^{s}, c_{66}^{s} are surface elastic constants; e_{31}^{s} is the surface piezoelectric constant; $\sigma_{\alpha\beta}^{0}(\alpha,\beta=x,y)$ and $D_{\alpha}^{0}(\alpha=x,y)$ are residual surface stress and residual surface electric displacement without applied strain and electric field.

The existence of the surface stresses of the PNP induces traction jumps exerted on the bulk of the plate, which has been commonly adopted in the surface elasticity model and surface piezoelectric model for nanostructures with a variety of configurations

(Huang and Yu, 2006; Lu *et al.*, 2006; Wang and Feng, 2007; 2009; He and Lilley 2008a; b; Yan and Jiang 2011a; b; c; Li *et al.*, 2011). According to the generalized Young-Laplace equations (Chen *et al.*, 2006b), these traction jumps T_x, T_y and T_z with the consideration of the plate deformation can be expressed as

$$\left.\begin{aligned}
T_x &= \frac{\partial \sigma_{xx}^{s}}{\partial x} + \frac{\partial \sigma_{yx}^{s}}{\partial y}; \\
T_y &= \frac{\partial \sigma_{xy}^{s}}{\partial x} + \frac{\partial \sigma_{yy}^{s}}{\partial y}; \\
T_z^{u} &= \sigma_{xx}^{s} \frac{\partial^2 w}{\partial x^2} + 2\sigma_{xy}^{s} \frac{\partial^2 w}{\partial x \partial y} + \sigma_{yy}^{s} \frac{\partial^2 w}{\partial y^2}; \\
T_z^{l} &= -\sigma_{xx}^{s} \frac{\partial^2 w}{\partial x^2} - 2\sigma_{xy}^{s} \frac{\partial^2 w}{\partial x \partial y} - \sigma_{yy}^{s} \frac{\partial^2 w}{\partial y^2},
\end{aligned}\right\}$$

(6.4)

where the superscripts 'u' and 'l' represent the upper and lower surfaces of the plate.

In order to make a vibration analysis for the PNP, a Kirchhoff plate model is used for modeling purposes. According to Kirchhoff's hypotheses, the displacements of the plate can be expressed as

$$\left.\begin{aligned}
u(x, y, z, t) &= u^0(x, y, t) - z \frac{\partial w(x, y, t)}{\partial x}; \\
v(x, y, z, t) &= v^0(x, y, t) - z \frac{\partial w(x, y, t)}{\partial y}; \\
w(x, y, z, t) &= w(x, y, t),
\end{aligned}\right\}$$

(6.5)

where $w(x, y, t)$ is the transverse displacement; $u^0(x, y, t)$ and $v^0(x, y, t)$ are the in-plane displacements of the midplane describing the membrane deformations. For an elastic bulk plate, these in-plane displacements are assumed as zero, according to conventional Kirchhoff plate theory. However, they may not be zero for the PNP, for example, the applied electrical load induces the in-plane displacements of the midplane owing to the electromechanical coupling. In addition, the existence of surface stresses may also cause the in-plane relaxation displacements, as discussed in the literature (Park and Klein, 2007; Zhang *et al.*, 2010b; Park 2012), *i.e.* for a PNP that is allowed to have free in-plane movement, when it is at equilibrium after relaxation without any applied external loads,

the bulk part usually presents initial in-plane deformations owing to the residual surface stresses. According to the displacement fields of equation (6.5), the in-plane strain fields can be obtained from

$$\varepsilon_{xx} = \frac{\partial u^0}{\partial x} - z\frac{\partial^2 w}{\partial x^2};\ \varepsilon_{yy} = \frac{\partial v^0}{\partial y} - z\frac{\partial^2 w}{\partial y^2};\ \gamma_{xy} = \frac{\partial u^0}{\partial y} + \frac{\partial v^0}{\partial x} - 2z\frac{\partial^2 w}{\partial x\partial y}. \tag{6.6}$$

For a differential element of the plate composed of the surface layers and the bulk part as shown in Fig. 6.1b, the motion equations are derived as

$$\left.\begin{aligned}
&\frac{\partial N_{xx}}{\partial x} + \frac{\partial N_{xy}}{\partial y} + T_x^{\mathrm{u}} + T_x^{\mathrm{l}} = \rho h\frac{\partial^2 u^0}{\partial t^2}; \\[4pt]
&\frac{\partial N_{xy}}{\partial x} + \frac{\partial N_{yy}}{\partial y} + T_y^{\mathrm{u}} + T_y^{\mathrm{l}} = \rho h\frac{\partial^2 v^0}{\partial t^2}; \\[4pt]
&\frac{\partial Q_x}{\partial x} + \frac{\partial Q_y}{\partial y} + T_z^{\mathrm{u}} - T_z^{\mathrm{l}} + q_z = \rho h\frac{\partial^2 w}{\partial t^2}; \\[4pt]
&\frac{\partial M_{xx}}{\partial x} + \frac{\partial M_{yx}}{\partial y} + Q_x - (T_x^{\mathrm{u}} - T_x^{\mathrm{l}})\frac{h}{2} = \frac{\rho h^3}{12}\frac{\partial^2}{\partial t^2}\left(\frac{\partial w}{\partial x}\right); \\[4pt]
&\frac{\partial M_{xy}}{\partial x} + \frac{\partial M_{yy}}{\partial y} + Q_y - (T_y^{\mathrm{u}} - T_y^{\mathrm{l}})\frac{h}{2} = \frac{\rho h^3}{12}\frac{\partial^2}{\partial t^2}\left(\frac{\partial w}{\partial y}\right),
\end{aligned}\right\} \tag{6.7}$$

where $N_{\alpha\beta}$ and Q_α are axial and shear forces with dimension of force per unit length, and $M_{\alpha\beta}$ is bending moment with dimension of moment per unit length. The axial forces and bending moments are related to stresses by $N_{\alpha\beta} = \int_{-h/2}^{h/2}\sigma_{\alpha\beta}\mathrm{d}z$ and $M_{\alpha\beta} = -\int_{-h/2}^{h/2}\sigma_{\alpha\beta}z\mathrm{d}z$, respectively. ρ is the mass density of the material. The transverse load q_z in the third equation is induced by the in-plane loads $N_{\alpha\beta}$ and the traction jumps, which can be derived as $q_z = N_{xx}\partial^2 w/\partial x^2 + 2N_{xy}\partial^2 w/\partial x\partial y + N_{yy}\partial^2 w/\partial y^2$, with the consideration of the first two equations of Eqs. (6.7).

In the absence of free electric charges, the electric displacement should satisfy the Gauss's law

$$\frac{\partial D_x}{\partial x} + \frac{\partial D_y}{\partial y} + \frac{\partial D_z}{\partial z} = 0. \tag{6.8}$$

Under the assumption that the electric field exists only in the z-direction, D_x and D_y are equal to zero and D_z is given in Eqs. (6.2). Solving the above equation with the applied electric boundary conditions results in the electric potential and electric field

$$\Phi = -\frac{e_{31}}{2\kappa_{33}}\left(\frac{\partial^2 w}{\partial x^2}+\frac{\partial^2 w}{\partial y^2}\right)\left(z^2-\frac{h^2}{4}\right)+\frac{V}{h}z+\frac{V}{2}\,;\, E_z = \frac{e_{31}}{\kappa_{33}}\left(\frac{\partial^2 w}{\partial x^2}+\frac{\partial^2 w}{\partial y^2}\right)z-\frac{V}{h}. \tag{6.9}$$

After the manipulation of the last three equations of (6.7) with the consideration of q_z defined earlier, the motion equation of the PNP for the transverse vibration can be derived as

$$\frac{\partial^2 M_{xx}^*}{\partial x^2}+2\frac{\partial^2 M_{xy}^*}{\partial x\partial y}+\frac{\partial^2 M_{yy}^*}{\partial y^2}+\rho h\frac{\partial^2 w}{\partial t^2}-\frac{\rho h^3}{12}\frac{\partial^2}{\partial t^2}\left(\frac{\partial^2 w}{\partial x^2}+\frac{\partial^2 w}{\partial y^2}\right)$$
$$=N_{xx}^*\frac{\partial^2 w}{\partial x^2}+2N_{xy}^*\frac{\partial^2 w}{\partial x\partial y}+N_{xx}^*\frac{\partial^2 w}{\partial y^2}, \tag{6.10}$$

where $N_{\alpha\beta}^*$ and $M_{\alpha\beta}^*$ are the generalized resultant forces and moments with the consideration of surface effects, which are defined by Lu *et al.* (2006)

$$N_{\alpha\beta}^* = N_{\alpha\beta}+\left(\sigma_{\alpha\beta}^s\right)^u+\left(\sigma_{\alpha\beta}^s\right)^l\,;\, M_{\alpha\beta}^* = M_{\alpha\beta}-\frac{h}{2}\left[\left(\sigma_{\alpha\beta}^s\right)^u-\left(\sigma_{\alpha\beta}^s\right)^l\right]. \tag{6.11}$$

It is obvious that without considering the surface effects, *i.e.* $N_{\alpha\beta}^* = N_{\alpha\beta}$ and $M_{\alpha\beta}^* = M_{\alpha\beta}$, the motion equation (6.10) is reduced to that for a conventional Kirchhoff plate (Reddy, 2007).

For case study, the vibrational behavior of a simply supported PNP is investigated with boundary conditions described by the out-plane displacement and the generalized resultant moments

$$w = 0,\, M_{xx}^* = 0 \text{ at } x = 0,\, x = a\,;\, w = 0,\, M_{yy}^* = 0 \text{ at } y = 0,\, y = b. \tag{6.12}$$

In addition to these boundary conditions, the in-plane boundary conditions for the PNP must also be prescribed in order to solve the motion equation (6.10).

These in-plane boundary conditions depend on the in-plane constraints, which are listed as the following two cases:

1. $N_{xx}^* = N_{xy}^* = 0$ at $x = 0, x = a$; $N_{yy}^* = N_{xy}^* = 0$ at $y = 0, \ y = b$.

This is a traction-free boundary condition on all the edges of the PNP. Assuming $\sigma_x^0 = \sigma_y^0 = \sigma^0$ and $\sigma_{xy}^0 = 0$, then equation (6.10) is rewritten in terms of the transverse displacement w as

$$D_{11}\left(\frac{\partial^4 w}{\partial x^4} + \frac{\partial^4 w}{\partial y^4}\right) + 2\left(D_{12} + 2D_{66}\right)\frac{\partial^4 w}{\partial x^2 \partial y^2} + \rho h \frac{\partial^2 w}{\partial t^2} - \frac{\rho h^3}{12}\frac{\partial^2}{\partial t^2}\left(\frac{\partial^2 w}{\partial x^2} + \frac{\partial^2 w}{\partial y^2}\right) = 0, \qquad (6.13)$$

with

$$\left.\begin{aligned} D_{11} &= \left(c_{11} + \frac{e_{31}^2}{\kappa_{33}}\right)\frac{h^3}{12} + \left(c_{11}^s + \frac{e_{31}^s e_{31}}{\kappa_{33}}\right)\frac{h^2}{2}; \\ D_{12} &= \left(c_{12} + \frac{e_{31}^2}{\kappa_{33}}\right)\frac{h^3}{12} + \left(c_{12}^s + \frac{e_{31}^s e_{31}}{\kappa_{33}}\right)\frac{h^2}{2}; \\ D_{66} &= \frac{c_{66}h^3}{12} + \frac{c_{66}^s h^2}{2}. \end{aligned}\right\} \qquad (6.14)$$

It should be mentioned that with these in-plane constraints, in-plane strains will be induced owing to the inherent electromechanical coupling of piezoelectric materials and the surface effects, which are derived from the first two equations of Eqs. (6.7) as

$$\varepsilon = -\frac{e_{31}V + 2\left[\sigma^0 + e_{31}^s\left(V/h\right)\right]}{\left(c_{11} + c_{12}\right)h + 2\left(c_{11}^s + c_{12}^s\right)}. \qquad (6.15)$$

It is obvious that without the applied electrical load (*i.e.* $V = 0$), the residual surface stress will still induce a relaxation strain for elastic nanomaterials, *i.e.* $\varepsilon_{\text{relax}} = -2\sigma^0 / \left[\left(c_{11} + c_{12}\right)h + 2\left(c_{11}^s + c_{12}^s\right)\right]$. However, this relaxation was not considered in the previous studies on the elastic nanoplate (Lim and He, 2004; Lu *et al*., 2006; Assadi and Farshi, 2010; Assadi *et al*., 2010) using modified continuum mechanics models, while atomistic or atomistic-based studies have confirmed and discussed this phenomenon (Park and Klein, 2007; Zhang *et al*., 2010b; Park 2012).

2. $u^0\left(x, y\right) = v^0\left(x, y\right) = 0$

This can be realized by clamping the edges of the PNP without in-plane movement. In this case, the in-plane displacements are assumed to be trivial compared with the transverse deflection as defined by conventional Kirchhoff plate theory. It should be noted that this boundary condition was adopted by Zhao *et al.* (2007) when conducting the electro-elastic analysis of a conventional piezoelectric plate. The equation governing the transverse vibration of the PNP is then simplified as

$$
D_{11}\left(\frac{\partial^4 w}{\partial x^4}+\frac{\partial^4 w}{\partial y^4}\right)+2\left(D_{12}+2D_{66}\right)\frac{\partial^4 w}{\partial x^2 \partial y^2}+\rho h\frac{\partial^2 w}{\partial t^2}-\frac{\rho h^3}{12}\frac{\partial^2}{\partial t^2}\left(\frac{\partial^2 w}{\partial x^2}+\frac{\partial^2 w}{\partial y^2}\right)
$$
$$
=\left[2\left(\sigma^0+e_{31}^{s}\frac{V}{h}\right)+e_{31}V\right]\left(\frac{\partial^2 w}{\partial x^2}+\frac{\partial^2 w}{\partial y^2}\right). \tag{6.16}
$$

We can see that under this condition, the electric potential and residual surface-stress-induced axial force $P=2\left(\sigma^0+e_{31}^{s}V/h\right)+e_{31}V$ will influence the transverse vibration of the PNP. Once this force becomes compressive, it may cause the mechanical buckling of the plate, as observed for the piezoelectric nanobeams in literature (Wang and Feng, 2010; Yan and Jiang, 2011b).

According to the boundary conditions of Eq. (6.12), the harmonic solution of Eqs. (6.13) and (6.16) can be expressed as

$$
w=\sum_{m=1}^{\infty}\sum_{n=1}^{\infty}W_{mn}\sin\frac{m\pi x}{a}\sin\frac{n\pi y}{b}\mathrm{e}^{i\omega t}, \tag{6.17}
$$

where W_{mn} is a constant representing the mode shape amplitude, m and n are the half wave numbers, and ω is the resonant frequency.

Substituting Eq. (6.17) into Eqs. (6.13) and (6.16), respectively, the square of the resonant frequency can be obtained for case 1 as

$$
\left(\omega_{mn}^{(1)}\right)^2=\frac{D_{11}\left(m^4\pi^4/a^4+n^4\pi^4/b^4\right)+2\left(D_{12}+2D_{66}\right)\left(m^2 n^2\pi^4/a^2 b^2\right)}{\rho h+\left(\rho h^3/12\right)\left(m^2\pi^2/a^2+n^2\pi^2/b^2\right)}, \tag{6.18}
$$

and for case 2 as

$$\left(\omega_{mn}^{(2)}\right)^2 = \frac{1}{\rho h + \left(\rho h^3 / 12\right)\left(m^2\pi^2 / a^2 + n^2\pi^2 / b^2\right)}$$

$$\times \left\{ D_{11}\left(\frac{m^4\pi^4}{a^4} + \frac{n^4\pi^4}{b^4}\right) + 2\left(D_{12} + 2D_{66}\right)\frac{m^2 n^2 \pi^4}{a^2 b^2} + \left[2\left(\sigma^0 + e_{31}^s \frac{V}{h}\right) + e_{31}V\right]\left(\frac{m^2\pi^2}{a^2} + \frac{n^2\pi^2}{b^2}\right)\right\}.$$

$$(6.19)$$

The mechanical buckling of the PNP is also an interesting phenomenon that requires further investigation. By letting $\omega_{mn}^{(2)} = 0$ in Eq. (6.19), the electric voltage V_{mn} corresponding to the buckling of the PNP with clamped in-plane constraints can be obtained in terms of (m, n) as

$$V_{mn} = \frac{-\left[D_{11}\left(m^4\pi^4 / a^4 + n^4\pi^4 / b^4\right) + 2\left(D_{12} + 2D_{66}\right)m^2 n^2 \pi^4 / a^2 b^2\right]}{\left(2e_{31}^s / h + e_{31}\right)\left(m^2\pi^2 / a^2 + n^2\pi^2 / b^2\right)}.$$

$$(6.20)$$

The lowest value of V_{mn} and associated (m, n) represents the critical electric voltage for buckling and the buckling mode, respectively.

6.3   Results and discussion

The formulation developed based on the modified plate theory will be employed to conduct the simulation of the vibrational behavior of a simply supported PNP with different in-plane constraints described in section 6.2. PZT-5H is selected as an example material with macroscopic material constants $c_{11} = 102$ GPa , $c_{12} = 31$ GPa , $c_{66} = 35.5$ GPa , $e_{31} = -17.05$ C m^{-2} and $\kappa_{33} = 1.76\times10^{-8}$ C V^{-1} m^{-1} for the bulk part. For the surface layers, the material constants which can be determined from atomic calculations (Dai *et al*., 2011) or experiments are not completely available in the literature for PZT-5H owing to the lack of such work. The estimated values of the surface material constants in the literature (Huang and Yu, 2006; Yan and Jiang 2011a; b) are taken as $c_{11}^s = 7.56$ N m^{-1}, $e_{31}^s = -3\times10^{-8}$ C m^{-1}, $c_{12}^s = 3.3$ N m^{-1} and $c_{66}^s = 2.13$ N m^{-1}. In addition, the residual surface stress σ^0 is assumed as 1.0 N m^{-1}. As suggested by Yao *et al.* (2009), an aspect ratio of the plate between 1/80 and 1/5 is adopted for a Kirchhoff plate. In the current analysis, the plate aspect ratio is set within such a range.
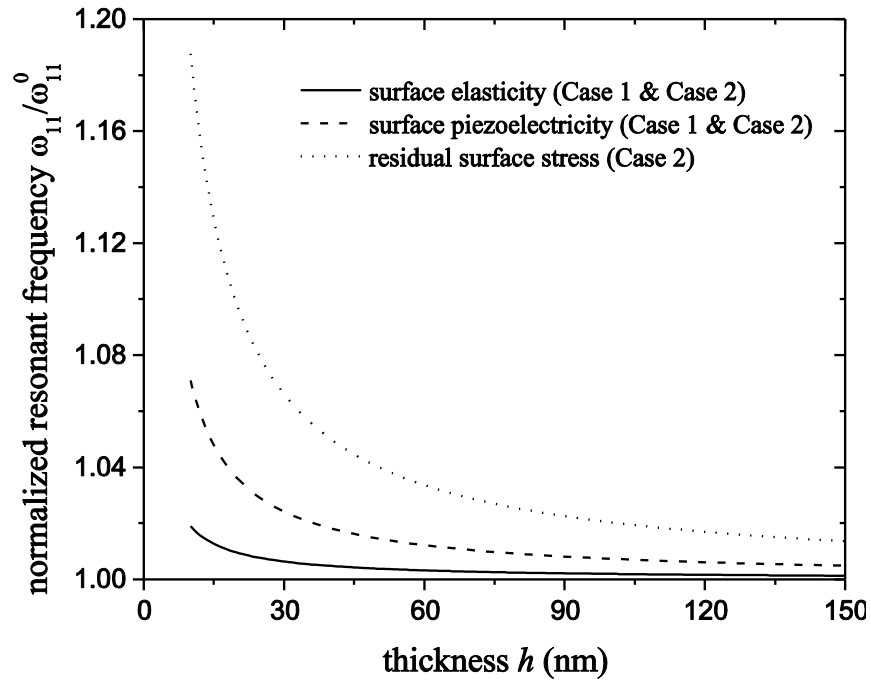
Figure 6.2: Separate surface effect on the free vibration of the PNP with different in-plane constraints ($a=b=20h$).
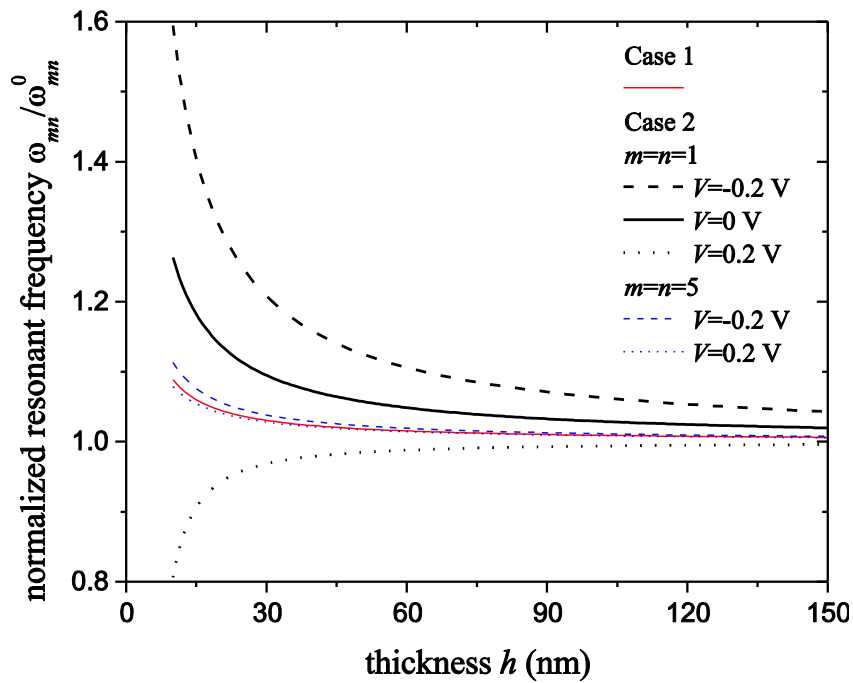
Figure 6.3: Normalized resonant frequency versus plate thickness for the PNP with different in-plane constraints ($a=b=20h$).

Firstly, we consider the separate influence of the surface elasticity, residual surface stress and surface piezoelectricity upon the vibrational behavior of the PNP. The normalized mode (1, 1) resonant frequency $\omega_{11}/\omega_{11}^0$ for the free vibration of a square PNP ($a = b = 20h$) with the variation of the plate thickness h is shown in Fig. 6.2, in which ω_{11}^0 is the resonant frequency without considering the surface effects. Without the applied electrical load, both surface elasticity and surface piezoelectricity have the same effect on the resonant frequency of the PNP with different in-plane constraints for case 1 and case 2, as indicated in Eqs. (6.18) and (6.19). However, the residual surface stress has no effect on the transverse vibration of the PNP with case 1 in-plane constraints, while it will induce in-plane relaxation, as shown in Eq. (6.15). For the PNP with case 2 in-plane constraints, it is observed in this figure that the residual surface stress has the most significant influence within the considered values of the surface material constants. It is also found in this figure that the surface piezoelectricity has a more prominent effect compared with the surface elasticity, which means the necessity of using this surface piezoelectricity model in the vibration analysis of the piezoelectric nanoplates. The individual influence of these surface effects is more significant for the thinner plate, and will eventually become negligible with the increase in the plate thickness.

Fig. 6.3 plots the normalized resonant frequency $\omega_{mn}/\omega_{mn}^0$ of a square PNP ($a = b = 20h$) against the plate thickness h when it is subjected to an electric voltage V, in which ω_{mn}^0 is the resonant frequency for the PNP without considering surface effects and the applied electric voltage. For the PNP with different in-plane constraints as described by case 1 and case 2 in section 6.2, the surface effects are found to be more pronounced for the PNP with a smaller thickness, while they diminish with increasing plate thickness, as expected. It is also demonstrated in this figure that the in-plane constraints have a significant effect on the vibrational behavior of the PNP, *i.e.* the influence of the surface effects on the resonant frequency of the PNP does not change with variation of the applied electrical load and the mode numbers (m, n) for the PNP with in-plane traction-free condition (case 1), while it is significantly altered by these factors for the PNP with in-plane clamped constraints (case 2). For example, the discrepancy between the curves for the PNP under the same electrical load for different mode numbers (m, n) indicates

that the contribution of the surface effects to the resonant frequency of the PNP varies with the vibration modes. It should be mentioned that the applied electric potential induces the in-plane strain, as shown in Eq. (6.15) for the PNP with in-plane traction-free conditions. This figure also reveals how the applied electrical load influences the vibrational behavior of the PNP with clamped in-plane constraints. As observed, for a lower vibration mode ($m = n = 1$ for example), the influence of the surface effects is significantly affected by the applied electrical load, which is similar to the results obtained for a piezoelectric nanobeam (Yan and Jiang, 2011b). However, for a higher vibration mode (*e.g.* $m = n = 5$), the electrical load will not influence the surface effects contribution that much. Such variation of the resonant frequency of the PNP with the applied electric voltage at lower modes proposes a possible avenue for frequency tuning of the PNP-based nanodevices by applying electrical load, which may either stiffen or soften the PNP, depending on the direction and amplitude of the electric potential. For example, for mode (1, 1), the PNP with thickness 10 nm is stiffened with $V = -0.2$ V and its resonant frequency is increased by approximately 60 per cent, while it is softened with $V = 0.2$ V and its resonant frequency is decreased by approximately 20 per cent. With a sufficient large electric voltage (*e.g.* $V = 0.2$ V), the drop down of the resonant frequency of the PNP with the thickness h in this figure indicates a possible mechanical buckling of the PNP, which will be discussed later. The results in this figure conclude that the in-plane constraints must be prescribed for the transverse vibration of the PNP; otherwise may lead substantial errors in prediction and characterization of the dynamic performance of the nanoplate.

The variation of the surface effects on the mode (1, 1) resonant frequency of the PNP with its thickness is demonstrated in Fig. 6.4 for the PNP with different aspect ratios. The surface effects on the resonant frequency of the PNP do not change with aspect ratio of the PNP when the in-plane constraints are described by case 1. However, for the PNP with clamped in-plane constraints (case 2), with a given value of b/a, the normalized resonant frequency increases when the aspect ratio a/h increases (*i.e.* the PNP becomes thinner). For a fixed value of a/h, the resonant frequency increases with the increase in aspect ratio b/a (*i.e.* the PNP has a larger surface area). Therefore, it is concluded that the surface effects on the resonant frequency of the PNP are more prominent for the thinner
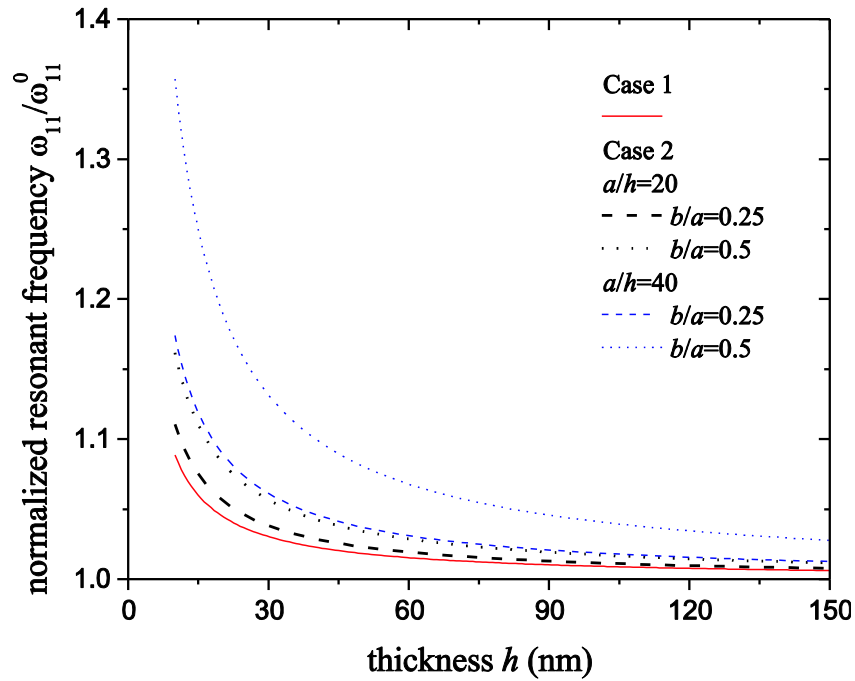
Figure 6.4: Normalized resonant frequency versus plate thickness for the PNP with different aspect ratios (*V*=0 V).
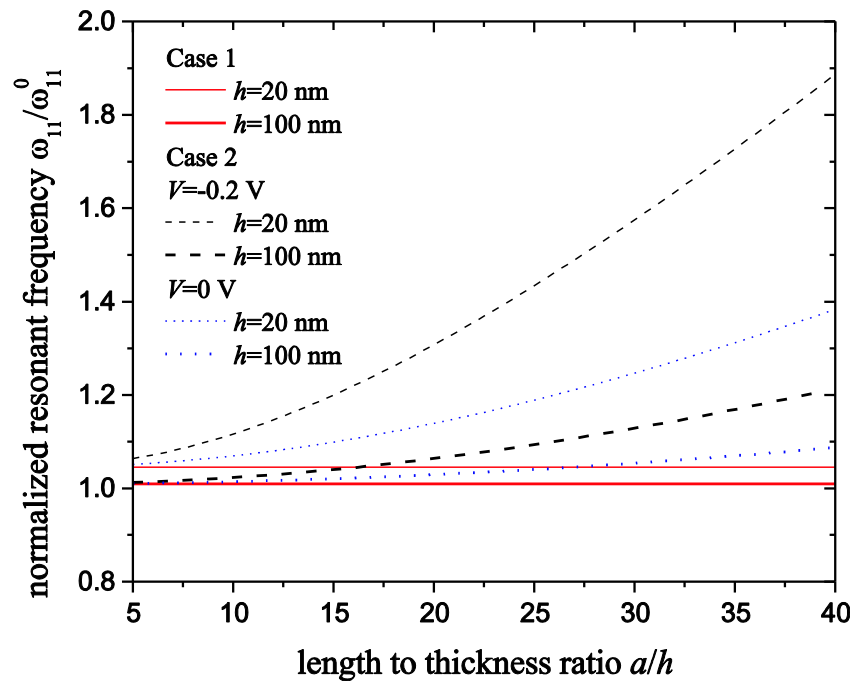
Figure 6.5: Normalized resonant frequency versus aspect ratio *a/h* of the PNP (*a=b*).

plate with larger surface area. The variation of the normalized resonant frequency $\omega_{11}/\omega_{11}^0$ with aspect ratio *a/h* is plotted in Fig. 6.5 for a square PNP (*a =b*). The straight

lines in this figure indicate the surface effects on the resonant frequency of the PNP with case 1 in-plane conditions are independent of a/h. However, the normalized resonant frequency is significantly influenced by a/h for case 2 in-plane conditions. For example, for the PNP under the same electrical load, the resonant frequency increases with an increase in a/h owing to the larger surface effects. Moreover, the resonant frequency will be further increased by the applied electric potential, as indicated by the difference between the curves for $V = -0.2$ V and $V = 0$ V. It is also seen that for both in-plane constraints of the PNP, the surface effects are more significant when the plate thickness h gets smaller.

As mentioned earlier, the normalized resonant frequency does not vary with the mode numbers for the PNP with case 1 in-plane constraints. Therefore, we only plot $\omega_{mn} / \omega_{mn}^0 \left(m = n \right)$ for a square PNP ($a = b = 20h$) with case 2 in-plane constraints in Fig. 6.6. As expected, the surface effects are more significant for the PNP with smaller thickness h. It is observed that the $\omega_{mn} / \omega_{mn}^0$ is larger in lower modes, while it tends to approach a constant value as the mode number increases. This indicates that the surface effects are more prominent in the lower vibration modes while such effects will not change much for higher mode vibration, which is similar to the results obtained for the vibration of an elastic nanoplate with the consideration of surface effects (Assadi *et al.*, 2010). It is also observed in this figure that the influence of the applied electric potential on the resonant frequency of the PNP decreases with an increase in the mode number and becomes negligible when the mode number becomes sufficient large, for example $m = n$ $= 8$. Therefore, the resonant frequency tuning concept by applying an electrical load for the PNP is applicable only for the lower vibration modes.

As discussed in section 6.2, for the PNP with case 2 in-plane constraints, the applied electric potential may induce a compressive force. When the compressive force reaches the critical value, it may cause mechanical buckling of the plate, which is also an interesting topic that needs further discussion. Fig. 6.7 plots the variation of the normalized critical electric voltage V_{cr} / V_{cr}^0 for buckling (V_{cr}^0 is the calculated critical electric voltage without the surface effects) with the plate thickness h. Similar to the observations in the previous figures, the surface effects are more prominent with a
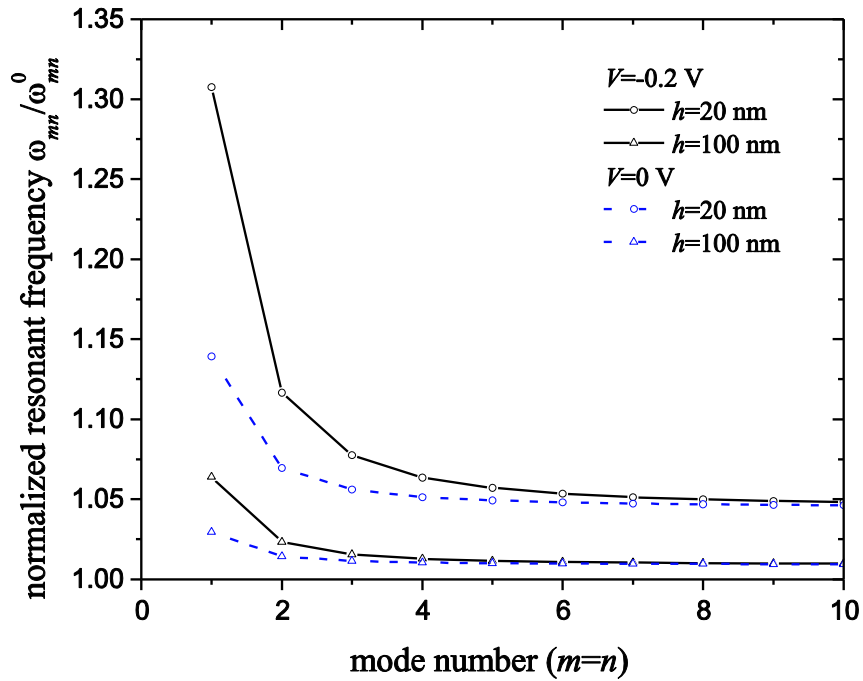
Figure 6.6: Variation of normalized resonant frequency with mode number for PNP with clamped in-plane constraints.
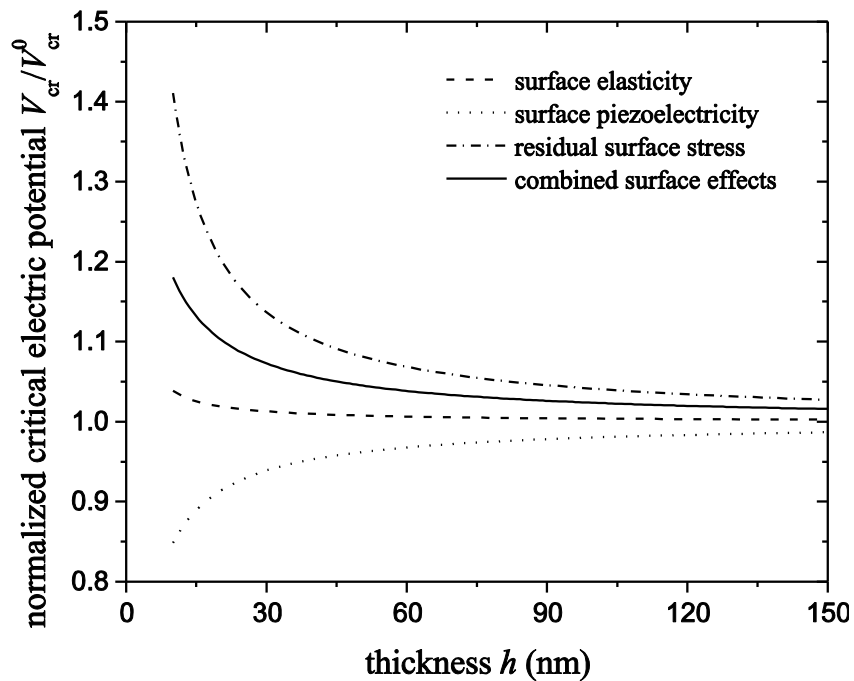
Figure 6.7: Separate surface effect on the buckling of the PNP ($a=b=20h$).

decrease in the plate thickness h. It is also found that both the surface elasticity and the residual surface stress increase this critical electric voltage, while the surface

piezoelectricity decreases it. In comparison, the residual surface stress and surface piezoelectricity have more effects on this critical electrical load for buckling than the surface elasticity, which again indicates the necessity of considering the surface piezoelectricity model for the piezoelectric nanostructures. Owing to the opposite effect of the surface piezoelectricity on the critical electrical buckling load to the other two separate surface effects, it is natural to believe that the combined surface effects on the critical electric voltage may vanish under some conditions. Fig. 6.8 plots the variation of the normalized critical electric voltage V_{cr}/V_{cr}^0 against the aspect ratio a/h for a square PNP ($a = b$) with different thickness. This figure clearly demonstrates how the combined surface effects influence the critical electric voltage for the buckling of the PNP with the change of plate size. It is interesting to note that the combined surface effects decrease the critical electric voltage when a/h is small, while increase it when a/h becomes larger. Therefore, a transition point exists within the considered range of the surface material constants, *i.e.* regardless of the value of the plate thickness h, the influence of the surface effects on the critical electrical load for buckling vanishes at this transition point $(a/h)_t$. Obviously $(a/h)_t$ depends on the in-plane aspect ratio b/a of the PNP. In particular, for a square PNP, $(a/h)_t$ is derived as

$$(a/h)_t = \sqrt{\frac{e_{31}^s\left[c_{11}+c_{12}+2c_{66}+2\left(e_{31}^2/\kappa_{33}\right)\right]-3e_{31}\left(c_{11}^s+c_{12}^s+2c_{66}^s+2e_{31}^s e_{31}/\kappa_{33}\right)}{12\sigma^0 e_{31}}} .$$
(6.21)

For a positive residual surface stress ($\sigma^0 > 0$), the surface effects decrease the critical electric voltage when $a/h < (a/h)_t$, while they increase it when $a/h > (a/h)_t$. However, if the residual surface stress $\sigma^0 \leq 0$, the surface effects always decrease the critical electric voltage for buckling.

From the simulation results in this work, it can be concluded that the transverse vibration behavior of PNPs is substantially influenced by the in-plane boundary conditions. It should also be noted that although the applied electric potential and the residual surface stress have no effect on the transverse vibration of the PNPs with case 1

in-plane constraints, they will significantly influence the in-plane mechanical behavior of the PNPs, such as the in-plane relaxation as indicated in Eq. (6.15).
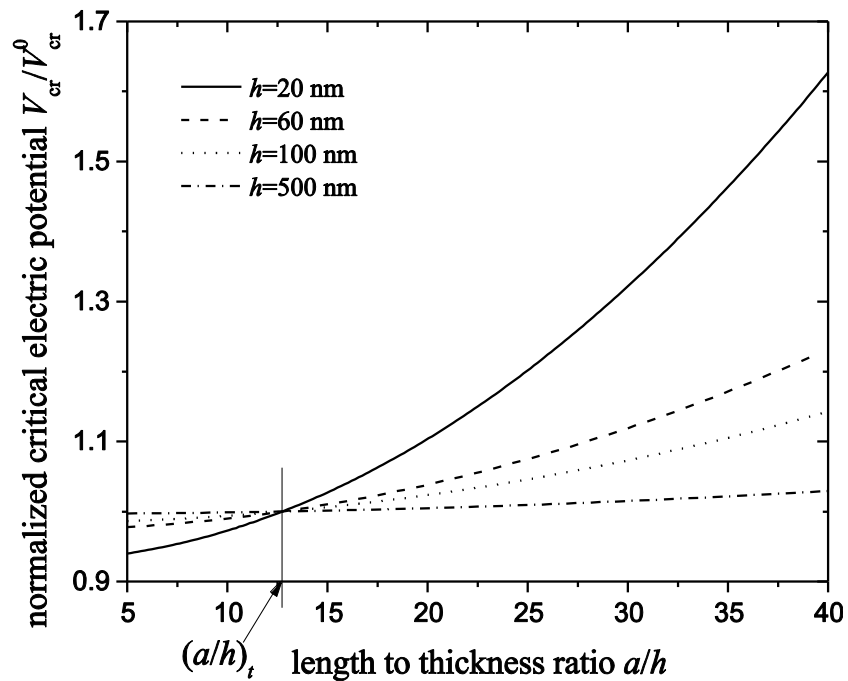
Figure 6.8: Variation of the normalized critical electric voltage for buckling with the aspect ratio a/h of the PNP ($a=b$).

6.4 Conclusions

A modified Kirchhoff plate model is developed to investigate the surface effects on the vibration and buckling behavior of a simply supported PNP under different in-plane constraints. The surface effects are accounted by employing a surface piezoelectricity model and generalized Young-Laplace equations. Surface effects are found more prominent for the plate with smaller thickness, while they decrease with increasing plate thickness. Simulation results show that the surface effects on the vibrational behavior of the PNP depend on the in-plane constraints. For the PNP with traction-free in-plane conditions, the residual surface stress and the applied electric potential have no effect on the transverse vibration of the PNP, while they induce an in-plane relaxation of the PNP. In addition, the influence of the surface effects on the resonant frequency of the PNP does not change with mode number and plate aspect ratio. However, the applied electric potential, mode number and plate aspect ratio significantly influence the surface effects

on the vibrational behavior of the PNP with clamped in-plane conditions. It is also concluded that for the PNP with clamped in-plane constraints, its resonant frequencies for lower vibration modes can be tuned by applying an electrical load. The possible mechanical buckling when the PNP is subject to an electrical load and the surface effects on the buckling behavior has also been studied. The influence of the surface effects is sensitive to the plate thickness and aspect ratio. It is found that a transition point at which surface effects vanish for all plate thickness may exist under certain conditions owing to the combined effects of the surface elasticity, residual surface stress and surface piezoelectricity. This work is expected to be helpful for understanding the size-dependent properties of piezoelectric nanostructured materials and provide guidelines for the design and applications of piezoelectric nanoplate-based device in the nanotechnology.

References

Agrawal, R., Peng, B., Gdoutos, E. E. and Espinosa, H. D., 2008. Elasticity size effects in ZnO nanowires: a combined experimental-computational approach. Nano Lett. **8**, 3668-3674.

Assadi, A. and Farshi, B., 2010. Vibration characteristics of circular nanoplates. J. Appl. Phys. **108**, 074312.

Assadi, A. and Farshi, B., 2011. Size dependent vibration of curved nanobeams and rings including surface energies. Physica E **43**, 975-978.

Assadi, A., Farshi, B. and Alinia-Ziazi, A., 2010. Size dependent dynamic analysis of nanoplates. J. Appl. Phys. **107**, 124310.

Chen, C. Q., Shi, Y., Zhang, Y. S., Zhu, J. and Yan, Y. J., 2006a. Size dependence of Young's modulus in ZnO nanowires. Phys. Rev. Lett. **96**, 075505.

Chen, T. Y., Chiu, M. S. and Weng, C. N., 2006b. Derivation of the generalized Young-Laplace equation of curved interfaces in nanoscaled solids. J. Appl. Phys. **100**, 074308.

Dai, S. X., Gharbi, M., Sharma, P. and Park, H. S., 2011. Surface piezoelectricity: Size effects in nanostructures and the emergence of piezoelectricity in non-piezoelectric materials. J. Appl. Phys. **110**, 104305.

Fei, P., Yeh, P. H., Zhou, J., Xu, S., Gao, Y. F., Song, J. H., Gu, Y. D., Huang, Y. Y. and Wang, Z. L., 2009. Piezoelectric potential gated field-effect transistor based on a free-standing ZnO wire. Nano Lett. **9**, 3435-3439.

Feng, X., Yang, B. D., Liu, Y. M., Wang, Y., Dagdeviren, C., Liu, Z. J., Carlson, A., Li, J. Y., Huang, Y. G. and Rogers, J. A., 2011. Stretchable ferroelectric nanoribbons with wavy configurations on elastomeric substrates. ASC Nano **5**, 3326-3332.

Gao, Y. F. and Wang, Z. L., 2007. Electrostatic potential in a bent piezoelectric nanowire: the fundamental theory of nanogenerator and nanopiezotronics. Nano Lett. **7**, 2499-2505.

Gurtin, M. E. and Murdoch, A. I., 1975. A continuum theory of elastic material surfaces. Arch. Ration. Mech. Anal. **57**, 291-323.

He, J. and Lilley, C. M., 2008a. Surface effect on the elastic behavior of static bending nanowires. Nano Lett. **8**, 1798-1802.

He, J. and Lilley, C. M., 2008b. Surface stress effect on bending resonance of nanowires with different boundary conditions. Appl. Phys. Lett. **93**, 263108.

Huang, G. Y. and Yu, S. W., 2006. Effect of surface piezoelectricity on the electromechanical behaviour of a piezoelectric ring. Phys. Status Solidi-Rapid Res. Lett. **243**, R22-R24.

Ke, L. L. and Wang, Y. S., 2012. Thermoelectric-mechanical vibration of piezoelectric nanobeams based on the nonlocal theory. Smart Mater. Struct. **21**, 025018.

Ke, L. L., Wang, Y. S. and Wang, Z. D., 2012. Nonlinear vibration of the piezoelectric nanobeams based on the nonlocal theory. Compos. Struct. **94**, 2038-2047.

Lao, C. S., Kuang, Q., Wang, Z. L., Park, M. C. and Deng, Y. L., 2007. Polymer functionalized piezoelectric-FET as humidity/chemical nanosensors. Appl. Phys. Lett. **90**, 262107.

Li, Y. H., Fang, B., Zhang, J. H. and Song, J. Z., 2011. Surface effects on the wrinkling of piezoelectric films on compliant substrates. J. Appl. Phys. **110**, 114303.

Lim, C. W. and He, L. H., 2004. Size-dependent nonlinear response of thin elastic films with nano-scale thickness. Int. J. Mech. Sci. **46**, 1715-1726.

Liu, C. and Rajapakse, R. K. N. D., 2010. Continuum models incorporating surface energy for static and dynamic response of nanoscale beams. IEEE Trans. Nanotechnol. **9**, 422-431.

Lu, P., He, L. H., Lee, H. P. and Lu, C., 2006. Thin plate theory including surface effects. Int. J. Solids Struct. **43**, 4631-4647.

Park, H. S., 2012. Surface stress effects on the critical buckling strains of silicon nanowires. Comp. Mater. Sci. **51**, 396-401.

Park, H. S. and Klein, P. A., 2007. Surface Cauchy-Born analysis of surface stress effects on metallic nanowires. Phys. Rev. B **75**, 085408.

Park, K. I., Xu, S., Liu, Y., Hwang, G. T., Kang, S. J. L., Wang, Z. L. and Lee, K. J., 2010. Piezoelectric $BaTiO_3$ thin film nanogenerator on plastic substrates. Nano Lett. **10**, 4939-4943.

Qi, Y., Kim, J., Nguyen, T. D., Lisko, B., Purohit, P. K. and McAlpine, M. C., 2011. Enhanced piezoelectricity and stretchability in energy harvesting devices fabricated from buckled PZT ribbons. Nano Lett. **11**, 1331-1336.

Reddy, J. N., 2007. Theory and analysis of elastic plates and shells, Boca Raton, FL: CRC Press.

Shen, S. P. and Hu, S. L., 2010. A theory of flexoelectricity with surface effect for elastic dielectrics. J. Mech. Phys. Solids **58**, 665-677.

Song, F., Huang, G. L., Park, H. S. and Liu, X. N., 2011. A continuum model for the mechanical behavior of nanowires including surface and surface-induced initial stresses. Int. J. Solids Struct. **48**, 2154-2163.

Stan, G., Ciobanu, C. V., Parthangal, P. M. and Cook, R. F., 2007. Diameter-dependent radial and tangential elastic moduli of ZnO nanowires. Nano Lett. **7**, 3691-3697.

Su, W. S., Chen, Y. F., Hsiao, C. L. and Tu, L. W., 2007. Generation of electricity in GaN nanorods induced by piezoelectric effect. Appl. Phys. Lett. **90**, 063110.

Tanner, S. M., Gray, J. M., Rogers, C. T., Bertness, K. A. and Sanford, N. A., 2007. High-Q GaN nanowire resonators and oscillators. Appl. Phys. Lett. **91**, 203117.

Wang, G. F. and Feng, X. Q., 2007. Effects of surface elasticity and residual surface tension on the natural frequency of microbeams. Appl. Phys. Lett. **90**, 231904.

Wang, G. F. and Feng, X. Q., 2009. Timoshenko beam model for buckling and vibration of nanowires with surface effects. J. Phys. D: Appl. Phys. **42**, 155411.

Wang, G. F. and Feng, X. Q., 2010. Effect of surface stresses on the vibration and buckling of piezoelectric nanowires. EPL **91**, 56007.

Wang, Z. L. and Song, J. H., 2006. Piezoelectric nanogenerators based on zinc oxide nanowire arrays. Science **312**, 242-246.

Yan, Z. and Jiang, L. Y., 2011a. Surface effects on the electromechanical coupling and bending behaviours of piezoelectric nanowires. J. Phys. D: Appl. Phys. **44**, 075404.

Yan, Z. and Jiang, L. Y., 2011b. The vibrational and buckling behaviors of piezoelectric nanobeams with surface effects. Nanotechnology **22**, 245703.

Yan, Z. and Jiang, L. Y., 2011c. Electromechanical response of a curved piezoelectric nanobeam with the consideration of surface effects. J. Phys. D: Appl. Phys. **44**, 365301.

Yao, W., Zhong, W. and Lim, C. W., 2009. Symplectic elasticity, 1st edn, pp. 225-226. Singapore: World Scientific Publishing.

Zhang, L. X. and Huang, H. C., 2006. Young's moduli of ZnO nanoplates: ab initio determinations. Appl. Phys. Lett. **89**, 183111.

Zhao, M. H., Wang, Z. L., and Mao, S. X., 2004. Piezoelectric characterization of individual zinc oxide nanobelt probed by piezoresponse force microscope. Nano Lett. **4**, 587-590.

Zhao, M. H., Qian, C. F., Lee, S. W. R., Tong, P., Suemasu, H. and Zhang, T. Y., 2007. Electroelastic analysis of piezoelectric laminated plates. Adv. Compos. Mater. **16**, 63-81.

Zhang, Y. H., Hong, J. W., Liu, B. and Fang, D. N., 2010a. Strain effect on ferroelectric behaviors of $BaTiO_3$ nanowires: a molecular dynamics study. Nanotechnology **21**, 015701.

Zhang, T. Y., Wang, Z. J. and Chan, W. K., 2010b. Eigenstress model for surface stress of solids. Phys. Rev. B **81**, 195427.

Chapter 7

7   Surface effects on the vibration and buckling of piezoelectric nanoplates[6]

7.1   Introduction

The enhanced piezoelectricity and unique coupling between piezoelectric and semiconducting properties of piezoelectric nanomaterials make them attractive for applications as sensors, resonators, generators and transistors in the nano-electro-mechanical systems (NEMS) (Wang *et al*., 2006a; b; Lao *et al*., 2007; Tanner *et al*., 2007; Qi *et al*., 2010; Feng *et al*., 2011). To better understand the underlying mechanisms and improve the performances of these advanced devices, some fundamental issues must be clearly addressed, for example, the vibration and buckling behaviors of piezoelectric nanostructures.

Different from their macroscopic counterparts, nanomaterials exhibit size-dependent mechanical and physical properties due to the large surface area to volume ratio. For example, experimental investigations and atomistic simulations have demonstrated that the elastic constants or the piezoelectric coefficients of some piezoelectric nanomaterials increase dramatically with the decrease of the material size to the nanoscale (Zhao *et al*., 2004; Kulkarni *et al*., 2005; Chen *et al*., 2006a; Stan *et al*., 2007). In literature, modified continuum mechanics theories have also been adopted as alternative and cost-effective tools to study the surface effects on the size-dependent properties of elastic nanostructures with various configurations (Lu *et al*., 2006; Wang *et al*., 2007; He and Lilley, 2008a; b; Assadi *et al*., 2010) based on the surface elasticity model developed by Gurtin and Murdoch (1975). However, this surface elasticity model is not sufficient in predicting the size-dependent properties of piezoelectric nanomaterials since it neglects surface piezoelectricity effect, which is unique for piezoelectric materials. As pointed out by Tagantsev (1986), the effect of surface piezoelectricity may become significant with

---

[6]A version of this chapter has been published.

Yan, Z. and Jiang, L.Y., EPL 99, 27007, (2012).

the miniaturization of piezoelectric materials into a nanoscale size. Therefore, it is essential to incorporating the effect of the surface piezoelectricity to investigate the electroelastic properties of piezoelectric nanomaterials. As an extension of the surface elasticity model, a surface piezoelectricity model with the consideration of the surface piezoelectricity as well as the residual surface stress and surface elasticity, was first proposed by Huang and Yu (2006) to study the electroelastic responses of a piezoelectric nanoring. Based on this model, the surface effects on the bending, vibration and buckling behaviors of piezoelectric nanobeams have been recently investigated in our previous work (Yan and Jiang, 2011a; b). It is found that the influence of the surface piezoelectricity on the static and dynamic behaviors of the piezoelectric nanobeams is significant. Li *et al*. (2011) studied the surface effects on the wrinkling of a piezoelectric nanofilm on a compliant substrate. Their results showed that the wavelength and amplitude of the wrinkling were significantly affected by the surface parameters for the films with nanoscale thickness. However, the investigation of the surface effects on two-dimensional piezoelectric nanostructures is very limited. In order to enrich the studies on the plate-like piezoelectric nanostructures, the present work aims to develop a modified piezoelectric plate model based on the classical Kirchhoff plate theory and the surface piezoelectric model to study the surface effects on the vibration and buckling behaviors of a piezoelectric nanoplate (PNP). Simulation results will show how the influence of the surface effects on the resonant frequency and the critical buckling potential changes with the PNP thickness and aspect ratio. In addition, the possibility of frequency tuning via applied electric potentials will also be investigated.

7.2   Modified plate model and formulation

The problem considered is a rectangular PNP with thickness h, in-plane length a and width b, as illustrated in Fig 7.1. A Cartesian coordinate (x_1, x_2, x_3) is used to describe the plate with x_1 and x_2 axes and the origin at the midplane of the undeformed plate, and x_3-axis in the thickness direction. The PNP is poled along x_3 direction and is subjected to an electric voltage V. Following Kirchhoff's hypotheses, the displacements at any point of the plate are expressed as

$$u_\alpha(x_1,x_2,x_3,t) = u_\alpha^0(x_1,x_2,t) - x_3 \frac{\partial u_3(x_1,x_2,x_3,t)}{\partial x_\alpha}; \ u_3(x_1,x_2,x_3,t) = w(x_1,x_2,t), \qquad (7.1)$$

where u_α^0 are the in-plane displacements of the midplane and w is the transverse displacement. Such midplane displacements describing the membrane deformations may be induced by the in-plane applied mechanical load, the applied electrical load due to the electromechanical coupling or the residual surface stress induced relaxation (Park *et al.*, 2007; Zhang *et al.*, 2010a). The usual convention of summation over repeated indices is used here, *e.g.* Greek indices run from 1 to 2. Accordingly, the in-plane strains for the Kirchhoff plate can be written as

$$\varepsilon_{\alpha\beta} = \frac{1}{2}\left(\frac{\partial u_\alpha^0}{\partial x_\beta} + \frac{\partial u_\beta^0}{\partial x_\alpha}\right) - x_3 \frac{\partial^2 w}{\partial x_\alpha \partial x_\beta}. \qquad (7.2)$$

The electric field E is assumed to exist only along the x_3 direction and can be expressed in terms of the electric potential Φ as

$$E_3 = -\frac{\partial \Phi}{\partial x_3}. \qquad (7.3)$$
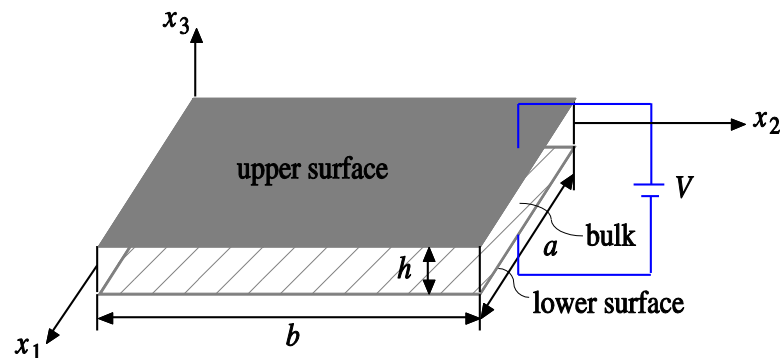
Figure 7.1: Schematic plot of a PNP with upper and lower surfaces.

Following the surface piezoelectricity model, the plate itself is composed of a bulk part with the upper and lower surface layers with negligible thickness. The constitutive equations for the surface layers of the PNP are different from the bulk, which are given as

$$\sigma_{\alpha\beta}^s = \sigma_{\alpha\beta}^0 + c_{\alpha\beta\gamma\delta}^s \varepsilon_{\gamma\delta} - e_{3\alpha\beta}^s E_3; \ D_\gamma^s = D_\gamma^0 + e_{\alpha\beta\gamma}^s \varepsilon_{\alpha\beta} + \kappa_{\gamma\delta}^s E_\delta, \qquad (7.4)$$

where $\sigma_{\alpha\beta}^{\text{s}}$ and D_γ^{s} are surface stresses and surface electric displacements; $c_{\alpha\beta\gamma\delta}^{\text{s}}$, $e_{3\alpha\beta}^{\text{s}}$ and $\kappa_{\gamma\delta}^{\text{s}}$ are elastic, piezoelectric and dielectric constants for the surfaces; $\sigma_{\alpha\beta}^0$ and D_γ^0 are residual surface stresses and residual surface electric displacements. Following the assumption (Zhao *et al.*, 2007) that the stress component in x_3-direction is negligible, the in-plane stresses $\sigma_{\alpha\beta}$ and electric displacement D_3 for the bulk can be expressed as

$$\sigma_{\alpha\beta} = c_{\alpha\beta\gamma\delta}\varepsilon_{\gamma\delta} - e_{3\alpha\beta}E_3;\ D_3 = e_{3\alpha\beta}\varepsilon_{\alpha\beta} + \kappa_{33}E_3,\tag{7.5}$$

with $c_{\alpha\beta\gamma\delta}$, $e_{3\alpha\beta}$ and κ_{33} being the bulk elastic, piezoelectric and dielectric constants for the plane stress problem.

According to the generalized Young-Laplace equations, the existence of surface can be represented by the traction jumps T_i exerting on the bulk of the plate, which are

$$T_\alpha = \frac{\partial\sigma_{\alpha\beta}^{\text{s}}}{\partial x_\beta};\ T_3^{\text{u}} = \sigma_{\alpha\beta}^{\text{s}}\frac{\partial^2 w}{\partial x_\alpha \partial x_\beta};\ T_3^{\text{l}} = -\sigma_{\alpha\beta}^{\text{s}}\frac{\partial^2 w}{\partial x_\alpha \partial x_\beta},\tag{7.6}$$

The superscripts "u" and "l" denote the upper and lower surfaces of the plate, respectively. It should be noted that the electric displacement jump across the surfaces is zero.

In the absence of free electric charges, the electric displacement should satisfy the Gauss's law

$$\frac{\partial D_3}{\partial x_3} = 0.\tag{7.7}$$

Applying the electric boundary conditions $\Phi(h/2) = V$ and $\Phi(-h/2) = 0$, the electric potential and the electric field distribution can be determined.

For the transverse vibration of the PNP, the motion equation is derived as

$$\frac{\partial^2 M_{\alpha\beta}^*}{\partial x_\alpha \partial x_\beta} - N_{\alpha\beta}^*\frac{\partial^2 w}{\partial x_\alpha \partial x_\beta} + \rho h\ddot{w} - \frac{1}{12}\rho h^3\frac{\partial^2\ddot{w}}{\partial x_\alpha^2} = 0,\tag{7.8}$$

where ρ is the mass density, $N_{\alpha\beta}^*$, $M_{\alpha\beta}^*$ are the generalized resultant forces and moments for the PNP with the consideration of surface effects, *i.e.*

$$N_{\alpha\beta}^* = N_{\alpha\beta} + \left(\sigma_{\alpha\beta}^s\right)^u + \left(\sigma_{\alpha\beta}^s\right)^1; \quad M_{\alpha\beta}^* = M_{\alpha\beta} - \frac{h}{2}\left[\left(\sigma_{\alpha\beta}^s\right)^u - \left(\sigma_{\alpha\beta}^s\right)^1\right], \tag{7.9}$$

with $N_{\alpha\beta}$ and $M_{\alpha\beta}$ being the axial forces and bending moments in the bulk of the plate defined as

$$N_{\alpha\beta} = \int_{-h/2}^{h/2} \sigma_{\alpha\beta}\,\mathrm{d}x_3; \quad M_{\alpha\beta} = -\int_{-h/2}^{h/2} \sigma_{\alpha\beta}x_3\,\mathrm{d}x_3. \tag{7.10}$$

It should be noted that the subscripts in the material constants as shown in Eqs. (7.4) and (7.5) can be relabeled in the contracted notation due to the symmetry of stress and strain tensors following $11 \rightarrow 1$; $22 \rightarrow 2$; $33 \rightarrow 3$; $23 \rightarrow 4$; $13 \rightarrow 5$; $12 \rightarrow 6$. In the following formulation and discussion, the material constants in the contracted notation, i.e. $c_{11}, c_{12}, c_{66}, c_{11}^s, c_{12}^s, c_{66}^s, e_{31}$ and e_{31}^s will be used. After the manipulation of the equations above, the transverse motion equation of the PNP with surface effects can be derived in terms of $w(x_1, x_2, t)$ as

$$D_{11}\left(\frac{\partial^4 w}{\partial x_1^4} + \frac{\partial^4 w}{\partial x_2^4}\right) + 2\left(D_{12} + 2D_{66}\right)\frac{\partial^4 w}{\partial x_1^2 \partial x_2^2} + \rho h \ddot{w} - \frac{1}{12}\rho h^3\left(\frac{\partial^2 \ddot{w}}{\partial x_1^2} + \frac{\partial^2 \ddot{w}}{\partial x_2^2}\right)$$
$$= N_{11}^* \frac{\partial^2 w}{\partial x_1^2} + 2N_{12}^* \frac{\partial^2 w}{\partial x_1 \partial x_2} + N_{22}^* \frac{\partial^2 w}{\partial x_2^2}, \tag{7.11}$$

with

$$\left.\begin{aligned}
D_{11} &= \left(c_{11} + \frac{e_{31}^2}{\kappa_{33}}\right)\frac{h^3}{12} + \left(c_{11}^s + \frac{e_{31}^s e_{31}}{\kappa_{33}}\right)\frac{h^2}{2}; \\[4pt]
D_{12} &= \left(c_{12} + \frac{e_{31}^2}{\kappa_{33}}\right)\frac{h^3}{12} + \left(c_{11}^s + \frac{e_{31}^s e_{31}}{\kappa_{33}}\right)\frac{h^2}{2}; \\[4pt]
D_{66} &= c_{66}\frac{h^3}{12} + c_{66}^s\frac{h^2}{2}; \\[4pt]
N_{11}^* &= 2\left(\sigma_{11}^0 + c_{11}^s\frac{\partial u_1^0}{\partial x_1} + c_{12}^s\frac{\partial u_2^0}{\partial x_2} + e_{31}^s\frac{V}{h}\right) + \left(c_{11}\frac{\partial u_1^0}{\partial x_1} + c_{12}\frac{\partial u_2^0}{\partial x_2} + e_{31}\frac{V}{h}\right)h; \\[4pt]
N_{12}^* &= 2\left[\sigma_{12}^0 + c_{66}^s\left(\frac{\partial u_1^0}{\partial x_2} + \frac{\partial u_2^0}{\partial x_1}\right)\right] + c_{66}\left(\frac{\partial u_1^0}{\partial x_2} + \frac{\partial u_2^0}{\partial x_1}\right)h; \\[4pt]
N_{22}^* &= 2\left(\sigma_{22}^0 + c_{12}^s\frac{\partial u_1^0}{\partial x_1} + c_{11}^s\frac{\partial u_2^0}{\partial x_2} + e_{31}^s\frac{V}{h}\right) + \left(c_{12}\frac{\partial u_1^0}{\partial x_1} + c_{11}\frac{\partial u_2^0}{\partial x_2} + e_{31}\frac{V}{h}\right)h.
\end{aligned}\right\} \tag{7.12}$$

Obviously, the in-plane constraints for the PNP must be prescribed first to solve Eq. (7.11). For a clamped-clamped plate with four edges being fully restrained, it is reasonable to set the displacements $u_\alpha^0(x_1, x_2)$ as zero, which was adopted by Zhao *et al.* (2007) for a conventional piezoelectric plate. Moreover, the residual surface stress are assumed as $\sigma_{11}^0 = \sigma_{22}^0 = \sigma^0$ and $\sigma_{12}^0 = 0$. The harmonic solution of Eq. (7.11) takes

$$w(x_1, x_2, t) = W(x_1, x_2)e^{i\omega t},\tag{7.13}$$

where ω is the resonant frequency and $W(x_1, x_2)$ represents the vibration mode. Substituting Eq. (7.13) into Eq. (7.11) results in

$$
\begin{aligned}
D_{11}\left(\frac{\partial^4 W}{\partial x_1^4} + \frac{\partial^4 W}{\partial x_2^4}\right) &+ 2\left(D_{12} + 2D_{66}\right)\frac{\partial^4 W}{\partial x_1^2 \partial x_2^2} - \rho h\omega^2 W + \\
&\frac{1}{12}\rho h^3 \omega^2\left(\frac{\partial^2 W}{\partial x_1^2} + \frac{\partial^2 W}{\partial x_2^2}\right) = f\left(\frac{\partial^2 W}{\partial x_1^2} + \frac{\partial^2 W}{\partial x_2^2}\right),
\end{aligned}\tag{7.14}
$$

with $f = 2\left(\sigma^0 + e_{31}^s V/h\right) + e_{31}V$ being the biaxial force induced by the applied electrical load and residual surface stress. Such a force may cause the buckling of the PNPs.

In order to do the vibration and buckling analysis, the Ritz method (Reddy, 2007) is adopted to get the approximate solutions. The weak form of the variational statement of Eq. (7.14) is written as

$$
\begin{aligned}
0 = \int_0^b \int_0^a \Bigg\{ & D_{11}\left[\frac{\partial^2 W}{\partial x_1^2}\frac{\partial^2(\delta W)}{\partial x_1^2} + \frac{\partial^2 W}{\partial x_2^2}\frac{\partial^2(\delta W)}{\partial x_2^2}\right] + D_{12}\left[\frac{\partial^2 W}{\partial x_2^2}\frac{\partial^2(\delta W)}{\partial x_1^2} + \frac{\partial^2 W}{\partial x_1^2}\frac{\partial^2(\delta W)}{\partial x_2^2}\right] \\
& + 4D_{66}\frac{\partial^2 W}{\partial x_1 \partial x_2}\frac{\partial^2(\delta W)}{\partial x_1 \partial x_2} - \omega^2 \rho h W \delta W - \frac{1}{12}\omega^2 \rho h^3\left[\frac{\partial W}{\partial x_1}\frac{\partial(\delta W)}{\partial x_1} + \frac{\partial W}{\partial x_2}\frac{\partial(\delta W)}{\partial x_2}\right] \\
& + f\left[\frac{\partial W}{\partial x_1}\frac{\partial(\delta W)}{\partial x_1} + \frac{\partial W}{\partial x_2}\frac{\partial(\delta W)}{\partial x_2}\right]\Bigg\}dx_1 dx_2.
\end{aligned}\tag{7.15}
$$

According to the Ritz method, the transverse deflection of the PNP can be approximated by

$$W(x_1, x_2) \approx \sum_{i=1}^m \sum_{j=1}^n c_{ij} X_i(x_1) Y_j(x_2),\tag{7.16}$$

where c_{ij} are the unknown constants, and $X_i(x_1)$ and $Y_j(x_2)$ are the coordinate functions satisfying the boundary conditions. For the clamped-clamped PNP, W should satisfy $W=0$ and $\partial W / \partial x_1 = 0$ at $x_1=0$ and $x_1=a$; $W=0$ and $\partial W / \partial x_2 = 0$ at $x_2=0$ and $x_2=b$. Accordingly, $X_i(x_1)$ and $Y_j(x_2)$ are chosen as (Reddy, 2007)

$$X_i(x_1) = \left(\frac{x_1}{a}\right)^{i+1} - 2\left(\frac{x_1}{a}\right)^{i+2} + \left(\frac{x_1}{a}\right)^{i+3}; \ Y_j(x_2) = \left(\frac{x_2}{b}\right)^{j+1} - 2\left(\frac{x_2}{b}\right)^{j+2} + \left(\frac{x_2}{b}\right)^{j+3}. \tag{7.17}$$

Substituting Eq. (7.16) into Eq. (7.15), we have

$$\left([R] - \omega^2[B]\right)\{c\} = 0, \tag{7.18}$$

with

$$
\begin{aligned}
R_{(ij)(kl)} = \int_0^b \int_0^a \Bigg[& D_{11}\left(\frac{\partial^2 X_i}{\partial x_1^2}Y_j\frac{\partial^2 X_k}{\partial x_1^2}Y_l + X_i\frac{\partial^2 Y_j}{\partial x_2^2}X_k\frac{\partial^2 Y_l}{\partial x_2^2}\right) \\
& + D_{12}\left(X_i\frac{\partial^2 Y_j}{\partial x_2^2}\frac{\partial^2 X_k}{\partial x_1^2}Y_l + \frac{\partial^2 X_i}{\partial x_1^2}Y_j X_k\frac{\partial^2 Y_l}{\partial x_2^2}\right) \\
& + 4D_{66}\frac{\partial X_i}{\partial x_1}\frac{\partial Y_j}{\partial x_2}\frac{\partial X_k}{\partial x_1}\frac{\partial Y_l}{\partial x_2} + f\left(\frac{\partial X_i}{\partial x_1}Y_j\frac{\partial X_k}{\partial x_1}Y_l + X_i\frac{\partial Y_j}{\partial x_2}X_k\frac{\partial Y_l}{\partial x_2}\right) \Bigg] dx_1 dx_2,
\end{aligned} \tag{7.19}
$$

and

$$B_{(ij)(kl)} = \int_0^b \int_0^a \left[\rho h X_i X_k Y_j Y_l + \frac{1}{12}\rho h^3\left(\frac{\partial X_i}{\partial x_1}\frac{\partial X_k}{\partial x_1}Y_j Y_l + X_i X_k\frac{\partial Y_j}{\partial x_2}\frac{\partial Y_l}{\partial x_2}\right)\right] dx_1 dx_2. \tag{7.20}$$

Then, the resonant frequency ω of the PNP can be obtained by solving the characteristic equations of Eq. (7.18).

Due to the inherent electromechanical coupling of piezoelectric materials, the applied electrical load generates in-plane forces when the in-plane displacements of the plate are constrained, which may cause the mechanical buckling of the PNP once the resulting forces become compressive. Moreover, the surface stresses may also contribute to these in-plane forces, as shown in Eq. (7.9). Therefore, it will be interesting to investigate the buckling behavior of the PNP with surface effects. The equation

governing the buckling behaviors of PNPs can be determined by letting $\omega = 0$ in Eq. (7.14). Similarly, substituting Eq. (7.16) into Eq. (7.15) with $\omega = 0$ results in

$$\left(\left[R^{'} \right] - f \left[B^{'} \right] \right) \{c\} = 0, \tag{7.21}$$

with

$$
R^{'}_{(ij)(kl)} = \int_0^b \int_0^a \left[D_{11} \left(\frac{\partial^2 X_i}{\partial x_1^2} Y_j \frac{\partial^2 X_k}{\partial x_1^2} Y_l + X_i \frac{\partial^2 Y_j}{\partial x_2^2} X_k \frac{\partial^2 Y_l}{\partial x_2^2} \right) \right.
$$
$$
\left. + D_{12} \left(X_i \frac{\partial^2 Y_j}{\partial x_2^2} \frac{\partial^2 X_k}{\partial x_1^2} Y_l + \frac{\partial^2 X_i}{\partial x_1^2} Y_j X_k \frac{\partial^2 Y_l}{\partial x_2^2} \right) + 4 D_{66} \frac{\partial X_i}{\partial x_1} \frac{\partial Y_j}{\partial x_2} \frac{\partial X_k}{\partial x_1} \frac{\partial Y_l}{\partial x_2} \right] dx_1 dx_2, \tag{7.22}
$$

and

$$
B^{'}_{(ij)(kl)} = -\int_0^b \int_0^a \left(\frac{\partial X_i}{\partial x_1} Y_j \frac{\partial X_k}{\partial x_1} Y_l + X_i \frac{\partial Y_j}{\partial x_2} X_k \frac{\partial Y_l}{\partial x_2} \right) dx_1 dx_2. \tag{7.23}
$$

After determining f from the characteristic solutions of Eq. (7.21), the critical electric potential for buckling is calculated as

$$
V_{\mathrm{cr}} = \frac{f - 2\sigma^0}{e_{31} + 2e_{31}^s / h}. \tag{7.24}
$$

7.3 Results and discussion

To qualitatively show the surface effects on the vibration and buckling behaviors of the PNP, PZT-5H is chosen as an example material for case study. Its macroscopic material constants are taken as $c_{11} = 102\ \mathrm{GPa}$, $c_{12} = 31\ \mathrm{GPa}$, $e_{31} = -17.05\ \mathrm{C\ m^{-2}}$ and $\kappa_{33} = 1.76 \times 10^{-8}\ \mathrm{C\ V^{-1}\ m^{-1}}$. Since the surface material constants are not completely available due to the lack of atomic calculations and experiments, the values adopted in Huang and Yu's work (2006) are used in the current work, *i.e.* $c_{11}^s = 7.56\ \mathrm{N\ m^{-1}}$, $e_{31}^s = -3.0 \times 10^{-8}\ \mathrm{C\ m^{-1}}$. In addition, the other surface material constants are taken as $\sigma^0 = 1.0\ \mathrm{N\ m^{-1}}$, $c_{12}^s = 3.3\ \mathrm{Nm^{-1}}$ and $c_{66}^s = 2.13\ \mathrm{N\ m^{-1}}$.

For a PNP ($a=b=20h$) subjected to $V = -0.1$ V, Fig. 7.2 shows the normalized first mode resonant frequency versus the plate thickness, where ω^V is the resonant frequency

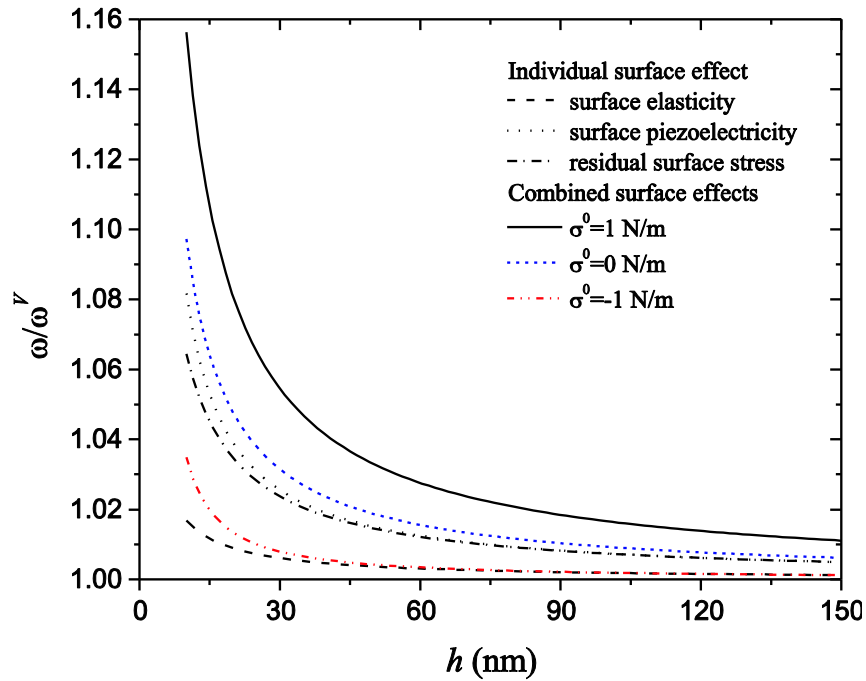Figure 7.2: Variation of normalized resonant frequency with plate thickness ($a = b=20h$, $V = -0.1$ V).
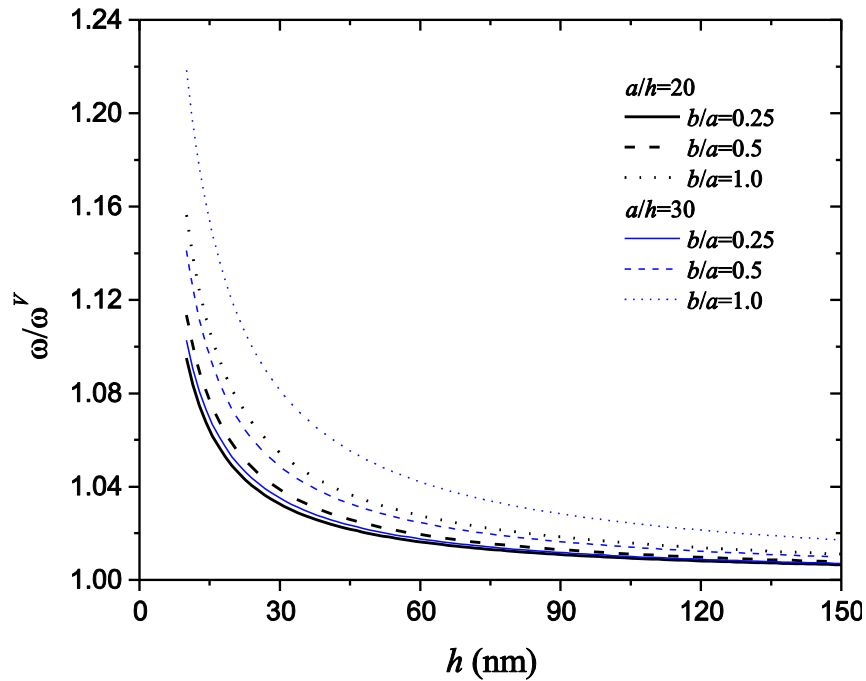

Figure 7.3: Normalized resonant frequency vs. plate thickness for different plate aspect ratios ($V = -0.1$ V).

of the PNP without the surface effects. With the considered values of the surface material constants, it is found that the separate influence of the surface piezoelectricity is obvious

the largest in comparison with the residual surface stress and the surface elasticity for the PNP with small thickness, for example, h<30 nm. This observation indicates the importance of using the surface piezoelectricity model to investigate the mechanical property of piezoelectric nanostructures. With the increase of the plate thickness h, the influence of the surface effects diminishes and this normalized resonant frequency tending to approach 1. As reported in He and Lilley's work (He and Lilley, 2008a), the residual surface stress may range from a negative value to a positive one. The combined surface effects with setting $\sigma^0 = 0$ N/m and $\sigma^0 = -1.0$ N/m are also provided in this figure for comparison with $\sigma^0 = 1.0$ N/m. The obvious discrepancy among these curves indicates that this surface piezoelectricity model is sensitive to the values of these surface material constants. Fig. 7.3 plots the normalized resonant frequency against the plate thickness for the PNP with different in-plane aspect ratio, b/a=0.25, 0.5 and 1.0 for example. It is observed that the influence of the surface effects on the normalized resonant frequency increases as b/a increases for a given a/h. When the in-plane aspect ratio b/a is fixed, the influence of the surface effects also increases with the aspect ratio a/h. These results indicate that the surface effects are more prominent for PNPs with smaller thickness and larger in-plane area.

Fig. 7.4 depicts the variation of ω/ω^0 against h with ω^0 being calculated without considering the surface effects and the applied electric potential. It is seen that the influence of the surface effects is significantly affected by the applied electrical load, which is similar to that observed for a simply-supported piezoelectric nanobeam (Yan and Jiang, 2011b). The variation of the resonant frequency with the applied electrical load suggests possible frequency tuning of PNPs by the applied electric potentials. Such frequency tuning concept is expected to provide guidelines for the design and applications of PNPs as resonators. It is interesting to note that with the increase of the electric potential or the decrease of the plate thickness, the resonant frequency may drop down. This phenomenon indicates a possible mechanical buckling of the PNP caused by the combined electrical load and the surface effects, which is an important issue needs to be addressed in order to keep the mechanical integrity of the structures. Fig. 7.5 shows the normalized critical electric potential V_{cr}/V_{cr}^0 for buckling (V_{cr}^0 is calculated without
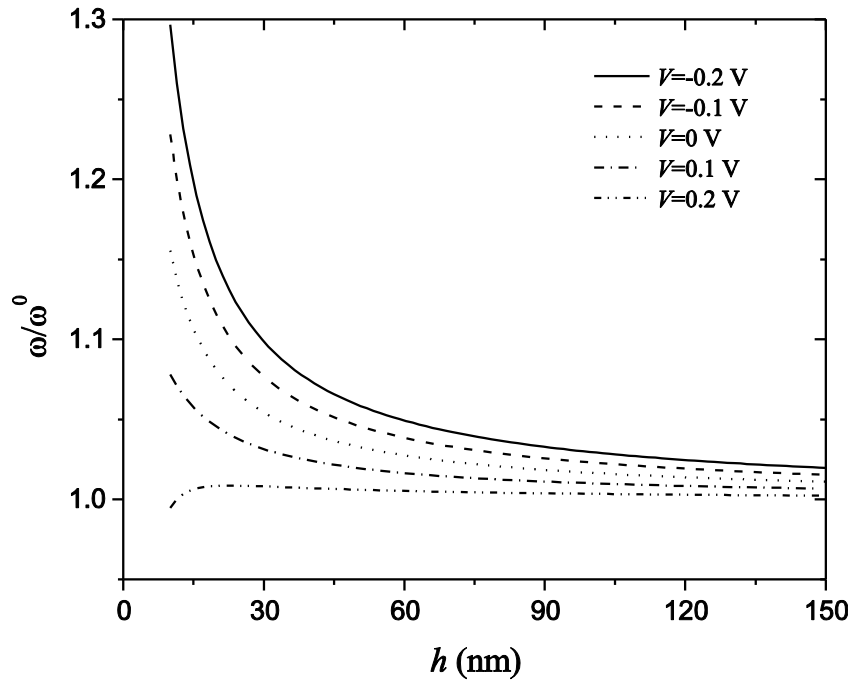
Figure 7.4: Normalized resonant frequency vs. plate thickness for different applied electric potentials ($a = b = 20h$).
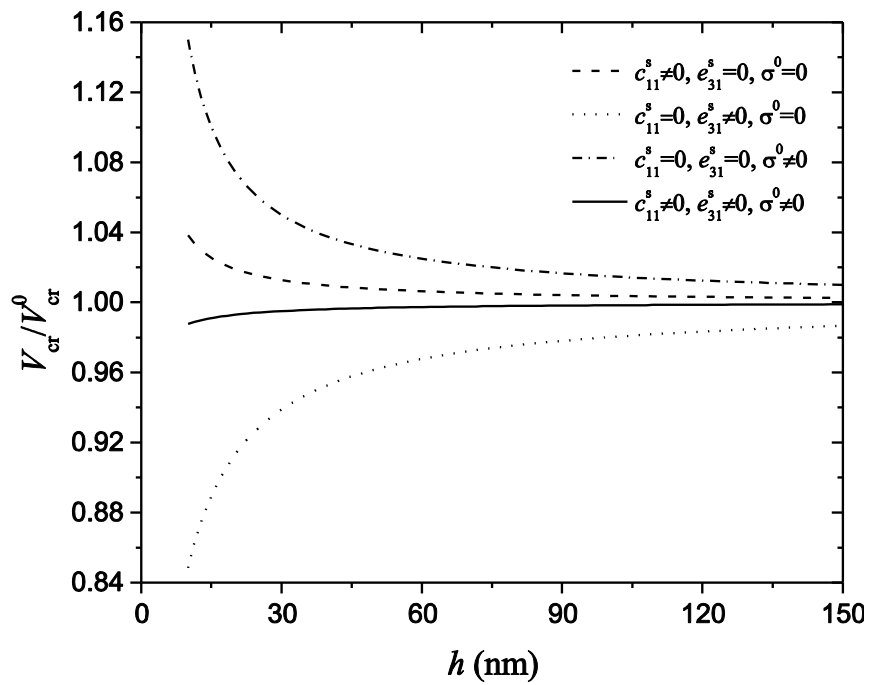
Figure 7.5: Variation of normalized critical electric potential for buckling with plate thickness ($a = b = 20h$).
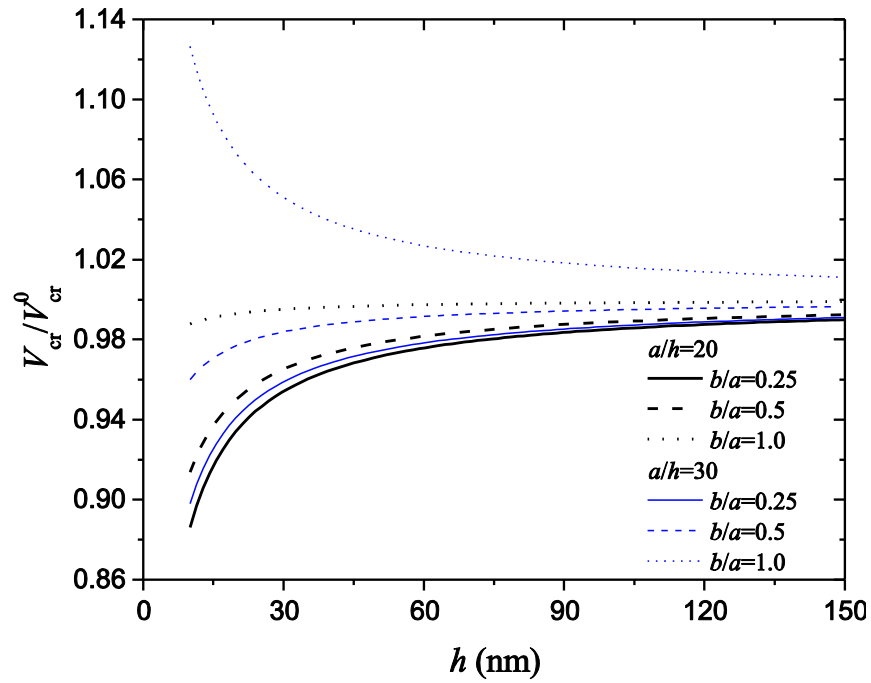
Figure 7.6: Normalized critical electric potential vs. plate thickness for different plate aspect ratios.
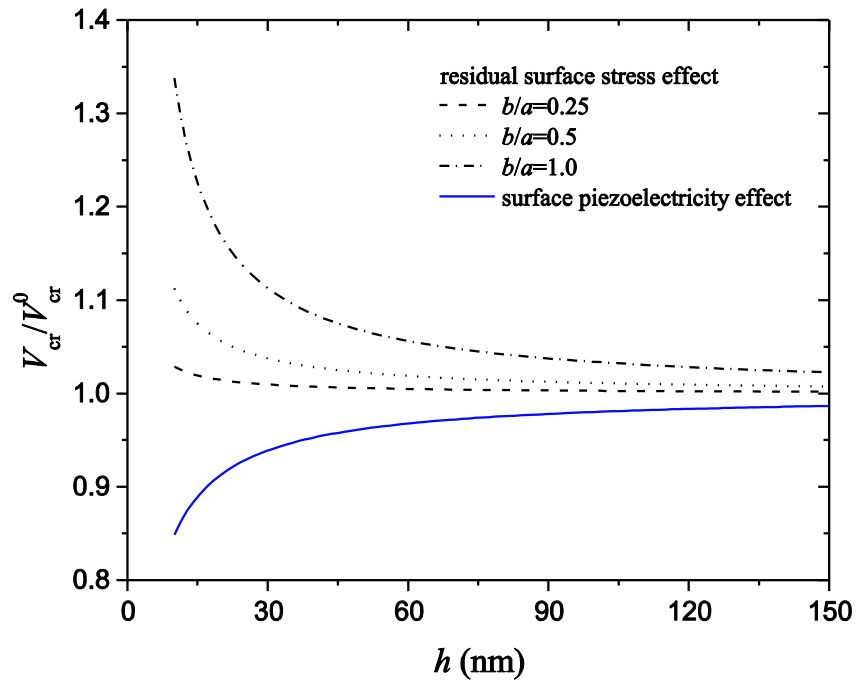
Figure 7.7: Normalized critical electric potential vs. plate thickness considering residual surface stress and surface piezoelectricity separately (a/h=30).

surface effects) versus the plate thickness h. Similar to the trend observed in Fig. 7.2, the surface effects on V_{cr}/V_{cr}^0 are more prominent for smaller h. Although the combined

surface effects are not significant, the separate influence of the surface piezoelectricity and the residual surface stress is obvious when h is small, for example, $h<30$ nm. It is the competition between these two surface effects that ends up with a smaller combined effect. Again this result suggests the importance of incorporating the surface piezoelectricity into the plate model to study the mechanical behavior of the PNP, otherwise may lead some misleading predictions. The influence of the surface effects on the critical electric potential of the PNP with different aspect ratios is displayed in Fig. 7.6. It is found that the influence of the surface effects is significantly affected by the aspect ratio. When $a/h=20$, the surface effects decrease the critical electric potential of the PNP for $b/a=0.25$, 0.5 and 1.0. However, such a trend is changed for a PNP with larger surface area, $a/h=30$ and $b/a=1.0$ for example. This phenomenon could be explained by studying the individual surface effect as presented in Fig. 7.7. Since the influence of the surface elasticity is much smaller than that of the residual surface stress and surface piezoelectricity, we just ignore the surface elasticity here. From Fig. 7.7, it is found that the residual surface stress always increases the critical electric potential, and such effect is further enhanced with the increase of the in-plane aspect ratio b/a. However, the surface piezoelectricity always decreases the critical electric potential and its influence is independent of the aspect ratio b/a. Therefore, the residual surface stress becomes dominant with the increase of b/a and a/h, resulting the trend change for the combined surface effects on the critical electric potential observed in Fig. 7.6.

7.4 Conclusions

In summary, a modified plate model is developed based on the classical Kirchhoff plate theory and the surface piezoelectricity model to investigate the surface effects on the vibration and buckling of the PNPs. Simulation results show that the surface piezoelectricity has a significant effect on the resonant frequency and critical electric potential for buckling, indicating the importance of using the surface piezoelectricity model in predicting the mechanical behavior of the PNPs. The surface effects on the resonant frequency of the PNPs are found more prominent for the PNPs with smaller thickness and larger in-plane aspect ratio, while the influence of the surface piezoelectricity on the critical electric potential for buckling is independent of such aspect

ratio. This study also suggests the possible frequency tuning of PNPs via applied electric potentials. The fundamental investigations on the mechanical behavior of PNPs carried out in this work might be helpful for the design and applications of PNP-based nanodevices.

References

Assadi, A., Farshi, B. and Alinia-Ziazi, A., 2010. Size dependent dynamic analysis of nanoplates. J. Appl. Phys. **107**, 124310.

Chen, C. Q., Shi, Y., Zhang, Y. S., Zhu, J. and Yan, Y. J., 2006. Size dependence of Young's modulus in ZnO nanowire. Phys. Rev. Lett. **96**, 075505.

Feng, X., Yang, B. D., Liu, Y. M., Wang, Y., Dagdeviren, C., Liu, Z. J., Carlson, A., Li, J. Y., Huang, Y. G. and Rogers, J. A., 2011. Stretchable ferroelectric nanoribbons with wavy configurations on elastomeric substrates. ACS Nano **5**, 3326-3332.

Gurtin, M. E. and Murdoch, A. I., 1975. A continuum theory of elastic material surfaces. Arch. Ration. Mech. Anal. **57**, 291-323.

He, J. and Lilley, C. M., 2008a. Surface effect on the elastic behavior of static bending nanowires. Nano Lett. **8**, 1798-1802.

He, J. and Lilley, C. M., 2008b. Surface stress effect on bending resonance of nanowires with different boundary conditions. Appl. Phys. Lett. **93**, 263108.

Huang, G. Y. and Yu, S. W., 2006. Effect of surface piezoelectricity on the electromechanical behaviour of a piezoelectric ring. Phys. Status Solidi-Rapid Res. Lett. **243**, R22-R24.

Kulkarni, A. J., Zhou, M. and Ke, F. J., 2005. Orientation and size dependence of the elastic properties of zinc oxide nanobelts. Nanotechnology **16**, 2749.

Lao, C. S., Kuang, Q., Wang, Z. L., Park, M. C. and Deng, Y. L., 2007. Polymer functionalized piezoelectric-FET as humidity/chemical nanosensors. Appl. Phys. Lett. **90**, 262107.

Li, Y. H., Fang, B., Zhang, J. Z. and Song, J. Z., 2011. Surface effects on the wrinkling of piezoelectric films on compliant substrates. J. Appl. Phys. **110**, 114303.

Lu, P., He, L. H., Lee, H. P. and Lu, C., 2006. Thin plate theory including surface effects. Int. J. Solids Struct. **43**, 4631-4647.

Park, H. S. and Klein, P. A., 2007. Surface Cauchy-Born analysis of surface stress effects on metallic nanowires. Phys. Rev. B **75**, 085408.

Qi, Y., Jafferis, N. T., Lyons, K., Lee, C. M., Ahmad, H. and McAlpine, M. C., 2010. Piezoelectric ribbons printed onto rubber for flexible energy conversion. Nano Lett. **10**, 524-528.

Reddy J. N., 2007. Theory and analysis of elastic plates and shells, CRC, Boca Raton, FL.

Stan, G., Ciobanu, C. V., Parthangal, P. M. and Cook, R. F., 2007. Diameter-dependent radial and tangential elastic moduli of ZnO nanowires. Nano Lett. **7**, 3691-3697.

Tagantsev, A. K., 1986. Piezoelectricity and flexoelectricity in crystalline dielectrics. Phys. Rev. B **34**, 5883-5889.

Tanner, S. M., Gray, J. M., Rogers, C. T., Bertness, K. A. and Sanford, N. A., 2007. High-Q GaN nanowire resonators and oscillators. Appl. Phys. Lett. **91**, 203117.

Wang, G. F., Feng, X. Q. and Yu, S. W., 2007. Surface buckling of a bending microbeam due to surface elasticity. EPL **77**, 44002.

Wang, X. D., Zhou, J., Song, J. H., Liu, J., Xu, N. S. and Wang, Z. L., 2006. Piezoelectric field effect transistor and nanoforce sensor based on a single ZnO nanowire. Nano Lett. **6**, 2768-2772.

Wang, Z. L. and Song, J. H., 2006. Piezoelectric nanogenerators based on zinc oxide nanowire arrays. Science **312**, 242-246.

Yan, Z. and Jiang, L. Y., 2011a. Surface effects on the electromechanical coupling and bending behaviours of piezoelectric nanowires. J. Phys. D: Appl. Phys. **44**, 075404.

Yan, Z. and Jiang, L. Y., 2011b. The vibrational and buckling behaviors of piezoelectric nanobeams with surface effects. Nanotechnology **22**, 245703.

Zhao, M., Qian, C., Lee, S. W. R., Tong, P., Suemasu, H. and Zhang, T. Y., 2007. Electro-elastic analysis of piezoelectric laminated plates. Adv. Compos. Mater. **16**, 63-81.

Zhao, M. H., Wang, Z. L. and Mao, S. X., 2004. Piezoelectric characterization of individual zinc oxide nanobelt probed by piezoresponse force microscope. Nano Lett. **4**, 587-590.

Zhang, T. Y., Wang, Z. J. and Chan, W. K., 2010. Eigenstress model for surface stress of solids. Phys. Rev. B. **81**, 195427.

Chapter 8

8 Flexoelectric effect on the electroelastic responses of bending piezoelectric nanobeams[7]

8.1 Introduction

The conventional electromechanical coupling between the electric polarization and the uniform strain is unique for noncentrosymmetric crystals, such as piezoelectric materials (Cady, 1946). However, the presence of a strain gradient or a nonuniform strain field can locally break the inversion symmetry and induce an electric polarization even in crystalline centrosymmetric dielectrics (Maranganti *et al*., 2006). This spontaneous electric polarization induced by strain gradient is referred as flexoelectricity, which is proportional to both the flexoelectric coefficient and the magnitude of the strain gradient. In general, flexoelectricity is expected to be rather weak compared with piezoelectricity. However, this effect may become prominent at the nanoscale since the strain gradient is inversely proportional to the feature scale of the structures (Majdoub *et al*., 2008). Thus, it is necessary to consider the flexoelectric effect in studying the electromechanical coupling of dielectrics at the nanoscale.

Recently, flexoelectricity has stimulated a surge of scientific interests and research activities. Particular application of flexoelectricity was focused on the possibility of creating piezoelectric nanomaterials without using piezoelectric materials (Sharma *et al*., 2007; 2010), in which a nonzero net polarization was induced in the nonpiezoelectric dielectric materials due to the flexoelectric effect. In literature, it was found that the flexoelectric effect played a crucial role in the physical characteristics of ferroelectrics, such as the dielectric constants (Catalan *et al*., 2004), the polarization hysteresis curves (Lee *et al*., 2011), the critical thickness of thin films below which the switchable spontaneous polarization vanishes (Zhou *et al*., 2012), and the critical phase transition temperature of nanowires and thin pills (Eliseev *et al*., 2009). A series of experiments

---

[7]A version of this chapter has been published.

Yan, Z. and Jiang, L. Y., J. Appl. Phys. 113, 194102, (2013).

have been carried out by Ma and Cross (2001a; b; 2005; 2006) to measure the flexoelectric coefficients μ_{ijkl} of some dielectrics. It was reported in their work that remarkably large flexoelectric coefficients were found for ferroelectrics with high dielectric permittivity. In contrast, the flexoelectric constants were estimated to be several orders of magnitude smaller than the aforementioned measurements from atomistic simulations (Maranganti and Sharma, 2009; Hong *et al*., 2010). Controversy on this issue has recently been interpreted in Ponomareva *et al*.'s work (2012) by the fact that the flexoelectric coefficients are temperature dependent. Some efforts have also been devoted to establishing theoretical frameworks for dielectrics with the consideration of flexoelectricity to quantitatively understand the underlying physics of electromechanical coupling of dielectrics at the nanoscale. For example, Maranganti *et al*. (2006) presented a mathematical framework with the flexoelectricity based on the extended linear theory for centrosymmetric dielectrics. Hu and Shen (Hu and Shen, 2010; Shen and Hu, 2010) developed the governing equations of dielectrics with the consideration of the flexoelectric effect by a variational principle. These existing studies provided fundamental physical and mathematical basis for incorporating the flexoelectric effect in nanoscale dielectrics and intrigued further investigations on this topic.

One-dimensional piezoelectric nanostructures, such as nanowires or nanobelts which can be mathematically classified as beams, are fundamental building blocks for the design of nanodevices in nanoelectromechanical systems (NEMS). Therefore, it is essential to predict their electromechanical coupling with the consideration of the nanoscale structure features. "Small is different", these piezoelectric nanobeams may exhibit different performance from their bulk counterparts, *i.e.* size-dependent properties. It is commonly believed that such size effects are attributed to the surface effects and the flexoelectricity for nanoscale piezoelectric materials (Tagantsev, 1986). With the consideration of the surface effects, a surface piezoelectricity model (Huang and Yu, 2006) was applied to study the size-dependent static bending and dynamic behavior of piezoelectric nanowires (Yan and Jiang, 2011a; b). It should be mentioned that there are very limited studies on the size-dependent properties of piezoelectric nanostructures induced by the flexoelectricity. Until recently, an analytical solution was obtained for the piezoelectric potential generated in a cantilever ZnO nanowire with the consideration of

the flexoelectricity due to a nonuniform bending strain (Liu *et al*., 2012). However, the flexoelectric effect on the electroelastic responses of piezoelectric nanobeams with different boundary conditions has not been reported thus far. Therefore, the objective of the current work is to investigate the influence of the flexoelectricity on the bending of piezoelectric nanobeams with different boundary conditions by using an Euler-Bernoulli beam model. Simulation results will be demonstrated to show how the flexoelectricity varies with the beam size and its influence on the electroelastic responses of the beams.

8.2 Modeling and formulation for piezoelectric beam with the consideration of flexoelectricity

In dealing with the problem of piezoelectric nanobeams with the consideration of the flexoelectricity, our mathematical modeling is based on the extended linear theory of piezoelectricity, in which the strain gradient is incorporated. The general expression for the internal energy density function U can be written as (Hu and Shen, 2010)

$$U = \frac{1}{2} a_{kl} P_k P_l + \frac{1}{2} c_{ijkl} \varepsilon_{ij} \varepsilon_{kl} + d_{ijk} \varepsilon_{ij} P_k + f_{ijkl} u_{i,jk} P_l + r_{ijklm} \varepsilon_{ij} u_{k,lm} + \frac{1}{2} g_{ijklmn} u_{i,jk} u_{l,mn}, \qquad (8.1)$$

where P_i are the components for the polarization vector, while u_i are the components for the displacement vector. a_{kl}, c_{ijkl} and d_{ijk} are the elements for the reciprocal dielectric susceptibility, elastic coefficient and piezoelectric coefficient tensors, respectively. These material constant tensors are exactly the same as those in the linear piezoelectricity theory. f_{ijkl} are the elements in the polarization and strain gradient coupling tensor, *i.e.* the flexocoupling coefficient tensor (Eliseev *et al*., 2009). r_{ijklm} and g_{ijklmn} are the elements for the strain and strain gradient coupling and strain gradient and strain gradient coupling tensors, respectively. The strain is defined as

$$\varepsilon_{ij} = \frac{1}{2}\left(u_{i,j} + u_{j,i}\right). \qquad (8.2)$$

For simplicity, the couplings between the strain and the strain gradient, and the strain gradient and the strain gradient are ignored in the current work as in Majdoub *et al*.'s work (2008), *i.e.* both r_{ijklm} and g_{ijklmn} are assumed as zero. In their work, such an

assumption in predicting the electromechanical coupling of piezoelectric nanobeams was validated through molecular dynamics. The constitutive equations can be expressed as

$$\sigma_{ij} = \frac{\partial U}{\partial \varepsilon_{ij}} = c_{ijkl}\varepsilon_{kl} + d_{ijk}P_k; \ \sigma_{ijm} = \frac{\partial U}{\partial u_{i,jm}} = f_{ijmk}P_k; \ E_i = \frac{\partial U}{\partial P_i} = a_{ij}P_j + d_{jki}\varepsilon_{jk} + f_{jkli}u_{j,kl}. \quad (8.3)$$

where σ_{ij} and E_i are the traditional stresses and the electric field, respectively. σ_{ijm} is defined as the higher order stress or the moment stress (Majdoub *et al*., 2008; Hu and Shen, 2010), which is induced by the flexoelectric effect while does not exist in the classical theory of piezoelectricity.
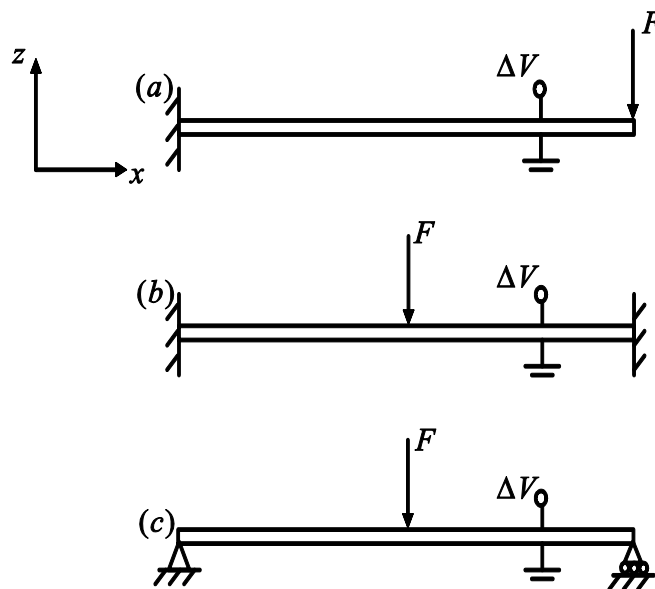
Figure 8.1: Schematic of piezoelectric nanobeams with various boundary conditions (a) cantilever (b) clamped-clamped (c) simply supported.

It is worth mentioning that unlike the elastic coefficient tensor, the flexocoupling coefficient tensor is asymmetric and its elements f_{ijkl} are related to the flexoelectric coefficient tensor elements μ_{ijkl} by $f_{ijkl} = a_{lm}\left(\mu_{ijkm} + \mu_{ikjm} - \mu_{jkim}\right)$ (Sharma *et al*., 2010). These two tensors have the same number of independent coefficients for a given material symmetry group. Le Quang and He (2011) have solved the fundamental problem of determining the number and types of all possible rotational symmetries for flexoelectric tensors. More recently, the non-zero and independent flexoelectric coefficients in a matrix form have been given in Shu *et al*.'s work (2011). In the current work,

the tetragonal barium titanate (point group 4 mm) is taken as the example material with the nonzero flexoelectric coefficients in the matrix form being given in Shu *et al.*'s work (2011), from which the nonzero f_{ijkl} in the matrix form are obtained accordingly.

In this paper, attention is focused on the static bending behavior of a piezoelectric nanobeam of length L, thickness h and width b with different boundary conditions, as shown in Fig. 8.1. A Cartesian coordinate system (x, y, z) is used to describe the beam with the x-axis being the centroidal axis of the undeformed beam, and the z-axis being along the thickness direction. The piezoelectric body is polarized along the z-axis. A constant electric potential ΔV is applied between the upper surface $z = h/2$ and the lower surface $z = -h/2$ of the beam, and a constant concentrated load F is applied at the free end $x = L$ of the cantilever (C-F) beam and at the midpoint $x = L/2$ of the clamped-clamped (C-C) and the simply supported (S-S) beams. If the transverse displacement of the bending beam is denoted as $w(x)$, the axial displacement at any point of the piezoelectric beam can be expressed under the Euler beam hypotheses as

$$u(x,z) = u_0(x) - z\frac{\mathrm{d}w(x)}{\mathrm{d}x}, \tag{8.4}$$

where $u_0(x)$ is the axial displacement along the centroidal axis of the beam, which may be induced by the applied mechanical load, the applied electrical load due to the electromechanical coupling or the flexoelectric effect. The only non-zero strain for the beam is obtained from Eq. (8.2) as $\varepsilon_x = \dfrac{\mathrm{d}u_0}{\mathrm{d}x} - z\dfrac{\mathrm{d}^2 w}{\mathrm{d}x^2}$. Note that $h \ll L$ is assumed for the Euler beam and the axial displacement is small compared to the transverse displacement for a bending beam; the strain gradient $\varepsilon_{x,x} = \dfrac{\mathrm{d}^2 u_0}{\mathrm{d}x^2} - z\dfrac{\mathrm{d}^3 w}{\mathrm{d}x^3}$ can be neglected in comparison with $\varepsilon_{x,z} = -\dfrac{\mathrm{d}^2 w}{\mathrm{d}x^2}$. Thus we only consider the flexoelectricity induced by the strain gradient $\varepsilon_{x,z}$ in the following analysis.

The electric field is assumed to exist only in the beam thickness direction as justified in Wang and Feng's work (2010), in which the authors stated that for a

piezoelectric nanobeam under an electric potential across its thickness, the electric field component in the length direction was negligible compared with that in the thickness direction based on the existing numerical simulation results (Gao and Wang, 2007). In the formulation, the following matrix notations are introduced for convenience, *i.e.* $c_{11} = c_{1111}$, $d_{31} = d_{311}$ and $f_{13} = f_{1133}$. From the third equation of Eqs. (8.3) and Eq. (8.4), the electric field in z direction can be written as

$$E_z = a_{33} P_z + d_{31} \left(\frac{du_0}{dx} - z \frac{d^2 w}{dx^2} \right) - f_{13} \frac{d^2 w}{dx^2},$$

(8.5)

in which the extra term $-f_{13} \dfrac{d^2 w}{dx^2}$ different from the linear piezoelectricity theory attributes to the flexoelectric effect.

In the absence of free body charges, the Gauss's law is satisfied as

$$-\epsilon_0 \frac{\partial^2 \Phi}{\partial z^2} + \frac{\partial P_z}{\partial z} = 0,$$

(8.6)

where $\epsilon_0 = 8.85 \times 10^{-12}$ F/m is the permittivity of the vacuum or air. Φ is the electric potential and is related to the electric field by $E_z = -\partial \Phi / \partial z$. With the consideration of the electric boundary conditions $\Phi(h/2) = \Delta V$ and $\Phi(-h/2) = 0$, the polarization and the electric field from Eqs. (8.5) and (8.6) can be determined in terms of u_0 and w as

$$P_z = \frac{\epsilon_0 d_{31}}{\epsilon_0 a_{33} + 1} z \frac{d^2 w}{dx^2} - \frac{d_{31}}{a_{33}} \frac{du_0}{dx} + \frac{f_{13}}{a_{33}} \frac{d^2 w}{dx^2} - \frac{\Delta V}{a_{33} h}; \; E_z = -\frac{d_{31}}{\epsilon_0 a_{33} + 1} z \frac{d^2 w}{dx^2} - \frac{\Delta V}{h}.$$

(8.7)

By substituting the first equation of Eqs. (8.7) into the first equation of Eqs. (8.3), the axial stress σ_x can be obtained as

$$\sigma_x = \left(c_{11} - \frac{d_{31}^2}{a_{33}} \right) \frac{du_0}{dx} - \left(c_{11} - \frac{\epsilon_0 d_{31}^2}{\epsilon_0 a_{33} + 1} \right) z \frac{d^2 w}{dx^2} + \frac{d_{31} f_{13}}{a_{33}} \frac{d^2 w}{dx^2} - \frac{d_{31}}{a_{33}} \frac{\Delta V}{h}.$$

(8.8)

It is seen from the above equation that an axial force

$$T_x = b \int_{-h/2}^{h/2} \sigma_x \, dz = bh \left[\left(c_{11} - \frac{d_{31}^2}{a_{33}} \right) \frac{du_0}{dx} + \frac{d_{31} f_{13}}{a_{33}} \frac{d^2 w}{dx^2} - \frac{d_{31}}{a_{33}} \frac{\Delta V}{h} \right]$$ is developed in the beam,

which originates from the strain, and the electromechanical couplings induced by the strain gradient and the applied electrical load. Obviously, for a C-F beam without any applied mechanical loads in the axial direction, this force is 0 due to the traction free condition, resulting in a relaxation strain $\varepsilon_0 = \dfrac{\mathrm{d}u_0}{\mathrm{d}x} = -\dfrac{d_{31}}{a_{33}c_{11} - d_{31}^2}\left(f_{13}\dfrac{\mathrm{d}^2 w}{\mathrm{d}x^2} - \dfrac{\Delta V}{h}\right)$. However, for a C-C or an S-S beam with the axial displacement being restricted ($u_0 = 0$), this resultant force becomes $F_x = bh\left(\dfrac{d_{31}f_{13}}{a_{33}}\dfrac{\mathrm{d}^2 w}{\mathrm{d}x^2} - \dfrac{d_{31}}{a_{33}}\dfrac{\Delta V}{h}\right)$, which is expected to influence the bending behaviors of the C-C and S-S beams. It should be mentioned that if this axial force becomes compressive and sufficient large, for example, when a large positive electric potential ($\Delta V > 0$) is applied, mechanical buckling may occur.

The energy method is used to obtain the governing equations of the bending piezoelectric nanobeams with the consideration of the flexoelectricity. From Eqs. (8.1) and (8.3), the internal energy density function is given as $U = \dfrac{1}{2}\left(\sigma_x \varepsilon_x + \sigma_{xxz}\varepsilon_{x,z} + E_z P_z\right)$ with $\sigma_{xxz} = f_{13}\left[\left(\dfrac{\epsilon_0 d_{31}}{\epsilon_0 a_{33} + 1}z + \dfrac{f_{13}}{a_{33}}\right)\dfrac{\mathrm{d}^2 w}{\mathrm{d}x^2} - \dfrac{d_{31}}{a_{33}}\dfrac{\mathrm{d}u_0}{\mathrm{d}x} - \dfrac{\Delta V}{a_{33}h}\right]$ (Hu and Shen, 2010). The electric enthalpy density H is defined as $H = U - \dfrac{1}{2}\epsilon_0 \Phi_{,z}\Phi_{,z} + \Phi_{,z}P_z$. In the entire volume Ω of the piezoelectric beam, the variational principle takes (Hu and Shen, 2010)

$$-\delta \int_\Omega H \mathrm{d}\Omega + \delta W = 0, \tag{8.9}$$

which gives the governing equations of the bending piezoelectric beams. For the C-C and S-S beams, the work done by the resultant axial force is $W = -\dfrac{1}{2}\int_0^L F_x \left(\mathrm{d}w/\mathrm{d}x\right)^2 \mathrm{d}x$ (Rao, 2007). While for the C-F beam, the relaxation strain as discussed before must be considered. Therefore, the governing equations are derived as

$$\left(EA\right)^* \dfrac{\mathrm{d}^2 u_0}{\mathrm{d}x^2} + C\dfrac{\mathrm{d}^3 w}{\mathrm{d}x^3} = 0; \quad \left(EI\right)^* \dfrac{\mathrm{d}^4 w}{\mathrm{d}x^4} + C\dfrac{\mathrm{d}^3 u_0}{\mathrm{d}x^3} = 0 \quad \text{(C-F)}, \tag{8.10}$$

and

$$\left(EI\right)^{*}\frac{\mathrm{d}^{4}w}{\mathrm{d}x^{4}}+D\frac{\mathrm{d}^{2}w}{\mathrm{d}x^{2}}=0 \quad \text{(C-C, S-S),} \tag{8.11}$$

where $C=\dfrac{d_{31}f_{13}}{a_{33}}bh$ and $D=\dfrac{d_{31}}{a_{33}}\Delta Vb$. $\left(EA\right)^{*}=\left(c_{11}-\dfrac{d_{31}^{2}}{a_{33}}\right)bh$ is the effective axial

rigidity and $\left(EI\right)^{*}=\left(c_{11}-\dfrac{\epsilon_{0}d_{31}^{2}}{\epsilon_{0}a_{33}+1}\right)\dfrac{bh^{3}}{12}-\dfrac{f_{13}^{2}}{a_{33}}bh$ is the effective bending rigidity.

Obviously, the bending rigidity is affected by the flexoelectricity through the extra term

$-\dfrac{f_{13}^{2}}{a_{33}}bh$, resulting in a smaller value as compared to the conventional piezoelectric beam.

The flexocoupling coefficient can be determined from the first principles calculation (Ponomareva *et al.*, 2012). According to Refs. (Eliseev *et al.*, 2009; Ponomareva *et al.*, 2012; Chen and Soh, 2012), the typical value of the flexocoupling tensor elements range

from 1 V to 10 V, thus the value of $\dfrac{f_{13}^{2}}{a_{33}}$ falls in the range of $10^{-8}\sim10^{-6}$ SI units, which is

comparable to $\left(c_{11}-\dfrac{\epsilon_{0}d_{31}^{2}}{\epsilon_{0}a_{33}+1}\right)\dfrac{h^{2}}{12}$ when the beam thickness scales down to nanometers.

Therefore, the flexoelectric effect cannot be neglected at the nanoscale but the condition $\left(EI\right)^{*}>0$ must be valid for the stability of the system without considering the higher

gradient term (*e.g.* strain gradient and strain gradient coupling term $\dfrac{1}{2}g_{ijklmn}u_{i,jk}u_{l,mn}$). In

fact, $\left(EI\right)^{*}<0$ can only be reached when the beam thickness h is below 5.39 nm with the considered material properties for barium titanate. At this truly small scale, one needs to resort to atomistic simulations for the accurate predictions of the properties of structures in order to capture the edge effects (He and Lilley, 2008), which is out of the scope of the current work. In addition, surface effects have been demonstrated to increase the bending rigidity of the piezoelectric structures prominently at the nanoscale (Yan and Jiang, 2011a; b; Li *et al.*, 2011), which are also ignored in the current work.

With the consideration of the applied concentrated force F, the boundary conditions can be deduced from Eq. (8.9) for the beams with different boundary constraints. For a C-

F beam, the transverse displacement and slope at the free end $x=0$ are zeros,
i.e. $w = \dfrac{\mathrm{d}w}{\mathrm{d}x} = 0$. The moment and force equilibrium at $x = L$ gives

$$\left(EI\right)^{*}\frac{\mathrm{d}^{2}w}{\mathrm{d}x^{2}}+C\frac{\mathrm{d}u_{0}}{\mathrm{d}x}+\frac{f_{13}}{a_{33}}\Delta Vb=0; \quad -\left(EI\right)^{*}\frac{\mathrm{d}^{3}w}{\mathrm{d}x^{3}}-C\frac{\mathrm{d}^{2}u_{0}}{\mathrm{d}x^{2}}+F=0. \tag{8.12}$$

The boundary condition for a C-C beam is the same as that for a C-F beam at $x = 0$. In
addition, $\dfrac{\mathrm{d}w}{\mathrm{d}x} = 0$ at $x=L/2$ due to the symmetry and the force equilibrium at $x=L/2$ results
in

$$-\left(EI\right)^{*}\frac{\mathrm{d}^{3}w}{\mathrm{d}x^{3}}-D\frac{\mathrm{d}w}{\mathrm{d}x}+\frac{F}{2}=0. \tag{8.13}$$

For an S-S beam, the displacement $w = 0$ at $x = 0$. The slope and force equilibrium at $x = L/2$ are the same as the C-C beam. The moment equilibrium condition at $x = 0$ is given by

$$\left(EI\right)^{*}\frac{\mathrm{d}^{2}w}{\mathrm{d}x^{2}}+\frac{f_{13}}{a_{33}}\Delta Vb+\frac{C}{2}\left(\frac{\mathrm{d}w}{\mathrm{d}x}\right)^{2}=0, \tag{8.14}$$

in which the term $\dfrac{C}{2}\left(\dfrac{\mathrm{d}w}{\mathrm{d}x}\right)^{2}$ can be neglected under the infinitesimal deformation

assumption. It should also be noted that the term $\dfrac{f_{13}}{a_{33}}\Delta Vb$ in the first equation of Eq.
(8.12) and Eq. (8.14) represents the nonhomogeneity of the boundary conditions for the
C-F and S-S beams caused by the flexoelectricity, which results in a relaxation moment.
It should be mentioned that this relaxation moment depends on the applied electric
potential and becomes zero for the beam without applied electrical load.

Solving the governing equations (8.10) and (8.11) with the consideration of the
beam boundary conditions as stated above, the explicit expressions of the transverse
deflections for the C-F ($0 \le x \le L$), C-C ($0 \le x \le L/2$) and S-S ($0 \le x \le L/2$) beams are
derived as

$$w^{CF} = \frac{Fx^2}{6(EI)^{CF}}(x-3L) - \frac{c_{11}f_{13}\Delta Vbx^2}{2(a_{33}c_{11}-d_{31}^2)(EI)^{CF}},$$

$$\left((EI)^{CF} = (EI)^* - \frac{d_{31}^2 f_{13}^2 bh}{a_{33}^2 c_{11} - a_{33}d_{31}^2} \simeq (EI)^*\right)$$

(8.15)

$$w^{CC} = \begin{cases} \dfrac{F}{2s_1^3(EI)^*}\left\{\dfrac{\cosh\left(\dfrac{s_1 L}{2}\right)-1}{\sinh\left(\dfrac{s_1 L}{2}\right)}\left[1-\cosh(s_1 x)\right] - s_1 x + \sinh(s_1 x)\right\}; & \Delta V < 0 \\[4ex] \dfrac{F}{2s_2^3(EI)^*}\left\{\dfrac{\cos\left(\dfrac{s_2 L}{2}\right)-1}{\sin\left(\dfrac{s_2 L}{2}\right)}\left[1-\cos(s_2 x)\right] + s_2 x - \sin(s_2 x)\right\}; & \Delta V > 0 \\[4ex] \dfrac{F(-3L+4x)x^2}{48(EI)^*}, & \Delta V = 0 \end{cases}$$

(8.16)

$$w^{SS} = \begin{cases} \dfrac{F}{2s_1^3(EI)^*}\left[-s_1 x + \dfrac{\sinh(s_1 x)}{\cosh\left(\dfrac{s_1 L}{2}\right)}\right] + \dfrac{f_{13}\Delta Vb}{a_{33}s_1^2(EI)^*}\left[1-\cosh(s_1 x) + \dfrac{\sinh\left(\dfrac{s_1 L}{2}\right)}{\cosh\left(\dfrac{s_1 L}{2}\right)}\sinh(s_1 x)\right]; \\[2ex] \hfill \Delta V < 0 \\[4ex] \dfrac{F}{2s_2^3(EI)^*}\left[s_2 x - \dfrac{\sin(s_2 x)}{\cos\left(\dfrac{s_2 L}{2}\right)}\right] - \dfrac{f_{13}\Delta Vb}{a_{33}s_2^2(EI)^*}\left[1-\cos(s_2 x) - \tan\left(\dfrac{s_2 L}{2}\right)\sin(s_2 x)\right]; \\[2ex] \hfill \Delta V > 0 \\[4ex] \dfrac{F(-3L^2+4x^2)x}{48(EI)^*}, \quad \Delta V = 0 \end{cases}$$

(8.17)

where $s_1 = \sqrt{-\dfrac{d_{31}\Delta Vb}{a_{33}(EI)^*}}$ and $s_2 = \sqrt{\dfrac{d_{31}\Delta Vb}{a_{33}(EI)^*}}$. Substituting these displacement fields into

Eqs. (8.7) and (8.8), the corresponding polarization, electric field and stress developed in the beams with different boundary conditions can be derived.

The analytical solutions obtained in the current work clearly show the dependence of the electroelastic fields of the beams on the flexoelectricity. If the flexoelectric effect is excluded in the formulation, these equations can be reduced to the electroelastic fields of the conventional piezoelectric beams based on the linear piezoelectricity theory.

8.3   Results and discussion

In this section, the electroelastic responses of a piezoelectric nanobeam loaded with a concentrated force $F = 1$ nN and an electric potential ΔV under different boundary constraints are investigated to see the flexoelectric effect. The geometry of the beam is set as $L = 20\ h$ and $b = h$. BaTiO$_3$ is taken as the example material with its material properties being given in Giannakopoulos and Suresh's work (1999). For a narrow beam ($b < 5h$), the material properties under the plane stress condition are calculated as $c_{11} = 131$ GPa , $d_{31} = 1.87 \times 10^8$ V m^{-1} and $a_{33} = 0.79 \times 10^8$ V m C^{-1} . In addition, $f_{13} = 5$ V is adopted in the simulation according to Refs. (Eliseev *et al*., 2009; Ponomareva *et al*., 2012; Chen and Soh, 2012).

Firstly, the flexoelectric effect on the elastic fields of the bending beams is investigated. As discussed in the previous section, the effective bending rigidity $\left(EI\right)^{*}$ of the beam with the consideration of the flexoelectricity is smaller than the bending rigidity of the conventional piezoelectric beam, resulting in a softer bending behavior of the nanobeam under pure mechanical loading, *i.e.* a larger transverse displacement is induced in the applied mechanical load direction. This softer bending behavior is always demonstrated by the C-C beam regardless of the electrical load. However, the bending behavior of the C-F and S-S beams is also affected by the applied electric potential as indicated by Eqs. (8.15) and (8.17). Example calculations of the transverse displacement along the beam longitudinal axis from Eqs. (8.15)-(8.17) for the beams with different boundary conditions are plotted in Fig. 8.2, in which the arbitrary unit (Arb. unit) is adopted to represent the displacement profile. The beam thickness is taken as $h = 20$ nm and the applied electrical load is $\Delta V = -0.1$ V. It is shown from this figure that the C-F beam exhibits a stiffer elastic behavior while the C-C and S-S beams exhibit a softer elastic behavior than the corresponding conventional beams under this electrical loading

condition. The stiffer or softer behavior is attributed to the flexoelectricity, which may result in a non-homogeneous boundary condition for the beam in addition to modifying the effective bending rigidity. For the C-F and S-S beams subjected to such a negative electric potential, the non-homogeneous boundary condition effect is equivalent to adding a positive moment $-\dfrac{f_{13}c_{11}\Delta Vb}{c_{11}a_{33}-d_{31}^2}$ at the free end $x = L$ of the C-F beam and $-\dfrac{f_{13}\Delta Vb}{a_{33}}$ at the two ends $x = 0$ and $x = L$ of the S-S beam, respectively. Such a relaxation moment induces a displacement in the opposite direction of the applied mechanical load for the C-F beam while in the same direction as the applied mechanical load for the S-S beam. Therefore, the effect of the flexoelectricity induced non-homogeneous boundary condition to the bending behavior of the C-F beam is opposite to that of the effective bending rigidity, but more dominant when the beam is under such a large negative electric potential, leading to an overall stiffer elastic behavior of the C-F beam as compared to a conventional one. However, for an S-S beam, both of these two effects soften the beam. Thus, a much softer behavior is observed for the S-S beam with larger discrepancy between the displacements predicted from the current model and the conventional one without the flexoelectric effect. If a positive electric potential ($\Delta V > 0$) is applied to the C-F and the S-S beams, the effect of the flexoelectricity induced non-homogeneous boundary condition is equivalent to applying a negative relaxation moment. Therefore, the overall effect of the flexoelectricity may cause a stiffer elastic behavior for the S-S beam while a softer elastic behavior for the C-F beam if the applied electric potential is sufficiently large. However, it should be mentioned that a large positive electric potential may cause the mechanical buckling of the S-S beam as discussed in the previous section, which must be avoided to keep the stability of the beam system. It is thus concluded that the flexoelectric effect on the bending behavior of the beam is sensitive to the beam boundary conditions and the applied electrical load, *i.e.* the flexoelectricity always softens the bending of a C-C piezoelectric nanobeam, while may soften or stiffen the bending of the C-F and S-S piezoelectric nanobeams depending on the applied electric potential.

The flexoelectric effect on the beam elastic behavior can also be revealed by the contact stiffness k, which is defined as the ratio of the applied force to the induced
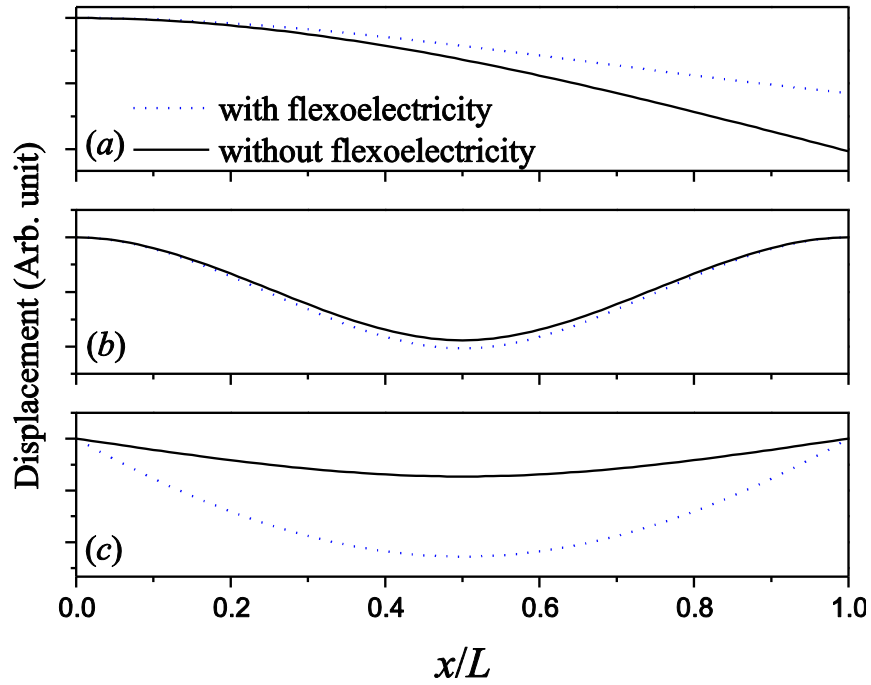
Figure 8.2: Transverse displacement along beam longitudinal direction with different boundary conditions (a) cantilever (b) clamped-clamped (c) simply supported ($\Delta V = -0.1$ V).
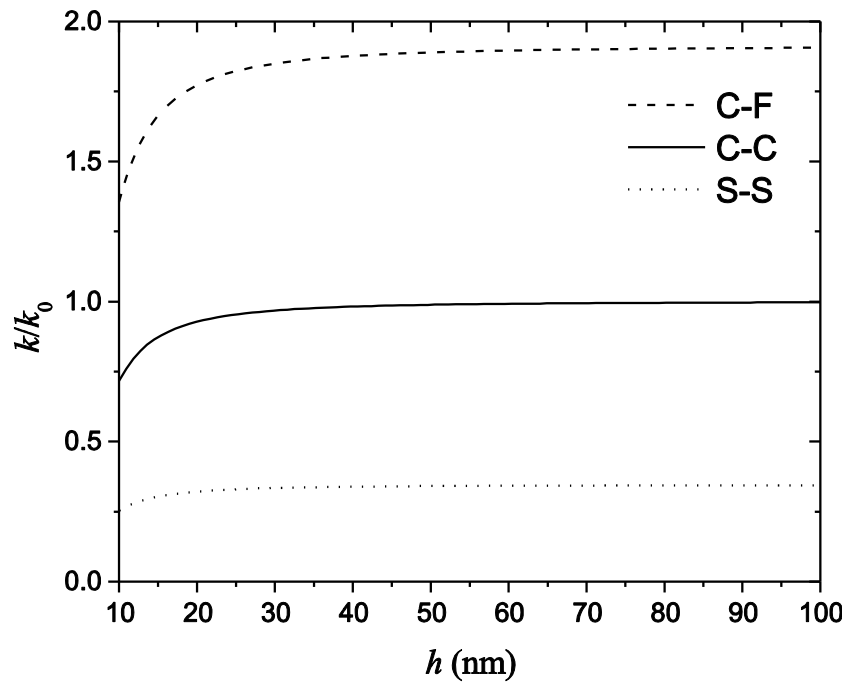

Figure 8.3: Variation of normalized contact stiffness with beam thickness for beams with different boundary conditions ($\Delta V = -0.1$ V).

displacement at the same point sustaining this force (Jing *et al*., 2006). Under the same loading condition as that in Fig. 8.2, the variation of the normalized contact stiffness k / k_0 with the beam thickness h is plotted in Fig. 8.3 with k_0 being the contact stiffness for a conventional beam. It is observed that the normalized contact stiffness increases with the scale up of the beam thickness for the beams with different boundary conditions. When the beam thickness is sufficiently large, k / k_0 approaches a constant. For a C-C beam, k / k_0 approaches unit due to the diminishing of the flexoelectric effect. However, for the C-F and S-S beams, the flexoelectricity induced relaxation moment prescribes a remanent contact stiffness for the beams, resulting in $k / k_0 = 1.9$ and $k / k_0 = 0.34$ for the C-F and S-S beams under such a loading condition. The stiffer bending behavior for the C-F beam and the softer elastic behavior for the S-S beam due to the combined effects of the flexoelectricity and the applied electrical load are consistent with the results in Fig. 8.2. Similarly, the flexoelectric effect on the contact stiffness will vary with the applied electric potential. For example, without the applied electrical load ($\Delta V = 0$), no relaxation moment develops for the C-F and the S-S beams, therefore, the normalized contact stiffness goes to unit for all these three kinds of beams with sufficiently large thickness.

It is obvious from the above discussion that for the bending piezoelectric nanobeams under a concentrated load, a residual deflection or contact stiffness exists for cantilevered and simply supported beams due to the strain gradient induced non-homogeneous boundary conditions, or namely non-local effects as stated in some literatures (Lim and Wang, 2007), which introduce a discontinuous jump at beam boundaries in a similar way as a concentrated load does. Under a pure electrical load, the residual quantities decay with the increase of the structural size. However, under both electrical and concentrated mechanical loads, these residual quantities depend on the flexocoupling coefficient, electrical load to mechanical load ratio V/F, location x and beam aspect ratio L/h while always become negligible for sufficient large aspect ratio L/h. Therefore, the predicted deflection and contact stiffness from the current model may not recover to the classical predictions when the structural size is beyond nanometer scale under certain circumstances (*e.g. L/h* is not sufficient large), as shown in Figs. 8.2 and 8.3. As is well

known that strain gradient theories can describe size effects in small scale problem; they also have important consequences in problems with concentrated sources. For example, significant difference between the solutions of the higher-order strain gradient model and classical model was revealed for a cantilevered nanobeam under a tip point load, particularly at the vicinity of the beam clamped end (Lim and Wang, 2007). A similar phenomenon was also observed by employing the polarization gradient theory (Yang *et al*., 2004), in which the potential field of a polarized ceramic due to a line charge source from polarization gradient theory was found to differ significantly from the classical solution near the source point. However, the merit of the current model lies in its capability of qualitatively predicting the trend of size-dependent bending properties of piezoelectric beams when their sizes scale down to nanometers. Moreover, the scaling effects of the relaxation strain, resultant force and polarization field of the piezoelectric beams under different boundary conditions could be efficiently predicted through the modeling with the flexoelectricity since the effects of classical terms in strain or electric fields are more dominant than the strain gradient induced extra terms in these quantities with the increase of the structural size, which will be demonstrated in later results and discussion.

Due to the inherent electromechanical coupling of piezoelectric materials, the applied electric potential in the beam polarization direction induces an axial strain along the beam centroidal axis under the free axial load condition. This relaxation strain is also influenced by the flexoelectricity, as indicated from the calculation in the previous Section, *i.e.* $\varepsilon_0 = -\dfrac{d_{31}}{a_{33}c_{11} - d_{31}^2}\left(f_{13}\dfrac{\mathrm{d}^2 w}{\mathrm{d}x^2} - \dfrac{\Delta V}{h}\right)$ for a C-F beam. The variation of this axial relaxation strain with the beam thickness h at both the beam free and fixed ends of a C-F beam under different electrical loads is plotted in Fig. 8.4, in which the relaxation strain without the consideration of the flexoelectric effect is also provided for comparison. In the absence of the flexoelectricity, $\varepsilon_0 = \dfrac{d_{31}\Delta V}{\left(a_{33}c_{11} - d_{31}^2\right)h}$ is independent of the beam longitudinal position x. However, this relaxation strain varies along the longitudinal position x when the flexoelectricity is considered since it depends on the changing strain
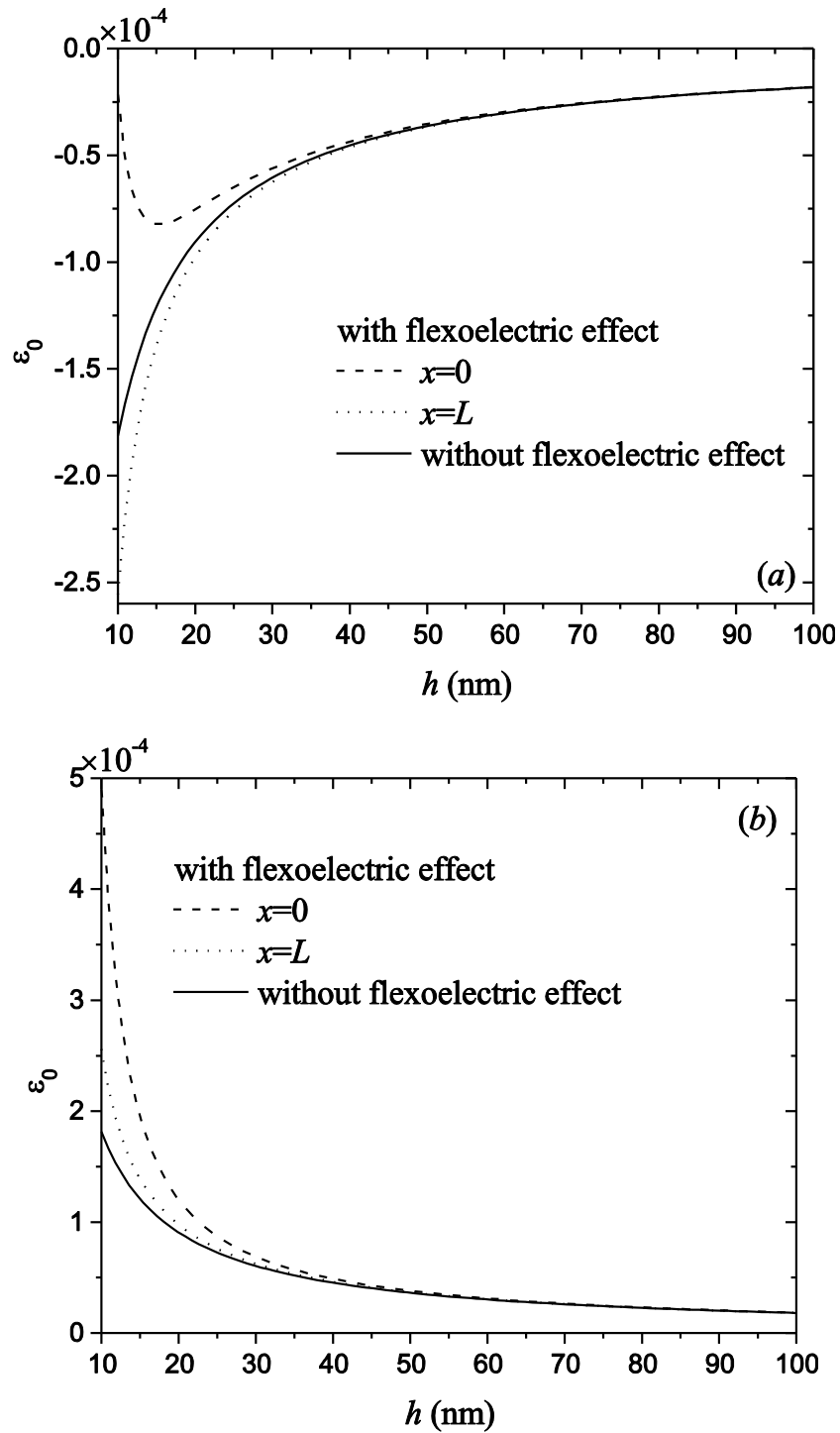
Figure 8.4: Variation of relaxation strain with beam thickness for a cantilever beam with different electrical loads (*a*) $\Delta V = -0.1$ V (*b*) $\Delta V = 0.1$ V.

gradient of the bending beam $\left(-\mathrm{d}^2 w / \mathrm{d}x^2\right)$ due to the mechanical load *F*. When a negative electric potential is applied, for example, $\Delta V = -0.1$ V, the relaxation strain is

negative and its absolute value at the beam fixed end ($x = 0$) first increases with h, then decreases with h as shown in Fig. 8.4(a). However, at the C-F beam free end ($x = L$), this negative relaxation strain always decreases with the increase of the beam thickness. It is observed from Fig. 8.4(b) that this strain becomes positive and decreases monotonously with the beam thickness h for both ends of the C-F beam when a positive voltage is applied, $\Delta V = 0.1$ V for example. The results in Fig. 8.4(a) and 8.4(b) demonstrate that the flexoelectric effect on the mechanical deformation is more pronounced for the C-F beam fixed end due to the higher strain gradient at this position. Moreover, the flexoelectric effect is observed to be more significant when the beam thickness h is small, and such an effect diminishes with the increase of h as indicated by the fact that the relaxation strain approaches to the result without the consideration of the flexoelectricity when h is sufficiently large. For a C-C beam and an S-S beam, the axial displacement is restricted while a nonzero axial force is developed in the beam as discussed before. Without considering the flexoelectricity, the resultant axial force $F_x^0 = -d_{31}\Delta Vb / a_{33}$ is a constant along the longitudinal axis of the beam and independent of the boundary conditions. In order to see the flexoelectric effect upon the developed axial force, Fig. 8.5 plots the normalized axial force F_x / F_x^0 versus the beam thickness h for both the C-C and S-S beams. Due to the symmetric deformation of the beams, this normalized force is plotted for both the end and the middle points of the beam. To avoid the mechanical buckling of the piezoelectric beam, a negative electric potential $\Delta V = -0.1$ V is applied. Similar to the relaxation strain observed in Fig. 8.4, this resultant axial force varies along the longitudinal axis of the beam. It is observed in this figure that the flexoelectric effect upon this axial force is more significant for the beams with smaller thickness. With the increase of the beam thickness h, the flexoelectric effect diminishes as expected. It is also found in this figure that the influence of the flexoelectricity upon the resultant axial force is sensitive to the beam boundary conditions. For the S-S beam, the flexoelectricity increases the resultant axial force along the whole length of the beam. However, for the C-C beam, the influence of the flexoelectricity has different trends for the material points along the beam length. For example, under the current loading condition, the flexoelectricity decreases the resultant axial force at the end of the beam ($x = 0$), while it

increases the axial force at the middle point ($x = L/2$) of the beam as compared to the results without the consideration of the flexoelectricity.
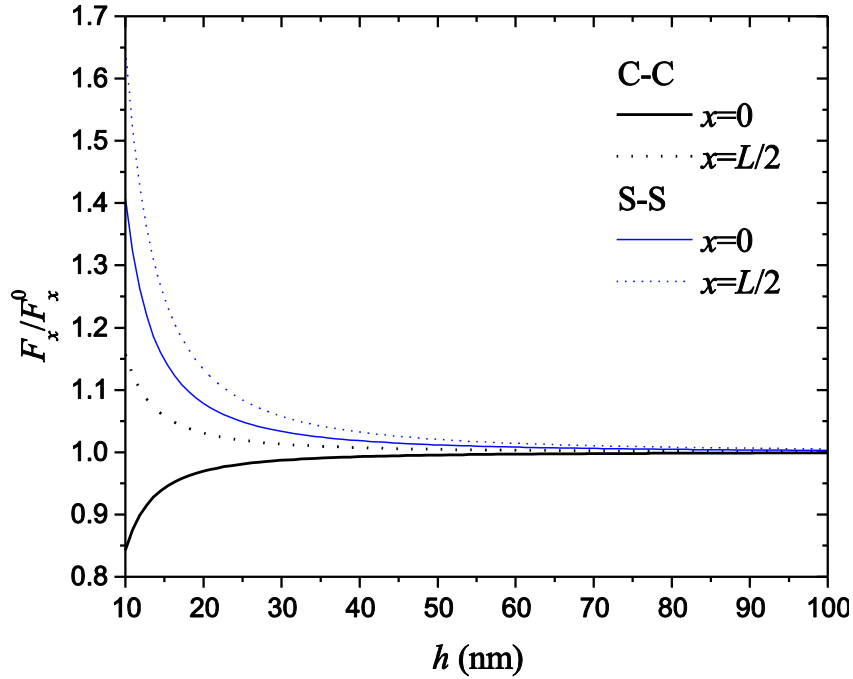

Figure 8.5: Variation of normalized axial force with beam thickness for both clamped-clamped and simply supported beams ($\Delta V = -0.1$ V).

The flexoelectric effect on the electrical field of the piezoelectric beam, such as the polarization, is also presented in the current work. Within the considered range of the beam thickness h and the material properties, the numerical value of $\dfrac{\epsilon_0 d_{31} h}{2(\epsilon_0 a_{33} + 1)}$ is $10^{-4} \sim 10^{-3}$ times of f_{13}/a_{33}. Therefore, the polarization contributed by the first term in the first equation Eq. (8.7) can be neglected and the polarization of the bending piezoelectric nanobeam can be regarded as uniformly distributed across the beam thickness. However, the polarization varies along the longitudinal axis of the nanobeam since the strain gradient effect is substantial and depends on the longitudinal position x. In Fig. 8.6, the polarization is plotted against the beam thickness h for a C-F beam under different electrical loads. The results for the cases with and without the consideration of the flexoelectricity are compared. Stronger dependence of the polarization on the flexoelectricity is observed for the beam with smaller thickness under both positive and
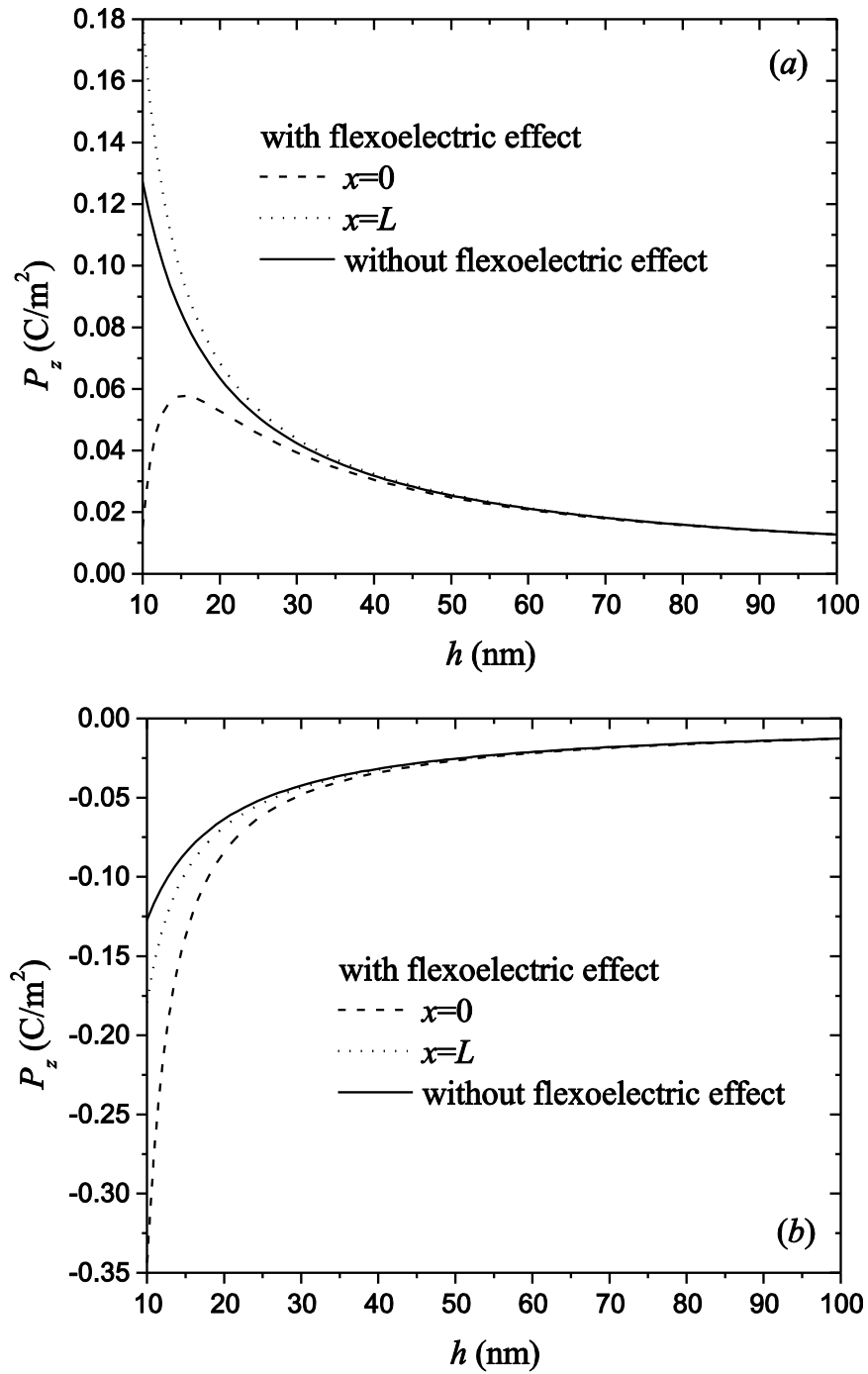
Figure 8.6: Variation of polarization with beam thickness for a cantilever beam under different electrical loads (a) $\Delta V = -0.1$ V (b) $\Delta V = 0.1$ V.
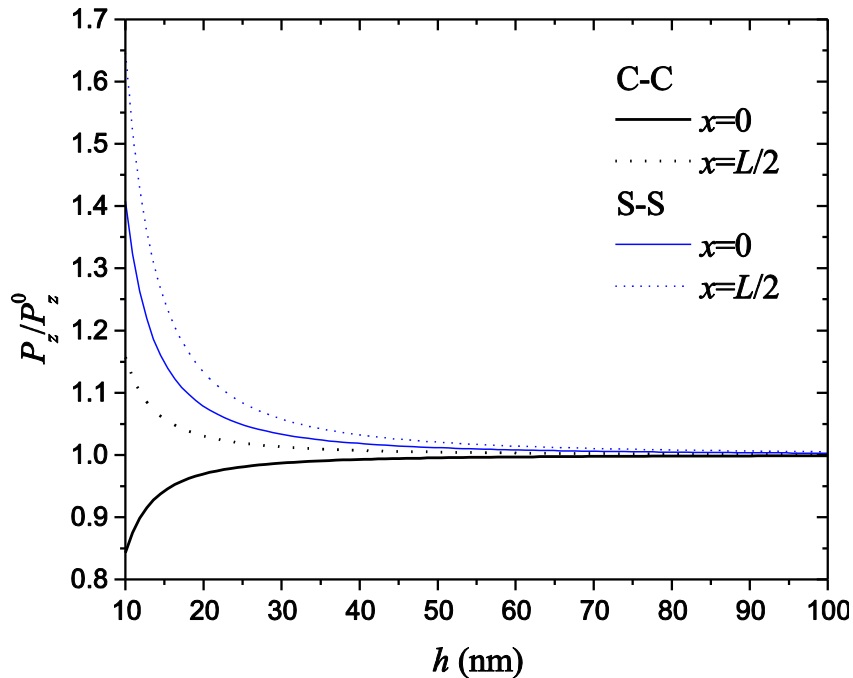
Figure 8.7: Variation of normalized polarization with beam thickness for both clamped-clamped and simply supported beams ($\Delta V = -0.1$ V).

negative applied electric potentials, while such dependence reduces with the increase of the beam thickness. As shown in Fig. 8.6(a), when a negative electric potential is applied, for example, $V = -0.1$ V, the polarization first increases then decreases with the increase of h at the beam fixed end ($x = 0$), while the flexoelectricity always increases the polarization of the beam at its free end ($x = L$). When a positive electric potential $V = 0.1$ V is applied, the variation trends of the polarization with the beam thickness h at both fixed end ($x = 0$) and the free end ($x = L$) are the same, $i.e.$ the magnitude of P_z decreases with the increase of the beam thickness h as shown in Fig. 8.6(b). The influence of the flexoelectricity on the polarization in the C-C and S-S piezoelectric nanobeams under $V = -0.1$ V is also studied by plotting the normalized polarization P_z / P_z^0 in Fig. 8.7, in which P_z^0 is the polarization in the beam without the consideration of the flexoelectric effect. Similarly, the flexoelectric effect on the polarization is more significant for the piezoelectric beams with smaller thickness, and such an effect is sensitive to the beam boundary conditions. It is worth mentioning that without the applied electric potential, the conventional electromechanical coupling effect (or the piezoelectric effect) induces a

polarization in the piezoelectric beams due to the bending deformation, which is negligible at the nanoscale. However, a much stronger polarization will present in these beams with different boundary conditions due to the flexoelectricity.

8.4 Conclusions

This work aims to provide a fundamental understanding on the flexoelectric effect upon the electroelastic responses of bending piezoelectric beams under different boundary conditions. A theoretical model based on the extended linear theory of piezoelectricity and the Euler-Bernoulli beam assumptions is developed for this purpose. Simulation results have demonstrated that the flexoelectricity has more significant effect on the electroelastic fields of the piezoelectric beams with smaller thickness and decays quickly with the increase of beam size. The results also indicate that for a cantilever beam, a relaxation strain is induced from the conventional electromechanical coupling and the flexoelectricity, which also result in the development of a resultant axial force in the clamped-clamped and simply supported beams. It is also observed in the current work that the flexoelectric effect on the electroelastic fields of the piezoelectric nanobeams is sensitive to the beam boundary conditions and the applied electric potential. The model developed here can be claimed as helpful for predicting a qualitative trend of the flexoelectric effect on the physical properties of piezoelectric nanostructures, suggesting that it is possible to use the flexoelectricity to modify the performance of piezoelectric nanobeam-based devices in NEMS. However, there are still some other factors that may exert influence on the properties of piezoelectric nanostructures, *e.g.* the higher order strain and strain gradient and strain gradient and strain gradient coupling effects, polarization gradient effect and surface effects. Such effects have not been taken into account in this study, which is the limitation of the current model. The development of a more comprehensive theoretical framework with the consideration of all these factors should be a further concentration of the future work.

References

Cady, W. G., 1946. Piezoelectricity: an introduction to the theory and applications of electromechanical phenomena in crystals, McGraw-Hill.

Catalan, G., Sinnamon, L. J. and Gregg, J. M., 2004. The effect of flexoelectricity on the dielectric properties of inhomogeneously strained ferroelectric thin films. J. Phys.: Condens. Matter **16**, 2253.

Chen, H. T. and Soh, A. K., 2012. Influence of flexoelectric effects on multiferroic nanocomposite thin bilayer films. J. Appl. Phys. **112**, 074104.

Eliseev, E. A., Morozovska, A. N., Glinchuk, M. D. and Blinc, R., 2009. Spontaneous flexoelectric/flexomagnetic effect in nanoferroics. Phys. Rev. B **79**, 165433.

Gao, Y. F. and Wang, Z. L., 2007. Electrostatic potential in a bent piezoelectric nanowire. The fundamental theory of nanogenerator and nanopiezotronics. Nano Lett. **7**, 2499-2505.

Giannakopoulos, A. E. and Suresh, S., 1999. Theory of indentation of piezoelectric materials. Acta Mater. **47**, 2153-2164.

He, J. and Lilley, C. M., 2008. Surface effect on the elastic behavior of static bending nanowires. Nano Lett. **8**, 1798-1802.

Hong, J. W., Catalan, G., Scott, J. F. and Artacho, E., 2010. The flexoelectricity of barium and strontium titanates from first principles. J. Phys.: Condens. Matter **22**, 112201.

Hu, S. L. and Shen, S. P., 2010. Variational principles and governing equations in nano-dielectrics with the flexoelectric effect. Sci. China-Phys. Mech. Astron. **53**, 1497-1504.

Huang, G. Y. and Yu, S. W., 2006. Effect of surface piezoelectricity on the electromechanical behaviour of a piezoelectric ring. Phys. Status Solidi-Rapid Res. Lett. **243**, R22-R24.

Jing, G. Y., Duan, H. L., Sun, X. M., Zhang, Z. S., Xu, J., Li, Y. D., Wang, J. X. and Yu, D. P., 2006. Surface effects on elastic properties of silver nanowires: Contact atomic-force microscopy. Phys. Rev. B **73**, 235409.

Lee, D., Yoon, A., Jang, S. Y., Yoon, J. G., Chung, J. S., Kim, M., Scott, J. F. and Noh, T. W., 2011. Giant flexoelectric effect in ferroelectric epitaxial thin films. Phys. Rev. Lett. **107**, 057602.

Li, Y. H., Fang, B., Zhang, J. H. and Song, J. Z., 2011. Surface effects on the wrinkling of piezoelectric films on compliant substrates. J. Appl. Phys. **110**, 114303.

Lim, C. W. and Wang, C. M., 2007. Exact variational nonlocal stress modeling with asymptotic higher-order strain gradients for nanobeams. J. Appl. Phys. **101**, 054312.

Liu, C. C., Hu, S. L. and Shen, S. P., 2012. Effect of flexoelectricity on electrostatic potential in a bent piezoelectric nanowire. Smart Mater. Struct. **21**, 115024.

Ma, W. H. and Cross, L. E., 2001a. Large flexoelectric polarization in ceramic lead magnesium niobate. Appl. Phys. Lett. **79**, 4420.

Ma, W. H. and Cross, L. E., 2001b. Observation of the flexoelectric effect in relaxor $Pb(Mg_{1/3}Nb_{2/3})O_3$ ceramics. Appl. Phys. Lett. **78**, 2920.

Ma, W. H. and Cross, L. E., 2005. Flexoelectric effect in ceramic lead zirconate titanate. Appl. Phys. Lett. **86**, 072905.

Ma, W. H. and Cross, L. E., 2006. Flexoelectricity of barium titanate. Appl. Phys. Lett. **88**, 232902.

Majdoub, M. S., Sharma, P. and Cagin, T., 2008. Size-dependent piezoelectricity and elasticity in nanostructures due to the flexoelectric effect. Phys. Rev. B **77**, 125424.

Maranganti, R., Sharma, N. D. and Sharma, P., 2006. Electromechanical coupling in nonpiezoelectric materials due to nanoscale nonlocal size effects: Green's function solutions and embedded inclusions. Phys. Rev. B **74**, 014110.

Maranganti, R. and Sharma, P., 2009. Atomistic determination of flexoelectric properties of crystalline dielectrics. Phys. Rev. B **80**, 054109.

Ponomareva, I., Tagantsev, A. K. and Bellaiche, L., 2012. Finite-temperature flexoelectricity in ferroelectric thin films from first principles. Phys. Rev. B **85**, 104101.

Le Quang, H. and He, Q. C., 2011. The number and types of all possible rotational symmetries for flexoelectric tensors. Proc. R. Soc. A **467**, 2369-2386.

Rao, S. S., 2007. Vibration of continuous systems, New York: Wiley.

Sharma, N. D., Landis, C. M. and Sharma, P., 2010. Piezoelectric thin-film superlattices without using piezoelectric materials. J. Appl. Phys. **108**, 024304.

Sharma, N. D., Maranganti, R. and Sharma, P., 2007. On the possibility of piezoelectric nanocomposites without using piezoelectric materials. J. Mech. Phys. Solids **55**, 2328-2350.

Shen, S. P. and Hu, S. L., 2010. A theory of flexoelectricity with surface effect for elastic dielectrics. J. Mech. Phys. Solids **58**, 665-677.

Shu, L. L., Wei, X. Y., Pang, T., Yao, X. and Wang, C. L., 2011. Symmetry of flexoelectric coefficients in crystalline medium. J. Appl. Phys. **110**, 104106.

Tagantsev, A. K., 1986. Piezoelectricity and flexoelectricity in crystalline dielectrics. Phys. Rev. B **34**, 5883-5889.

Wang, G. F. and Feng, X. Q., 2010. Effect of surface stresses on the vibration and buckling of piezoelectric nanowires. EPL **91**, 56007.

Yan, Z. and Jiang, L. Y., 2011a. Surface effects on the electromechanical coupling and bending behaviours of piezoelectric nanowires. J. Phys. D: Appl. Phys. **44**, 075404.

Yan, Z. and Jiang, L. Y., 2011b. The vibrational and buckling behaviors of piezoelectric nanobeams with surface effects. Nanotechnology **22**, 245703.

Yang, X. M., Hu, Y. T. and Yang, J. S., 2004. Electric field gradient effects in anti-plane problems of polarized ceramics. Int. J. Solids Struct. 41, 6801-6811.

Zhou, H., Hong, J. W., Zhang, Y. H., Li, F. X., Pei, Y. M. and Fang, D. N., 2012. Flexoelectricity induced increase of critical thickness in epitaxial ferroelectric thin films. Physica B **407**, 3377-3381.

Chapter 9

9   Size-dependent bending and vibration behavior of piezoelectric nanobeams aroused by flexoelectricity[8]

9.1   Introduction

The past decade has witnessed the successful development of nanoscale field effect transistors, piezoelectric-gated diodes, mechanical sensors, resonators and energy harvesters for meeting the demand of high precision and wireless NEMS devices (Wang, 2007). In these devices, the electromechanical coupling of dielectrics (including piezoelectric materials) plays a key role in their performance, particularly piezoelectricity, which refers to the generation of electric charges in response to a uniform strain. Recently, flexoelectricity, a spontaneous electric polarization generated in dielectric crystals due to a nonuniform strain or a strain gradient, has stimulated a surge of scientific interests and is believed to contribute to the electromechanical coupling of dielectrics under certain conditions. Since strain gradient is closely linked with the feature scale of structures, materials tend to exhibit stronger flexoelectricity when their structural size scales down to nanometer (Majdoub *et al*., 2008; Ma, 2008; 2010). Thus, it is necessary to explore the influence of flexoelectricity on the size-dependent mechanical and physical properties of nanostructured dielectric materials.

In literature, the flexoelectric effect was found to play an important role in explaining some unusual physical properties in ferroelectric thin films such as the reduction of dielectric constant (Catalan *et al*., 2004; 2005), polarization instability (Chu *et al*., 2004), shift in phase transition temperature (Eliseev *et al*., 2009) and asymmetry of hysteresis curves (Tagantsev and Gerra, 2006). Flexoelectric effect was also responsible for the non-switchable dead layer formed at the interface between the thin film and the contact electrode, resulting in a decrease in stored charge in the thin film capacitors (Tagantsev and Gerra, 2006; Majdoub *et al*., 2009). Due to the flexoelectric effect, electric polarization can be induced even in a non-piezoelectric dielectric material.

---

[8]A version of this chapter has been submitted to J. Phys. D: Appl. Phys.

Therefore, flexoelectricity in principle can be exploited to produce piezoelectric composites from non-piezoelectric constituents (Fousek *et al*., 1999; Sharma *et al*., 2007; 2010), which could be realized by either tailoring non-piezoelectric structure into a tapered pyramidal shape (Zhu *et al*., 2006) or designing it in the flexure mode (Chu *et al*., 2009) to obtain a non-homogeneous strain gradient. Investigation also showed that the physical properties of ferroelectric epitaxial thin films, such as domain configurations and hysteresis curves, could be tuned by means of the flexoelectric effect (Lee *et al*., 2011). Furthermore, flexoelectricity could be employed as a dynamic tool for polarization control and might enable data-storage application in which memory bits are written mechanically and read electrically (Lu *et al*., 2012).

For dealing with the practical device applications of piezoelectric nanostructures, it is necessary to establish theoretical frameworks to understand the fundamental physics of these materials at the nanoscale. The conventional electromechanical coupling has been well interpreted by the linear piezoelectricity theory developed by Toupin (1956). Mindlin (1969) extended this linear theory by incorporating the polarization gradient effect in a later work. Maranganti *et al*. (2006) developed a variation principle for dielectrics including both the strain gradient and polarization gradient effects. Recently, with the consideration of the flexoelectricity, electroelastic force and surface effects, a comprehensive theoretical framework for nanoscale dielectrics has been established (Hu and Shen, 2010; Shen and Hu, 2010). Owing to these pioneer works, the electromechanical coupling behavior of piezoelectric nanomaterials can be characterized and interpreted to some extend. For example, the flexoelectric effect was found to enhance the electromechanical coupling coefficient of piezoelectric nanowires by employing a modified Euler-Bernoulli model (Majdoub *et al*., 2008). The flexoelectricity was also incorporated in calculating the piezoelectric potential distribution in ZnO nanowire, and the predictions were in good agreement with experimental data (Liu *et al*., 2012). In our previous work, based on the Euler-Bernoulli beam theory, the size-dependent electroelastic reponses of a piezoelectric nanobeam were predicted with the consideration of the flexoelectricity (Yan and Jiang, 2013). However, understanding of the flexoelectric effect on the electromechanical coupling of nanostructured piezoelectric materials is still far from complete. To the authors' best knowledge, all the existing

continuum modeling on the size-dependent properties of one-dimensional piezoelectric nanostructures aroused by the flexoelectricity was based on the Euler-Bernoulli beam theory. As another effective mathematical model, the Timoshenko beam theory accounts for the effects of shear deformation and rotary inertia for vibrating beams, thus it is expected to be more accurate, particulary for beams with low length-to-thickness aspect ratio. To complement the theoretical modeling on the piezoelectric nanobeams, a comprehensive model based on the extended linear theory of piezoelectricity and Timoshenko beam theory will be developed in the current work to investigate the static bending and free vibration of a simply supported piezoelectric nanobeam with the consideration of the flexoelectricity. Simulations will be conducted to show how the flexoelectricity varies with the beam size and its influence on the static and dynamic behaviors of the beam. Since beam model mathematically represents fundamental building blocks in NEMS devices, such as nanowires and nanobelts, this work is expected to be beneficial for the design and applications of one-dimensional piezoelectric structure-based nanodevices.

9.2   Formulation of the problem

The problem envisaged in the current work is a simply supported piezoelectric nanobeam with length L, width b and thickness h under an electric potential V and a distributed transverse load q, as shown in Fig. 9.1. A Cartesian coordinate system (oxz) is applied to describe the beam position with the x-axis being along the beam centroidal axis. The poling direction of the piezoelectric material coincides with the z-axis. To conduct the bending analysis of the piezoelectric nanobeam with the flexoelectricity, Timoshenko beam theory is adopted with the displacement field being defined as (Rao, 2007)

$$u = -z\phi(x,t); \quad w = w(x,t),$$

(9.1)

where t is the time, u and w are the displacement components along the x and z directions for an arbitrary point in the beam, respectively. ϕ is the rotation angle of the beam cross section due to pure bending. In particular, $\phi = \partial w/\partial x$ for an Euler-Bernoulli beam. Accordingly, the strains can be derived as

$$S_x = -z\frac{\partial\phi}{\partial x}; \quad S_{xz} = \frac{1}{2}\left(-\phi+\frac{\partial w}{\partial x}\right). \tag{9.2}$$

The electric field is assumed to exist only in the z direction, which is expressed in terms of the electric potential as

$$E_z = -\frac{\partial\Phi}{\partial z}. \tag{9.3}$$

To account for the flexoelectric effect, the extended linear theory of piezoelectricity incorporating the strain gradient and the electric polarization coupling is employed in the current study. Neglecting the effect of higher order terms (fifth order tensors and higher), the general expression for the internal energy density function U can be written as (Majdoub *et al*., 2008; Hu and Shen, 2010)

$$U = \frac{1}{2}\mathbf{P}\cdot\mathbf{a}\cdot\mathbf{P}+\frac{1}{2}\mathbf{S:c:S+S:d}\cdot\mathbf{P+P}\cdot\mathbf{f:}\nabla\nabla\mathbf{u}, \tag{9.4}$$

where $\mathbf{P}$ and $\mathbf{u}$ are the polarization and displacement vectors; $\mathbf{S}$ is the strain tensor; $\mathbf{a}$, $\mathbf{c}$ and $\mathbf{d}$ are the reciprocal dielectric susceptibility, elastic coefficient and piezoelectric coefficient tensors, respectively; $\mathbf{f}$ is the fourth order polarization and strain gradient coupling tensor, *i.e.* the flexocoupling coefficient tensor (Eliseev *et al*., 2009).
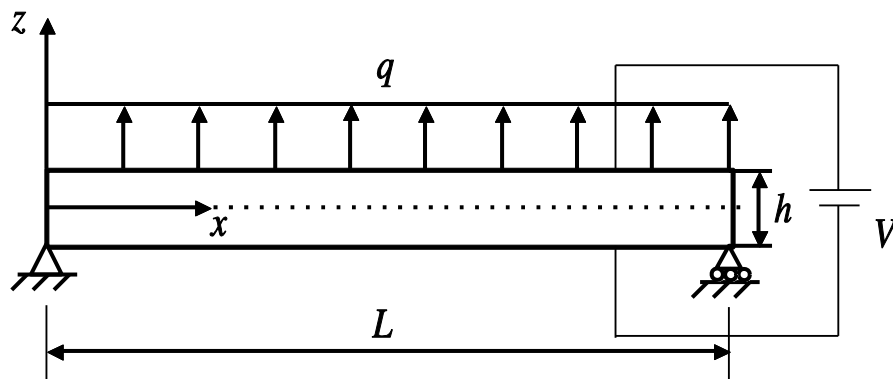
Figure 9.1: Schematic of a simply supported piezoelectric nanobeam subjecting to a distributed mechanical load q and an electrical load V.

The constitutive equations can thus be expressed as

$$\mathbf{T}=\frac{\partial U}{\partial\mathbf{S}}=\mathbf{c:S+d}\cdot\mathbf{P};\ \overline{\mathbf{T}}=\frac{\partial U}{\partial\nabla\nabla\mathbf{u}}=\mathbf{f}\cdot\mathbf{P};\ \mathbf{E}=\frac{\partial U}{\partial\mathbf{P}}=\mathbf{a}\cdot\mathbf{P+d:S+f:}\nabla\nabla\mathbf{u}, \tag{9.5}$$

where **T** and **E** are the stress tensor and the electric field vector, respectively. $\overline{\mathbf{T}}$ was defined as the higher order stress or the moment stress tensor (Majdoub *et al.*, 2008; Hu and Shen, 2010), which is induced by the flexoelectric effect. From the above equations, the constitutive relations for the one-dimensional Timoshenko piezoelectric nanobeam are derived as

$$
\left.
\begin{aligned}
T_x &= c_{11}S_x + d_{31}P_z; \\
T_{zx} &= kc_{44}\left(-\phi + \frac{\partial w}{\partial x}\right); \\
\overline{T}_{xxz} &= f_{13}P_z; \\
E_z &= a_{33}P_z + d_{31}S_x + f_{13}S_{x,z},
\end{aligned}
\right\}
\tag{9.6}
$$

where k is the shear correction factor and is taken as 5/6 for a rectangular cross section (Abbasion *et al.*, 2009). In order to obtain the analytical solutions of the problem, the piezoelectric effect contributed by d_{15} is neglected although nonzero shear strain exists (Wang, 2013). In addition, only the strain gradient along the beam thickness direction, *i.e.* $S_{x,z} = -\partial\phi/\partial x$ is considered, while the strain gradients along the beam length direction $S_{x,x}$ and $S_{zx,x}$ are neglected for simplicity.

In the absence of free electric charges, the Gauss's law requires

$$
-\varepsilon_0 \frac{\partial^2 \Phi}{\partial z^2} + \frac{\partial P_z}{\partial z} = 0,
\tag{9.7}
$$

where $\varepsilon_0 = 8.85 \times 10^{-12}$ C V^{-1} m^{-1} is the permittivity of the vacuum or air. Considering Eq. (9.3), the third equation of Eqs. (9.6) and Eq. (9.7), and the electric boundary conditions $\Phi(-h/2) = 0$ and $\Phi(h/2) = V$, the electric polarization and electric field are determined as

$$
P_z = \frac{\varepsilon_0 d_{31}}{\varepsilon_0 a_{33} + 1}\frac{\partial\phi}{\partial x}z + \frac{f_{13}}{a_{33}}\frac{\partial\phi}{\partial x} - \frac{V}{a_{33}h}; E_z = -\frac{d_{31}}{\varepsilon_0 a_{33} + 1}\frac{\partial\phi}{\partial x}z - \frac{V}{h}.
\tag{9.8}
$$

Substituting the first equation of Eqs. (9.8) into the first two equations of Eqs. (9.6), the expressions of the stresses and the higher order stresses can be obtained in terms of ϕ and w accordingly.

In this study, Hamilton's principle is adopted to derive the governing equations and boundary conditions of the piezoelectric nanobeam with the consideration of the flexoelectric effect, which follows

$$\delta \int_{t_1}^{t_2} \left(-\int_{\Omega} H d\Omega + K + W \right) dt = 0 \tag{9.9}$$

where Ω is the entire volume occupied by the piezoelectric beam. $H = U - \frac{1}{2}\varepsilon_0 \Phi_{,z}\Phi_{,z} + \Phi_{,z}P_z$ is the electric enthalpy density. From Eqs. (9.5), Eq. (9.4) is reduced to $U = \frac{1}{2}T_x S_x + T_{xz}S_{xz} + \frac{1}{2}\bar{T}_{xxz}S_{x,z} + \frac{1}{2}E_z P_z$ for the one-dimensional piezoelectric beam. $K = \frac{1}{2}\int_0^L \left[\rho A \left(\frac{\partial w}{\partial t} \right)^2 + \rho I \left(\frac{\partial \phi}{\partial t} \right)^2 \right] dx$ is the kinetic energy, in which ρ is the mass density, $A = bh$ and $I = \frac{1}{12}bh^3$ are the area and second moment of area of the rectangle beam, respectively. The work done by external loads is defined as $W = \int_0^L qw dx - \frac{1}{2}\int_0^L F_x \left(\partial w / \partial x \right)^2 dx$ with $F_x = \int_A T_x dA = d_{31} \left(\frac{f_{13}}{a_{33}} \frac{\partial \phi}{\partial x} - \frac{V}{a_{33}h} \right) A$. For simplicity, we ignore the length change of the beam induced by the shear deformation, then $\partial w / \partial x$ in the second term of W is approximated by ϕ in the derivation of the governing equations. It should be mentioned that the axial force F_x originates from the inherent electromechanical coupling of piezoelectric materials (d_{31}) and the flexoelectric effect (f_{13}). When the flexoelectric effect is excluded, F_x is a constant. Applying the variational principle of Eq. (9.9), the following governing equations are obtained in terms of the beam transverse displacement w and rotation angle ϕ as

$$-\left(EI \right)^* \frac{\partial^2 \phi}{\partial x^2} - kAc_{44}\left(-\phi + \frac{\partial w}{\partial x} \right) - \frac{d_{31}Vb}{a_{33}}\phi + \rho I \frac{\partial^2 \phi}{\partial t^2} = 0, \tag{9.10}$$

$$-kAc_{44}\left(-\frac{\partial \phi}{\partial x} + \frac{\partial^2 w}{\partial x^2} \right) + \rho A \frac{\partial^2 w}{\partial t^2} = q, \tag{9.11}$$

with the effective bending rigidity $(EI)^* = \left(c_{11} - \dfrac{\varepsilon_0 d_{31}^2}{\varepsilon_0 a_{33}+1}\right)I - \dfrac{f_{13}^2}{a_{33}}A$. Obviously, the flexoelectricity reduces the bending rigidity of the beam as compared with the conventional one. The associated boundary conditions for the simply supported piezoelectric beam at $x = 0$ and $x = L$ are expressed as

$$w = 0 \text{ and } (EI)^* \frac{\partial \phi}{\partial x} + \frac{f_{13}}{a_{33}}bV + \frac{1}{2}A\frac{d_{31}f_{13}}{a_{33}}\phi^2 = 0, \tag{9.12}$$

in which the term $\dfrac{1}{2}A\dfrac{d_{31}f_{13}}{a_{33}}\phi^2$ is ignored under the infinitesimal deformation assumption.

It is noted that the flexoelectric effect not only modifies the bending rigidity but also causes a non-homogeneous boundary condition for the beam, as shown in Eq. (9.12).

A. Static bending of a piezoelectric nanobeam

For static bending of a piezoelectric nanobeam, the governing equations are simplified from Eqs. (9.10) and (9.11) as

$$-(EI)^* \frac{\mathrm{d}^2\phi}{\mathrm{d}x^2} - kAc_{44}\left(-\phi + \frac{\mathrm{d}w}{\mathrm{d}x}\right) - \frac{d_{31}Vb}{a_{33}}\phi = 0, \tag{9.13}$$

$$-kAc_{44}\left(-\frac{\mathrm{d}\phi}{\mathrm{d}x} + \frac{\mathrm{d}^2w}{\mathrm{d}x^2}\right) = q. \tag{9.14}$$

Combining Eq. (9.13) and (9.14), we have

$$(EI)^* \frac{\mathrm{d}^3\phi}{\mathrm{d}x^3} + \frac{d_{31}Vb}{a_{33}}\frac{\mathrm{d}\phi}{\mathrm{d}x} = q. \tag{9.15}$$

The general solution of Eq. (9.15) can be expressed as

$$\phi = \begin{cases} C_1 e^{\lambda x} + C_2 e^{-\lambda x} + \dfrac{qa_{33}}{d_{31}Vb}x + C_3 ; (V \neq 0) \\[2ex] \dfrac{q}{6(EI)^*}x^3 + D_1 x^2 + D_2 x + D_3, (V = 0) \end{cases} \tag{9.16}$$

with $\lambda = \sqrt{-\dfrac{d_{31}Vb}{a_{33}(EI)^*}}$. Integrating Eq. (9.13) with the consideration of Eq. (9.16), the

expression for w is obtained as

$$w = \begin{cases} \dfrac{1}{\lambda}\left(C_1 e^{\lambda x} - C_2 e^{-\lambda x}\right) + \dfrac{qx^2}{2}\left(\dfrac{a_{33}}{d_{31}Vb} - \dfrac{1}{kAc_{44}}\right) + C_3\left(1 - \dfrac{d_{31}V}{a_{33}hkc_{44}}\right)x + C_4; \ (V \neq 0) \\[4mm] \dfrac{q}{24(EI)^*}x^4 + \dfrac{D_1}{3}x^3 + \dfrac{1}{2}\left(D_2 - \dfrac{q}{kAc_{44}}\right)x^2 + \left(D_3 - \dfrac{2(EI)^*}{kAc_{44}}D_1\right)x + D_4, \ (V = 0) \end{cases} \tag{9.17}$$

with $C_1 - C_4$ and $D_1 - D_4$ being determined from the boundary conditions Eq. (9.12) as

$$\left.\begin{array}{l} C_1 = \dfrac{e^{-\lambda L}-1}{\lambda\left(e^{\lambda L} - e^{-\lambda L}\right)}\left[\dfrac{qa_{33}}{d_{31}Vb} + \dfrac{f_{13}bV}{a_{33}(EI)^*}\right]; \ C_2 = \dfrac{e^{\lambda L}-1}{\lambda\left(e^{\lambda L} - e^{-\lambda L}\right)}\left[\dfrac{qa_{33}}{d_{31}Vb} + \dfrac{f_{13}bV}{a_{33}(EI)^*}\right]; \\[6mm] C_3 = -\dfrac{qL\left(\dfrac{a_{33}}{d_{31}Vb} - \dfrac{1}{kAc_{44}}\right)}{2\left(1 - \dfrac{d_{31}V}{a_{33}khc_{44}}\right)}; \ C_4 = \dfrac{1}{\lambda^2}\left[\dfrac{qa_{33}}{d_{31}Vb} + \dfrac{f_{13}bV}{a_{33}(EI)^*}\right], \end{array}\right\} \tag{9.18}$$

and

$$D_1 = -\dfrac{qL}{4(EI)^*}; \ D_2 = 0; \ D_3 = \dfrac{qL^3}{24(EI)^*}; \ D_4 = 0. \tag{9.19}$$

Thus the completed electroelastic fields of the Timoshenko piezoelectric beam with the flexoelectric effect are determined. When the terms associated with the shear coefficient k are set as zeros, the corresponding solution reduces to that for an Euler-Bernoulli piezoelectric beam with the flexoelectricity. Moreover, the solution is further reduced to that for a classical Euler-Bernoulli piezoelectric beam when the flexoelectric effect is excluded.

B. Free vibration of a piezoelectric nanobeam

Combining Eq. (9.10) and Eq. (9.11), the governing equation for the free transverse vibration of a piezoelectric nanobeam can be written in terms of w as

$$\left(EI\right)^{*}\frac{\partial^{4}w}{\partial x^{4}}+\frac{d_{31}Vb}{a_{33}}\frac{\partial^{2}w}{\partial x^{2}}-\rho\left(I+\frac{\left(EI\right)^{*}}{kc_{44}}\right)\frac{\partial^{4}w}{\partial x^{2}\partial t^{2}}+\rho A\left(1-\frac{d_{31}V}{a_{33}kc_{44}h}\right)\frac{\partial^{2}w}{\partial t^{2}}+\frac{\rho^{2}I}{kc_{44}}\frac{\partial^{4}w}{\partial t^{4}}=0.$$

(9.20)

The harmonic solution of Eq. (9.20) for the simply supported beam takes the format of

$$w\left(x,t\right)=\sum_{n=1}^{\infty}C_{n}\sin\frac{n\pi x}{L}\cos\omega_{n}t,$$

(9.21)

where C_n is a constant, n is the mode number, and ω_n is the resonant frequency of the n-th mode. Substitution of Eq. (9.21) into Eq. (9.20) gives the characteristics equation for determining the beam resonant frequency, *i.e.*

$$\frac{\rho^{2}I}{kc_{44}}\omega_{n}^{4}-\rho\left[\left(I+\frac{\left(EI\right)^{*}}{kc_{44}}\right)\left(\frac{n\pi}{L}\right)^{2}+A\left(1-\frac{d_{31}V}{a_{33}khc_{44}}\right)\right]\omega_{n}^{2}+\left(EI\right)^{*}\left(\frac{n\pi}{L}\right)^{4}-\frac{d_{31}Vb}{a_{33}}\left(\frac{n\pi}{L}\right)^{2}=0.$$

(9.22)

Eq. (9.22) is a quadratic equation in ω_n^2 and gives two values of ω_n for any mode number n. The smaller value of ω_n corresponds to the bending deformation mode, while the larger one corresponds to the shear deformation mode. In the following case study, we will show how the flexoelectricity influences the first resonant frequency of the bending deformation mode of the piezoelectric nanobeam.

9.3 Results and discussion

In this work, the influence of the flexoelectric effect on the static and dynamic responses of a simply supported piezoelectric nanobeam is investigated. For case study, $BaTiO_3$ is taken as the example material with its material properties being given in Giannakopoulos and Suresh's work (1999). Under the plane stress condition, the elastic, piezoelectric and dielectric constants of $BaTiO_3$ are calculated as $c_{11}=131\,\text{GPa}$, $c_{44}=42.9\,\text{GPa}$, $d_{31}=1.87\times10^{8}\,\text{V m}^{-1}$ and $a_{33}=0.79\times10^{8}\,\text{V m C}^{-1}$, respectively. The mass density is $\rho=6.02\times10^{3}\,\text{kg m}^{-3}$. The flexocoupling coefficient of $BaTiO_3$ is not available in the open literatures due to the lack of experimental work and atomistic simulations, but should fall into the range of 1−10 V (Tagantsev and Yurkov, 2012). In the current

simulations, the flexocoupling coefficient takes $f_{13} = 5$ V following the following works (Eliseev *et al*., 2009; Tagantsev and Yurkov, 2012; Chen and Soh, 2012; Ponomareva *et al*., 2012). In the presented results and the corresponding discussion, symbols EB, TB, CEB and CTB are used to represent Euler beam, Timoshenko beam, classical Euler beam, and classical Timoshenko beam, respectively.

To demonstrate the flexoelectric effect on the static bending of the piezoelectric nanobeam, the transverse deflection of a simply supported beam with geometries $b = h = 10$ nm, $L = 50$ nm is plotted in Fig. 9.2 under the same mechanical load $q = 0.2$ nN/nm but different electrical loads $V = 0.1$ V and $V = -0.1$ V, respectively. The predictions based on the current modified Timoshenko and Euler theories with the consideration of the flexoelectricity are provided in this figure to compare with the results from the classical beam models. Obviously, the flexoelectric effect is significant for the bending of the beam as evidenced by the large discrepancies between the results of the current models and the classical models. Moreover, the flexoelectric effect is sensitive to the applied electrical load. In particular, when the applied electrical load is positive ($V = 0.1$ V), flexoelectricity increases the beam deflections for both TB and EB in comparison to CTB and CEB, as shown in Fig. 9.2(a); when the applied electrical load is negative and sufficient large, for example, $V = -0.1$ V as shown in Fig. 9.2(b), it is observed that the direction of the deflection can even be reversed due to the flexoelectric effect. This phenomenon can be interpreted by the nonhomogeneous boundary conditions induced by the flexoelectricity as shown in Eq. (9.12), *i.e.* the equivalent relaxation moment $-f_{13}bV/a_{33}$ at the beam ends $x = 0$ and $x = L$, which does not exist in classical beam theories. It is indicated from Eqs. (9.17) and (9.18) that the deflection of the beams depends on both the mechanical load q and the equivalent moment $-f_{13}bV/a_{33}$. Under $q = 0.2$ nN/nm, a positive deflection is produced for the Timoshenko and Euler beams. In addition, a positive electrical load V is equivalent to a negative relaxation moment at the beam ends, which induces a deflection in the same direction as that of the applied mechanical load; while a negative electrical load V is equivalent to a positive moment at the beam ends, resulting in a deflection in the opposite direction as that of the applied mechanical load. Therefore, the overall deflection of the beam depends on the combined
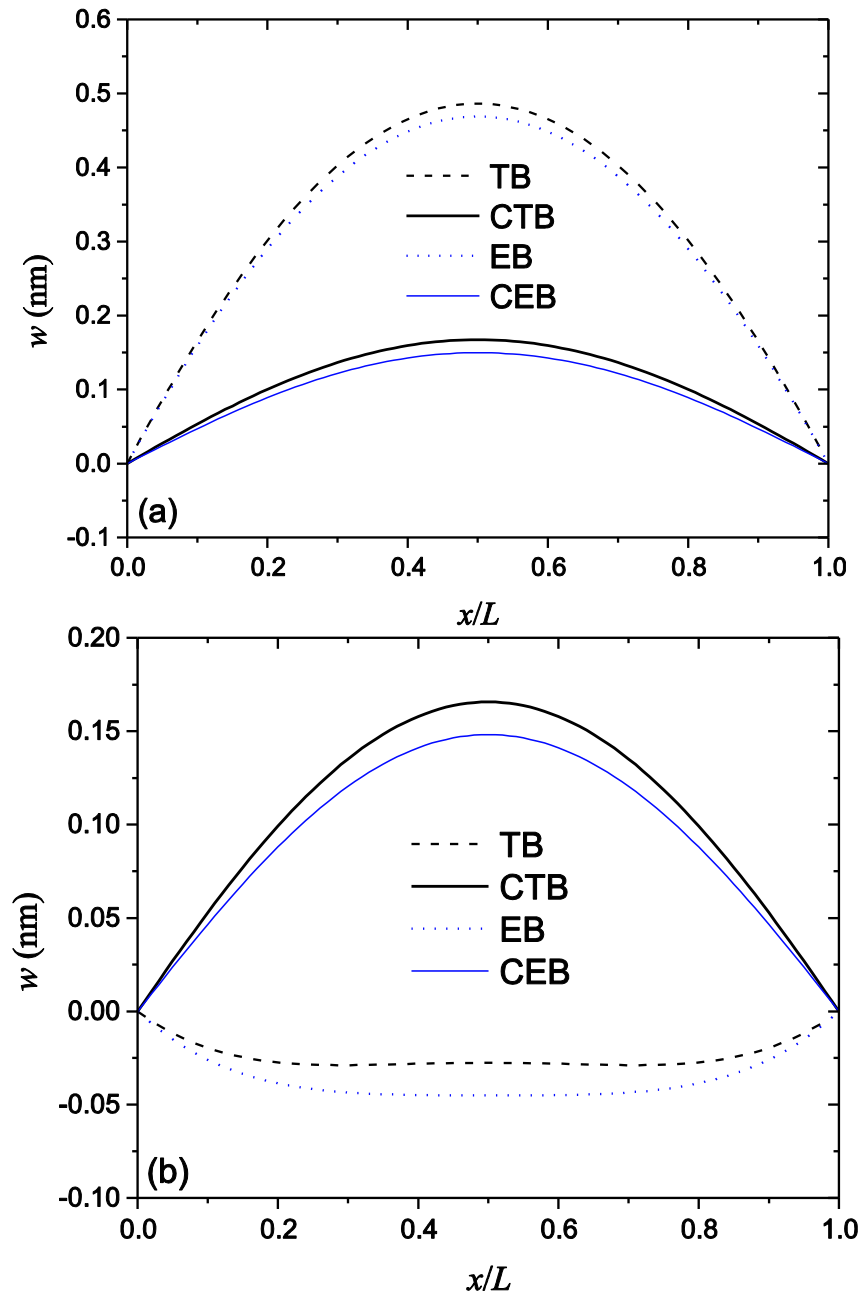
Figure 9.2: Deflections of the beams under distributed load (a) V=0.1 V and (b) V=−0.1 V.

effects of the mechanical load and the equivalent relaxation moment induced by the flexoelectricity, for example, the flexoelectricity may even change the mechanical deflection direction under certain conditions. This phenomenon indicates that the flexoelectricity can be used to control the displacement profile of a piezoelectric nanobeam at the nanoscale, which is useful for the design of piezoelectric nanobeam-based actuators.
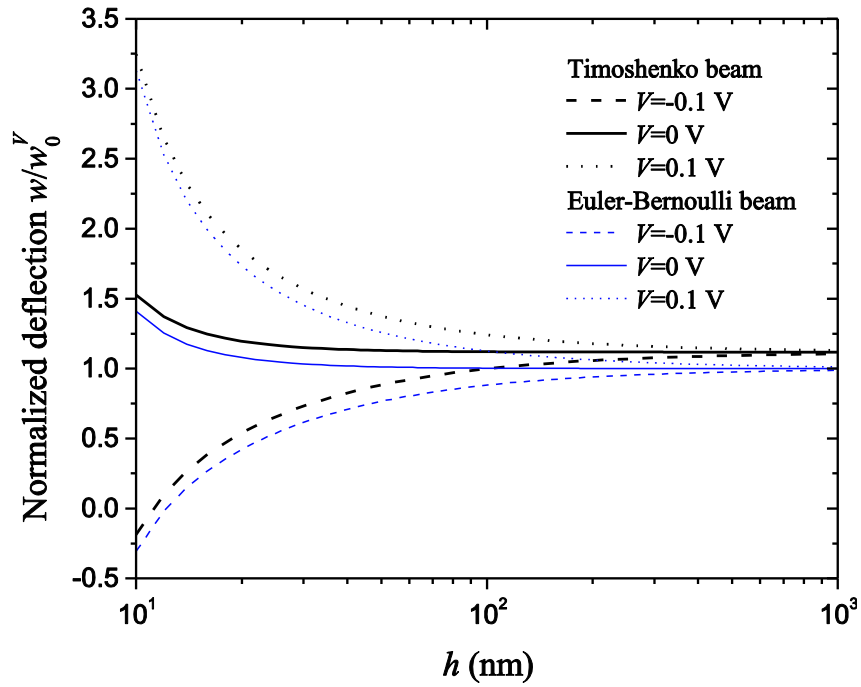
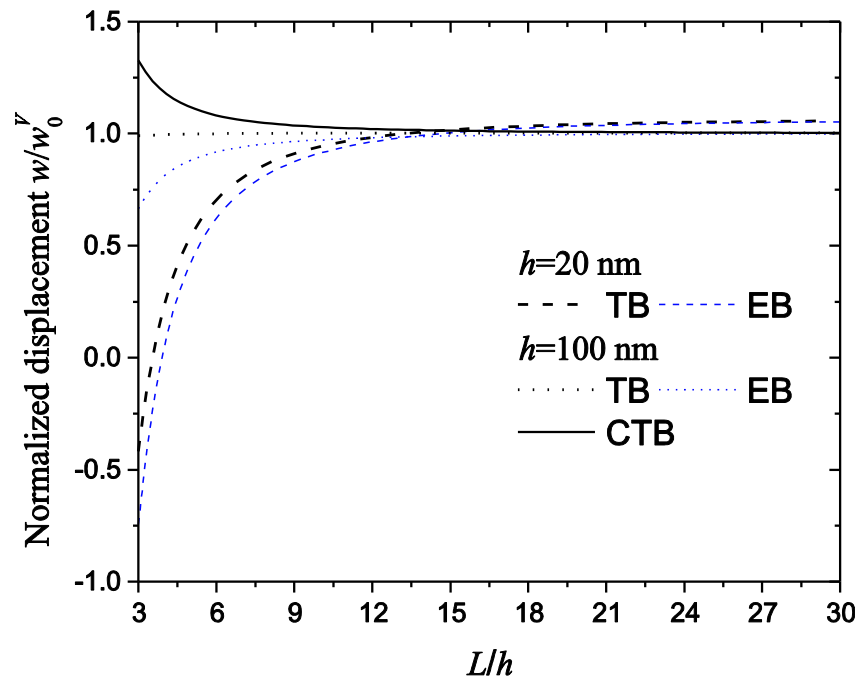Figure 9.3: Variation of the normalized beam deflection with the beam thickness.

Figure 9.4: Variation of the normalized beam deflection with the beam length to thickness ratio when

$V=-0.1$ V.

Fig. 9.3 shows the variation of the normalized beam deflection w/w_0^V at the midpoint ($x = L/2$) of the beam with the beam thickness for both Timoshenko and Euler beam models. w_0^V is the deflection for an Euler-Bernoulli beam without considering the flexoelectric effect. The beam is subjected to the same mechanical load as that in Fig. 9.2 and different electrical loads. The geometry of the beam is set as $b = h$, $L = 5h$. It is obvious from this figure that the flexoelectric effect leads to the size-dependent bending behavior of the piezoelectric nanobeam. With the increase of the beam thickness, the flexoelectric effect decreases with the beam deflection approaching to the classical result. It is also observed from this figure that the flexoelectric effect on the mechanical deflection of the beam depends on the applied electrical load prominently, for example, the deflection direction could be reversed by the flexoelectricity when the applied negative electrical load is sufficient large, which is consistent with the observations in Fig. 9.2. In order to see the shear deformation effect, Fig. 9.4 plots the normalized deflection w/w_0^V against the beam length to thickness aspect ratio (L/h) for the beam with $b = h$ when subjected to $q = 0.2$ nN/nm and $V = -0.1$ V. It is indicated from this figure that the shear deformation has significant effect on both beams with and without the flexoelectric effect when the length-to-thickness ratio L/h is small, as evidenced by the discrepancy between the results from the Timoshenko and Euler-Bernoulli beam models. With the increase of L/h, the predictions from the Timoshenko beam models tend to approach the results from the Euler-Bernoulli beam model as expected. It is also seen that the shear deformation effect increases the beam deflection as indicated by the deflection values of the CTB higher than 1; while the flexoelectric effect decreases the beam deflection and becomes more prominent for the beam with smaller beam thickness h. Therefore, the shear deformation effect on the beam deflection may be compromised with the consideration of the flexoelectricity. For example, when the beam thickness h=100 nm, the result from the Timoshenko beam model with the consideration of the flexoelectricity (curve TB) is close to that from the classical Euler-Bernoulli beam due to the combined effects of the shear deformation and the flexoelectricity. Once again, the large discrepancy between the results from the modified beam models with the consideration of the flexoelectricity and the classical beam models for piezoelectric nanobeams with

smaller thickness indicates the necessity of incorporating the flexoelectricity in predicting their size-dependent bending properties.
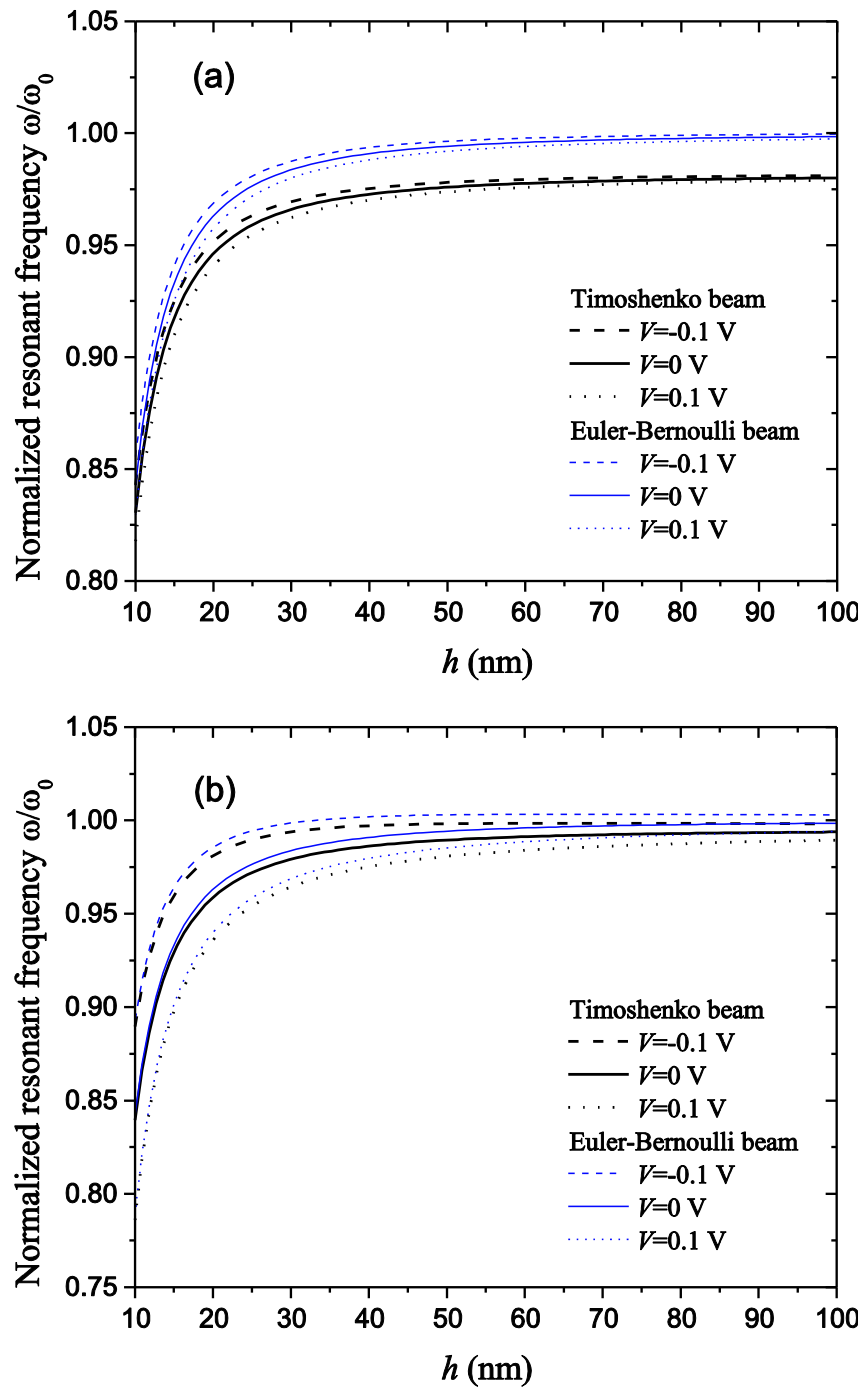

Figure 9.5: Variation of the normalized resonant frequency with the beam thickness for beams with different length to thickness ratios (a) $L/h=10$ and (b) $L/h=20$.

To investigate how the flexoelectricity influences the vibration behavior of the piezoelectric nanobeams, the normalized resonant frequencies from both Timoshenko and Euler-Bernoulli beam predictions are plotted against the beam thickness in Fig. 9.5. ω_0 is the resonant frequency of an Euler-Bernoulli beam without considering the flexoelectric effect and the applied electrical load. It is found that the resonant frequency of the Timoshenko model is always lower than that from the Euler-Bernoulli prediction. In addition, the flexoelectricity decreases the beam resonant frequency and such flexoelectric effect on the vibration behavior of the piezoelectric nanobeam is more pronounced for the beam with smaller thickness. The discrepancy between the curves for different electrical loads indicates that it is possible to tune the frequency of piezoelectric nanobeams by adjusting the applied electrical load, which has also been also been discussed in the works (Wang and Feng, 2010; Yan and Jiang, 2011). By comparing Figs. 9.5(a) and (b), it is observed that the variation of the resonant frequency with the applied electrical load is more significant for slender beams with larger length to thickness ratio (*L*/*h*=20 for example), which means that the frequency tuning for piezoelectric nanobeams with electrical load is more efficient for slender beams. Such frequency tuning concept is expected to provide helpful guidelines for the design and application of piezoelectric nanowires/belts as nanoresonators.

9.4 Conclusions

In this work, Timoshenko beam model with the consideration of the flexoelectric effect is adopted to investigate the static bending and free vibration of piezoelectric nanobeams. By employing the extended linear theory of piezoelectricity and Hamilton's principle, the explicit expressions for the deflection and the resonant frequency of a simply supported piezoelectric nanobeam are obtained. The results show that due to the flexoelectricity induced nonhomogeneous boundary conditions, the flexoelectric effect on the static bending behavior of the piezoelectric nanobeams is prominent and depends on the applied electrical load considerably. The shear deformation is also found to effectively influence the deflection of piezoelectric nanobeams at small length to thickness ratio. The vibration analysis of the piezoelectric nanobeam indicates that the flexoelectricity, the rotary inertia and shear deformation tend to reduce the resonant frequency of the beams.

In addition, the variation of the resonant frequency with the applied electric potential suggests that frequency tuning of piezoelectric nanobeams can be achieved by adjusting the applied electrical load. This work provides a methodology to predict the mechanical properties of piezoelectric nanobeams with a wider range of beam length to thickness ratios. It should be mentioned that the surface effects and the polarization gradient effect are not taken into account in the current study, which will be our future work concentration.

References

Abbasion, S., Rafsanjani, A., Avazmohammadi, R. and Farshidianfar, A., 2009. Free vibration of microscaled Timoshenko beams. Appl. Phys. Lett. **95**, 143122.

Catalan, G., Noheda, B., McAneney, J., Sinnamon, L. J. and Gregg, J. M., 2005. Strain gradients in epitaxial ferroelectrics. Phys. Rev. B **72**, 020102 (R).

Catalan, G., Sinnamon, L. J. and Gregg, J. M., 2004. The effect of flexoelectricity on the dielectric properties of inhomogeneously strained ferroelectric thin film. J. Phys.: Condens. Matter **16**, 2253.

Chen, H. T. and Soh, A. K., 2012. Influence of flexoelectric effects on multiferroic nanocomposite thin bilayer films. J. Appl. Phys. **112**, 074104.

Chu, B. J., Zhu, W. Y., Li, N. and Cross, L. E., 2009. Flexure mode flexoelectric piezoelectric composites. J. Appl. Phys. **106**, 104109.

Chu, M. W., Szafraniak, I., Scholz, R., Harnagea, C., Hesse, D., Alexe, M. and Gösele, U., 2004. Impact of misfit dislocations on the polarization instability of epitaxial nanostructured ferroelectric perovskites. Nat. Mater. **3**, 87-90.

Eliseev, E. A., Morozovska, A. N., Glinchuk, M. D. and Blinc, R., 2009. Spontaneous flexoelectric/flexomagnetic effect in nanoferroics. Phys. Rev. B **79**, 165433.

Fousek, J., Cross, L. E. and Litvin, D. B., 1999. Possible piezoelectric composites based on the flexoelectric effect. Mater. Lett. **39**, 287-291.

Giannakopoulos, A. E. and Suresh, S., 1999. Theory of indentation of piezoelectric materials. Acta Mater. **47**, 2153-2164.

Hu, S. L. and Shen, S. P., 2010. Variational principles and governing equations in nano-dielectrics with the flexoelectric effect. Sci. China-Phys. Mech. Astron. **53**, 1497-1504.

Lee, D., Yoon, A., Jang, S. Y., Yoon, J. G., Chung, J. S., Kim, M., Scott, J. F. and Noh, T. W., 2011. Giant flexoelectric effect in ferroelectric epitaxial thin films. Phys. Rev. Lett. **107**, 057602.

Liu, C. C., Hu, S. L. and Shen, S. P., 2012. Effect of flexoelectricity on electrostatic potential in a bent piezoelectric nanowire. Smart Mater. Struct. **21**, 115024.

Lu, H., Bark, C.-W., Esque de los Ojos, D., Alcala, J., Eom, C. B., Catalan, G. and Gruverman, A., 2012. Mechanical writing of ferroelectric polarization. Science **336**, 59-61.

Ma, W. H., 2008. A study of flexoelectric coupling associated internal electric field and stress in thin film ferroelectrics. Phys. Status Solidi B-Basic Solid State Phys. **245**, 761-768.

Ma, W. H., 2010. Flexoelectric charge separation and size dependent piezoelectricity in dielectric solids. Phys. Status Solidi B-Basic Solid State Phys. **247**, 213-218.

Majdoub, M. S., Maranganti, R. and Sharma, P., 2009. Understanding the origins of the intrinsic dead layer effect in nanocapacitors. Phys. Rev. B **79**, 115412.

Majdoub, M. S., Sharma, P. and Cagin, T., 2008. Enhanced size-dependent piezoelectricity and elasticity in nanostructures due to the flexoelectric effect. Phys. Rev. B **77**, 125424.

Maranganti, R., Sharma, N. D. and Sharma, P., 2006. Electromechanical coupling in nonpiezoelectric materials due to nanoscale nonlocal size effects: Green's function solutions and embedded inclusions. Phys. Rev. B **74**, 014110.

Mindlin, R. D., 1969. Continuum and lattice theories of influence of electromechanical coupling on capacitance of thin dielectric films. Int. J. Solids Struct. **5**, 1197-1208.

Ponomareva, I., Tagantsev, A. K. and Bellaiche, L., 2012. Finite-temperature flexoelectricity in ferroelectric thin films from first principles. Phys. Rev. B **85**, 104101.

Rao, S. S., 2007. Vibration of continuous systems, New York: Wiley.

Sharma, N. D., Landis, C. M. and Sharma, P., 2010. Piezoelectric thin-film superlattices without using piezoelectric materials. J. Appl. Phys. **108**, 024304.

Sharma, N. D., Maranganti, R. and Sharma, P., 2007. On the possibility of piezoelectric nanocomposites without using piezoelectric materials. J. Mech. Phys. Solids **55**, 2328-2350.

Shen, S. P. and Hu, S. L., 2010. A theory of flexoelectricity with surface effect for elastic dielectrics. J. Mech. Phys. Solids **58**, 665-677.

Tagantsev, A. K. and Gerra, G., 2006. Interface-induced phenomena in polarization response of ferroelectric thin films. J. Appl. Phys. **100**, 051607.

Tagantsev, A. K. and Yurkov, A. S., 2012. Flexoelectric effect in finite samples. J. Appl. Phys. **112**, 044103.

Toupin, R. A., 1956. The elastic dielectric. J. Rat. Mech. Anal. **5**, 849-915.

Wang, G. F. and Feng, X. Q., 2010. Effect of surface stresses on the vibration and buckling of piezoelectric nanowires. EPL **91**, 56007.

Wang, G., 2013. Analysis of bimorph piezoelectric beam energy harvesters using Timoshenko and Euler-Bernoulli beam theory. J. Intell. Mater. Syst. Struct. **24**, 226-239.

Wang, Z. L., 2007. The new field of nanopiezotronics. Mater. Today. **10**, 20-28.

Yan, Z. and Jiang, L. Y., 2011. The vibrational and buckling behaviors of piezoelectric nanobeams with surface effects. Nanotechnology **22**, 245703.

Yan, Z. and Jiang, L. Y., 2013. Flexoelectric effect on the electroelastic responses of bending piezoelectric nanobeams. J. Appl. Phys. **113**, 194102.

Zhu, W. Y., Fu, J. Y., Li, N. and Cross, L. E., 2006. Piezoelectric composite based on the enhanced flexoelectric effects. J. Appl. Phys. **89**, 192904.

Chapter 10

10 Conclusions and future work

10.1 Conclusions

Different from conventional bulk piezoelectric structures, piezoelectric nanostructures show size-dependent mechanical and electromechanical coupling properties, which cannot be captured by conventional continuum mechanics models. In addition, the coupling of electromechanical coupling of piezoelectric materials and size effects at the nanoscale complicates the theoretical analysis of such novel structures. In this work, within the continuum mechanics framework, the size-dependent bending, vibration and buckling behaviors of piezoelectric straight and curved nanobeams, and piezoelectric nanoplates have been firstly predicted by modified beam or plate continuum models accounting for size effects. The contributions of the current work include:

(1) This work is the first to provide a comprehensive study on the size-dependent mechanical and electromechanical coupling properties of different piezoelectric nanostructures with surface effects. By applying the surface piezoelectricity model, we firstly develop various modified beam and plates models, which are capable of predicting the size-dependent properties of piezoelectric nanostructures. These models can recover the conventional continuum mechanics models when surface effects are neglected;

(2) By controlling the beam axial constraints or plate in-plane boundary constraints, the relaxation phenomenon of nanostructures, which was observed in both experiments and atomistic simulations, is captured through the methodologies and models presented in the current work. Such a relaxation phenomenon has not been reported thus far through continuum mechanics approaches in existing literatures;

(3) The phenomenon of flexoelectricity observed in ferroelectric materials at the nanoscale has attracted significant scientific interest recently. However, there are very limited studies on modeling the effect of flexoelectrity on the static and dynamic behavior of piezoelectric nanostructures. The current work fills this gap and is the

first to develop modified beam models for piezoelectric nanobeams with different boundary conditions accounting for flexoelectricity. Based on the developed models, the flexoelectricity induced size-dependent mechanical and electrical properties of piezoelectric nanobeams can be captured.

In addition, significant conclusions drawn from the current work are listed as:

(1) The electromechanical coupling coefficient of piezoelectric nanobeams may be significantly enhanced with the decrease of nanobeam thickness due to surface effects, implying the possible performance improvement of piezoelectric nanobeam based devices in NEMS;

(2) The influence of surface effects including residual surface stress, surface elasticity and surface piezoelectricity on the bending, vibration and buckling behaviors of piezoelectric nanobeams and nanoplates is more prominent with the decrease of beam or plate thickness;

(3) Although some individual influence of the residual surface stress, surface elasticity and surface piezoelectricity on the electroelastic fields of curved piezoelectric nanobeam is small under some circumstances, the combined influence of these surface effects is significant;

(4) The in-plane boundary conditions influence the surface effects on the static bending and vibration behaviors of a simply supported piezoelectric nanoplate prominently.

(5) A transition length to thickness ratio of a piezoelectric nanoplate is found, at which surface effects on the critical electric potential for the mechanical buckling of the plate disappear for all plate thickness.

(6) Flexoelectric effect on the electroelastic fields of the piezoelectric nanobeam is sensitive to the beam boundary conditions and the applied electric potential, and such an influence is more significant for a beam with smaller thickness and decays quickly with the increase of beam size.

10.2 Future work

This work provides a general methodology to study the size-dependent properties of piezoelectric nanobeams and nanoplates under different loading conditions. The models developed in the work can be claimed as helpful for predicting a qualitative trend of the surface effects and the flexoelectric effect on the mechanical and electromechanical coupling properties of piezoelectric nanostructures. Based on the results from the current study, some other aspects of the size-dependent properties of piezoelectric nanostructures are suggested to be further conducted:

(1) In this study, the surface effects and the flexoelectric effect on the properties of piezoelectric nanostructures are investigated separately. For a dielectric material (including piezoelectric materials), both effects exist simultaneously. Therefore, further investigation on the size-dependent properties of piezoelectric nanostructures considering both surface effects and flexoelectric effect is necessary. Due to the complexity of the problem induced by the electromechanical coupling of piezoelectric materials and the small scale effects, analytical solutions may only be obtained for specific piezoelectric nanostructure configurations. Therefore, appropriate numerical methods are required to implement the investigations.

(2) Recently, there is an increasing scientific interest in designing new multifunctional devices at the nanoscale. The functionality of such novel devices depends on the multi-physics coupling of their structural constituents, *e.g.* layered composites, which exhibit coexistence of at least two material properties, such as elasticity, electricity and magnetism. To fulfill the practical requirements, it is important to model these advanced materials with size effects and clarify the size effects on their physical properties. For the layered structures, in addition to surface effects and flexoelectric effect, the interface effects should also be taken into consideration.

(3) To study the flexoelectric effect on the piezoelectric nanobeams, the strain gradient along the beam thickness direction is considered while the one along the beam axial direction is ignored. This is a limitation of the current work. In fact, when the strain gradients along both directions are considered, differential governing equations with higher-order terms compared to the conventional governing equations will be

obtained. Meantime, in addition to the classical boundary conditions, new boundary conditions are required to solve the modified governing equations with higher-order terms. Therefore, a more accurate model should be developed with the consideration of all the strain gradients. Numerical studies may need to be conducted to investigate the strain gradient effects on the properties of the piezoelectric nanobeams.

(4) The current study based on continuum mechanics is not applicable for extremely small nanostructures (*i.e.* $h < 10$ nm in the current work), in which edge and corner effects play an important role in the overall properties of structures. At such an extremely small scale, atomistic simulations should be employed to conduct the analyses. Therefore, modified continuum mechanics modeling should be combined with atomistic studies to investigate the size-dependent properties of piezoelectric nanostructures.

(5) With the development of advanced synthesis techniques, various configurations of piezoelectric nanostructures have been successfully synthesized with potential applications in the NEMS. It is thus necessary to acquire a fundamental understanding of the size-dependent properties of these nanostructured piezoelectric materials. However, it is very difficult if it is not impossible to fully conduct analytical analysis on these materials with complex structures due to the mathematical obstacles. Therefore, numerical methods such as a finite element model with the consideration of surface effects and flexoelectricity within the framework of classical finite element method should be conducted for the numerical simulation purpose. Such a numerical approach incorporating the nanoscale features of piezoelectric materials is expected to be more accurate and reliable.

Appendix A: Influence of axial boundary constraint on the vibration of piezoelectric nanobeams with surface effects

This appendix has been provided to supplement the work presented in Chapter 3 by considering the axial boundary constraint of piezoelectric nanobeams. The schematic of the piezoelectric nanobeams is referred to Fig. 3.1. In addition, notations will only be given to physical quantities that do not appear in Chapter 3, otherwise, they are the same as those defined in Chapter 3. The axial strain is expressed based on the Euler-Bernoulli beam theory as

$$\varepsilon_x = \frac{\partial u_0(x,t)}{\partial x} - z\frac{\partial^2 w(x,t)}{\partial x^2}, \tag{A.1}$$

with $u_0(x,t)$ being the axial displacement at $z=0$, which was assumed as zero in Chapter 3 based on the conventional Euler-Bernoulli model. Such assumption is reasonable for a clamped-clamped beam. However, for a cantilevered or a simply supported beam, this axial displacement may not be zero depending on the boundary constraints. Following the derivation procedure given in Chapter 3, the following governing equations for a general case can be obtained as

$$\left[c_{11}bh + (2b+2h)c_{11}^s\right]\frac{\partial^2 u_0(x)}{\partial x^2} = 0, \tag{A.2}$$

$$(EI)^*\frac{\partial^4 w(x,t)}{\partial x^4} - N^*\frac{\partial^2 w(x,t)}{\partial x^2} = -\rho bh\frac{\partial^2 w(x,t)}{\partial t^2}, \tag{A.3}$$

in which $(EI)^* = \left(c_{11} + e_{31}^2/\kappa_{33}\right)bh^3/12 + \left(c_{11}^s + e_{31}^s e_{31}/\kappa_{33}\right)\left(h^3/6 + bh^2/2\right)$ is the effective bending rigidity of the beam and $N^* = \left[c_{11}\partial u_0/\partial x + e_{31}V/h\right]bh + 2\left[\sigma_x^0 + c_{11}^s\partial u_0/\partial x + e_{31}^s V/h\right]b$.

The boundary conditions in both the axial and transverse directions are prescribed as

$$u_0 = w = \frac{\partial w}{\partial x} = 0 \text{ at } x = 0; \ P^* = M^* = Q^* = 0 \text{ at } x = L \ \text{(C-F)}, \tag{A.4}$$

$$\begin{cases} u_0 = w = M^* = 0 \text{ at } x = 0 \text{ and } x = L \text{ (Case 1)} \\ P^* = w = M^* = 0 \text{ at } x = 0 \text{ and } x = L \text{ (Case 2)} \end{cases} \text{(S-S)}, \tag{A.5}$$

$$u_0 = w = \frac{\partial w}{\partial x} = 0 \text{ at } x = 0 \text{ and } x = L \text{ (C-C),} \tag{A.6}$$

where $P^* = \int \sigma_x \mathrm{d}y\mathrm{d}z + \int_c \sigma_x^s \mathrm{d}c = [c_{11}\partial u_0/\partial x + e_{31}V/h]bh + 2[\sigma_x^0 + c_{11}^s \partial u_0/\partial x + e_{31}^s V/h](b+h)$ is

the effective axial force; $M^* = (EI)^* \partial^2 w/\partial x^2$ is the effective moment; and

$Q^* = (EI)^* \partial^3 w/\partial x^3 - N^* \partial w/\partial x$ is the effective shear force. It should be mentioned that

two different axial boundary conditions may apply for simply-supported piezoelectric

beam, as shown from Eq. (A.5). The beam is constrained without axial moving under the

Case 1 boundary condition while traction free is adopted under the Case 2 boundary

condition. The traction free boundary condition is also adopted for the cantilever beam as

indicated in Eq. (A.4). Under this condition, a uniform strain

$\varepsilon = \partial u_0/\partial x = -[e_{31}Vb + 2\sigma_x^0(b+h) + 2e_{31}^s V(b+h)/h]/[c_{11}bh + 2c_{11}^s(b+h)]$ is induced by

the applied electrical load and surface effects, which will influence the vibration behavior

of piezoelectric nanobeams. After applying these boundary conditions, the resonant

frequencies of the piezoelectric nanobeams can be determined.

Firstly, the variation of the normalized resonant frequency ω^s/ω^0 of a simply-

supported piezoelectric nanobeam with beam thickness h under both Case 1 and Case 2

axial boundary conditions is plotted in Fig. A.1. ω^0 is the resonant frequency calculated

without the consideration of surface effects and the applied electrical load. The beam

geometry is set as $b=h$ and $L=10h$. It is clearly seen from this figure that the axial

boundary constraint has a significant influence on the vibration of the piezoelectric

nanobeam, as evidenced by the dissimilar variation trends. For example, when the axial

boundary constraint is set as described in Case 1, the combined effects of surfaces and

electrical load increase the resonant frequency of the piezoelectric nanobeams. When $V=$−

0.1 V, the influence is the largest (ω^s/ω^0 is about 1.2 at $h=10$ nm). However, under Case

2 boundary constraint, the resonant frequency can be either enhanced or reduced by the

surface effects and the applied electrical load. For example, ω^s/ω^0 is about 1.01 and

0.95 for a beam with $h=10$ nm when $V=0.1$ V and −0.1 V, respectively. It is noted that the

variation of resonant frequency with the applied electric potential in this figure indicates

a possible avenue for frequency tuning of piezoelectric nanobeams. It is also observed that the surface effects have more prominent influence on the resonant frequency of a beam with smaller thickness. While such surface effects decrease with the increase of beam thickness h. Fig. A.2 shows the variation of the normalized resonant frequency of a piezoelectric nanobeam against the beam thickness. The beam has the same geometric parameters as the one in Fig. A.1 without any applied electrical load. It demonstrates that the surface effects on the resonant frequencies of piezoelectric nanobeams are significantly influenced by the beam boundary conditions. For the S-S beam with Case 1 boundary constraint and the C-C beam, surface effects increase the resonant frequencies, while the trend is opposite for the S-S beam with Case 2 boundary constraint and the C-F beam. Again, surface effects are more significant for the beam with smaller thickness h and reduce with the increase of h. From these two figures, it is conduced that the axial boundary condition plays a substantial role in the transverse vibration of piezoelectric nanobeams with surface effects. Therefore, it is essential to consider the axial boundary constraints in predicting the vibration behavior of piezoelectric nanobeams.
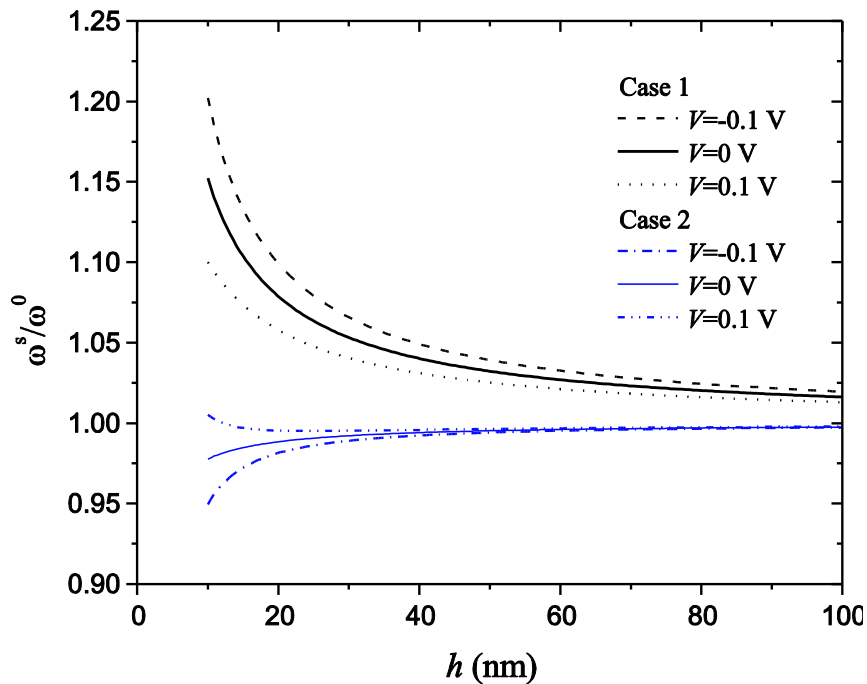

Figure A.1: The normalized resonant frequency ω^s / ω^0 versus beam thickness h for a simply-supported piezoelectric nanobeam with surface effects under different axial boundary conditions.
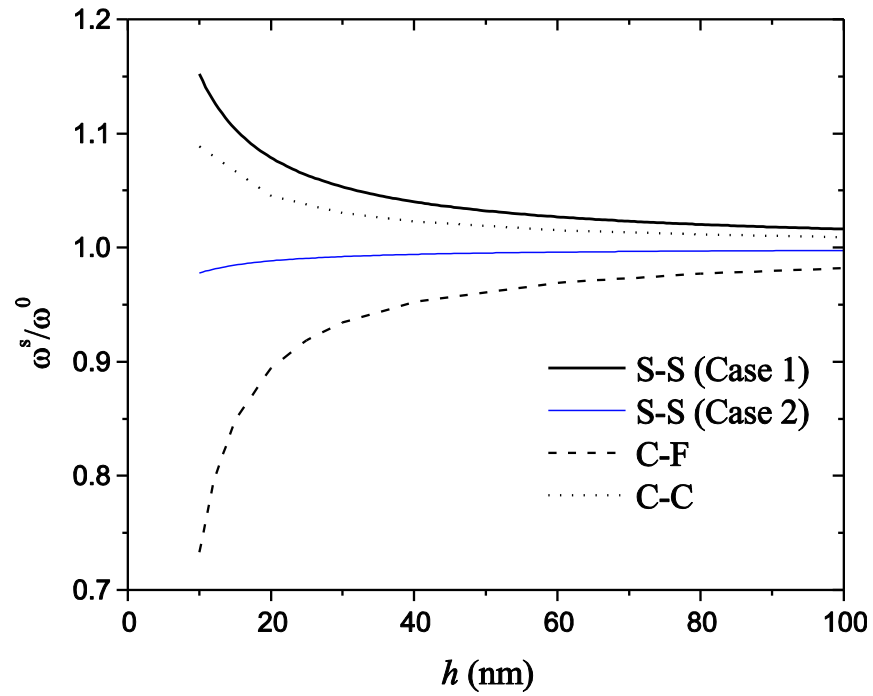
Figure A.2: The normalized resonant frequency ω^s / ω^0 versus beam thickness h for a piezoelectric nanobeam with surface effects under different boundary conditions.
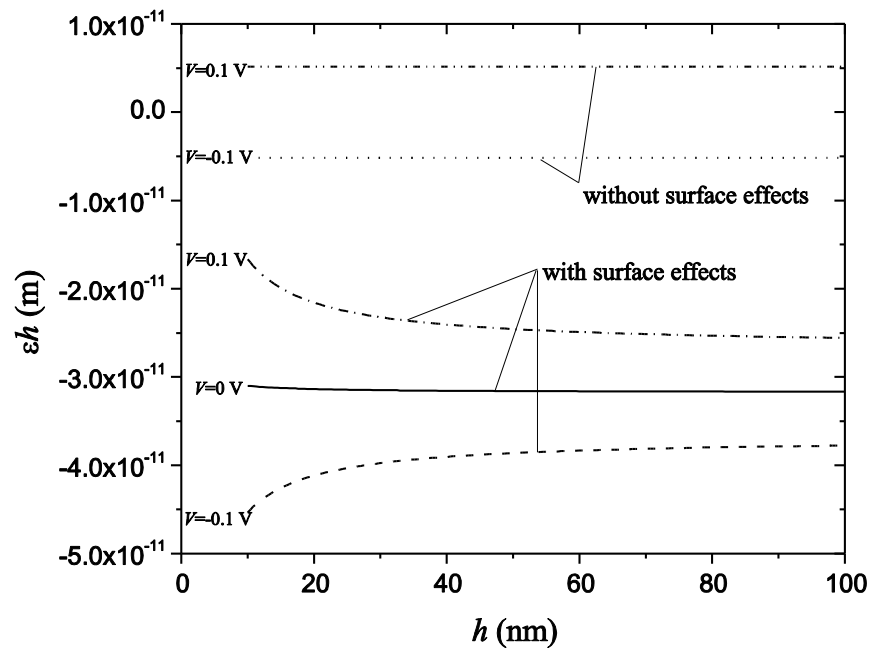

Figure A.3: Axial strain εh versus beam thickness h for a piezoelectric nanobeam under different applied electrical loads.

As mentioned before, the applied electrical load and surface effects will induce an axial strain when the axial traction free condition is prescribed for the beam. As shown in Fig. A.3, without the consideration of the surface effects, the product of this axial strain with the beam thickness is a constant, *i.e.* $\varepsilon h = -e_{31}V/c_{11}$. When V=0 V, no axial strain is induced for the beam without considering the surface effects. However, the existence of the residual surface stress will still induce a relaxation strain as shown by the curve V=0 V with surface effects in Fig. A.3. It is also observed in this figure that the surface effects lead to the size-dependency of this axial strain. From the above analysis, it is indicated that both axial and transverse boundary constraints significantly influence the surface effects on the resonant frequencies of piezoelectric nanobeams. And an axial strain relaxation is also observed under axial traction free boundary condition for a C-F beam. This applied electrical load and surface effects dependent relaxation phenomenon has not been observed in Chapter 3.

Curriculum Vitae

Name:	Zhi Yan
Post-secondary Education and Degrees:	Huazhong University of Science & Technology Wuhan, Hubei, China 2002-2006 B.E.Sc. 2006-2007 M.E.Sc. The University of Western Ontario London, Ontario, Canada 2007-2009 M.E.Sc 2009-2013 Ph.D.
Honours and Awards:	Ontario Graduate Scholarship (OGS) 2011-2012, 2012-2013 Graduate Thesis Research Award 2008, 2010, 2012
Related Work Experience	Teaching Assistant, Research Assistant The University of Western Ontario 2007-2013

Publications:

1. Yan, Z. and Jiang, L.Y., 2013. Flexoelectric effect on the electroelastic responses of bending piezoelectric nanobeams. J. Appl. Phys. 113: 194102.

2. Yan, Z. and Jiang, L.Y., 2012. Surface effects on the vibration and buckling of piezoelectric nanoplates. EPL 99: 27007.

3. Yan, Z. and Jiang, L.Y., 2012. Vibration and buckling analysis of a piezoelectric nanoplate considering surface effects and in-plane constraints. Proc. R. Soc. A 458: 3458-3475.

4. Yan, Z. and Jiang, L.Y., 2012. Surface effects on the electroelastic responses of a thin piezoelectric plate with nanoscale thickness. J. Phys. D: Appl. Phys. 45: 255401.

5. Yan, Z. and Jiang, L.Y., 2011. Electromechanical response of a curved piezoelectric nanobeam with the consideration of surface effects. J. Phys. D: Appl. Phys. 44: 365301.

6. Yan, Z. and Jiang, L.Y., 2011. The vibrational and buckling behaviors of piezoelectric nanobeams with surface effects. Nanotechnology 22: 245703.

7. Yan, Z. and Jiang, L.Y., 2011. Surface effects on the electromechanical coupling and bending behaviors of piezoelectric nanowires. J. Phys. D: Appl. Phys. 44: 075404.

8. Yan, Z., Zaman, M. and Jiang, L.Y., 2011. Thermo-electro-mechanical analysis of a curved functionally graded piezoelectric actuator with sandwich structure. Materials (special issue: Advances in Functionally Graded Materials) 4: 2151-2170.

9. Jiang, L.Y and Yan, Z., 2010. Timoshenko beam model for static bending of nanowires with surface effects. Physica E. 42: 2274-2279.

10. Zaman, M., Yan, Z., and Jiang, L.Y., 2010. Thermal effect on the bending behavior of curved functionally graded piezoelectric actuators. Int. J. Appl. Mech. 2: 787-805.

11. Yan, Z., and Jiang, L.Y., 2010. Interaction of parallel dielectric cracks in functionally graded piezoelectric materials (FGPMs). Acta Mech. 211: 251-269.

12. Yan, Z., and Jiang, L.Y., 2009. Investigation of the critical states of dielectric cracks in functionally graded piezoelectric materials. Proc. R. Soc. A 465: 3187-3207.

13. Yan, Z., Jiang, L.Y. and Dryden, J. R., 2009. The fracture behaviour of functionally graded piezoelectric materials containing collinear dielectric cracks. Proc. R. Soc. A 465: 1779-1798.

14. Yan, Z. and Jiang, L.Y., 2009. On a moving dielectric crack in a piezoelectric interface with spatially varying properties. Eng. Frac. Mech. 76: 560-579.

15. Yan, Z. and Jiang, L.Y., 2009. Study of a propagating finite crack in functionally graded piezoelectric materials considering dielectric medium effect. Int. J. Solids Struct. 46: 1362-1372.